Study of New Adsorbents and Operation Cycles for Medical PSA Units

João Carlos Godinho de Faria dos Santos

Dissertation presented for the degree of
Doctor in Chemical Engineering

by ***Universidade do Porto***

Supervisors
Fernão Domingos M. B. M. de Magalhães
Adélio Miguel Magalhães Mendes

Departamento de Engenharia Química
Faculdade de Engenharia da Universidade do Porto
2005

To my parents and to Marta…

Acknowledgments

I would like to thank Professors Adélio Mendes and Fernão Magalhães for all their support and motivation they gave me during the PhD and for having always assured the best conditions. I would also like to thank Fundação para a Ciência e a Tecnologia for the PhD grant and to Departamento de Engenharia Química, namely to Professors Sebastião Feyo de Azevedo and Romualdo Salcedo and LEPAE for the resources made available and to Professor Miguel Madeira, Mrs. Fátima Faustino, Mr. Luís Carlos Matos, Mr. Sousa Vale, Mr. Meireles and to Mrs. Rosa Ramos for their support.

I would like to thank to Air Products and Chemicals, namely Dr. Roger Whitley, Dr. Timothy Golden and Dr. James Occhialini and all the people I was with during my stay in Allentown, for their support and for providing samples of zeolites.

I would also like to thank Weinmann, namely Dr. Ulrich Palm for offering the PSA unit.

I thank to my friends and colleagues in the laboratory, namely, Vasco Silva, Paulo and Luciana Cruz, Pedro Taveira and Valter Silva.

I would like to thank my fiancée, Marta, for the help and strength she always gave me and her parents for all their support.

I would like to thank to my parents and brothers for their support and guidance and for always being there for me.

Abstract

The simulation of pressure swing adsorption units for oxygen separation from air using zeolites with high capacities and selectivities requires the use of fast and accurate numerical methods. An algorithm that combines the finite volume method with the use of high resolution schemes was presented and it was concluded that it allows good accuracy of the results while maintaining a high convergence.

The adsorption capacities of the zeolites Oxysiv 5, Oxysiv 7, KEG415 (formerly from Bayer) and Oxysiv MDX from UOP, MS S 624 and MS C 544 from Grace Davison and AgLiLSX from Air Products and Chemicals, Inc., were determined. AgLiLSX is the only adsorbent that allows the production of oxygen with a concentration higher than 96%.

The regeneration of the adsorbents was studied and it was concluded that special care must be taken to avoid an irreversible degradation of the adsorbent. Carbon dioxide and water vapour were found to contaminate all the adsorbents studied and the extent of this contamination was determined. The contamination of an experimental working pressure swing adsorption unit with MS S 624 was also studied.

Pressure swing adsorption cycles were compared with a vacuum and pressure swing adsorption cycle. Cycles with three different types of equalization (top-to-top, bottom-to-bottom and crossed), cycles with backfill and units with multiple columns were compared as well.

The simulator was able to accurately represent a real unit. With the optimization strategy it was possible to achieve better operating conditions and design characteristics that improved the performance of the units.

Sumário

A simulação de unidades de adsorção com modulação da pressão para a separação de oxigénio do ar, utilizando zeólitos com elevadas capacidades e selectividades, requer o uso de métodos numéricos rápidos e precisos. Foi apresentado um algoritmo que combina o uso do método dos elementos finitos com os esquemas de alta resolução e concluiu-se que esse algoritmo possibilita uma boa precisão dos resultados mantendo, ao mesmo tempo, uma convergência elevada.

Determinaram-se as capacidades de adsorção dos zeólitos Oxysiv 5, Oxysiv 7, KEG415 (previamente da Bayer) e Oxysiv MDX da UOP, MS S 624 e MS C 544 da Grace Davison e AgLiLSX da Air Products and Chemicals, Inc. O adsorvente AgLiLSX é o único que permite a produção de oxigénio com uma pureza superior a 96%.

Estudou-se a regeneração dos adsorventes e concluiu-se que são necessários cuidados especiais para evitar a degradação irreversível dos mesmos. Demonstrou-se que o dióxido de carbono e o vapor de água contaminam todos os adsorventes estudados e determinou-se a extensão dessa contaminação. Foi também estudada a contaminação de uma unidade laboratorial de adsorção com modulação da pressão com MS S 624 após o seu funcionamento.

Compararam-se ciclos de adsorção com modulação da pressão com ciclos de adsorção com modulação da pressão e vácuo. Ciclos com três tipos de igualização (topo-a-topo, base-a-base e cruzada), ciclos com *backfill* e unidades com múltiplas colunas foram também comparados.

O simulador foi capaz de representar uma unidade real de forma precisa. Através da estratégia de optimização foi possível obter melhores condições de operação e características de desenho e melhorar o desempenho das unidades.

Sommaire

La simulation des unités d'adsorption modulée en pression pour la séparation de l'oxygène de l'air, en utilisant des zéolithes avec de hautes capacités et sélectivités, requiert l'usage de méthodes numériques rapides et précis. On a présenté un algorithme qui combine l'usage de la méthode des éléments finis avec les schémas de haute résolution et on a conclu que cet algorithme rend possible une bonne précision des résultats en maintenant, en même temps, une convergence élevée.

On a déterminé les capacités d'adsorption des zéolithes Oxysiv 5, Oxysiv 7, KEG415 (préalablement de la Bayer) et Oxysiv MDX de l'UOP, MS S 624 et MS C 544 de la Grace Davison et AgLiLSX de l'Air Products and Chemicals, Inc. L'adsorbant AgLiLSX est le seul qui permet la production d'oxygène d'une pureté supérieure à 96%.

On a étudié la régénération des adsorbants et on a conclu qu'il faut avoir des soins spéciaux pour éviter leur dégradation irréversible. On a démontré que le dioxyde de carbone et la vapeur d'eau contaminent tous les adsorbants étudiés et on a déterminé l'extension de cette contamination. On a aussi étudié la contamination d'une unité laboratoiriale d'adsorption modulée en pression avec MS S 624 après son fonctionnement.

On a comparé des cycles d'adsorption modulée en pression avec des cycles d'adsorption modulée en pression et vacuum. Des cycles avec trois types d'égalisation (haut-à-haut, base-à-base et croisée), des cycles avec *backfill*, et des unités avec des multiples colonnes ont été aussi comparés.

Le simulateur a été capable de représenter une unité réelle de forme précise. À travers la stratégie d'optimisation on a pu obtenir de meilleures conditions d'opération et de meilleures caractéristiques de dessin et améliorer l'exécution des unités.

Index

1. INTRODUCTION 1

1.1 Oxygen production by pressure swing adsorption 1

1.2 References 5

2. NUMERICAL METHODS 6

2.1 Introduction 6

2.2 Equations for modelling cyclic adsorption processes 8

2.3 Methods for modelling cyclic adsorption processes 9
2.3.1 Finite difference method 10
2.3.1.1 Velocity profile without pressure drop (isothermal) 10
2.3.1.2 Velocity profile with pressure drop (non-isothermal) 11
2.3.2 Successive stages method 11
2.3.2.1 Velocity profile without pressure drop (isothermal) 12
2.3.2.2 Velocity profile with pressure drop (non-isothermal) 13
2.3.3 Finite volume method 14
2.3.3.1 Velocity profile without pressure drop (isothermal) 15
2.3.3.2 Velocity profile with pressure drop (non-isothermal) 16

2.4 HRS and WENO schemes 17

2.5 χ-Schemes 19

2.6 Temporal integration 20

2.7 Application to simulation of cyclic adsorption processes 21
2.7.1 Cyclic steady state 21
2.7.2 Process model 21
2.7.3 Considerations about the numerical methods to be applied 22

2.8 Conclusions 24

2.9 Notation 26

2.10 References 28

3. ADSORPTION EQUILIBRIUM 33

3.1 Introduction 33

3.2 Adsorbents studied 36

3.3 Monocomponent adsorption equilibrium 37
3.3.1 Monocomponent Langmuir isotherm 37
3.3.2 Monocomponent Freundlich isotherm 38

3.3.3 Monocomponent Sips isotherm 39

3.4 Multicomponent adsorption equilibrium 40
3.4.1 Multicomponent Langmuir isotherm 40
3.4.2 Multicomponent Sips isotherm 40
3.4.3 Ideal adsorption solution theory (IAST) 40

3.5 Experimental part 42
3.5.1 Methods for the determination of adsorption equilibrium points 42
3.5.1.1 Volumetric method 42
3.5.1.2 Gravimetric method 44
3.5.1.3 Comparison between the gravimetric and volumetric methods 46
3.5.2 Adsorption isotherms 47
3.5.2.1 Oxysiv 5 from UOP 47
3.5.2.2 Oxysiv 7 from UOP 49
3.5.2.3 MS S 624 from Grace Davison 50
3.5.2.4 MS C 544 from Grace Davison 51
3.5.2.5 KEG415 from UOP/Bayer 52
3.5.2.6 Oxysiv MDX from UOP 53
3.5.2.7 AgLiLSX from Air Products and Chemicals, Inc. 55
3.5.3 Regeneration of the adsorbents 56
3.5.4 Contamination of the adsorbents 57
3.5.5 Contamination of the adsorbents in a pressure swing adsorption unit 59
3.5.5.1 MS S 624 from Grace Davison 59

3.6 Conclusions 63

3.7 Notation 65

3.8 References 67

Appendix 3.1 Volumetric method 69

Appendix 3.2 Gravimetric method 84

Appendix 3.3 Contamination of the adsorbents 95

4. MASS TRANSPORT 122

4.1 Introduction 122

4.2 Mass transport characterization 123
4.2.1 Gas flux in pores 123
4.2.1.1 Knudsen diffusion 123
4.2.1.2 Molecular diffusion 123
4.2.1.3 Combination of the mechanisms Knudsen diffusion and molecular diffusion 125

4.3 Characterization of the adsorbents 125
4.3.1 Pore size distribution 125

4.4 Models for mass transport 126
4.4.1 Linear driving force (LDF) 126

4.5 Experimental part 127
4.5.1 Particles and pores average diameters and porosity of the adsorbents 127
4.5.2 LDF kinetic coefficients 128

4.6 Conclusions **129**

4.7 Notation **130**

4.8 References **132**

5. OPTIMIZATION OF PRESSURE SWING ADSORPTION PROCESSES 134

5.1 Introduction **134**

5.2 PSA units **136**
5.2.1 Description of PSA units 136
5.2.2 Cycles used in PSA units 139
5.2.2.1 Standard cycle without equalization (Skarstrom's cycle) 139
5.2.2.2 Standard cycle with equalization 139
5.2.2.3 Backfill 140

5.3 Commercial PSA units **141**
5.3.1 PSA unit from Weinmann 141
5.3.2 PSA unit from Sequal 144
5.3.3 VPSA unit from Air Products and Chemicals, Inc. 144

5.4 PSA units for high purity oxygen production **146**

5.5 Mathematical model **148**
5.5.1 Boundary conditions 153
5.5.1.1 Standard cycle without equalization 153
5.5.1.2 Standard cycle with equalization 155
5.5.1.3 Cycle with backfill 156
5.5.1.4 Cycle of the unit from Weinmann without equalization 157
5.5.1.5 Cycle of the unit from Weinmann 158
5.5.1.6 Cycle of the unit from Weinmann with backfill 159
5.5.1.7 Cycle of the unit from Air Products and Chemicals 160
5.5.1.8 Output molar velocity 163
5.5.2 Initial conditions 163

5.6 Optimization strategy **164**
5.6.1 Definition of the objective function 164
5.6.2 Optimization variables 167
5.6.2.1 PSA unit from Weinmann 167
5.6.2.2 Other PSA units 168

5.7 Experimental part **169**
5.7.1 PSA unit from Weinmann 169
5.7.1.1 Characteristics of the unit 169
5.7.1.2 Cycle without equalization – comparison between PSA and VPSA 170
5.7.1.3 Cycle with equalization 175
5.7.1.4 Cycle with backfill 186
5.7.2 PSA unit from Sequal 191
5.7.2.1 Experimental results 191
5.7.3 VPSA unit from Air Products and Chemicals 191
5.7.3.1 Description of the unit 191
5.7.3.2 Experimental results 191
5.7.4 Small experimental PSA unit with Oxysiv MDX 193
5.7.4.1 Description of the unit 193
5.7.4.2 Experimental results 195
5.7.5 Small experimental PSA unit for high purity oxygen production 197

5.7.5.1 Description of the unit 197
5.7.5.2 Experimental results 197

5.8 Conclusions **200**

5.9 Notation **202**

5.10 References **205**

Appendix 5.1 Optimization algorithm **210**

6. GENERAL CONCLUSIONS AND FUTURE WORK 213

1. Introduction

1.1 Oxygen production by pressure swing adsorption

The pressure swing adsorption (PSA) technology has experienced many developments since 1932 when Finlayson and Sharp developed the first PSA single bed process. Ten years later, Khale released a German Patent describing a two bed PSA process. Back then, only modest separations could be obtained due to the low separation factor between oxygen and nitrogen on the available zeolites (Yang, 1987). In the following years this technology and the adsorbents used went through many developments. From 1949 to the early 1950s, Milton and Breck discovered the commercially significant zeolites. In 1960, Skarstrom developed several PSA cycles. Most applications were for air drying. In 1964 (U.S. Patent 3,142,547), Skarstrom proposed an equalization step which allowed the decrease of the power consumption (Espitalier-Noel, 1988). In this step, some of the gas inside the column that was producing is used to pressurize the other column increasing, this way, the recovery.

Along with process improvements, zeolites for oxygen production also experienced enhancements in terms of nitrogen capacity and selectivity. Zeolites such as NaX made possible the development of the first economical PSA process for oxygen production (Sherman, 1999). In 1964 (U.S. Patent 3,140,931), McRobbie, from Union Carbide Corporation, specified a zeolite for O_2 PSA plants. In 1966 (U.S. Patent 3,237,377), a patent was filled by Skarstrom describing a PSA unit for producing oxygen from air, in a 2 bed process with an equalization step and using a 13X type zeolite (Espitalier-Noel, 1988).

These developments allowed, in 1970, the commercialization of pressure swing adsorption units for separating oxygen from air. However, the goal of decreasing even more the power consumption was still being pursued. In 1982 (G.B. Patent 2,091,121), Armond and Deverell proposed the use of smaller particles claiming that this allows reduced power consumption, bed size and cycle times (Espitalier-Noel, 1988). Other developments have been made in the zeolite field, such as the decrease of the quantity of the inert inorganic material that binds the zeolite crystallites (binder - zeolites for equilibrium air separations contain about 20% of this material). This modification in the

zeolite structure aimed at increasing the adsorption capacity and, consequently, the performance of the PSA units (Gaffney et al., 1993). New adsorbents, such as LiX, used commercially since 1997, together with process improvements, allowed the reduction of both capital and operating costs (Sherman, 1999).

Many applications have been found for PSA units, such as the production of oxygen for medical use. In 1975, these units became widely used in hospitals for treating patients with respiratory illness, providing 2-4 L/min of 85-95% oxygen. Also in this year, Ruder and Isles patented a PSA unit to produce enriched air for use on-board jet aircrafts (U.S. Patent 3,922,149). One year later, Armond described an electric powered compact PSA apparatus (DE Patent 2,559,120) using zeolite molecular sieve to generate breathing air for medical use. In 1984 (U.S. Patent 4,477,265), Kratz and Sircar patented a medical oxygen generator for domiciliary use which generated a product with 90% of oxygen (Espitalier-Noel, 1988). Currently, about 500,000 of these units are sold per year worldwide.

For economical reasons, the cycle and configuration of these units differ from the ones proposed by Skarstrom: the solenoid on-off valves used for controlling the pressurization step are replaced by check valves and this step will become dependent on the volume of the storage tank and on the production flow rate. The units that incorporate an equalization step operate in four stages: one stage that begins with pressurization and finishes at the end of production, one equalization stage, one stage that begins with depressurization and finishes at the end of purge and another equalization stage.

One of the consequences of using these units and cycles is that the pressure history during a cycle depends on the product flow rate while it is independent when using the Skarstrom cycle. For this reason, the first cycle is more difficult to simulate and optimize and thumb rules valid for Skarstrom cycles are not applicable.

New pressure swing adsorption cycles and adsorbents are still being developed: Sequal Technologies, Inc. developed a portable multicolumn pressure swing adsorption unit for medical oxygen production (Hill and Hill, 1998) which makes use of a rotary valve (Hill et al., 2001); an LiLSX type zeolite was developed, having a large nitrogen capacity and a high selectivity; Air Products and Chemicals Inc., patented an AgLiLSX type zeolite in 2002 (U.S. Patent 6,432,170) and in 2003 (U.S. Patent 6,544,318) a PSA cycle that makes use of it, which allow the production of high purity oxygen (above 95%).

Among other applications, high purity oxygen is used for surgeries. The legal minimum oxygen concentration limit in the United States is 99% while in Europe is 99.5%.

Another application for high purity oxygen is on fuel cells. According to Nernst's equation, in a fuel cell that produces electromotive force by electrochemical reactions when supplied with an oxidizing gas containing oxygen on the cathode size, increasing the oxygen partial pressure of the oxidizing gas elevates the electromotive force of the cell and improves also the power generating efficiency (Nitta et al., 2000). This can be achieved by either increasing the total pressure of the oxidizing gas or by increasing the oxygen concentration of this gas. For the first case, a widely adopted practice is the incorporation of a compressor in the fuel cell system providing compressed air as oxidizing gas. For the second case, a possible solution is the use of a pressure swing adsorption (PSA) unit to concentrate oxygen from air as it can be described in several patents (Hildebrandt and Schram, 1992, Kaufmann et al., 2002, Keefer et al., 2000, St-Pierre et al., 2003).

Heat and water are typically removed from the fuel cell stack by circulating excessive air across the cathode (Dighe, 1982). To avoid this energy loss, especially on systems that make use of a PSA unit to generate the oxidizing gas, recirculation systems are employed on the cathode and a small purge may be used to avoid excessive build-up of the other components (Dighe, 1982, Hildebrandt and Schram, 1992, Keefer et al., 2000). Since a PSA with a tradition adsorbent can only produce 95% of oxygen, being the rest argon, the average concentration of oxygen in the recirculation loop is only around 55% (Keefer et al., 2000). To minimize the amount of oxygen that is lost in the purge, which can be seen as an energy loss, a higher concentration of oxygen may be used, which will result in a reduction of the argon build-up and a reduction of the purge flow rate and thus in a smaller requirement of this gas. However, for this solution to be viable an energetically efficient technology for high purity oxygen production must be used.

In this Thesis, the results obtained with finite differences and finite volumes combined with high resolution schemes are compared for solving the equations commonly used for modelling adsorption separation processes. The adsorption capacities and physical properties of several commercial adsorbents are presented as well as a contamination study involving carbon dioxide, water vapour and these two

contaminants together. The contamination of a working experimental pressure swing adsorption unit is also presented.

The performance obtained in pressure swing adsorption and in vacuum and pressure swing adsorption modes is compared as well as the performance obtained with three different equalization steps and with a backfill step. An optimization procedure based on process modelling and simulation is used for optimizing all these cycles. Experimental results obtained with commercial and with laboratorial PSA units are compared with the results obtained from the simulator developed in the framework of this Thesis. An experimental PSA unit for high purity oxygen production directly from air using AgLiLSX is also described and studied.

1.2 References

Dighe, S. V. Fuel Cell Cooling and Recirculation System. U.S. Patent 4,362,789, 1982.

Espitalier-Noel, P. M. Waste recycle pressure swing adsorption to enrich oxygen from air. Ph.D. Thesis, University of Surrey, Guildford, Surrey, U.K., 1988.

Gaffney, T. R.; Kirner, J. F.; Kumar, R.; Maliszewskyj, R. J.; Schmidt, W. P. O_2 VSA Process with Low O_2 Capacity Adsorbents. U.S. Patent 5,266,102, 1993.

Hildebrandt, U.; Schram, W. High-temperature Fuel Cells with Oxygen-enriched Gas. U.S. Patent 5,175,061, 1992.

Hill, C. C.; Hill, T. B. Fluid fractionator. U.S. Patent 5,730,778, 1998.

Hill, T. B.; Hill, C. C.; Hansen, A. C. Rotary valve assembly for pressure swing adsorption system. U.S. Patent 6,311,719, 2001.

Kaufmann, L.; Parker, I. S.; Boulet, A. J. Fuel Cell System having a Pressure Swing Adsorption Unit. WO Patent 02/067353, 2002.

Keefer, B. G.; McLean, C.; Brown, M. J. Electrical Current Generation System. WO Patent 00/16425, 2000.

Nitta, S.; Taki, M.; Kawahara, T.; Miura, M. Fuel-Cells System. U.S. Patent 6,106,963, 2000.

Sherman, J. D., Synthetic zeolites and other microporous oxide molecular sieves. *Proceedings of the National Academy of Sciences of the United States of America*, **1999,** 96, (7), 3471-3478.

St-Pierre, J.; Wilkinson, D. P.; Wainwright, D. S. Integrated Fuel Cell and Pressure Swing Adsorption System. U.S. Patent 6,627,338, 2003.

Yang, R. T., *Gas separation by adsorption processes*. Butterworth: Boston, 1987.

2. Numerical Methods

2.1 Introduction

The simulation and optimization of adsorption separation processes have been under close study in the last decade (Cruz et al., 2003b, Nilchan and Pantelides, 1998, Purnomo and Alpay, 2000, Santos et al., 2004b, Zhang et al., 2002), due to the development of new adsorbents with high sorption capacity and selectivity (Sherman, 1999) and processes (Cruz et al., 2005).

Transient sorption separation processes can be modelled by using convection-dominated partial differential equations (PDEs) for mass conservation in the fluid phase, ordinary differential equations (ODEs) for the sorption rate in the stationary phase, and eventually, algebraic equations for the sorption equilibrium between phases. The coupled system of partial differential equations should be solved numerically, because the analytic solution can only be derived for ideal conditions (usually under some assumptions such as: isothermal system, instantaneous equilibrium between the fluid and the stationary phases, negligible pressure drop, linear isotherm and frozen concentration profile during pressure variation stages) (Cruz et al., 2005).

For solving such system of equations, two different numerical approaches are normally used. The first one consists on the simultaneous space and time discretization of each PDE, and then resolution of the resulting system of non-linear algebraic equations (for example: double collocation). The other approach consists on the spatial discretization of each PDE and subsequent integration of the resulting initial value problem of ordinary differential equations with an appropriate integrator (method of lines). Usually, the integrator used is based on the backward differentiation formulas (BDF) (Byrne et al., 1977, Hindmarsh, 1974, Petzold, 1983), known as Gear method (Gear, 1971), which is suitable for the solution of stiff problems (Cruz et al., 2005).

Different numerical methods are usually applied in space and time discretization: orthogonal collocation, orthogonal collocation on finite elements, Galerkin finite elements and finite differences. These numerical methods are usually unbounded, which means that unphysical oscillations can appear in the computed solution. In the context of finite volume formulation, Harten et al., (1987) proposed the

use of ENO (essentially non-oscillatory) schemes and Shu & Osher (Shu, 1997, Shu and Osher, 1988, 1989) the WENO (Weighted ENO) schemes for the solution of partial differential equations in the presence of steep moving fronts (Cruz et al., 2005).

The simulation of adsorption separation processes such as the ones that will be studied in this Thesis require fast and accurate numerical methods. Cyclic adsorption processes are based on the selective retention (based on adsorption equilibrium selectivity or diffusion selectivity) of one or more components in a gas mixture, with the adsorbent regeneration being performed by total or partial pressure decrease (pressure swing adsorption – PSA, vacuum swing adsorption – VSA or vacuum and pressure swing adsorption - VPSA) or by temperature increase (temperature swing adsorption - TSA). These processes are intrinsically dynamic, operating in a periodic fashion with a fixed (or variable) period (Cruz et al., 2005).

Usually one of the following strategies is applied to solve the model equations in cyclic adsorption processes simulation: simultaneous space and time discretization and posterior resolution of the resulting non-linear algebraic system of equations, for example: double collocation (Raghavan and Ruthven, 1985) and space and time finite differences (Cen and Yang, 1985, Yang and Lee, 1998); spatial discretization and subsequent integration of the resulting initial value system of ordinary differential equations (ODE) with an appropriate integrator (Finlayson, 1992) – this method is known as the method of lines (MOL). Usually the integrator used is based on the BDF (backward differentiation formulas), known as Gear formulas (Gear, 1971), that are suitable for the solution of stiff problems (Byrne et al., 1977, Hindmarsh, 1974, Petzold, 1983) or Runge-Kutta Fehlberg method (RKF45 - (Fehlberg, 1969)) unsuitable for the solution of stiff problems but commonly used in cyclic adsorption processes simulation (Cruz et al., 2005).

Different numerical methods have been applied to the solution of cyclic adsorption processes models using the method of lines: successive stages method (Cheng and Hill, 1985), orthogonal collocation (Arvind et al., 2002, Raghavan et al., 1985), finite differences (Ko and Moon, 2000), orthogonal collocation on finite elements (Da Silva et al., 1999), Galerkin finite elements (Teague and Edgar, 1999). The use of high resolution schemes has been mentioned in the work of Cruz et al. (2003b). The use of such schemes conduces always to stable solutions with a high convergence to the reference solution (Cruz et al., 2005).

Some of the numerical methods mentioned before, such as the successive stages, the finite volumes and the finite differences are presented in this Chapter. The simulation results obtained with these methods are compared with experimental data and the error and convergence of these results is analysed. The influence of the mesh refinement on the optimization results is also discussed. Conclusions are withdrawn about the best strategy to be followed in this Thesis.

2.2 Equations for modelling cyclic adsorption processes

The main assumptions that were considered for modeling cyclic adsorption processes are: perfect gas behavior, axially dispersed plug-flow, uniform bed properties along the axial and radial coordinates and negligible radial gradients. According to these assumptions, the model equations can be written as follows:

Total mass balance

$$\frac{\partial c_{\mathrm{T}}}{\partial t} = -\frac{\partial \left(u c_{\mathrm{T}}\right)}{\partial z} - \sum_{i=1}^{\mathrm{nc}} N_i = 0 \tag{2.1}$$

Partial mass balance

$$\frac{\partial c_i}{\partial t} = \frac{\partial}{\partial z}\left(D_{\mathrm{ax}}\ c_{\mathrm{T}} \frac{\partial (c_i / c_{\mathrm{T}})}{\partial z} \right) - \frac{\partial \left(u c_i\right)}{\partial z} - N_i ,\ i = 1, \mathrm{nc} , \tag{2.2}$$

where c_{T} is the total molar concentration, u is the average (interstitial) molar velocity, z is the spatial coordinate, D_{ax} is the effective axial dispersion coefficient, N_i is the molar flow rate of component *i*, c_i is the molar concentration of component *i* in the fluid phase, t is the time variable and nc the number of components in the mixture.

Equations (2.1) and (2.2) can be written in dimensionless form as follows:

Total mass balance

$$\frac{\partial c_{\mathrm{T}}^*}{\partial \theta} = -\frac{\partial \left(u^* c_{\mathrm{T}}^*\right)}{\partial x} - \sum_{i=1}^{\mathrm{nc}} N_i^* \tag{2.3}$$

Partial mass balance

$$\frac{\partial c_i^*}{\partial \theta} = \frac{1}{\mathrm{Pe}} \frac{\partial}{\partial x}\left[c_\mathrm{T}^* \frac{\partial}{\partial x}(c_i^* / c_\mathrm{T}^*) \right] - \frac{\partial \left(u^* c_i^* \right)}{\partial x} - N_i^* , \tag{2.4}$$

Where c_i^* is the dimensionless total molar concentration, $c_i^* = c_i / c_\mathrm{ref}$; c_T^* is the dimensionless total molar concentration, $c_\mathrm{T}^* = c_\mathrm{T} / c_\mathrm{ref}$; θ the dimensionless time variable, $\theta = t / \theta_\mathrm{ref}$, θ_ref the bed time constant, $\theta_\mathrm{ref} = L / u_\mathrm{ref}$; u^* the dimensionless molar average velocity, $u^* = u / u_\mathrm{ref}$; x the dimensionless axial coordinate, $x = z / L$; N_i^* is the dimensionless molar flow rate of component i , $N_i^* = N_i \theta_\mathrm{ref} / c_\mathrm{ref}$ and Pe the Peclet number for mass transfer, $\mathrm{Pe} = u_\mathrm{ref} L / D_\mathrm{ax}$.

For convenience, the asterisk will be omitted from the dimensionless variables in the following sections.

The boundary conditions are obtained from a balance in the vicinity of $x = 0$ and $x = 1$:

$$x = 0 : \frac{1}{\mathrm{Pe}} \frac{\partial}{\partial x}(c_i / c_\mathrm{T}) = u_{x=0} \left(c_i - c_{i,x=0^-} \right) / c_\mathrm{T} \tag{2.5}$$

$$x = 1 : \frac{1}{\mathrm{Pe}} \frac{\partial}{\partial x}(c_i / c_\mathrm{T}) = u_{x=1} \left(c_{i,x=1^+} - c_i \right) / c_\mathrm{T} \tag{2.6}$$

2.3 Methods for modelling cyclic adsorption processes

As mentioned before, different numerical methods may be applied to the solution of cyclic adsorption processes models and some of the most promising ones are: finite difference methods, successive stages and finite volume methods. These methods are briefly presented in this section.

2.3.1 Finite difference method

In the finite differences method, the partial differential equations of the model are transformed in ordinary differential equations by applying finite differences formulas to the derivatives in specific points of the domain.

An extensive work has been done on this field with the aim of reducing the computational effort. Efficient interpolating wavelet-based adaptive-grid numerical methods have been developed for 1D (Cruz et al., 2001, 2002) and for 2D (Santos et al., 2003). These methods are inspired on the wavelets theory and result on the use of a variable number of discretization points along time. These points will be concentrated in the vicinity of discontinuities such as concentration fronts and more dispersed in smoother regions. Recently, methods that combine the use of high-resolution schemes (such as SMART) with an adaptive multiresolution approach inspired by wavelet theory have also been presented for 1D (Alves et al., 2002, Cruz et al., 2003a) and for 2D (Santos et al., 2004a). Despite the high efficiency of these numerical methods, mass conservation is not assured which makes them less attractive when dealing with adsorption separation processes using high adsorption capacity and selectivity adsorbents.

2.3.1.1 Velocity profile without pressure drop (isothermal)

When the pressure drop and temperature variations can be considered negligible, two of the following three boundary conditions must be imposed (Cruz et al., 2005):

$$u(x=0) = u_{\text{in}} \tag{2.7}$$

$$u(x=1) = u_{\text{out}} \tag{2.8}$$

$$\frac{\partial c_{\text{T}}}{\partial \theta} = \text{constant}\,, \tag{2.9}$$

where u_{in} and u_{out} are the molar average velocity in the inlet and outlet streams, respectively.

2.3.1.2 Velocity profile with pressure drop (non-isothermal)

When the pressure drop and temperature variations can not be considered negligible, one must impose one boundary condition in $x = 0$ and another in $x = 1$ (Cruz et al., 2005):

$$u(x=0) = u_{\text{in}} \text{ or } c_{\text{T}}(x=0) = c_{\text{T,in}} \tag{2.10}$$

$$u(x=1) = u_{\text{out}} \text{ or } c_{\text{T}}(x=1) = c_{\text{T,out}} \tag{2.11}$$

The pressure drop along a packed column can be described the Blake-Kozeny equation (Bird et al., 1960):

$$-\frac{\partial p_{\text{T}}}{\partial x} = \beta \cdot u \tag{2.12}$$

For packed columns, β is given by:

$$\beta = \frac{150\mu_{\text{mix}}(1-\varepsilon_{\text{b}})^2}{\varepsilon_{\text{b}}^3 d_{\text{p}}^2}, \tag{2.13}$$

where d_{p} is the particle diameter, ε_{b} is the bed void fraction and μ_{mix} is the mixture viscosity given by Wilke's formula.

2.3.2 Successive stages method

The successive stages method (or mixed cells in series model or cascade of perfectly mixed tanks), is a widely used method for the solution of separation processes (see, for example, Cheng and Hill, 1985). A representation of this method is presented in Figure 2.1.

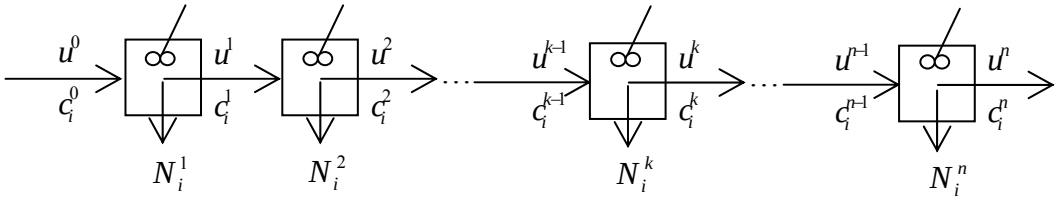

Figure 2.1 - Successive stages method applied to a separation process (Cruz et al., 2005).

The equivalent total mass balance equation using the successive stages method is given by the following equation:

$$\frac{\partial c_{\mathrm{T}}^{k}}{\partial \theta} = -n \cdot \left(u^{k} c_{\mathrm{T}}^{k} - u^{k-1} c_{\mathrm{T}}^{k-1} \right) - \sum_{i=1}^{\mathrm{nc}} N_{i}^{k} \ , \ k = 1, n \, , \tag{2.14}$$

where n is the number of stages. The i^{th} component mass balance is given by:

$$\frac{\partial c_{i}^{k}}{\partial \theta} = -n \cdot \left(u^{k} c_{i}^{k} - u^{k-1} c_{i}^{k-1} \right) - N_{i}^{k} \, , \tag{2.15}$$

and

$$c_{\mathrm{T}}^{k} = \sum_{i=1}^{\mathrm{nc}} c_{i}^{k} \ ; \ c_{\mathrm{T}}^{k} = p_{\mathrm{T}}^{k} / T^{k} \, , \tag{2.16}$$

where T is the absolute temperature.

The pressure drop equation is given by:

$$u^{k} = -n \cdot \left(p_{\mathrm{T}}^{k+1} - p_{\mathrm{T}}^{k} \right) / \beta \tag{2.17}$$

2.3.2.1 Velocity profile without pressure drop (isothermal)

If the boundary conditions are: $\partial c_{\mathrm{T}} / \partial \theta = c_{\mathrm{T}}^{\theta}$ and $u^{0} = u_{\mathrm{in}}$, the velocity profile is calculated by the following equation (Cruz et al., 2005):

$$u^{k} = u^{k-1} - \frac{1}{n \cdot c_{\mathrm{T}}} \left(c_{\mathrm{T}}^{\theta} + \sum_{i=1}^{\mathrm{nc}} N_{i}^{k} \right), \ k = 1, n \tag{2.18}$$

If the boundary conditions are: $\partial c_{\mathrm{T}} / \partial \theta = c_{\mathrm{T}}^{\theta}$ and $u^{n} = u_{\mathrm{out}}$, the velocity profile is calculated by the following equations:

$$\begin{aligned} & u^{0} = 0 \\ & u^{k} = u^{k-1} - \frac{1}{n \cdot c_{\mathrm{T}}} \left(c_{\mathrm{T}}^{\theta} + \sum_{i=1}^{\mathrm{nc}} N_{i}^{k} \right), \ k = 1, \ldots, n \\ & u^{k} = u^{k} + (u_{\mathrm{out}} - u^{n}), \ k = 1, \ldots, n \end{aligned} \tag{2.19}$$

If the boundary conditions are: $u^0 = u_{\text{in}}$ and $u^n = u_{\text{out}}$, the velocity profile is calculated by the following equations(Cruz et al., 2005):

$$c_{\text{T}}^{\theta} = -c_{\text{T}} \cdot \left(u_{\text{out}} - u_{\text{in}}\right) + \sum_{k=1}^{n} \sum_{i=1}^{\text{nc}} \left(N_i^k \cdot \Delta x^k\right) \tag{2.20}$$

$$u^k = u^{k-1} - \frac{1}{n \cdot c_{\text{T}}} \left(c_{\text{T}}^{\theta} + \sum_{i=1}^{\text{nc}} N_i^k \right), \; k = 1, n-1 \tag{2.21}$$

2.3.2.2 Velocity profile with pressure drop (non-isothermal)

The velocity profile is calculated by the following equation (Cruz et al., 2005):

$$u^k = -n \cdot \left(p_{\text{T}}^{k+1} - p_{\text{T}}^k \right) / \beta \tag{2.22}$$

For boundary conditions such as: $p_{\text{T}}^0 = p_{\text{T,in}}$ and $p_{\text{T}}^n = p_{\text{T,out}}$,

$$u_{\text{in}} = -\frac{2 \cdot n}{\beta} \cdot \left(p_{\text{T}}^1 - p_{\text{T,in}} \right) \tag{2.23}$$

$$u_{\text{out}} = -\frac{2 \cdot n}{\beta} \cdot \left(p_{\text{T,out}} - p_{\text{T}}^n \right) \tag{2.24}$$

For boundary conditions such as: $u^0 = u_{\text{in}}$ and $u^n = u_{\text{out}}$,

$$p_{\text{T,in}} = \frac{\beta}{2 \cdot n} u_{\text{in}} + p_{\text{T}}^1 \tag{2.25}$$

$$p_{\text{T,out}} = p_{\text{T}}^n - \frac{\beta}{2 \cdot n} u_{\text{out}} \tag{2.26}$$

The pressure profile is calculated by the integration of the following equation:

$$\frac{\partial c_{\text{T}}^k}{\partial \theta} = -n \cdot \left(u^k c_{\text{T}}^k - u^{k-1} c_{\text{T}}^{k-1} \right) - \sum_{i=1}^{\text{nc}} N_i^k \;, \; k = 1, n \tag{2.27}$$

2.3.3 Finite volume method

In the finite volume method the values of the conserved variables (for example: molar concentration) are averaged across the volume and the conservation principle is always assured. This is the reason why it has been successfully used for heat transfer and mass flow problems (Cruz et al., 2005).

Figure 2.2 presents the finite volume discretization method in a schematic form. u_{F}^{k} is the velocity in the face k and $c_{\mathrm{F},i}^{k}$ is the concentration of i species in the face k.

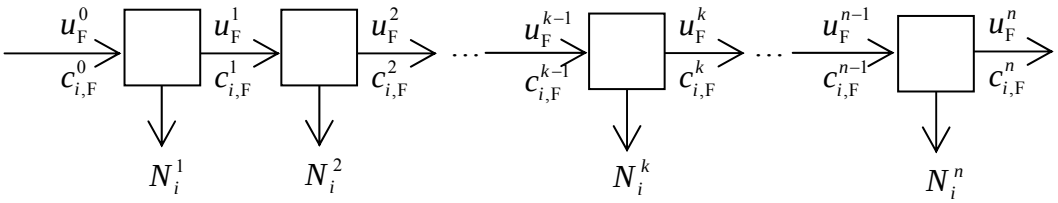

Figure 2.2 - Finite volume method applied to a separation process (Cruz et al., 2005).

The equivalent total mass balance equation using the finite volume method is given by the following equation (Cruz et al., 2005):

$$\frac{\partial \widehat{c}_{\mathrm{T}}^{k}}{\partial \theta} = -\frac{\left(u_{\mathrm{F}}^{k} c_{\mathrm{T,F}}^{k} - u_{\mathrm{F}}^{k-1} c_{\mathrm{T,F}}^{k-1}\right)}{\Delta x^{k}} - \sum_{i=1}^{\mathrm{nc}} \widehat{N}_i^{k}\ ,\ k = 1, n \tag{2.28}$$

where Δx^{k} is the volume in k stage. And the partial mass balance is given by:

$$\frac{\partial \widehat{c}_{i}^{k}}{\partial \theta} = \frac{1}{\mathrm{Pe}} \frac{c_{\mathrm{T,F}}^{k}\left(c_i^{k}/c_{\mathrm{T}}^{k}\right)_{\mathrm{F}}' - c_{\mathrm{T,F}}^{k-1}\left(c_i^{k-1}/c_{\mathrm{T}}^{k-1}\right)_{\mathrm{F}}'}{\Delta x^{k}} - \frac{\left(u_{\mathrm{F}}^{k} c_{i,\mathrm{F}}^{k} - u_{\mathrm{F}}^{k-1} c_{i,\mathrm{F}}^{k-1}\right)}{\Delta x^{k}} - \widehat{N}_i^{k} \tag{2.29}$$

where $\widehat{c}_i^{k}$ is the cell average concentration that is a function of c_i^{k} as follows (Leonard, 1995):

$$\widehat{c}_i^{k} = c_i^{k} + \frac{(\Delta x^{k})^2}{24}(c_i^{k})'' + \frac{(\Delta x^{k})^4}{1920}(c_i^{k})^{(\mathrm{iv})} + \ldots \tag{2.30}$$

$\left(c_i^k / c_{\mathrm{T}}^k\right)_{\mathrm{F}}'$ is the derivative of $\left(c_i^k / c_{\mathrm{T}}^k\right)$ in the face k and is a function of the neighboring cells. Using a second order approximation (central difference scheme - CDS2) the following expression is obtained:

$$\left(c_i^k / c_{\mathrm{T}}^k\right)_{\mathrm{F}}' = \frac{(c_i^{k+1} / c_{\mathrm{T}}^{k+1}) - (c_i^k / c_{\mathrm{T}}^k)}{\frac{1}{2}(\Delta x^{k+1} + \Delta x^k)}, \tag{2.31}$$

where $c_{i,\mathrm{F}}^k$ is the concentration of species i in the face k and is a function of the neighboring cells, as follows:

$$c_{i,\mathrm{F}}^k = f(c_i^{k-1}, c_i^k, c_i^{k+1}, c_i^{k+2}) \text{ and } c_{\mathrm{T,F}}^k = \sum_{i=1}^{nc} c_{i,\mathrm{F}}^k \tag{2.32}$$

Several methods have been proposed in the literature for the calculation of $c_{i,\mathrm{F}}^k$ (concentration of species i in the face k), such as the first-order upwind differencing scheme (UDS) of Courant et al. (1952), $c_{i,\mathrm{F}}^k = c_i^k$, $i = 1,...,\mathrm{nc}$, the second-order linear upwind scheme (LUDS) of Shyy (1985), $c_{i,\mathrm{F}}^k = \frac{3}{2}c_i^k - \frac{1}{2}c_i^{k-1}$, $i = 1,...,\mathrm{nc}$, or the third-order QUICK scheme of Leonard (1979), $c_{i,\mathrm{F}}^k = \frac{1}{2}\left(c_i^{k+1} + c_i^k\right) - \frac{1}{8}\left(c_i^{k+1} + 2c_i^k + c_i^{k-1}\right)$, $i = 1,...,\mathrm{nc}$, which are all upwind biased. Central schemes are often used, such as the second-order central (CDS2), $c_{i,\mathrm{F}}^k = \frac{1}{2}\left(c_i^{k+1} + c_i^k\right)$, $i = 1,...,\mathrm{nc}$, or the fourth-order central differences (CDS4). All these methods, with the exception of the first-order UDS, suffer from lack of boundedness and, for highly convective flows, the occurrence of unphysical oscillations is usual. Two different bounded approaches are nowadays commonly used: high-resolution schemes (HRS) and weighted essentially non oscillatory (WENO) schemes. These are, by definition, bounded higher-order schemes and will be briefly described below (Cruz et al., 2005).

2.3.3.1 Velocity profile without pressure drop (isothermal)

If the boundary conditions are: $\partial c_{\mathrm{T}} / \partial \theta = c_{\mathrm{T}}^{\theta}$ and $u_{\mathrm{F}}^0 = u_{\mathrm{in}}$, the velocity profile is calculated by the following equation (Cruz et al., 2005):

$$u_{\mathrm{F}}^k = u_{\mathrm{F}}^{k-1} - \frac{\Delta x^k}{c_{\mathrm{T}}}\left(c_{\mathrm{T}}^{\theta} + \sum_{i=1}^{\mathrm{nc}} N_i^k\right),\ k = 1, n \tag{2.33}$$

If the boundary conditions are: $\partial c_T / \partial \theta = c_T^{\theta}$ and $u^n = u_{out}$, the velocity profile is calculated by the following equations:

$$\begin{aligned} u_F^0 &= 0 \\ u_F^k &= u_F^{k-1} - \frac{\Delta x^k}{c_T}\left(c_T^{\theta} + \sum_{i=1}^{nc} N_i^k \right),\ k = 1,...,n \\ u_F^k &= u_F^k + (u_{out} - u_F^n),\ k = 1,...,n \end{aligned} \tag{2.34}$$

If the boundary conditions are: $u_F^0 = u_{in}$ and $u_F^n = u_{out}$, the velocity profile is calculated by the following equations:

$$c_T^{\theta} = \sum_{k=1}^{n}\sum_{i=1}^{nc}\left(N_i^k \cdot \Delta x^k \right) - c_T \cdot \left(u_{out} - u_{in} \right) \tag{2.35}$$

$$u_F^k = u_F^{k-1} - \frac{\Delta x^k}{c_T}\left(c_T^{\theta} + \sum_{i=1}^{nc} N_i^k \right),\ k = 1, n-1 \tag{2.36}$$

2.3.3.2 Velocity profile with pressure drop (non-isothermal)

Using a second order approximation (CDS2), the pressure drop equation is given by (Cruz et al., 2005):

$$u_F^k = -\frac{2}{\beta} \cdot \frac{\left(p_T^{k+1} - p_T^k \right)}{\left(\Delta x^{k+1} + \Delta x^k \right)} \tag{2.37}$$

where

$$c_T^k = \sum_{i=1}^{nc} c_i^k \ ;\ c_T^k = p_T^k / T^k \tag{2.38}$$

For boundary conditions such as: $p_{T,F}^0 = p_{T,in}$ and $p_{T,F}^n = p_{T,out}$,

$$u_F^0 = u_{in} = -\frac{2}{\beta} \cdot \frac{\left(p_T^1 - p_{T,F}^0 \right)}{\Delta x^1} \tag{2.39}$$

$$u_F^n = u_{out} = -\frac{2}{\beta} \cdot \frac{\left(p_{T,F}^n - p_T^n \right)}{\Delta x^n} \tag{2.40}$$

For boundary conditions such as: $u_F^0 = u_{in}$ and $u_F^n = u_{out}$,

$$p_{T,in} = \frac{\beta \cdot \Delta x^1}{2} u_{in} + p_{T,F}^1 \tag{2.41}$$

$$p_{T,out} = p_{T,F}^n - \frac{\beta \cdot \Delta x^n}{2} u_{out} \tag{2.42}$$

The equations presented for the boundaries (2.41) and (2.42) are only first order accurate. That should not be a problem in common separation problems. However for processes with high pressure drop these equations should be replaced by at least a second order accurate approximation (Cruz et al., 2005).

2.4 HRS and WENO schemes

As mentioned before, the application of conventional higher-order discretization schemes to the advective term (convection term) of hyperbolic or parabolic equations dominated by convection is not adequate, due to the occurrence of non-physical oscillations (Cruz et al., 2005).

In order to overcome this issue, an extensive amount of research has been directed towards the development of accurate and bounded nonlinear convective schemes. Several discretization schemes were proposed on the total variation-diminishing framework (TVD) (Harten, 1983, Shyy, 1985) and more recently on the normalized variable formulation (NVF) (Leonard, 1987) and its extension, the normalized variable and space formulation (NVSF) of Darwish and Moukalled (1994).

Considering a general grid, as illustrated in Figure 2.3, the labeling of the nodes depends on the local velocity, u_F, calculated at face F. For a given face F, the U and D nodes refer to the upstream and downstream points, relative to node P, which is itself upstream to the face F under consideration (Cruz et al., 2005).

According to the NVSF, the face values are interpolated as (Darwish and Moukalled, 1994):

$$y_F = y_U + \tilde{y}_F (y_D - y_U), \tag{2.43}$$

where y is the convected variable (for example c_i).

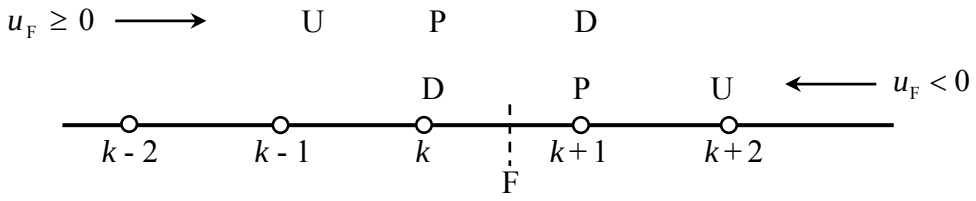

Figure 2.3 - Definition of local variables (Cruz et al., 2005).

The normalized face value, $\tilde{y}_F$, is calculated using an appropriate nonlinear limiter. As an example, the SMART (Gaskell and Lau, 1988) limiter (third order convergence in smooth regions) is presented:

$$\tilde{y}_F = \max\left[\tilde{y}_P, \min\left(\frac{\tilde{x}_F\left(1-3\tilde{x}_P+2\tilde{x}_F\right)}{\tilde{x}_P\left(1-\tilde{x}_P\right)}\tilde{y}_P, \frac{\tilde{x}_F\left(1-\tilde{x}_F\right)}{\tilde{x}_P\left(1-\tilde{x}_P\right)}\tilde{y}_P + \frac{\tilde{x}_F\left(\tilde{x}_F-\tilde{x}_P\right)}{1-\tilde{x}_P}, 1\right)\right] \quad (2.44)$$

and so is the MINMOD limiter (Harten, 1983) (second order convergence in smooth regions):

$$\tilde{y}_F = \max\left[\tilde{y}_P,\ \min\left(\frac{\tilde{x}_F}{\tilde{x}_P}\tilde{y}_P,\ \frac{1-\tilde{x}_F}{1-\tilde{x}_P}\tilde{y}_P + \frac{\tilde{x}_F-\tilde{x}_P}{1-\tilde{x}_P}\right)\right], \quad (2.45)$$

where the normalized variables $\tilde{y}_P$, $\tilde{x}_P$ and $\tilde{x}_F$ are calculated using:

$$\tilde{y}_P = \frac{y_P - y_U}{y_D - y_U},\ \tilde{x}_P = \frac{x_P - x_U}{x_D - x_U},\ \tilde{x}_F = \frac{x_F - x_U}{x_D - x_U} \quad (2.46)$$

More details on this issue, and other high-resolution schemes, can be found in the work of Darwish and Moukalled (1994) and Alves et al. (2003).

According to the third-order WENO scheme, the face fluxes are interpolated as (Shu, 1997, Shu and Osher, 1988, 1989):

$$y_F = w_0 y_F^0 + w_1 y_F^1, \quad (2.47)$$

with $y_F^0 = \frac{1}{2}(y_D + y_P)$ (CDS2), $y_F^1 = \frac{3}{2}y_P - \frac{1}{2}u_U$ (LUDS) and w_i defined by:

$$w_j = \frac{\alpha_j}{\alpha_0 + \alpha_1},\ \alpha_j = \frac{d_j}{(\varepsilon + \beta_j)^2},\ j = 0,1, \tag{2.48}$$

where $\varepsilon > 0$ is introduced to avoid the denominator to become zero. The value of $\varepsilon = 1 \times 10^{-6}$ was used in all the simulations presented. The smoothness measurement is defined by:

$$\beta_0 = (y_D - y_P)^2,\ \beta_1 = (y_P - y_U)^2 \tag{2.49}$$

and $d_0 = \frac{2}{3}$ and $d_1 = \frac{1}{3}$ (Cruz et al., 2005).

2.5 χ-Schemes

Although the schemes presented before are very efficient and bounded, for systems with more than two components, the use of these schemes may result in inconsistencies in the mass balances and may lead to unphysical solutions. For these cases, the χ-schemes should be used. These schemes are a new class of high-resolution schemes that combine consistency, accuracy and boundedness across systems of equations (Darwish and Moukalled, 2003). This new formulation is based on the observation that the upwind scheme and all high-order schemes are consistent. And so, if the high-resolution (HR) scheme at a control volume face is forced to share across the system of equations the same linear combination of high-order (HO) schemes then it will be consistent (Darwish and Moukalled, 2003). Otherwise the mass balance may not close. In this formulation, the value at a control volume face using a high-resolution scheme is written as:

$$\tilde{y}_F^{HR} = \tilde{y}_U + \chi(\tilde{y}_F^{HR} - \tilde{y}_U) \tag{2.50}$$

The NVF form of the SMART scheme is written as (Darwish and Moukalled, 2003):

$$\tilde{y}_F = \begin{cases} 3\tilde{y}_U & 0 < \tilde{y}_U < \frac{1}{6} \\ \frac{3}{8} + \frac{3}{4}\tilde{y}_U & \frac{1}{6} < \tilde{y}_U < \frac{5}{6} \\ 1 & \frac{5}{6} < \tilde{y}_U < 1 \\ \tilde{y}_U & \text{elsewhere} \end{cases} \tag{2.51}$$

The equivalent χ formulation is (Darwish and Moukalled, 2003):

$$\chi = \begin{cases} \frac{16\tilde{y}_U}{3\text{-}2\tilde{y}_U} & 0 < \tilde{y}_U < \frac{1}{6} \\ 1 & \frac{1}{6} < \tilde{y}_U < \frac{5}{6} \\ \frac{8(1-\tilde{y}_U)}{3\text{-}2\tilde{y}_U} & \frac{5}{6} < \tilde{y}_U < 1 \\ 0 & \text{elsewhere} \end{cases} \tag{2.52}$$

Forcing all the related equations to have the same values of χ at any control volume face ensures consistency (Darwish and Moukalled, 2003).

2.6 Temporal integration

The time integration of the resulting system of ordinary differential equations (ODE's initial value problem) can be accomplished using the solver LSODA (Petzold, 1983). This routine solves initial boundary problems for stiff or non-stiff systems of first-order ODE's. For non-stiff systems, it makes use of the Adams method with variable order (up to 12 th order) and step size, while for stiff systems it uses the Gear (or BDF) method with variable order (up to 5 th order) and step size. In the simulations presented, the error in time integration was always set small enough to ensure that the numerical errors are mainly due to inaccuracies resultant from spatial discretization.

2.7 Application to simulation of cyclic adsorption processes

2.7.1 Cyclic steady state

These processes, unlike other separation processes, have as an intrinsic characteristic the fact that the steady state is not reached. Since each adsorption column passes through different stages, a cyclic steady state (CSS) must be considered. It is reached when, after a certain time, the process starts exhibiting periodically, identical dependent variables values and these recurrences occur in a constant cycle time. In all simulations presented in this Thesis, the CSS was considered to be reached when the purity and recovery did not change, in two consecutive cycles, more than 0.001%.

2.7.2 Process model

The process used for testing these numerical methods was the oxygen production from air with a commercial pressure swing adsorption (PSA) oxygen concentrator, Oxymat 3, from Weinmann, without the equalization step (Figure 5.7). This unit operates between 1 and 3 bara and is composed by two adsorption columns and a storage tank. It operates in two stages: stage 1 where pressurization and production take place and stage 2 where depressurization and purge occur. The duration of each stage, defined by $\theta_{\text{press/prod}}$, is 9 s. Calibrated orifices are used to control the flow rates of the purge, vent, feed and product entering the storage tank. These orifices have a discharge coefficient represented as C_v^F, for the feed, C_v^P, for the purge, C_v^V, for the vent and C_v^T for the valve before the storage tank. This unit is described in detail in Chapter 5, Section 5.2. The model of this process is also presented in Chapter 5, Section 5.5.

Since oxygen and argon are adsorbed very similarly by the adsorbent used, a pseudo-binary mixture was considered to be fed to the columns. For this reason, the results regarding the product purity presented in this Chapter will consider a mixture of these two components.

2.7.3 Considerations about the numerical methods to be applied

The effect of mesh refinement in the simulation results (oxygen plus argon purity, Pur, and recovery, Rec) for different production flow rates using finite volume method with QUICK scheme is presented in Table 2.1. As it can be seen, using this scheme, for low product flow rates, oxygen plus argon purity is higher than 100%. Simultaneously the concentration profile inside the column presents unphysical oscillations, which do not disappear with mesh refinement. For higher product flow rates the concentration profile inside the column tends to be smoother and unphysical oscillations tend to disappear. These results give an indication of the number of volumes that are required to accurately simulate this separation unit. A number of 32 volumes are apparently acceptable.

Table 2.1. Effect of mesh refinement in simulation results (oxygen purity, Pur, and recovery, Rec) for different production flow rates using finite volume method with QUICK scheme.

n	1 L_{STP}/min		3 L_{STP}/min		5 L_{STP}/min	
	Rec	Pur	Rec	Pur	Rec	Pur
4	0.070	1.213	0.179	1.045	0.247	0.844
8	0.060	1.041	0.178	1.039	0.245	0.837
16	0.057	0.995	0.172	1.006	0.228	0.779
32	0.057	1.000	0.171	1.001	0.222	0.757
64	0.057	1.000	0.171	1.000	0.222	0.756
128	0.057	1.000	0.171	1.000	0.222	0.756

The error of the solution, ϕ, is presented in Figure 2.4 as a function of the number of discretization volumes for two different schemes: QUICK and SMART for a product flow rate of 1L_{STP}/min. In this figure, ϕ is defined as follows:

$$\phi_i = \frac{\left| X_i - X_i^{ref} \right|}{\left| X_i^{QUICK} - X_i^{ref} \right|}, \tag{2.53}$$

where X_i^{ref} is the reference oxygen purity (or recovery) in the outlet stream, X_i is the oxygen purity (or recovery) using i discretization volumes, X_i^{QUICK} is the oxygen purity (or recovery) using 4 discretization volumes and QUICK scheme. As we can see, the error in the simulation results using QUICK scheme tends, with mesh refinement, to an

asymptotic error which is not obvious from the analysis of Table 2.1. This is due to the unbounded properties of QUICK scheme.

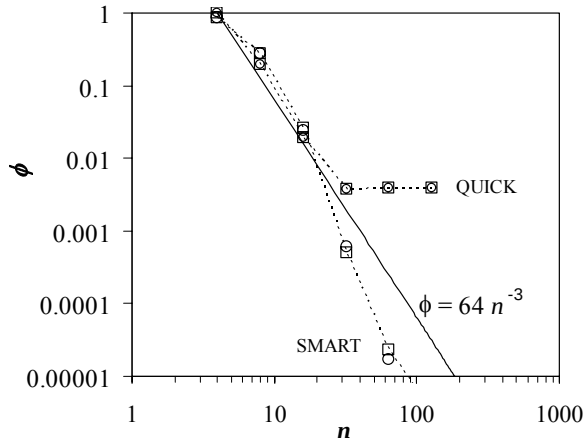

Figure 2.4 - Effect of mesh refinement on oxygen purity and recovery (cyclic steady state): □ purity and ○ recovery, using finite volume method with QUICK and SMART schemes.

The comparison between experimental results, simulation results using finite volumes with the SMART scheme (with 32 volumes), and the simulation results using finite differences, using also SMART scheme (with 128 discretization points) are presented in Figure 2.5. A good agreement between experimental and simulation results can be observed. As it can be seen, the use of the finite volumes method will result in the solution of fewer equations than when using the finite differences method which will be translated in less computational time.

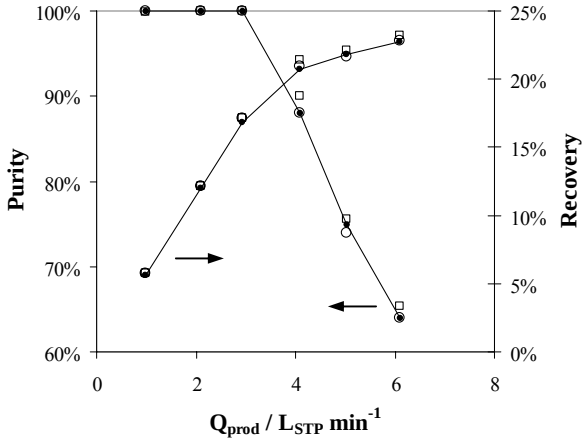

Figure 2.5 - Purity and recovery as a function of production flow rate: □ SMART scheme using finite volumes, ○ SMART scheme using finite differences and —●— experimental.

This strategy was also used to analyse the influence of the discretization scheme and mesh refinement in the results of numerical optimization of the comercial unit using 6 decision variables: L/L^{T} (ratio between the column and storage tank lengths), $\theta_{press/prod}$, C_v^F, C_v^T, C_v^P and C_v^V.

Table 2.2 presents the optimization results at 20ºC (for details see Chapter 5, Section 5.8). An R_p^b value of 110 was considered and a restriction of oxygen plus argon purity of 0.99 was imposed in the optimization. The cycle time, $\theta_{press/prod}$, is the variable that is the most affected by mesh refinement. The maximum recovery obtained increases with mesh refinement as expected.

Table 2.2. Effect of mesh refinement in optimization results using finite volumes with SMART scheme.

n	L/L^{T}	$\theta_{press/prod}$	C_v^F	C_v^T	C_v^P	C_v^V	Rec
4	2.06	0.73	155	73.4	9.0	229	0.252
8	2.09	0.90	155	73.4	8.9	229	0.288
16	2.10	1.06	155	73.4	8.9	229	0.317
32	2.02	1.10	155	73.4	8.8	229	0.324
64	2.10	1.11	155	73.4	8.9	229	0.324
128	2.10	1.11	155	73.4	8.9	229	0.324

It is possible to conclude that the use of unbounded schemes should be avoided in the solution of cyclic adsorption processes, namely when the problem involves sharp moving fronts, since with these schemes the error in the problem solution decreases with mesh refinement very slowly (in the case of QUICK scheme the third order accuracy is completely lost).

2.8 Conclusions

The application of finite volume method for the solution of separation processes involving adsorption was described. The algorithm presented enforces both local and global flux conservation in space and time. The convection terms can be discretized using high-resolution schemes, ensuring boundedness.

A cyclic adsorption process was simulated for better understanding the convergence of different discretization schemes. The use of 32 volumes was found to be sufficient for assuring a good accuracy of the results. The simulation results were verified to be in very good agreement with the experimental results. The unit was also optimized and the influence of the number of discretization volumes in the optimization variables and results was studied. The optimal recovery increases with mesh refinement and the pressurization/ production step duration is highly influenced by the number of volumes.

A minimum of 32 discretization volumes was used for the simulations presented in this Thesis. The solutions were verified with 64 volumes and in some cases with 128 volumes. The simulation of processes using zeolites with increased capacity and selectivity such as Oxysiv MDX from UOP and AgLiLSX from Air Products and Chemicals, Inc., required 64 volumes for obtaining accurate results. χ-schemes with SMART formulation were used whenever the feed gas was a mixture with more than two components.

2.9 Notation

c	fluid phase molar concentration, mol m^{-3}
C_v	valve parameter
D_{ax}	effective axial dispersion coefficient , m^2 s^{-1}
D_M^e	effective homogeneous diffusion coefficient, m s^{-1}
k	iteration or LDF coefficient, $k_i = 15 D_{M,i}^e / r_p^2$, s^{-1}
L	length of the adsorption column, m
n	number of stages or number of discretization points or number of finite volumes
nc	number of components in the mixture
N	molar flow rate, mol s^{-1}
p	pressure , Pa
Pe	Peclet number, $\mathrm{Pe} = u_{ref} / D_{ax}$
Pur	product purity
R_p^b	ratio between bed time constant and particle diffusion time constant (LDF approximation), $R_p^b = \theta_{ref} \cdot k_{ref}$
Rec	product recovery
t	time, s
T	absolute temperature, K
u	average (interstitial molar) velocity, m s^{-1}
x	dimensionless spatial coordinate
z	spatial coordinate, m

Greek symbols

β	pressure drop parameter
ϕ	error of the solution
θ_{ref}	bed time constant, $\theta_{ref} = L/u_{ref}$
θ	dimensionless time variable, $\theta = t/\theta_{ref}$

Subscripts

i	component
in	feed stream (inlet)
out	outlet stream
press	pressurization
prod	production
ref	reference
T	total

Superscripts

*	dimensionless variable
$\cap$	average
F	feed
P	purge
T	storage tank
V	vent

2.10 References

Alves, M. A.; Cruz, P.; Mendes, A.; Magalhães, F. D.; Pinho, F. T.; Oliveira, P. J., Adaptive multiresolution approach for solution of hyperbolic PDEs. *Computer Methods in Applied Mechanics and Engineering*, **2002,** 191, (36), 3909-3928.

Alves, M. A.; Oliveira, P. J.; Pinho, F. T., A convergent and universally bounded interpolation scheme for the treatment of advection. *International Journal for Numerical Methods in Fluids*, **2003,** 41, (1), 47-75.

Arvind, R.; Farooq, S.; Ruthven, D. M., Analysis of a piston PSA process for air separation. *Chemical Engineering Science*, **2002,** 57, (3), 419-433.

Bird, R. B.; Stewart, W. E.; Lightfoot, E. N., *Transport Phenomena*. Wiley International Edition: Singapore, 1960.

Byrne, G. D.; Hindmarsh, A. C.; Jackson, K. R.; Brown, H. G., Comparison of 2 Ode Codes - Gear and Episode. *Computers & Chemical Engineering*, **1977,** 1, (2), 133-147.

Cen, P.; Yang, R. T., Separation of a 5-Component Gas-Mixture by Pressure Swing Adsorption. *Separation Science and Technology*, **1985,** 20, (9-10), 725-747.

Cheng, H. C.; Hill, F. B., Separation of Helium-Methane Mixtures by Pressure Swing Adsorption. *Aiche Journal*, **1985,** 31, (1), 95-102.

Courant, R.; Isaacson, E.; Rees, M., On the Solution of Nonlinear Hyperbolic Differential Equations by Finite Differences. *Communications on Pure and Applied Mathematics*, **1952,** 5, (3), 243-255.

Cruz, P.; Alves, M. A.; Magalhães, F. D.; Mendes, A., Solution of hyperbolic PDEs using a stable adaptive multiresolution method. *Chemical Engineering Science*, **2003a,** 58, (9), 1777-1792.

Cruz, P.; Mendes, A.; Magalhães, F. D., Using wavelets for solving PDEs: an adaptive collocation method. *Chemical Engineering Science*, **2001,** 56, (10), 3305-3309.

Cruz, P.; Mendes, A.; Magalhães, F. D., Wavelet-based adaptive grid method for the resolution of nonlinear PDEs. *Aiche Journal*, **2002,** 48, (4), 774-785.

Cruz, P.; Santos, J. C.; Magalhães, F. D.; Mendes, A., Cyclic adsorption separation processes: analysis strategy and optimization procedure. *Chemical Engineering Science*, **2003b,** 58, (14), 3143-3158.

Cruz, P.; Santos, J. C.; Magalhães, F. D.; Mendes, A., Simulation of separation processes using finite volume method. *Computers & Chemical Engineering*, **2005,** 30, (1), 89-98.

Da Silva, F. A.; Silva, J. A.; Rodrigues, A. E., A general package for the simulation of cyclic adsorption processes. *Adsorption-Journal of the International Adsorption Society*, **1999,** 5, (3), 229-244.

Darwish, M.; Moukalled, F., The χ-schemes: a new consistent high-resolution formulation based on the normalized variable methodology. *Computer Methods in Applied Mechanics and Engineering*, **2003,** 192, (13-14), 1711-1730.

Darwish, M. S.; Moukalled, F. H., Normalized Variable and Space Formulation Methodology for High-Resolution Schemes. *Numerical Heat Transfer Part B-Fundamentals*, **1994,** 26, (1), 79-96.

Fehlberg, E. *Low-order classical Runge-Kutta formulas with stepsize control and their application to some heat transfer problems*; NASA TR R-315; NASA: 1969.

Finlayson, B., *Numerical Methods for Problems with Moving Fronts*. Ravenna Park Publishing Inc: Seattle, Washington, USA, 1992.

Gaskell, P. H.; Lau, A. K. C., Curvature-Compensated Convective-Transport - Smart, a New Boundedness-Preserving Transport Algorithm. *International Journal for Numerical Methods in Fluids*, **1988,** 8, (6), 617-641.

Gear, G. W., *Numerical initial-value problems in ordinary differential equations*. Englewood Cliffs: Prentice Hall, 1971.

Harten, A., High-Resolution Schemes for Hyperbolic Conservation-Laws. *Journal of Computational Physics*, **1983,** 49, (3), 357-393.

Harten, A.; Engquist, B.; Osher, S.; Chakravarthy, S. R., Uniformly High-Order Accurate Essentially Nonoscillatory Schemes .3. *Journal of Computational Physics*, **1987,** 71, (2), 231-303.

Hindmarsh, A. C. *Gear: Ordinary differential equation system solver*; Technical Report UICD-30001, Rev.3; Lawrence Livermore Laboratories: California, 1974.

Ko, D.; Moon, I., Optimization of start-up operating condition in RPSA. *Separation and Purification Technology*, **2000,** 21, (1-2), 17-26.

Leonard, B. P., Stable and Accurate Convective Modeling Procedure Based on Quadratic Upstream Interpolation. *Computer Methods in Applied Mechanics and Engineering*, **1979,** 19, (1), 59-98.

Leonard, B. P., Locally modified QUICK scheme for highly convective 2-D and 3-D flows. In *Numerical Methods in Laminar and Turbulent Flow*, C. Taylor and K. Morgan, e., Pineridge Press: Swansea, U. K., 1987; 5, 35-47.

Leonard, B. P., Order of Accuracy of Quick and Related Convection-Diffusion Schemes. *Applied Mathematical Modelling*, **1995,** 19, (11), 640-653.

Nilchan, S.; Pantelides, C. C., On the optimisation of periodic adsorption processes. *Adsorption-Journal of the International Adsorption Society*, **1998,** 4, (2), 113-147.

Petzold, L., Automatic Selection of Methods for Solving Stiff and Nonstiff Systems of Ordinary Differential-Equations. *Siam Journal on Scientific and Statistical Computing*, **1983,** 4, (1), 136-148.

Purnomo, I. S. K.; Alpay, E., Membrane column optimisation for the bulk separation of air. *Chemical Engineering Science*, **2000,** 55, (18), 3599-3610.

Raghavan, N. S.; Hassan, M. M.; Ruthven, D. M., Numerical-Simulation of a Psa System .1. Isothermal Trace Component System with Linear Equilibrium and Finite Mass-Transfer Resistance. *Aiche Journal*, **1985,** 31, (3), 385-392.

Raghavan, N. S.; Ruthven, D. M., Pressure Swing Adsorption .3. Numerical-Simulation of a Kinetically Controlled Bulk Gas Separation. *Aiche Journal*, **1985,** 31, (12), 2017-2025.

Santos, J. C.; Cruz, P.; Alves, M. A.; Oliveira, P. J.; Magalhães, F. D.; Mendes, A., Adaptive multiresolution approach for two-dimensional PDEs. *Computer Methods in Applied Mechanics and Engineering*, **2004a,** 193, (3-5), 405-425.

Santos, J. C.; Cruz, P.; Magalhães, F. D.; Mendes, A., 2-d wavelet-based adaptive-grid method for the resolution of PDEs. *Aiche Journal*, **2003,** 49, (3), 706-717.

Santos, J. C.; Portugal, A. F.; Magalhães, F. D.; Mendes, A., Simulation and optimization of small oxygen pressure swing adsorption units. *Industrial & Engineering Chemistry Research*, **2004b,** 43, (26), 8328-8338.

Sherman, J. D., Synthetic zeolites and other microporous oxide molecular sieves. *Proceedings of the National Academy of Sciences of the United States of America*, **1999,** 96, (7), 3471-3478.

Shu, C.-W., Essentially nonoscillatory (ENO) and weighted essentially nonoscillatory (WENO) schemes for hyperbolic conservation laws. In *Advanced Numerical Approximation of Nonlinear Hyperbolic Equations, Lecture Notes in Mathematics*, B. Cockburn, C. J., C.-W. Shu, E. Tadmor, and A. Quarteroni, Springer-Verlag: Berlin, 1997; 1697, 325 -432.

Shu, C. W.; Osher, S., Efficient Implementation of Essentially Non-Oscillatory Shock-Capturing Schemes. *Journal of Computational Physics*, **1988,** 77, (2), 439-471.

Shu, C. W.; Osher, S., Efficient Implementation of Essentially Non-Oscillatory Shock-Capturing Schemes .2. *Journal of Computational Physics*, **1989,** 83, (1), 32-78.

Shyy, W., A Study of Finite-Difference Approximations to Steady-State, Convection-Dominated Flow Problems. *Journal of Computational Physics*, **1985,** 57, (3), 415-438.

Teague, K. G.; Edgar, T. F., Predictive dynamic model of a small pressure swing adsorption air separation unit. *Industrial & Engineering Chemistry Research*, **1999,** 38, (10), 3761-3775.

Yang, J. Y.; Lee, C. H., Adsorption dynamics of a layered bed PSA for H2 recovery from coke oven gas. *Aiche Journal*, **1998,** 44, (6), 1325-1334.

Zhang, Z. Y.; Hidajat, K.; Ray, A. K.; Morbidelli, M., Multiobjective optimization of SMB and Varicol process for Chiral Separation. *AIChE Journal*, **2002,** 48, (12), 2800-2816.

3. Adsorption Equilibrium

3.1 Introduction

The study of the adsorption equilibrium is of great importance for simulation and selection of the adsorbent to be used in pressure swing adsorption (PSA) units.

The zeolites most commonly used are of the type A and X. These zeolites are composed by silica and tetrahedral alumina connected in an octahedral structure. These units are, by its turn, connected to tertiary units and form the unitary cell of the zeolite. While the groups SiO_2 are neutral, the groups $(AlO_2)^-$ introduce a negative charge to the structure which is compensated by the presence of cations, such as Na^+, Li^+ or Ca^{2+} (Hutson et al., 2001). Zeolites can be produced with smaller or greater amounts of SiO_2 than the ones that appear in natural zeolites. Larger amounts of SiO_2 generally give greater hydrothermal stability and originate more hydrophobic zeolites. Lesser amounts of SiO_2 give higher cation exchange capabilities and higher capacity to adsorb polar molecules (Sherman, 1999).

In zeolites, cations are usually responsible for the selectivity to nitrogen. These zeolites adsorb preferentially nitrogen instead of oxygen (usually at a rate of about 4:1) mainly due to the interactions between the cations of the zeolite and the quadrupolar moment of the adsorbed gas. Nitrogen quadrupolar moment is about four times the one of oxygen. Since these cations influence in such a significant way the zeolites adsorption capacity, numerous tries have been conducted with the intent of optimizing the zeolites properties by increasing the number of sites destined for cations, by creating zeolites with a higher content of aluminium; or by the synthesis of zeolites with different combinations of cations (Hutson et al., 2001).

The first mineral zeolite (stilbite) was presented in Sweden by Cronstedt in 1756 (Sherman, 1999). Since then, zeolites have undergone major developments. In Table 3.1 are presented, in chronological order, the most important progresses and patents in the zeolites field.

Table 3.1. Most important progresses and patents in the zeolites field.

Year	Patent	Description
1756	-	The first mineral zeolite (stilbite) was presented in Sweden by Cronstedt in 1756 [(1)].
1932	-	McBain introduced the term "molecular sieve" to describe porous solids[(2)].
1949 to 1950	-	Zeolites A, X and Y were discovered by Milton and Breck in New York, in Linde Air Products Division laboratories of Union Carbide Corporation (currently UOP) [(1)].
1964	US 3,140,931	McRobbie, from Union Carbide Corporation, presents a zeolite for PSA units for the production of oxygen [(2)].
1966	US 3,237,377	Skratrstom *et al.*, from Exxon, describe the use of a 13X type zeolite in a PSA unit for oxygen production [(2)].
1967	US 3,356,450	Heinze, from Bayer, describe the production of a binderless zeolite and explain its advantages [(3)].
1974	DE 2,347,574	Vayghan, from W.R. Grace & Co., (currently Grace Davison) describes the zeolites developed by this company [(2)].
1980	GB 1,567,856	The company W.R.Grace & Co. patents the process for manufacturing a binderless type A zeolite[(3)].
1982	GB 2,091,121	Armond and Deverell of the BOC group describe a zeolite with a reduced diameter and affirm that this reduction allows a decrease of the power consumption, bed length and cycle times [(2)].
1986	US 4,603,040	Kuznicki et al. present a process for the production of a type X zeolite with a smaller amount of silica (LSX) and binderless [(3)].
1988	-	The 2nd generation of zeolites for the separation of air by vacuum swing appears, making this technology competitive with cryogenic distillation up to 100 tons/day [(4)].
1989	US 4,859,217	Chao, from the company UOP, presents the use of a binderless LiX type zeolite with Si/Al ratios smaller than 1.5 and affirms that these adsorbents have large adsorption capacities and selectivities for nitrogen.
1996	-	Teruji suggests the use of a X type zeolite where the sodium or calcium ions are exchanged with a silver ion (AgX) for the production of high purity oxygen [(5)].
1999	-	Hutson et al. suggest the addition of silver to the LiX type zeolites to increase its performance in air separation (AgLiX) [(5)].
2002	US 6,432,170	Chiang et al., from the company Air Products and Chemicals Inc., present a zeolite called AgLiLSX with argon/ oxygen selectivity.

[(1)] (Sherman, 1999); [(2)] (Espitalier-Noel, 1988); [(3)] (Gaffney et al., 1993); [(4)] (Ruthven et al., 1994); [(5)] (Chiang et al., 2002)

The first pressure swing adsorption unit (PSA), composed by two beds, and using a 13X type zeolite was patented by Skarstrom in 1966 (Espitalier-Noel, 1988). Since then, the development of zeolites with higher nitrogen capacities and higher selectivities led to improvements in PSA and in vacuum swing adsorption (VSA) processes (Sherman, 1999).

The adsorbents commonly used in equilibrium air separations, have typically about 20% of an inorganic inert material - binder. This material has the function of connecting the zeolitic crystallites in an agglomerate with high physical strength and friction resistance, so that these crystallites may be used in adsorption processes. The addition of binder reduces the adsorption capacity between 15 and 20% (Gaffney et al., 1993). The tendency has been to reduce the amount of binder, many times down to 5% while maintaining the physical resistance of the adsorbent. In 1967 Heinze patented a production process of a binderless adsorbent and affirms that the production of this type of zeolites is advantageous since it allows higher adsorption capacities (Gaffney et al., 1993).

From the beginning to the middle of the 70's, zeolites of type NaX and CaA allowed the development and commercialization of the first economically viable PSA units, in a relatively small scale, for the separation of oxygen from air (Espitalier-Noel, 1988, Sherman, 1999). In 1982, Armond and Deverell patented a PSA process for separating oxygen from air, using adsorbents with a diameter between 0.4 and 3 mm (Armond and Deverell, 1982). According to them, the use of adsorbents with reduced diameters allows the decrease of the energetic consumption, of the bed size and of the cycle times (Espitalier-Noel, 1988). In 1988 the second generation of zeolites appeared for air separations by vacuum swing adsorption (VSA). These adsorbents made VSA processes competitive with cryogenic distillation up to 100 tons/day (Ruthven et al., 1994).

Second generation adsorbents, such as CaX, and third generation adsorbents, such as LiX, LiCaX or LiSrC and MgA, together with the progresses obtained in PSA and VSA processes allowed a significant reduction of the investment and operating costs of these units (Sherman, 1999).

In 1986, Kuznicki et al. presented the production process of a type X zeolite with a smaller amount of silica (LSX – low silica X-type) and binderless (Gaffney et al., 1993). This material is a type X zeolite saturated in aluminium with a silica/alumina ratio of 2 (or Si/Al =1). Commercial zeolites of type X, typically available in the form Na^+ (commercially known as 13X), are not saturated in aluminium and contain 86 atoms of aluminium per unitary cell while zeolites of the type LSX contain 96 atoms of aluminium per unitary cell.

With respect to the interactions with N_2, the cation Li^+ is among the strongest cations. Its use increased with some recent discoveries: it was discovered that the ionic

exchange of Li^+ in X type zeolites must exceed 70% so that this ion has some influence in the zeolite adsorption capacity; a significant increase of the N_2 adsorption capacity was noted in LSX type zeolites exchanged with the Li^+ ion, when compared to the commercial adsorbents (these adsorbents have a Si/Al ratio of 1.25) (Hutson et al., 2001).

In 1999, Hutson et al. suggested the addition of a small amount of silver to the zeolites of the type LiX (giving birth to the zeolites of the type AgLiX) to improve the performance of the adsorbent in oxygen separation from air. In 2002 an AgLiLSX type zeolite was patented by Air Products and Chemicals, Inc. This adsorbent, obtained by exchanging silver ions in LiLSX type zeolites, present high nitrogen adsorption capacities and high selectivity of nitrogen over oxygen, at sub-atmospheric pressures. AgLiLSX type zeolites, such as the 40% silver exchanged zeolite from Air Products and Chemicals may even present a selectivity of argon over oxygen, which allows the production of high purity oxygen (above 99%). This adsorbent can then be used for high purity oxygen production for medical applications (above 99.5% of oxygen), directly from air, allowing, this way, the production of PSA units for use in campaign hospitals or other places where the circumstances demand the immediate use of large quantities of this type of oxygen or where liquid oxygen cylinders are not enough or even a possibility for fulfilling the needs.

In this Chapter, the adsorption equilibrium data for several adsorbents are presented as well as the results of a study of the contamination caused by water vapour and carbon dioxide alone and together. The contamination of a working laboratorial pressure swing adsorption unit is also presented.

3.2 Adsorbents studied

With the aim of selecting the best adsorbents for oxygen separation from air, adsorption equilibrium data were determined for the following adsorbents: Oxysiv 5, Oxysiv 7, KEG415 (this adsorbent was previously from Bayer) and Oxysiv MDX from UOP, SYLOBEAD MS S 624 and SYLOBEAD MS C 544 from Grace Davison. All these adsorbents, except MS S 624, were indicated for oxygen separation from air. MS S 624, despite from being indicated for natural gas purification, has nitrogen and

oxygen isotherms favourable for the desired separation and so, was included in the study.

The adsorbent AgLiLSX from Air Products and Chemicals, Inc was also studied. This adsorbent may be used for the production of high purity oxygen (>95%) since it adsorbs more argon than oxygen.

Oxysiv 5 is a 13X (NaX) type zeolite (Teague and Edgar, 1999); Oxysiv 7 is a LiX type zeolite with a ratio SiO_2/Al_2O_3 =2,5 (Si/Al=1.25) (Ackley and Zhong, 2003); KEG415 is a 5A type zeolite; according to the company Grace Davison, MS S 623 is a binderless 5A type zeolite; MS C 544 is also a 13X (NaX) type zeolite. Oxysiv MDX is a low silica X-type zeolite (LiLSX) with a ratio Si/Al=1.

The adsorbent AgLiLSX is a 40% silver exchanged zeolite and its starting material was Oxysiv MDX from UOP.

3.3 Monocomponent adsorption equilibrium

3.3.1 Monocomponent Langmuir isotherm

The first coherent theory of adsorption onto a flat surface, based on the kinetic point of view, was proposed by Langmuir in 1918. According to this theory, there is a continuous process of bombardment of molecules onto the surface and a corresponding evaporation (desorption) of molecules from the surface, so that the accumulation rate at the surface in equilibrium is null (Do, 1998).

The Langmuir model considers that (Do, 1998):

- The surface is homogeneous, i.e., the energy of adsorption is constant in all the adsorption sites;
- The adsorption at the surface is localized, i.e., the atoms or molecules are adsorbed at localized and definitive sites;
- Each adsorption site can only accommodate one molecule or atom.

The Langmuir equation is written as follows (Do, 1998):

$$C_{\mu} = C_{\mu s} \frac{b(T) \cdot P}{1 + b(T) \cdot P} \tag{3.1}$$

and

$$b(T) = b_{\infty}\, \mathrm{e}^{\frac{Q}{\Re T}}, \tag{3.2}$$

where C_{μ} is the adsorbed amount in mol/kg, $C_{\mu s}$ is the maximum adsorbed amount or saturation capacity, which corresponds to the total coverage of the monolayer, P is the total pressure, b is the affinity constant, b_{∞} is the pre-exponential factor of the affinity constant, Q is the heat of adsorption and is equal to the activation energy for desorption, $\Re$ is the universal gas constant and T is the absolute temperature.

3.3.2 Monocomponent Freundlich isotherm

This equation is one of the oldest empiric models used for describing equilibrium data. It assumes that the surface is heterogeneous: the adsorption energy is distributed and the surface presents a patchwise topography, i.e., the adsorption sites that have the same adsorption energy are grouped together in one patch (the adsorption energy in this patch is the energy of the interaction between the solute and adsorbent). Each patch is independent, i.e., there is no interaction between patches. Another assumption is that in each patch, a molecule of the solute adsorbs only in one adsorption site, i.e., the Langmuir equation may be applied to the description of the equilibrium in each patch.

The Freundlich equation may be written as follows (Do, 1998):

$$C_{\mu} = K \cdot P^{1/n} \tag{3.3}$$

and

$$K = (\delta A_0) \cdot P_0^{-\Re T/A_0} \tag{3.4}$$

$$\frac{1}{n} = \frac{\Re T}{A_0}, \tag{3.5}$$

where K and n are equation parameters, δ is a parameter of the distribution function and A_0 is the potential characteristic of the adsorption. The parameter n, is usually

above unity and when the pressure tends to infinity the adsorption amount also tends (Do, 1998).

3.3.3 Monocomponent Sips isotherm

In 1948, Sips, aware of the continuous increase, in the Freundlich equation, of the adsorbed amount with pressure, proposed a similar equation to the Freundlich equation but with a finite limit for high pressures. This equation is also similar to the Langmuir equation and can be written as follows (Do, 1998):

$$C_{\mu} = C_{\mu s} \frac{(bP)^{1/n}}{1+(bP)^{1/n}} \tag{3.6}$$

and

$$b = b_{\infty} \exp\left(\frac{Q}{\Re T}\right) = b_0 \exp\left[\frac{Q}{\Re T_0}\left(\frac{T_0}{T}-1\right)\right] \tag{3.7}$$

$$\frac{1}{n} = \frac{1}{n_0} + \alpha\left(1-\frac{T_0}{T}\right), \tag{3.8}$$

where b_{∞} is the affinity constant at infinite temperature, b_0 is the affinity constant at the reference temperature T_0, n_0 is the parameter n at the reference temperature and α is a parameter of the equation.

The saturation capacity may be considered constant or the following dependency with the temperature may be assumed (Do, 1998):

$$C_{\mu s} = C_{\mu s,0} \exp\left[\chi\left(1-\frac{T}{T_0}\right)\right], \tag{3.9}$$

where $C_{\mu s,0}$ is the saturation capacity at the reference temperature and χ a parameter of the equation.

3.4 Multicomponent adsorption equilibrium

3.4.1 Multicomponent Langmuir isotherm

The multicomponent Langmuir isotherm is based on the same assumptions of the monocomponent equilibrium equation and may be written as follows (Do, 1998):

$$C_{\mu,i} = C_{\mu s,i} \frac{b_i P_i}{1 + \sum_{j=1}^{nc} b_j P_j}, \tag{3.10}$$

where $C_{\mu,i}$ is the adsorbed amount of component i, P_i is the partial pressure of component i and nc is the number of components.

This equation is only valid from the thermodynamic point of view if the saturation capacities for all species are the same (Do, 1998).

3.4.2 Multicomponent Sips isotherm

The multicomponent Sips isotherm may be written as follows (Do, 1998):

$$C_{\mu,i} = C_{\mu s} \frac{b_i P_i \left(\sum_{k=1}^{nc} b_k P_k \right)^{1/n-1}}{1 + \left(\sum_{k=1}^{nc} b_k P_k \right)^{1/n}} \tag{3.11}$$

This equation is only valid from the thermodynamic point of view if the saturation capacities and the parameters n are the same for all species (Do, 1998).

3.4.3 Ideal adsorption solution theory (IAST)

The ideal adsorption solution theory was developed in 1965 by Myers and Prausnitz for the multicomponent adsorption equilibrium prediction using a monocomponent equilibrium equation (Do, 1998).

The IAST prediction of the multicomponent adsorption equilibrium may be achieved using the following algorithm (Do, 1998):

1. With the parameters of a monocomponent adsorption equilibrium equation, estimate the reduced spreading pressure, z :

Langmuir	Sips
$\bar{C}_{\mu s} = \dfrac{\sum_{i=1}^{nc} C_{\mu s,i}}{nc}$	$\bar{C}_{\mu s} = \dfrac{\sum_{i=1}^{nc} C_{\mu s,i}}{nc};\ \bar{n} = \dfrac{\sum_{i=1}^{nc} n_i}{nc}$
$z = \bar{C}_{\mu s} \ln\left[1 + \sum_{i=1}^{nc} (b_i P_i)\right]$	$z = \bar{n} \cdot \bar{C}_{\mu s} \ln\left[1 + \sum_{i=1}^{nc} (b_i P_i)^{1/n}\right]$

2. Evaluate the pressure of the pure component, P_i^0 , for each component:

Langmuir	Sips
$P_i^0 = \dfrac{1}{b_i}\left[\exp\left(\dfrac{z}{C_{\mu s}}\right) - 1\right]$	$P_i^0 = \dfrac{1}{b_i}\left[\exp\left(\dfrac{z}{nC_{\mu s}}\right) - 1\right]^n$

3. Evaluate the adsorbed amount, $C_{\mu,i}^0$, for each pure component:

Langmuir	Sips
$C_{\mu,i}^0 = C_{\mu s,i} \dfrac{b_i P_i^0}{1 + b_i P_i^0}$	$C_{\mu,i}^0 = C_{\mu s,i} \dfrac{\left(b_i P_i^0\right)^{1/n}}{1 + \left(b_i P_i^0\right)^{1/n}}$

4. Evaluate the value of the following function:

$$F(z) = \sum_{i=1}^{nc} \left(\frac{y_i P}{P_i^0}\right) - 1$$

5. Estimate the new reduced spreading pressure and repeat steps 2 to 4 until $F(z) = 0$:

$$z^{(k+1)} = z^{(k)} - \frac{F(z^{(k)})}{F'(z^{(k)})},$$

where

$$F(z^{(k)}) = \sum_{i=1}^{nc} \left(\frac{y_i P}{P_i^0(z^{(k)})} \right) - 1$$

$$F'(z^{(k)}) = \left\{ -\sum_{i=1}^{nc} \frac{y_i P}{\left[P_i^0(z^{(k)}) \right] C_{\mu,i}^0} \right\}_{z=z^{(k)}}$$

6. Evaluate the adsorbed amount of each component, $C_{\mu,i}$, in equilibrium:

$$x_i = \frac{y_i P}{P_i^0}$$

$$\frac{1}{C_{\mu T}} = \sum_{i=1}^{nc} \frac{x_i}{C_{\mu,i}^0}$$

$$C_{\mu,i} = x_i C_{\mu T},$$

where $C_{\mu T}$ is the total concentration of the adsorbed phase in equilibrium and x_i is the molar fraction of the adsorbed phase.

3.5 Experimental part

3.5.1 Methods for the determination of adsorption equilibrium points

The adsorption equilibrium points were determined by two distinct methods: volumetric method and gravimetric method.

3.5.1.1 Volumetric method

The unit for determining the adsorption equilibrium points by the volumetric method is presented in Figure 3.1.

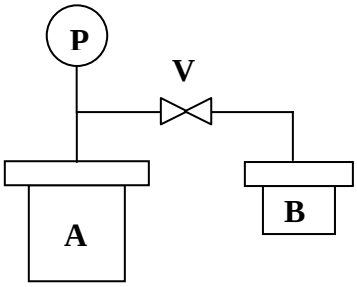

Figure 3.1. Sketch of the unit for determining adsorption equilibrium points by the volumetric method.

The determination of monocomponent adsorption equilibrium points by the volumetric method is based on the measurement of the variation of the pressure of the gas after an expansion. For this, two tanks with known volume are used (tank A and tank B in Figure 3.1), connected between themselves by a tube with an on-off valve (V in Figure 3.1). A given mass of adsorbent is introduced in tank B and the system is evacuated. Next, tank A is pressurized with the gas in study; after the opening of the valve between the two tanks, the decrease of the pressure is due to the expansion and to the adsorption. Knowing the pressure variation and assuming ideal gas behaviour for the system in study it is possible to determine the concentration of the adsorbed solute. For determining bicomponent adsorption equilibrium points it is also necessary to measure the composition of the gas mixture after equilibrium is reached. The procedure for determining adsorption equilibrium points is described in detail in Appendix 3.1.

The adsorbed solute concentration, q, for a given pressure, P, is given by:

$$q = \frac{1}{\Re T}\left[(P_A - P)\frac{V_A}{V_S} + (P - P^0)(1 - \frac{V_B}{V_S}) \right], \tag{3.12}$$

where $\Re$ is the universal gas constant, P_A is the initial pressure of tank A, V_A is the volume of tank A, P^0 is the initial pressure of the gas in the tanks, V_B is the volume of tank B, V_S is the volume of the adsorbent and T is the absolute temperature.

For bicomponent adsorption equilibrium, the adsorbed amount of component 1, q_1, and of component 2, q_2, for a given pressure, P, is given by:

$$q_1 = \frac{n_{ads,1}}{V_S} = \frac{1}{\Re T}\left[\left(P_{A,1} - P^0 - y_1 P \right)\frac{V_A}{V_S} + y_1 P\left(1 - \frac{V_B}{V_S} \right) \right] \tag{3.13}$$

$$q_2 = \frac{n_{ads,2}}{V_S} = \frac{1}{\Re T}\left[\left(P_{A,2} - P_{A,1} - P^0 - y_2 P\right)\frac{V_A}{V_S} + y_2 P\left(1 - \frac{V_B}{V_S}\right)\right], \quad (3.14)$$

where $P_{A,1}$ is the pressure of component 1 in tank A, $P_{A,2}$ is the total pressure after adding component 2 in tank A and y_1 and y_2 are the molar fractions of component 1 and 2, respectively. The deduction of these equations, as well as the ones used for determining the volume of the tanks and of the adsorbent are presented in Appendix 3.1.

3.5.1.2 Gravimetric method

The gravimetric method consists in measuring the variation of the mass of the adsorbent when a perturbation is made to the pressure of the gas it is exposed to. For this, a magnetic suspension balance is used. The variation of mass allows the determination of the adsorbed amount.

A magnetic suspension balance from Rubotherm was used for determining adsorption equilibrium data. This unit is presented in Figure 3.2.

This balance has the particularity of having the microbalance physically separated from the weighting system which allows the use of high pressures and temperatures.

The balance measures the mass at three different positions of the shaft:

- Position 0, where nothing is weighted (this position is used to tare the balance);
- Position 1, where the shaft is moved upward and the basket with the sample and the metallic shaft are weighted;
- Position 2, where besides the objects weighted in position 1, the titanium piece is also weighted.

The masses of the titanium piece, shaft and basket, as well as its volumes and the initial mass of the sample and its volume are determined before the measurement of the adsorption equilibrium points is begun. Hence, the measurement of the mass at position 2 is only for determining the impulsion caused by the gas inside the balance and so allowing the correction of the mass measured in position 1.

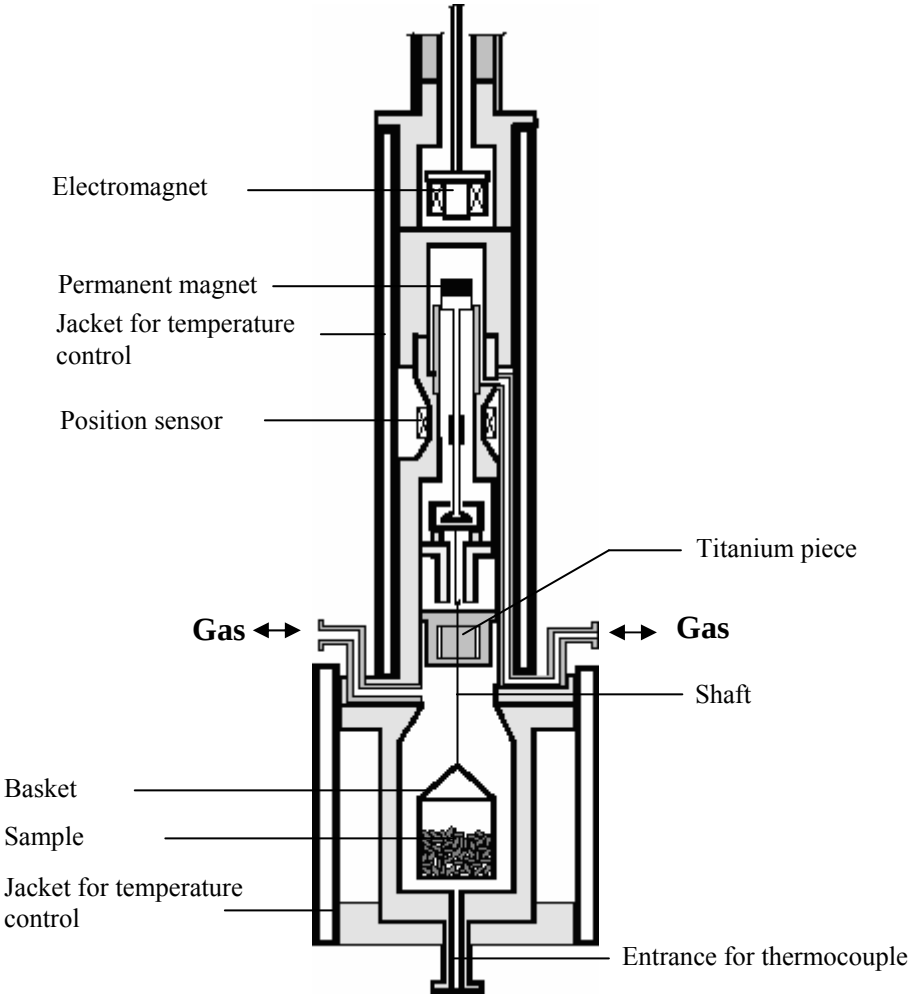

Figure 3.2. Sketch of the magnetic suspension balance from Rubotherm [adapted from (Dreisbach et al., 2002)].

The solute concentration in the adsorbed phase, q, is given by:

$$q = \frac{\Delta m_S}{V_S}, \tag{3.15}$$

where V_S is the volume of the adsorbent and Δm_S is the variation of the mass of the adsorbent and is given by:

$$\Delta m_S = m_S^{i-1} - m_S^i, \tag{3.16}$$

where m_S^{i-1} is the mass of the adsorbent at pressure P^{i-1} and m_S^i is the mass of the adsorbent at pressure P^i. The mass of the adsorbent for a certain pressure is given by the following expression:

$$m_S = m_1 + \frac{V_{HBS}}{V_T} \cdot \left[m_T - (m_2 - m_1) \right] - m_{HB}, \tag{3.17}$$

where m_1 and m_2 are the masses measured at positions 1 and 2, respectively, m_T is the mass of the titanium piece, m_{SB} is the mass of the set shaft/ basket, V_T is the volume of the titanium piece and V_{HBS} is the volume of the system composed by the metallic shaft (H), basket (B) and sample (S). The deduction of this expression and of the equations for determining m_T, V_T, m_{HB} and V_{HBS} are presented in Appendix 3.2, as well as the detailed experimental procedure for the determination of the adsorption equilibrium points using this method.

3.5.1.3 Comparison between the gravimetric and volumetric methods

The adsorption equilibrium points of oxygen, nitrogen and argon where determined at 20ºC for the adsorbent MS S 624 with the intent of comparing the gravimetric and volumetric methods. Figure 3.3 presents the adsorption equilibrium points determined with each method for a) nitrogen, b) oxygen and c) argon at 20ºC.

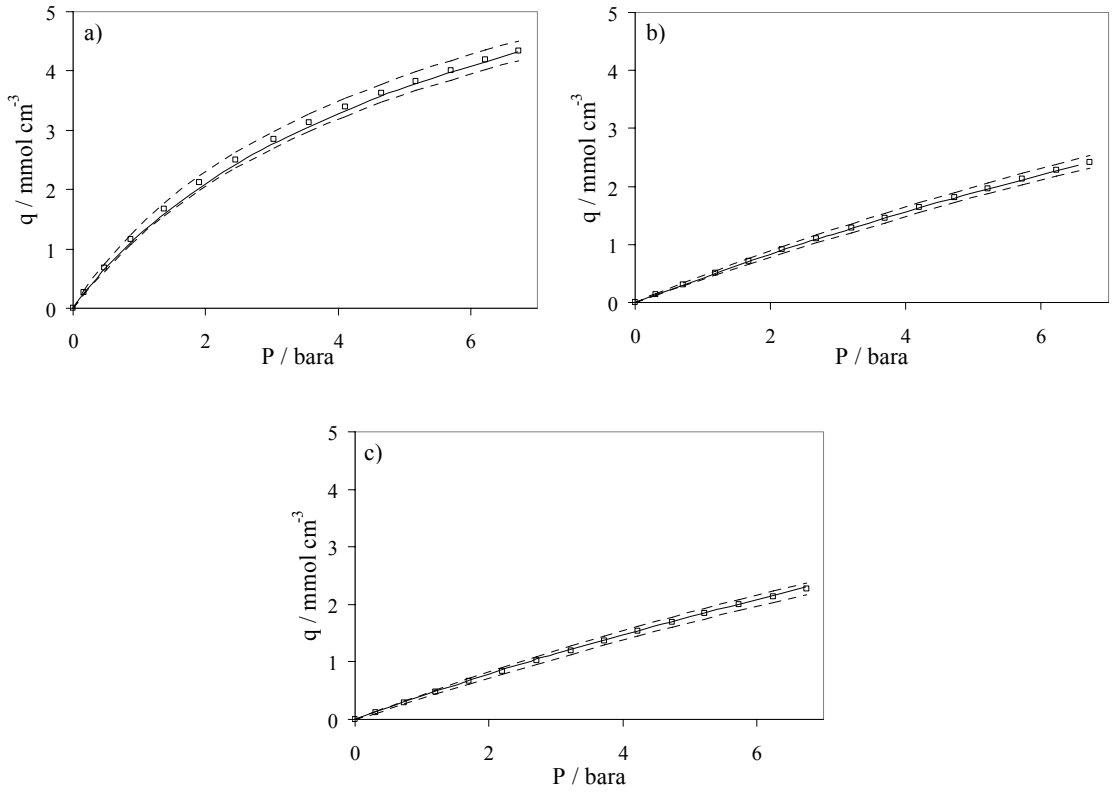

Figure 3.3. Adsorption equilibrium points determined by each method of a) nitrogen, b) oxygen and c) argon at 20ºC for the adsorbent MS S 624. □ volumetric method, — gravimetric method, --- error of the volumetric method.

As it can be seen, the values obtained by each method are in agreement. Nevertheless, the errors of the values obtained by the volumetric method are much higher than the ones obtained when using the gravimetric method (the error of the gravimetric method is of the magnitude of 2×10^{-5} g).

3.5.2 Adsorption isotherms

The parameters of the equations that describe the monocomponent adsorption equilibrium were fit to the adsorption equilibrium points determined experimentally at different temperatures. These parameters were obtained by minimization of the sum of the absolute value of the differences between the adsorbed quantity, q, and the adsorbed quantity predicted by the equation, q^*, for all gases and temperatures, divided by the number of experimental points, np (number of experimental points at each pressure for each gas and at each temperature):

$$\min\left(\frac{\sum_{i=1}^{\text{np}}\left|q-q^*\right|_i}{\text{np}}\right) \tag{3.18}$$

3.5.2.1 Oxysiv 5 from UOP

The monocomponent adsorption equilibrium in the adsorbent Oxysiv 5 from UOP is well described by Langmuir equation. Table 3.2 presents the parameters of this equation obtained from the adsorption equilibrium points, for the three gases, at 11.7ºC, 19.9ºC, and 36.4ºC determined by the gravimetric method.

Table 3.2. Parameters of the monocomponent Langmuir equation for Oxysiv 5.

	N_2	**O_2**	**Ar**
$C_{\mu s,j}$ (mol/kg)	3.091	3.091	3.091
b_∞ (Pa^{-1})	1.982	8.823	7.473
$Q/\Re$ (K)	2501.07	1767.86	1791.15
$\sum\left\|q-q^*\right\|/\text{np}$		1.37×10^{-3}	

The result of the fit at 19.9ºC is presented in Figure 3.4. The lines represent the adsorption equilibrium equation and the squares the experimental data.

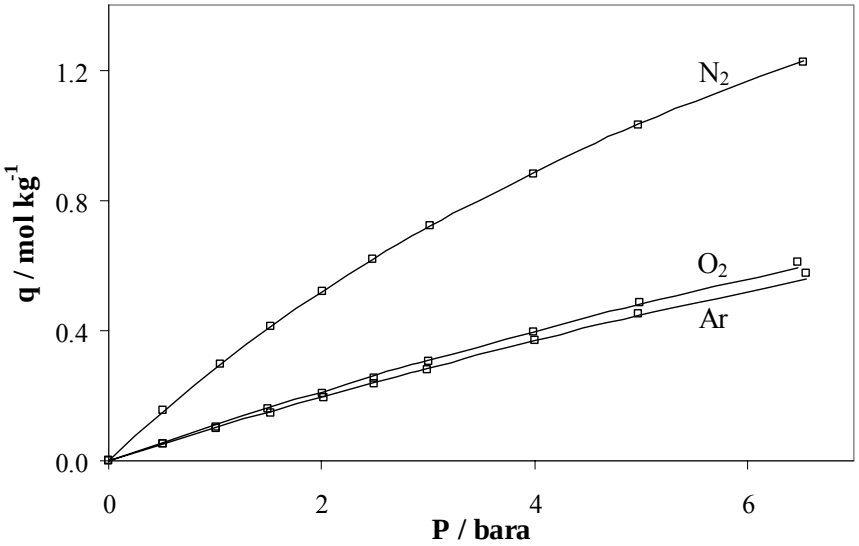

Figure 3.4. Result of the fit for Oxysiv 5 at 19.9ºC. □ Experimental data, — adsorption equilibrium equation.

The multicomponent adsorption equilibrium may be predicted by the Langmuir multicomponent equation since the saturation capacity is the same for the three species, which indicates consistency from a thermodynamic point of view (Do, 1998).

The multicomponent adsorption equilibrium prediction given by this equation was validated experimentally. Table 3.4 presents the differences between the experimental results of the determination of the bicomponent (nitrogen and oxygen) adsorption equilibrium at 19.9ºC by the volumetric method and the values predicted by the Langmuir and Sips multicomponent equations. The estimated adsorbed amount, q_i^*, given by the multicomponent Sips equation, was calculated using the monocomponent adsorption equilibrium parameters obtained from the experimental data (Table 3.3).

Table 3.3. Parameters of the monocomponent Sips equation for Oxysiv 5 at 20ºC.

	N_2	**O_2**	**Ar**
$C_{\mu s,0}$ (mol/kg)	3.137	3.137	3.137
b_0 (Pa^{-1})	1.282×10^5	4.174×10^4	3.905×10^4
$1/n_0$	1.0224	1.0224	1.0224

Table 3.4. Differences between the experimental results of the bicomponent adsorption equilibrium points obtained by the volumetric method at 19.9ºC and the values predicted by the Langmuir and Sips multicomponent equations.

P (bar)	y_{O_2}	$\sum_{i=1}^{2}\left(\frac{\lvert q_i - q_i^* \rvert}{q_i}\times 100\right)$	
		Langmuir	Sips
2.974	0.2193	3.6	3.1
2.986	0.2208	5.0	6.2

As it can be seen, the prediction of the bicomponent adsorption equilibrium obtained by each equation is acceptable, being the prediction given by the multicomponent Langmuir equation slightly better than the one given by the multicomponent Sips equation.

3.5.2.2 Oxysiv 7 from UOP

The monocomponent adsorption equilibrium in the adsorbent Oxysiv 7 from UOP is well described by the Sips equation. Table 3.5 presents the parameters of this equation, obtained from the adsorption equilibrium experimental points for nitrogen, oxygen and argon at 11.7ºC, 19.8ºC, 28.2ºC and 44.5ºC determined by the gravimetric method.

Table 3.5. Parameters of the monocomponent Sips equation for Oxysiv 7 at the reference temperature of $T_0 = 20^{\circ}\mathrm{C}$.

	N_2	**O_2**	**Ar**
$C_{\mu s,0}$ (mol/kg)	4.580	6.384	9.223
b_0 (Pa^{-1})	5.470×10^{3}	1.951×10^{3}	1.095×10^{3}
$1/n_0$	0.7100	0.9707	0.9539
$Q/\Re$ (K)	3156.82	1761.76	1829.54
α		0.3694	
χ		-0.6114	
$\sum\lvert q-q^*\rvert/\mathrm{np}$		1.38×10^{-3}	

The result of the fit at 19.8ºC is presented in Figure 3.5. The lines represent the adsorption equilibrium equation and the squares the experimental data.

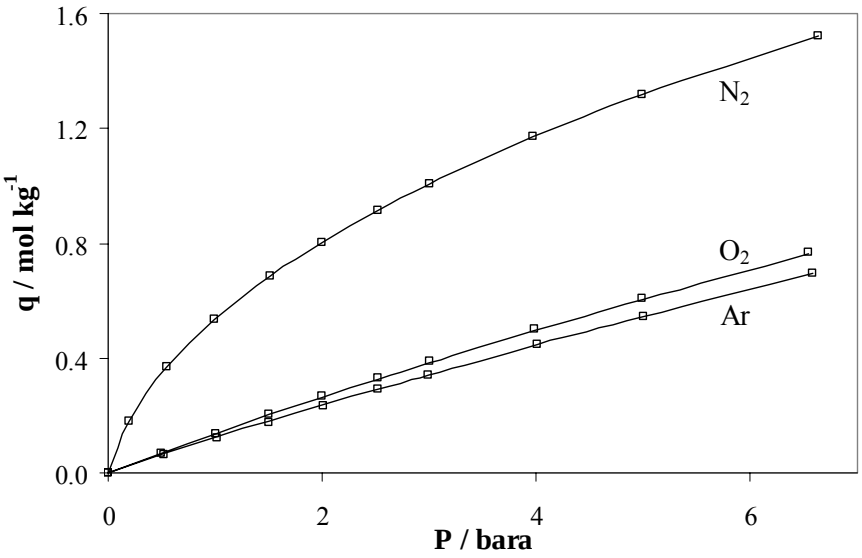

Figure 3.5. Result of the fit for Oxysiv 7 at 19.8ºC. □ Experimental data, — adsorption equilibrium equation.

Since the saturation capacity and the parameter *n* are not the same for all species, the multicomponent adsorption equilibrium may not be predicted by the multicomponent Sips equation and so, the ideal adsorption solution theory (IAST), for example, should be used.

3.5.2.3 MS S 624 from Grace Davison

The monocomponent adsorption equilibrium for the adsorbent MS S 624 from Grace Davison is well described by the Sips equation. Table 3.6 presents the parameters of this equation obtained from the adsorption equilibrium data, for the three gases, at 11.6ºC, 19.9ºC, 28.3ºC and 44.7ºC, determined by the gravimetric method.

Table 3.6. Parameters of the monocomponent Sips equation for MS S 624 at the reference temperature of $T_0 = 20^{\circ}\mathrm{C}$.

	N_2	O_2	Ar
$C_{\mu s,0}$ (mol/kg)	2.733	2.733	2.733
b_0 (Pa^{-1})	2.159×10^{4}	7.515×10^{3}	7.042×10^{3}
$1/n_0$	1.0711	1.0711	1.0711
$Q/\Re$ (K)	2208.40	1786.28	1704.03
α		-0.4329	
χ		1.1250	
$\sum\lvert q-q^{*}\rvert/\mathrm{np}$		2.45×10^{-3}	

The result of the fit at 19.9ºC is presented in Figure 3.6. The lines represent the adsorption equilibrium equation and the squares the experimental data.

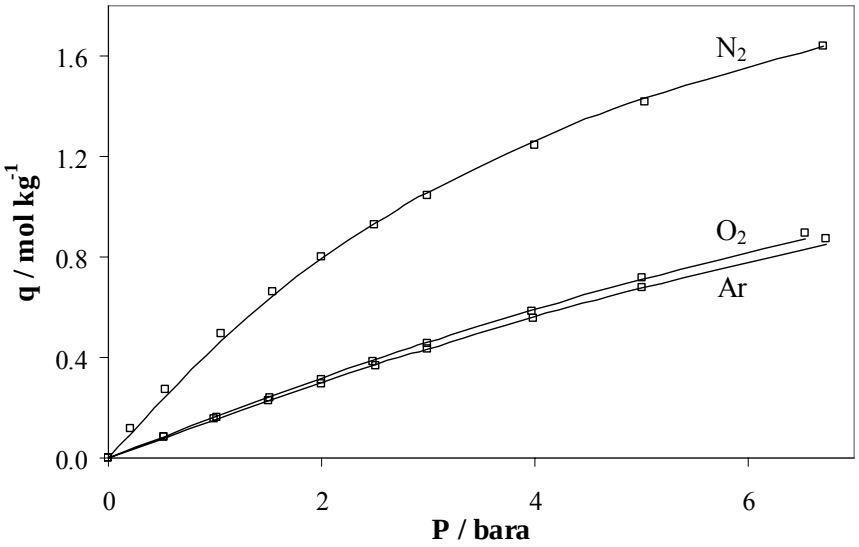

Figure 3.6. Result of the fit for MS S 624 at 19.9ºC. □ Experimental data, — adsorption equilibrium equation.

The multicomponent adsorption equilibrium may be predicted by the Sips equation since the saturation capacity and the parameter *n* are the same for the three components.

3.5.2.4 MS C 544 from Grace Davison

The monocomponent adsorption equilibrium of MS C 544 from Grace Davison is well described by the Langmuir equation. Table 3.7 presents the parameters of this equation obtained from the adsorption equilibrium experimental points, for the three gases, at 9.9ºC, 20.1ºC, 29.8ºC and 39.7ºC determined by the volumetric method.

Table 3.7. Parameters of the monocomponent Langmuir equation for MS C 544.

	N_2	**O_2**	**Ar**
$C_{\mu s,j}$ (mol/kg)	3.278	3.278	3.278
b_∞ (Pa-1)	1.710	7.096	1.741
$Q/\Re$ (K)	2096.92	1559.37	1535.16
$\sum\left\|q-q^*\right\|/\mathrm{np}$		1.88×10^{-3}	

The result of the fit at 20.1ºC is presented in Figure 3.7. The lines represent the adsorption equilibrium equation and the squares the experimental data.

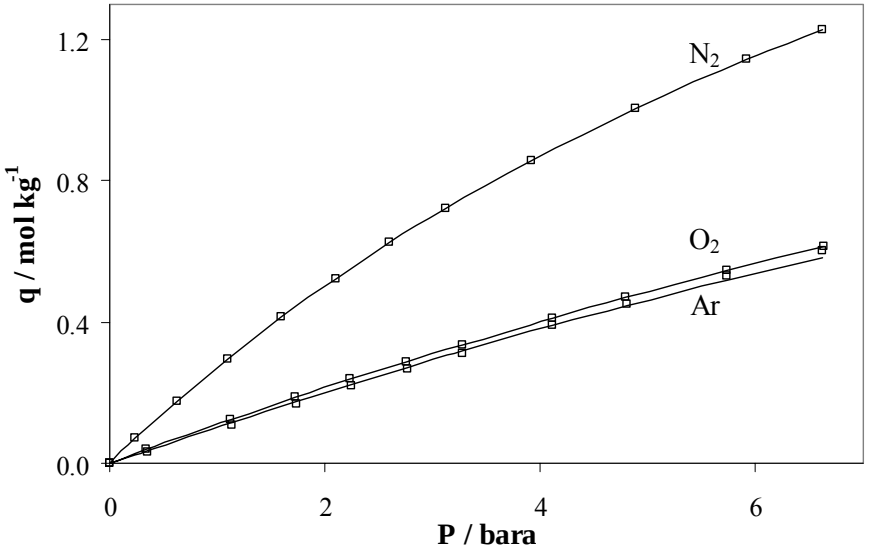

Figure 3.7. Result of the fit for MS C 544 at 20.1ºC. □ Experimental data, — adsorption equilibrium equation.

At this temperature, the multicomponent adsorption equilibrium may be predicted by the multicomponent Langmuir equation since the saturation capacities of all species are the same.

3.5.2.5 KEG415 from UOP/Bayer

The monocomponent adsorption equilibrium for the adsorbent KEG415 from UOP/Bayer is well described by the Sips equation. Table 3.8 presents the parameters of this equation obtained from the adsorption equilibrium experimental points, for the three gases, at 10.2ºC, 20.0ºC, 30.0ºC and 39.8ºC determined by the volumetric method.

The result of the fit at 20ºC is presented in Figure 3.8. The lines represent the adsorption equilibrium equation and the squares the experimental data.

Table 3.8. Parameters of the monocomponent Sips equation for KEG415 at the reference temperature of $T_0 = 20^{\circ}\mathrm{C}$.

	$\mathbf{N_2}$	$\mathbf{O_2}$	**Ar**
$C_{\mu s,0}$ (mol/kg)	2.324	2.324	2.324
b_0 (Pa^{-1})	2.942×10^{4}	9.730×10^{3}	8.448×10^{3}
$1/n_0$	1.0913	1.0913	1.0913
$Q/\Re$ (K)	1512.64	1189.13	1276.47
α		-0.3558	
χ		1.7727	
$\sum\lvert q-q^{*}\rvert/\mathrm{np}$		4.41×10^{-3}	

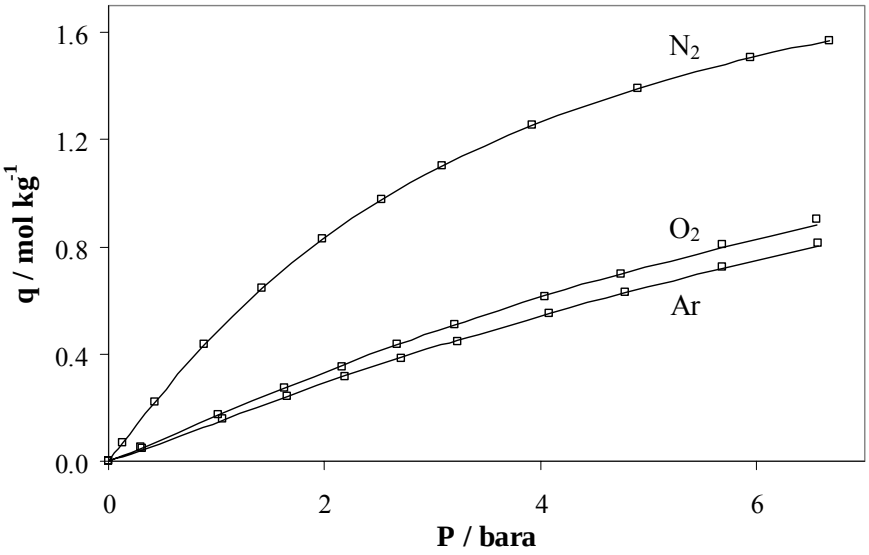

Figure 3.8. Result of the fit for KEG415 at 20ºC. □ Experimental data, — adsorption equilibrium equation.

The multicomponent adsorption equilibrium may be predicted by the Sips equation since the saturation capacity and the parameter *n* are the same for the three components.

3.5.2.6 Oxysiv MDX from UOP

The monocomponent adsorption equilibrium for the adsorbent Oxysiv MDX from UOP is well described by the Sips equation. Table 3.9 presents the parameters of this equation obtained from the adsorption equilibrium experimental points, for the three gases, at 10.0ºC, 20.0ºC, 30.0ºC and 40.0ºC determined by the gravimetric method.

Table 3.9. Parameters of the monocomponent Sips equation for Oxysiv MDX at the reference temperature of $T_0 = 20^{\circ}\mathrm{C}$.

	$\mathbf{N_2}$	$\mathbf{O_2}$	**Ar**
$C_{\mu s,0}$ (mol/kg)	3.425	6.056	7.946
b_0 ($\mathrm{Pa^{-1}}$)	3.356×10^{4}	2.665×10^{3}	1.610×10^{3}
$1/n_0$	0.8227	0.9797	0.9787
$Q/\Re$ (K)	3160.37	1820.15	1673.81
α		0.0556	
χ		0.0213	
$\sum\lvert q-q^{*}\rvert/\mathrm{np}$		6.82×10^{-4}	

The result of the fit at 20ºC is presented in Figure 3.9. The lines represent the adsorption equilibrium equation and the squares the experimental data.

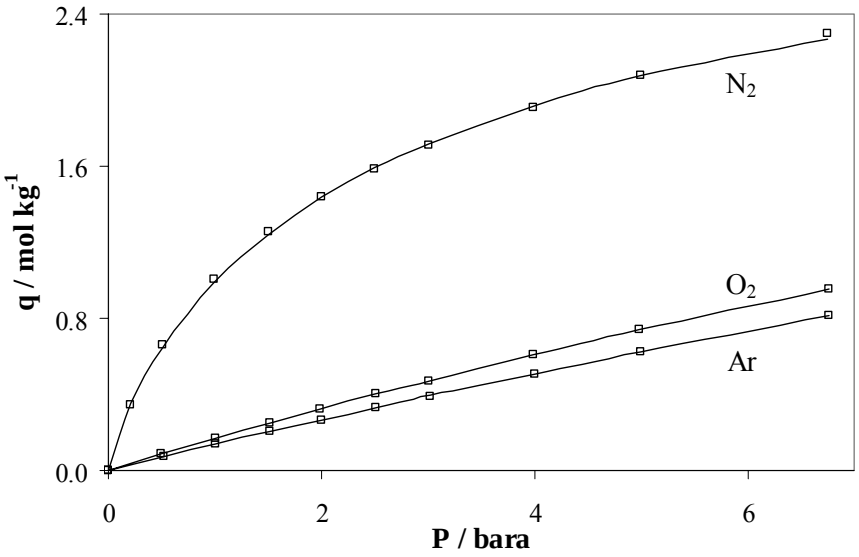

Figure 3.9. Result of the fit for Oxysiv MDX at 20ºC. □ Experimental data, — adsorption equilibrium equation.

Since the saturation capacity and the parameter *n* are not the same for all species, the multicomponent adsorption equilibrium may not be predicted by the multicomponent Sips equation and so, the ideal adsorption solution theory (IAST), for example, should be used.

3.5.2.7 AgLiLSX from Air Products and Chemicals, Inc.

The monocomponent adsorption equilibrium in the adsorbent AgLiLSX from Air Products and Chemicals, Inc. is well described by the Sips equation. Table 3.10 presents the parameters of this equation, obtained from the adsorption equilibrium experimental points for nitrogen, oxygen and argon at 11.7ºC, 23.0ºC, 29.9ºC and 39.8ºC determined by the gravimetric method.

Table 3.10. Parameters of the monocomponent Sips equation for AgLiLSX at the reference temperature $T_0 = 20^{\circ}\mathrm{C}$.

	$\mathbf{N_2}$	$\mathbf{O_2}$	**Ar**
$C_{\mu s,0}$ (mol/kg)	2.636	5.481	7.270
b_0 ($\mathrm{Pa^{-1}}$)	2.581×10^{4}	3.013×10^{3}	2.300×10^{3}
$1/n_0$	0.4856	0.9484	0.9216
$Q/\Re$ (K)	2740.70	1873.82	1771.33
α		0.3007	
χ		0.0112	
$\sum\lvert q-q^{*}\rvert/\mathrm{np}$		1.96×10^{-3}	

The result of the fit at 23.0ºC is presented in Figure 3.10. The lines represent the adsorption equilibrium equation and the squares the experimental data.

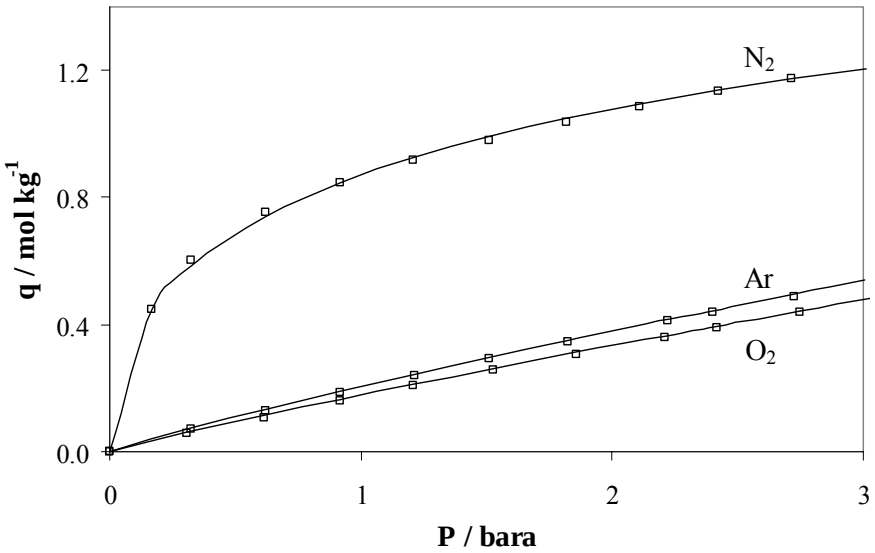

Figure 3.10. Result of the fit for AgLiLSX at 23.0ºC. □ Experimental data, — adsorption equilibrium equation.

Since the saturation capacity and the parameter *n* are not the same for all species, the multicomponent adsorption equilibrium may not be predicted by the multicomponent Sips equation and so, the ideal adsorption solution theory (IAST), for example, should be used.

3.5.3 Regeneration of the adsorbents

A deactivation of the adsorbents was noted after some time of operation of a experimental pressure swing adsorption unit. Due to this fact it was necessary to regenerate the adsorbents. Some adsorbents, like Oxysiv 7, require some caution in its regeneration. The following study was conducted for determining the conditions at which the adsorbents should be regenerated: samples of Oxysiv 7 were regenerated in a muffle at 375ºC, at different conditions, and the adsorption capacity of these samples were compared with the adsorption capacity of a "fresh" sample. For this study the magnetic suspension balance was used for determining the adsorption equilibrium points. Table 3.11. presents the results of this study.

Table 3.11. Results of the regeneration study of Oxysiv 7 at 375ºC.

Test	Description of the sample	q/q^*		α
		O_2	N_2	
1	Contaminated adsorbent without any regeneration	0.5	-	-
2	Contaminated adsorbent regenerated in the surrounding atmosphere	-	0.1	-
3	Fresh adsorbent regenerated in the surrounding atmosphere	0.5	0.1	1.5
4	Fresh adsorbent regenerated passing a current of helium through it	1	1	4.1
5	Contaminated adsorbent regenerated passing a current of helium through it	1	1	4.1
6	Contaminated adsorbent regenerated passing a current of dried air through it	1	1	4.1
7	Contaminated adsorbent regenerated in the surrounding atmosphere and afterwards regenerated passing a current of helium through it	0.5	-	-

The ratio q/q^* represents the ratio between the quantity adsorbed in the sample and the quantity of the same component adsorbed in a sample of the fresh adsorbent; α represents the selectivity of the adsorbent (ratio between the nitrogen adsorbed quantity and the oxygen adsorbed quantity).

The contamination of the adsorbent caused a decrease of about 50% of the capacity of the adsorbent. The incorrect regeneration of this adsorbent caused a decrease of 90% of the capacity as well as the loss of selectivity. Analysing the results of this study it is possible to conclude that the regeneration of fresh zeolite or of contaminated zeolite, in the surrounding atmosphere, causes an irreversible degradation of it (see results of test 7). The regeneration of this adsorbent may be achieved by passing a current of helium through it at 375ºC. Alternatively a current of dried air may also be used. This current may be obtained by passing compressed air through a column packed with silica gel followed by a column packed with activated carbon or activated alumina.

3.5.4 Contamination of the adsorbents

A study was conducted with the aim of determining the causes of loss of capacity of the adsorbents after being used in a pressure swing adsorption unit.

The study consisted in exposing the adsorbent to water vapour, carbon dioxide and both simultaneously, at 20ºC, and after regenerating it, determining a nitrogen adsorption equilibrium point to obtain the loss of efficiency. Three types of regeneration were considered: regeneration at 70ºC, evacuating and pressurizing with helium, alternatively; regeneration in a muffle at 375ºC without any gas flowing and regeneration in a muffle at 375ºC passing a current of dried air through the sample. The amount of carbon dioxide and water vapour used are close to the amounts the adsorbents are exposed to during the operation of a pressure swing adsorption unit.

The results of this study are presented in Table 3.12. The percentage of deactivation was defined as the ratio between the quantity of nitrogen adsorbed after exposure and the quantity of nitrogen adsorbed after full regeneration.

The regeneration in a muffle at 375ºC and passing a current of dried air through the adsorbent allowed, in all cases, the total recovery of the adsorbent.

All these results as well as the experimental procedure are presented in detail in Appendix 3.3.

As it can be seen from Table 3.12, carbon dioxide and water vapour contaminate the adsorbents studied. Except for MS C 544, the presence of carbon dioxide and water vapour, simultaneously, does not cause a deactivation superior than the one caused by each of these contaminants alone. When both contaminants are

together, it seems that carbon dioxide protects the adsorbent from water vapour probably by blocking the access of water vapour to the adsorption sites. The regeneration with vacuum and helium is the closest to the regeneration that occurs in pressure swing adsorption units and, as it can be seen, is not enough for recovering the total capacity of the adsorbents. Even the regeneration at 375ºC in a muffle, without passing a current of dried air is not enough, except for MS S 624.

Although the starting material for AgLiLSX is a LiLSX type zeolite such as Oxysiv MDX, these zeolites behave very differently when in contact with the contaminants. Oxysiv 5 and MS C 544 are both a 13X type zeolite and show also different behaviours when in contact with the contaminants. This may be due to the different size of these zeolites.

The adsorbent that revealed to be less affected by the contamination by carbon dioxide and water vapour was MS C 544.

Table 3.12. Results of the study where the adsorbents were exposed to water vapour, carbon dioxide and water vapour and carbon dioxide, simultaneously.

Experiment	Adsorbent	Deactivation (%) with		
		CO_2	H_2O	CO_2+H_2O
Regeneration at 70ºC during 2h, evacuating and pressurizing with helium, alternatively, after exposure to the contaminant at 20ºC	Oxysiv 5	5	70	35
	Oxysiv 7	31	82	38
	KEG415	17	59	29
	MS C 544	8	18	66
	MS S 624	18	95	13
	Oxysiv MDX	34	61	57
	AgLiLSX	34	91	65
Regeneration at 375ºC in a muffle without passing a dried air current	Oxysiv 5	5	8	4
	Oxysiv 7	34	65	40
	KEG415	9	2	6
	MS C 544	4	6	26
	MS S 624	0	0	0
	Oxysiv MDX	88	92	87
	AgLiLSX	28	97	70

When water vapour or carbon dioxide adsorbed in the zeolite are desorbed (such as what happens when the temperature is raised) and if they are kept in the gas phase surrounding the zeolite, the aluminium in the zeolite structure changes to alumina

and the zeolite structure changes itself. This change is irreversible and can only be avoided by removing the contaminants in the gas phase away from the zeolite, for instance, by passing an inert gas through the zeolite. There is still some work to be done for identifying the precise structure of the zeolites with adsorbed water (Hutson et al., 2000).

3.5.5 Contamination of the adsorbents in a pressure swing adsorption unit

A study was conducted for determining the degree of contamination of a zeolite during the operation of a pressure swing adsorption unit (PSA). This study consisted in operating the PSA unit at constant product flow rate during some days and following the product purity. After this purity stabilized, several layers of adsorbent were removed from both columns and the nitrogen adsorption capacity at 20ºC and the adsorbent density were determined. These measurements were done after regenerating the adsorbent at 70ºC during 2h with vacuum and helium, alternatively.

3.5.5.1 MS S 624 from Grace Davison

The characteristics of the adsorption columns used are presented in Table 3.13. The high pressure was 3 bara and the low pressure the atmospheric pressure.

Table 3.13. Characteristics of the adsorption columns.

Lenght (cm)	Diameter (cm)	Mass of adsorbent (g)	
		Left column	Right column
40	12	398	401

Table 3.14 presents the operating conditions of the pressure swing adsorption unit.

Table 3.14. Operating conditions of the pressure swing adsorption unit.

Time			Flow rate	
Operation (h)	Pressurization (s)	Production (s)	Production (L_{STP}/min)	Purge (L_{STP}/min)
141	12	7	9.5	0.74

The unit started producing oxygen at 80% and ended producing at 65%.

Figure 3.11 presents the percentage of activation of the adsorbent for each column along the axial coordinate, z. The percentage of activation is defined as the ratio between the nitrogen capacity and the maximum nitrogen capacity at 20ºC. The dashed line represents the percentage of activation of the adsorbent after contamination with water and the line represents the activation of the adsorbent after contamination with carbon dioxide. These results were obtained in the experiments presented in the previous section.

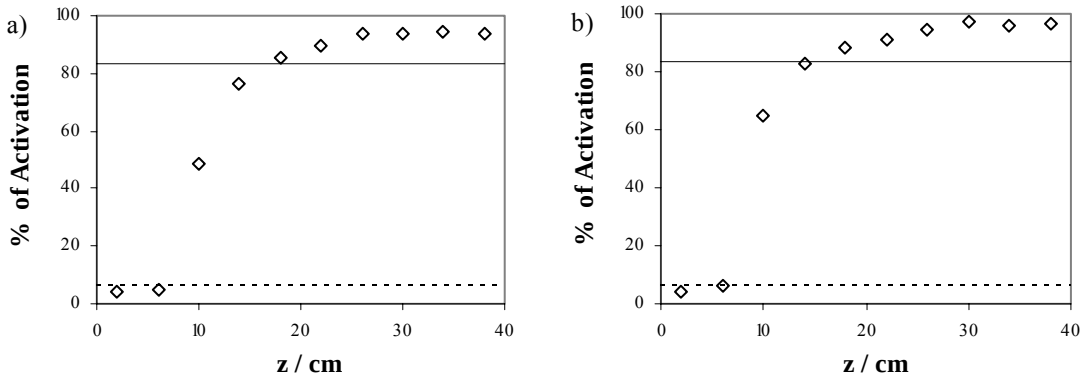

Figure 3.11. Percentage of activation of the adsorbent at 20ºC along the axial coordinate for the a) left column and b) right column. The dashed line represents the activation of the adsorbent after contamination with water and the line represents the percentage of activation of the adsorbent after contamination with carbon dioxide.

Analysing Figure 3.11, it is possible to see that the two first sections of the adsorption columns were contaminated mainly with water. The last sections appear to be partially contaminated, probably with carbon dioxide. It is also possible to see that the activation of the adsorbent along the axial column is very similar in both columns.

Figure 3.12 presents the density of the adsorbent in several sections of the columns, determined by helium picnometry. Analysing Figure 3.12 it is possible to see that the density of the adsorbent contaminated is inferior to that of the regenerated. It is possible to conclude that the density of the adsorbent is a good indicator of its activation.

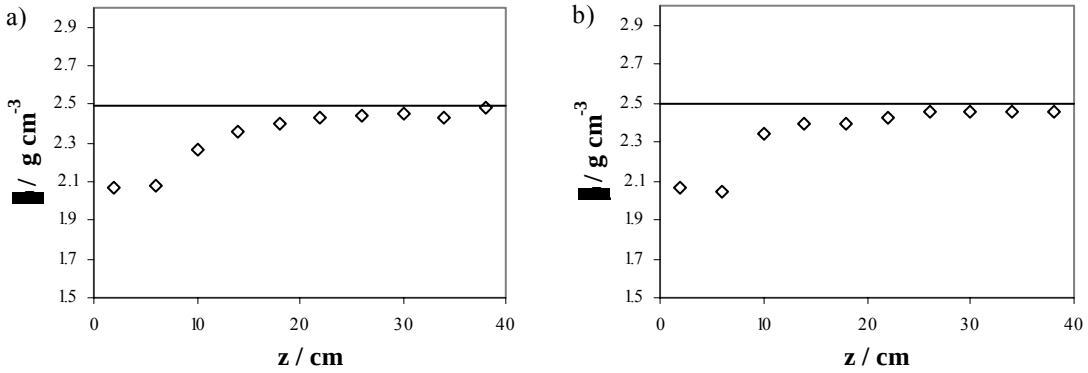

Figure 3.12. Density of the adsorbent in the sections of a) left column and b) right column. The line represents the density of the adsorbent completely regenerated.

Some work has been done regarding the adsorption of water on zeolites. Ahn and Lee (2003) studied the adsorption dynamics of water in layered bed for an air-drying temperature swing adsorption process and later on, in 2004 (Ahn and Lee, 2004), studied the effect of capillary condensation on adsorption and thermal desorption dynamics of water in 13X type zeolites and layered beds with silica gel and activated alumina before the zeolite. They refer that due to the strong adsorption of water in the 13X type zeolite, it takes a long time to regenerate the bed with a high level of energy consumption and so they performed a study about the regeneration dynamics but they do not mention the contamination of the zeolite nor the possibility that it can occur.

Rege et al. (2001) studied the air-prepurification by pressure swing adsorption (PSA) using single/layered beds and mention that in this process impurities such as water (present in atmospheric air up to 3%) and carbon dioxide (about 350 ppm are present in atmospheric air) are found to adsorb strongly, and to some extend, irreversibly on the adsorbents used for separation of air. They also state that this effect drastically affects the capacity as well as the selectivity of the adsorbent for air separation and thus requiring frequent plant shutdowns. They conclude that in order to prevent such malfunctions in the air separation units it is critical to pre-treat the feed air and reduce the impurity content to tolerable levels. They simulate a PSA unit with only three components: carbon dioxide (350ppm), water vapour (3000ppm) and the rest nitrogen and they assume the adsorption of each component by the adsorbents to be fully reversible. With these simulations they study the performance of 13X type zeolite, $\gamma - Al_2O_3$ and chabazite as sorbents for air prepurification and conclude that no single adsorbent can provide a nitrogen product with a satisfactorily low content of water

vapour and carbon dioxide impurities at a reasonable bed length. They also conclude that $\gamma - Al_2O_3$ sorbents appear to be the best for water removal and 13X type zeolite seem to be the better choice for carbon dioxide removal. With these remarks they suggest the use of a layered bed for air prepurification, composed by a first layer of $\gamma - Al_2O_3$ followed by a zeolite layer and after studying this system they find that for a particular set of operating conditions, the optimal alumina/ zeolite ratio is 7/3. They fail however to discuss the effect of the irreversible adsorption of these contaminants on their results.

Wilson et al. (2001) studied the effects of readily adsorbed trace component (water) in oxygen separation from air by vacuum swing adsorption (VSA). They mention that most molecular sieves used for oxygen VSA do not reversibly desorb water under VSA process conditions and so, a prelayer of activated alumina or NaX is required to protect the main adsorbent layer of a lithium- or calcium-based adsorbent from water and carbon dioxide. They perform some experiments with layered columns with activated alumina and a 13X type zeolite from UOP and remove all the carbon dioxide from the feed gas with a desiccant dryer. In these experiments they studied the length of penetration of water into the adsorption bed by removing samples of adsorbent at predefined distances and measured the nitrogen adsorption capacity of these samples and inferred the presence of water by the reduction in nitrogen loading (this is the same method that was used in the experiments presented in this section). They claim that this method is better than a TGA analysis since it provides the information on the extent of nitrogen loading. They refer that levels of water above approximately 1% w/w prevent nitrogen and oxygen from adsorbing. They conclude that in industrial practice, activated alumina might be more appropriate and at some extreme conditions, two pre-treating layers should be used, the first of activated alumina and the second of NaX. The conclusions of their study cannot, however, be applied in medical oxygen concentrators since desiccant dryers are not used and so, carbon dioxide along with water vapour will enter the unit and contaminate the adsorbent.

Brandani and Ruthven (2004) studied the effect of small amounts of water, in regard to inhibiting the adsorption of carbon dioxide, on several different cationic forms of zeolite X (LiLSX, NaLSX, NaX and CaX) using the zero length column technique, coupled with the temperature-programmed desorption. For all systems studied, it was observed that the Henry constant declines exponentially with the loading of water.

There are some patents that describe the removal of the contaminants through a separate pre-treatment material or a separate pre-treatment stage (Ackley, 1998, Dee et al., 2004, Notaro et al., 1998).

3.6 Conclusions

The gravimetric and volumetric methods used in the determination of adsorption equilibrium points give agreeable results. Nevertheless, the errors of the values obtained by the volumetric method are much higher than the ones obtained by the gravimetric method.

From the analysis of the monocomponent adsorption equilibrium isotherms it was concluded that Oxysiv MDX, from UOP, is the best adsorbent for the separation of oxygen from air. Good results were also obtained with AgLiLSX from Air Products and Chemicals, Inc. and Oxysiv 7 from UOP. However, a significant decrease of the performance of a pressure swing adsorption unit was observed with time, using this last adsorbent. From the study focusing the regeneration of Oxysiv 7 it was concluded that the regeneration in a stagnated atmosphere causes an irreversible degradation of this adsorbent. It was also concluded that it is possible to fully regenerate a contaminated sample at about 375ºC and passing continuously helium or dried air.

It was concluded that the monocomponent adsorption equilibrium data of the adsorbents Oxysiv 5 from UOP and MS C 544 from Grace Davison are well represented by a Langmuir type isotherm and this equation may be used for predicting the multicomponent adsorption equilibrium (this prediction was validated experimentally for Oxysiv 5). These two adsorbents are in fact very similar from an adsorption equilibrium point of view. The monocomponent adsorption equilibrium data of the adsorbents MS S 624 from Grace Davison and KEG415 from UOP/Bayer are well represented by a Sips type isotherm and it was verified that it is possible, from a thermodynamic point of view, to use this equation to predict the multicomponent adsorption equilibrium. The monocomponent adsorption equilibrium data of the adsorbents Oxysiv 7 and Oxysiv MDX from UOP and AgLiLSX from Air Products and Chemicals, Inc. are also well represented by a Sips type isotherm. However, the multicomponent adsorption equilibrium prediction should only be made using, for example, IAST.

From the study of the contamination that occurs in an adsorption column with MS S 624 during the operation of a pressure swing adsorption unit separating oxygen from air, it was concluded that 30% of the column was contaminated, water vapour being the main contaminant. It was also concluded that the density of the adsorbent gives a good indication about the activation state of the adsorbent.

3.7 Notation

A_0	adsorption characteristic potential
b	affinity constant, Pa^{-1}
b_0	affinity constant at reference temperature, Pa^{-1}
b_∞	affinity constant at infinit temperature, Pa^{-1}
C_μ	adsorbed quantity, mol/kg
$C_{\mu s}$	maximum adsorbed quantity or saturation capacity, mol/kg
$C_{\mu s,0}$	saturation capacity at reference temperature, mol/kg
K	parameter of the Freundlich equation
n	parameter of the Freundlich and of the Sips equations
n_0	parameter n of the Sips equation at reference temperature
nc	number of components
P	total pressure, Pa
P_i	partial pressure of component i, Pa
P_i^0	pressure of the pure component i, Pa
Q	heat of adsorption, J/mol
q	adsorbed quantity, mol/kg
q^*	predicted adsorbed quantity, mol/kg
$\Re$	universal gas constant, $(Pa \cdot m^3)/ (mol \cdot K)$
T	absolute temperature, K
T_0	reference temperature, K

x_i molar fraction of the adsorbed phase

z reduced spreading pressure

Greek variables

α Sips equation parameter

χ Sips equation parameter

δ distribution function parameter of the Sips equation

ρ density, $g \cdot cm^{-3}$

Subscripts

i component i

3.8 References

Ackley, M. W. Multilayer adsorbent beds for PSA gas separation. CA 2,234,924, 1998.

Ackley, M. W.; Zhong, G. Medical Oxygen Concentrator. U.S. Patent 6,551,384, 2003.

Ahn, H.; Lee, C. H., Adsorption dynamics of water in layered bed for air-drying TSA process. *Aiche Journal*, **2003,** 49, (6), 1601-1609.

Ahn, H.; Lee, C. H., Effects of capillary condensation on adsorption and thermal desorption dynamics of water in zeolite 13X and layered beds. *Chemical Engineering Science*, **2004,** 59, (13), 2727-2743.

Armond, J. W.; Deverell, B. E. T. Separation of gas mixtures. GB 2,091,121A, 1982.

Brandani, F.; Ruthven, D. M., The effect of water on the adsorption of CO2 and C3H8 on type X zeolites. *Industrial & Engineering Chemistry Research*, **2004,** 43, (26), 8339-8344.

Chiang, R. L.; Ridge, B.; Whitley, R. D.; Ostroski, J. E.; Dee, D. P. Argon/oxygen selective x-zeolite. U.S. Patent 6,432,170B1, 2002.

Dee, D. P.; Chiang, R. L.; Gondecki, G. J.; Whitley, R. D.; Ostroski, J. E. Use of lithium-containing FAU in air separation processes including water and/or carbon dioxide removal. U.S. Patent 6,824,590, 2004.

Do, D. D., *Adsorption Analysis: Equlibria and Kinetics*. Imperial College Press: London, 1998.

Dreisbach, F.; Lösch, H. W.; Harting, P., Highest Pressure Adsorption Equilibria Data: Measurement with Magnetic Suspension Balance and Analysis with a New Adsorbent/ Adsorbate-volume. *Adsorption*, **2002,** 8, (2), 95-109.

Espitalier-Noel, P. M. Waste recycle pressure swing adsorption to enrich oxygen from air. PhD Thesis, University of Surrey, Guildford, Surrey, UK, 1988.

Gaffney, T. R.; Kirner, J. F.; Kumar, R.; Maliszewskyj, R. J.; Schmidt, W. P. O_2 VSA Process with Low O_2 Capacity Adsorbents. U.S. Patent 5,266,102, 1993.

Hutson, N. D.; Zajic, S. C.; Rege, S. U.; Yang, R. T., *Air Separation by Pressure Swing Adsorption Using Superior Adsorbents*. University of Michigan: Ann Arbor, 2001.

Hutson, N. D.; Zajic, S. C.; Yang, R. T., Influence of residual water on the adsorption of atmospheric gases in Li-X zeolite: Experiment and simulation. *Industrial & Engineering Chemistry Research*, **2000,** 39, (6), 1775-1780.

Notaro, F.; Mullhaupt, J. T.; Leavitt, F. W.; Ackley, M. W. Adsorption process and system using multilayer adsorbent beds. U.S. Patent 5,810,909, 1998.

Rege, S. U.; Yang, R. T.; Qian, K. Y.; Buzanowski, M. A., Air-prepurification by pressure swing adsorption using single/layered beds. *Chemical Engineering Science*, **2001,** 56, (8), 2745-2759.

Ruthven, D. M.; Farooq, S.; Knaebel, K. S., *Pressure Swing Adsorption*. VCH Publishers: New York, 1994.

Sherman, J. D., Synthetic zeolites and other microporous oxide molecular sieves. *Proceedings of the National Academy of Sciences of the United States of America*, **1999,** 96, (7), 3471-3478.

Teague, K. G., Jr.; Edgar, T. F., Predictive dynamic model of a small pressure swing adsorption air separation unit. *Industrial & Engineering Chemical Research*, **1999,** 38, (10), 3761-3775.

Wilson, S. J.; Beh, C. C. K.; Webley, P. A.; Todd, R. S., The effects of a readily adsorbed trace component (water) in a bulk separation PSA process: The case of oxygen VSA. *Industrial & Engineering Chemistry Research*, **2001,** 40, (12), 2702-2713.

Appendix 3.1 Volumetric method

A 3.1.1 Experimental Procedure

In the next figure is represented one of the units used for determining adsorption equilibrium points by the volumetric method.

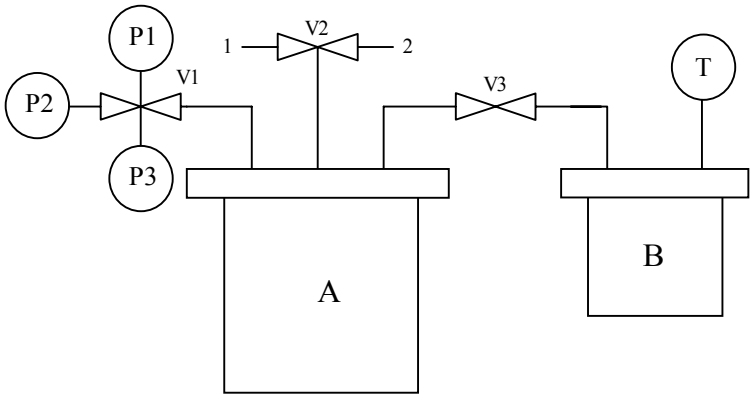

Legend: 1 – Gas inlet; 2 – Vacuum outlet
V1 – 5-Ways valve; V2 – 3-Ways valve; V3 – On-off valve
P1 – Pressure sensor 0-2 bara; P2 – Pressure sensor 0-17 bara; P3 – Pressure sensor 0-68.9 bara
T – Thermocouple.

Figure 3.13. Sketch of the unit used for determining adsorption equilibrium points.

The unit is composed by two stainless steel tanks, A and B. The 5-ways valve V1 is used for selecting the pressure sensor with the most adequate range. The 3-ways valve V2 allows the pressurization of the tanks with the desired gas or their evacuation. The on-off valve V3 allows the connection between the two tanks.

The tanks are immerged in water with temperature controlled by a thermostatic bath.

A 3.1.1.1 Measurement of the volumes of the tanks

The system is evacuated with both tanks immerged in water at controlled temperature and the pressure is registered. Valve V3 is closed, with valve V3, the pressure sensor with the range 0-2 bara is selected and valve V2 is rotated towards position 1. Tank A is filled with helium until the desired pressure is reached. Valve V2 is closed and the pressure is registered. The system is once again evacuated and this procedure should be repeated 30 times.

A given mass of glass spheres with known specific mass is measured. These spheres are introduced in tank A and the system is evacuated by the vacuum pump. Both tanks must be immerged in water at controlled temperature. After registering the pressure, valve V3 is closed and tank A is pressurized. The pressure in this tank is registered and valve V3 is opened. After the pressure stabilizes its value is registered. The system is evacuated and this procedure should be repeated 30 times.

A 3.1.1.2 Measurement of the volume of the sample

After regeneration a given mass of the adsorbent is determined and the sample is immediately inserted in tank B. Tank A should be empty. The temperature of the water in which both tanks are immerged is raised to 70ºC and the system is evacuated until no pressure variation is observed. From times to times the system is filled with helium and emptied afterwards. This procedure allows the desorption of any gas that might eventually been adsorbed before the sample was put in the tank. The temperature of the bath is set to a lower temperature and after stabilizing the pressure of the system is registered. Valve V3 is closed and tank A is filled with helium until a given pressure, which is registered afterwards. Valve V3 is opened and after the pressure stabilizes, its value is registered. The system is then evacuated and this procedure should be repeated 30 times.

A 3.1.1.3 Measurement of single component adsorption equilibrium points

The temperature of the bath is set for that at which the equilibrium points will be determined. The system is evacuated and the pressure registered. Valve V3 is closed and tank A is filled with the desired gas. The pressure inside this tank is registered and valve V3 is opened. After the pressure stabilizes its value is registered. Valve V3 is closed and tank A is filled with the same gas use before until another previously chosen pressure is reached. This procedure is repeated for several pressures.

Every time the gas is changed, the temperature of the water where the tanks are immerged is raised for 70ºC and the system is evacuated until no pressure variation is observed. From times to times the system is filled with helium and evacuated afterwards.

A 3.1.1.4 Measurement of bicomponent adsorption equilibrium points

The procedure used for determining bicomponent adsorption equilibrium points is very similar to that described before for single component measurements. At controlled temperature and after the system has been evacuated, a mixture of the two desired gases is introduced in tank A. After the adsorption equilibrium has been reached, valve V3 is closed and the composition of one of the gases in tank A is measured.

A 3.1.2 Determination of the volume of the tanks

For determining the volume of the tanks, two sets of experiments must be performed: expansion of helium with both tanks empty and expansion of helium with one of the tanks filled with spheres of glass with mass and specific mass previously determined.

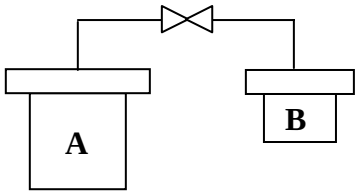

Figure 3.14. Empty tanks.

Considering two tanks such as the ones presented in Figure 3.14, the number of moles remaining after the evacuation (the system's total pressure is never nil since, with the vacuum pump, it is not possible to completely remove all the gas inside the tanks) is given by the following expression (perfect gases law):

$$n_A^0 + n_B^0 = \frac{P^0 \left(V_A + V_B\right)}{\Re T}, \tag{3.19}$$

where n is the number of moles of the gas, V the volume, P the pressure, $\Re$ the universal gas constant and T the absolute temperature. Subscripts "A" and "B" stand for tank A and B, respectively. The superscript "0" stands for the initial condition.

After the system has been evacuated, the valve between both tanks is closed and helium is introduced in tank A until a given pressure, P_A, is reached. The number of moles of the gas, n, that was introduced in tank A, at this instant, is given by the following expression (perfect gases law):

$$n = \frac{(P_{\mathrm{A}} - P^0) \cdot V_{\mathrm{A}}}{\Re T} \tag{3.20}$$

After opening the valve between the two tanks, the number of moles of the gas in both tanks is given by (perfect gases law):

$$n_{\mathrm{A}} + n_{\mathrm{B}} = \frac{P \cdot (V_{\mathrm{A}} + V_{\mathrm{B}})}{\Re T}, \tag{3.21}$$

where P is the system's total pressure. And

$$n_{\mathrm{A}} + n_{\mathrm{B}} = n + n_{\mathrm{A}}^0 + n_{\mathrm{B}}^0 \tag{3.22}$$

Replacing Equations (3.19), (3.20) and (3.22) in Equation (3.22) and after some algebraic manipulation it is possible to obtain the following relation between the tanks' volumes:

$$\frac{V_{\mathrm{A}}}{V_{\mathrm{B}}} = \frac{P - P^0}{P_{\mathrm{A}} - P} = R_{\mathrm{I}}, \tag{3.23}$$

where R_{I} is the ratio between the pressures measured with the tanks empty.

For a 95% confidence interval the error of R_{I}, $u(R_{\mathrm{I}})$, is given by (Wadsworth, 1989):

$$u(R_{\mathrm{I}}) = t_{0.025} \cdot \frac{\sigma}{\sqrt{\mathrm{N}}} = 2.042 \cdot \frac{\sigma}{\sqrt{30}}, \tag{3.24}$$

where σ is the standard deviation and N the number of measurements.

In the next figure the two tanks are represented but now tank B is filled with spheres of glass.

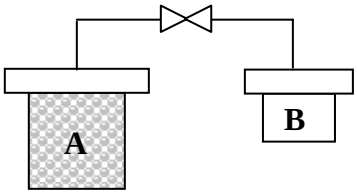

Figure 3.15. Tank A with spheres of glass and tank B empty.

The number of moles of gas inside the tanks, in the beginning, is given by (perfect gases law):

$$n_A^0 + n_B^0 = \frac{P^0 \left(V_A - V_E + V_B\right)}{\Re T}, \tag{3.25}$$

where V_E is the volume of the spheres of glass.

Such as when the two tanks were empty, helium is introduced in tank A until a given pressure, P_A is reached. The number of moles of gas, n, that was introduced in tank A, at this instant, is given by the following expression (perfect gases law):

$$n = \frac{(P_A - P^0) \cdot (V_A - V_E)}{\Re T} \tag{3.26}$$

The number of moles of helium in the tanks, after the valve between them is opened, is given by (perfect gases law):

$$n_A + n_B = \frac{P \cdot (V_A - V_E + V_B)}{\Re T} \tag{3.27}$$

And,

$$n_A + n_B = n + n_A^0 + n_B^0 \tag{3.28}$$

Replacing Equations (3.25), (3.26) and (3.27) in Equation (3.28) and after some algebraic manipulations it is possible to obtain the relation between the two tanks' volumes:

$$V_A = V_B \cdot R_2 + V_E, \tag{3.29}$$

where R_2 is the ratio of the pressures measured with tank A filled with spheres of glass and is given by:

$$R_2 = \frac{P - P^0}{P_A - P} \tag{3.30}$$

For a 95% confidence interval, the error of R_2, $u(R_2)$, is given by:

$$u(R_2) = t_{0.025} \cdot \frac{\sigma}{\sqrt{N}} = 2.042 \cdot \frac{\sigma}{\sqrt{30}} \tag{3.31}$$

Solving the system of equations composed by Equations (3.23) and (3.30) it is possible to determine the volume of each tank with the following expressions:

$$V_A = \frac{R_1}{R_1 - R_2} V_E \tag{3.32}$$

$$V_B = \frac{1}{R_1 - R_2} V_E \tag{3.33}$$

According to the error propagation theory, the general formula for calculating the error associated with a function f is as follows (Spiegel and Abellanas, 1989):

$$u(f) = \sqrt{\sum_{i=1}^{k} \left(\frac{\partial f}{\partial x_i} \cdot u(x_i) \right)^2}\ , \tag{3.34}$$

where k is the number of variables and x_i the ith variable.

Hence, the error associated with the determination of the volumes of the tanks is given by:

$$u(V_A) = \sqrt{\left(\frac{R_2 V_E}{(R_1 - R_2)^2} u(R_1) \right)^2 + \left(\frac{R_1 V_E}{(R_1 - R_2)^2} u(R_2) \right)^2 + \left(\frac{R_1}{R_1 - R_2} u(V_E) \right)^2} \tag{3.35}$$

and

$$u(V_B) = \sqrt{\left(\frac{V_E}{(R_1 - R_2)^2} u(R_1) \right)^2 + \left(\frac{V_E}{(R_1 - R_2)^2} u(R_2) \right)^2 + \left(\frac{1}{R_1 - R_2} u(V_E) \right)^2} \tag{3.36}$$

A 3.1.3 Determination of the volume of the sample

In Figure 3.16 two tanks are represented: tank A, which is empty, and tank B filled with the adsorbent.

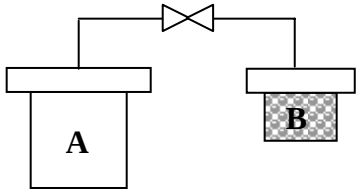

Figure 3.16. Tank A empty and tank B with the adsorbent.

The determination of the volume of the sample is conducted in a similar way of that used for determining the volume of the tanks: an expansion of helium is made from tank A to tank B.

The number of moles of gas in the tank at the initial moment is given by (perfect gases law):

$$n_A^0 + n_B^0 = \frac{P^0 \left(V_A + V_B - V_S \right)}{\Re T}, \tag{3.37}$$

where V_S is the volume of the adsorbent.

After filling tank A with helium until a given pressure, P_A, the number of moles of the gas, n, at this instant, is given by Equation (3.20).

After the valve between the tanks is opened, the number of moles of helium inside them is given by (perfect gases law):

$$n_A + n_B = \frac{P \cdot (V_A + V_B - V_S)}{\Re T} \tag{3.38}$$

By its turn,

$$n_A + n_B = n + n_A^0 + n_B^0 \tag{3.39}$$

Replacing Equations (3.20), (3.37) and (3.38) in Equation (3.39) and after some algebraic manipulations, it is possible to obtain the following equation:

$$V_S = V_B - \frac{V_A}{R_S}, \tag{3.40}$$

where R_S is the ratio of the pressures measured with tank B filled with adsorbent and is given by:

$$R_S = \frac{P - P^0}{P_A - P}, \tag{3.41}$$

where P^0 is the initial pressure in the two tanks, P_A is the pressure at which tank A was filled with helium and P is the pressure measured after the valve was opened.

According to Equation (3.34), the error associated to the determination of the volume of the sample is given by:

$$u(V_S) = \sqrt{\left(\frac{1}{R_S}u(V_A)\right)^2 + u(V_B)^2 + \left(\frac{V_A}{R_S^2}u(R_S)\right)^2} \tag{3.42}$$

For a confidence interval of 95%, the error associated to the determination of R_S, $u(R_S)$, is given by:

$$u(R_S) = t_{0.025} \cdot \frac{\sigma}{\sqrt{N}} = 2.042 \cdot \frac{\sigma}{\sqrt{30}} \tag{3.43}$$

A 3.1.4 Determination of the solute concentration in the adsorbed phase

A 3.1.4.1 Monocomponent adsorption equilibrium points

The determination of the monocomponent adsorption equilibrium points is similar to the determination of the volumes of the tanks and of the adsorbent. The decrease of the pressure in the moment the valve is opened is due both to the expansion of the gas and to the adsorption.

Hence, the number of moles initially present in the system, n^0, is given by (perfect gases law):

$$n_A^0 + n_B^0 = \frac{P^0 \left(V_A + V_B - V_S\right)}{\Re T}, \tag{3.44}$$

where V is the volume, P^0 is the pressure at this instant, $\Re$ is the universal gas constant and T the abolute temperature. The subscripts A, B and S stand for the tanks A and B and the sample, respectively.

After tank A is filled to the desired pressure, P_A, the number of moles of the gas which adsorption equilibrium points will be determined, n, is given by the following expression (perfect gases law):

$$n = \frac{(P_A - P^0) \cdot V_A}{\Re T} \tag{3.45}$$

Considering that the volume of the gas in the adsorbed phase can be considered negligible, the number of moles, in the gas phase, in both tanks, after the valve is opened is given by (perfect gases law):

$$n_A + n_B = \frac{P \cdot (V_A + V_B - V_S)}{\Re T} \tag{3.46}$$

By its turn,

$$n_A + n_B + n_{ads} = n + n_A^0 + n_B^0, \tag{3.47}$$

where n_{ads} is the number of moles adsorbed. Replacing Equations (3.44), (3.45) and (3.46) in Equation (3.47), and dividing by the volume of the adsorbent, the following expression is obtained:

$$\frac{n_{ads}}{V_S} = \frac{1}{\Re T}\left[(P_A - P)\frac{V_A}{V_S} + (P - P^0)(1 - \frac{V_B}{V_S})\right] = q, \tag{3.48}$$

where q is the concentration of the solute in the adsorbed phase.

According to the general formula of the error propagation theory, the error associated to the determination of the quantity of gas adsorbed is given by:

$$u(q)=\frac{1}{\Re T}\left\{\left[\frac{P_{\mathrm{A}}-P}{V_{\mathrm{S}}}u(V_{\mathrm{A}})\right]^2+\left[\frac{P-P^0}{V_{\mathrm{S}}}u(V_{\mathrm{B}})\right]^2+\left[\frac{(P-P_{\mathrm{A}})V_{\mathrm{A}}+(P-P^0)V_{\mathrm{B}}}{V_{\mathrm{S}}{}^2}u(V_{\mathrm{S}})\right]^2+\right.$$

$$\left.+\left[\frac{V_{\mathrm{A}}}{V_{\mathrm{S}}}u(P_{\mathrm{A}})\right]^2+\left[\left(1+\frac{V_{\mathrm{A}}-V_{\mathrm{B}}}{V_{\mathrm{S}}}\right)u(P)\right]^2+\left[\left(1-\frac{V_{\mathrm{B}}}{V_{\mathrm{S}}}\right)u(P^0)\right]^2+\left[q\cdot\Re\cdot u(T)\right]^2\right\}^{\frac{1}{2}} \tag{3.49}$$

For the successive determination of adsorption equilibrium points for the same gas, the variation of the concentration of solute in the adsorbed phase, Δq, is given by:

$$\Delta q^i=\frac{1}{\Re T}\left[(P_{\mathrm{A}}^i-P^i)\frac{V_{\mathrm{A}}}{V_{\mathrm{S}}}+(P^i-P^{i-1})(1-\frac{V_{\mathrm{B}}}{V_{\mathrm{S}}})\right], \tag{3.50}$$

where P^i is the pressure of the point which one wants to determine and P^{i-1} is the pressure of the point determined before.

The error associated to the calculation of the variation of the concentration of solute in the adsorbed phase is given by:

$$u(\Delta q^i)=\frac{1}{\Re T}\left\{\left[\frac{P_{\mathrm{A}}^i-P^i}{V_{\mathrm{S}}}u(V_{\mathrm{A}})\right]^2+\left[\frac{P^i-P^{i-1}}{V_{\mathrm{S}}}u(V_{\mathrm{B}})\right]^2+\right.$$

$$+\left[\frac{(P^i-P_{\mathrm{A}}^i)V_{\mathrm{A}}+(P^i-P^{i-1})V_{\mathrm{B}}}{V_{\mathrm{S}}{}^2}u(V_{\mathrm{S}})\right]^2+\left[\frac{V_{\mathrm{A}}}{V_{\mathrm{S}}}u(P_{\mathrm{A}}^i)\right]^2+\left[\left(1+\frac{V_{\mathrm{A}}-V_{\mathrm{B}}}{V_{\mathrm{S}}}\right)u(P^i)\right]^2+$$

$$\left.+\left[\left(1-\frac{V_{\mathrm{B}}}{V_{\mathrm{S}}}\right)u(P^{i-1})\right]^2+\left[\Delta q^i\cdot\Re\cdot u(T)\right]^2\right\}^{\frac{1}{2}} \tag{3.51}$$

The concentration of the solute in the adsorbed phase, at that pressure, is then given by:

$$q^i=q^{i-1}+\Delta q^i \tag{3.52}$$

The error associated to the calculation of the concentration of the solute in the adsorbed phase is:

$$u(q^i)=\sqrt{u(q^{i-1})^2+u(\Delta q^i)^2} \tag{3.53}$$

A 3.1.4.2 Bicomponent adsorption equilibrium points

As referred before, the determination of bicomponent adsorption equilibrium points is very similar to the determination of the monocomponent adsorption equilibrium points.

Considering that at the initial instant, none of the components is present in the system, the initial number of moles of the components 1, n_1^0, and 2, n_2^0 inside the tanks is nil. This hypothesis is valid since in the beginning the tanks are alternatively evacuated and filled with helium.

After tank A is filled with the component 1 and assuming perfect gas behaviour, the number of moles of this component introduced in the system is given by:

$$n_1 = \frac{(P_{A,1} - P^0) \cdot V_A}{\Re T} \tag{3.54}$$

In the same way, after tank A is filled with component 2 and assuming perfect gas behaviour, the number of moles of this component introduced in the system is:

$$n_2 = \frac{(P_{A,2} - P_{A,1} - P^0) \cdot V_A}{\Re T} \tag{3.55}$$

Assuming that the volume of the gas in the adsorbed phase can be considered negligible, the number of moles of the component *i*, in the gas phase, after the valve is opened, in both tanks, is given by (perfect gases law):

$$n_{A,i} + n_{B,i} = \frac{y_i P \cdot (V_A + V_B - V_S)}{\Re T}, \tag{3.56}$$

where y_i is the molar fraction of component *i*.

After performing a balance to component *i,* in the system, the following equation may be obtained:

$$n_{A,i} + n_{B,i} + n_{ads,i} = n_i + n_i^0 \tag{3.57}$$

The adsorbed quantity of components 1 and 2 may be given by:

$$q_1 = \frac{n_{ads,1}}{V_S} = \frac{1}{\Re T}\left[\left(P_{A,1} - P^0 - y_1 P\right)\frac{V_A}{V_S} + y_1 P\left(1 - \frac{V_B}{V_S}\right)\right] \tag{3.58}$$

$$q_2 = \frac{n_{ads,2}}{V_S} = \frac{1}{\Re T}\left[\left(P_{A,2} - P_{A,1} - P^0 - y_2 P\right)\frac{V_A}{V_S} + y_2 P\left(1 - \frac{V_B}{V_S}\right)\right] \tag{3.59}$$

According to the general formula of the error propagation theory, the error associated to the determination of the adsorbed quantity is given by:

$$\begin{aligned} u(q_1) = \frac{1}{\Re T}\Bigg\{ & \left[q_1 \cdot \Re \cdot u(T)\right]^2 + \left[\frac{V_A}{V_S}\cdot u(P_{A,1})\right]^2 + \left[\frac{V_A}{V_S}\cdot u(P^0)\right]^2 + \\ & + \left[P\cdot\left(1 - \frac{V_A}{V_S} - \frac{V_B}{V_S}\right)\cdot u(y_1)\right]^2 + \left[y_1\cdot\left(1 - \frac{V_A}{V_S} - \frac{V_B}{V_S}\right)\cdot u(P)\right]^2 + \\ & + \left[\frac{1}{V_S}\cdot\left(P_{A,1} - P^0 - y_1 P\right)\cdot u(V_A)\right]^2 + \left[\frac{y_1 P}{V_S}\cdot u(V_B)\right]^2 + \\ & + \left[\left(\frac{\left(y_1 P + P^0 - P_{A,1}\right)\cdot V_A}{{V_S}^2} + \frac{y_1 P\cdot V_B}{{V_S}^2}\right)\cdot u(V_S)\right]^2\Bigg\}^{\frac{1}{2}} \end{aligned} \tag{3.60}$$

$$\begin{aligned} u(q_2) = \frac{1}{\Re T}\Bigg\{ & \left[q_2 \cdot \Re \cdot u(T)\right]^2 + \left[\frac{V_A}{V_S}\cdot u(P_{A,2})\right]^2 + \left[\frac{V_A}{V_S}\cdot u(P_{A,1})\right]^2 + \left[\frac{V_A}{V_S}\cdot u(P^0)\right]^2 + \\ & + \left[P\cdot\left(1 - \frac{V_A}{V_S} - \frac{V_B}{V_S}\right)\cdot u(y_2)\right]^2 + \left[y_2\cdot\left(1 - \frac{V_A}{V_S} - \frac{V_B}{V_S}\right)\cdot u(P)\right]^2 + \\ & + \left[\frac{1}{V_S}\cdot\left(P_{A,2} - P_{A,1} - P^0 - y_2 P\right)\cdot u(V_A)\right]^2 + \left[\frac{y_2 P}{V_S}\cdot u(V_B)\right]^2 + \\ & + \left[\left(\frac{\left(y_2 P + P_{A,1} + P^0 - P_{A,2}\right)\cdot V_A}{{V_S}^2} + \frac{y_2 P\cdot V_B}{{V_S}^2}\right)\cdot u(V_S)\right]^2\Bigg\}^{\frac{1}{2}} \end{aligned} \tag{3.61}$$

A 3.1.5 Detailed description of the unit

Two units were used for measuring adsorption equilibrium points by the volumetric method, been one of them assembled in the framework of this Thesis. The

previous existent unit will be briefly described while the assembled unit will be described in more detail.

The previously existent unit is composed by two stainless steel tanks, A and B, as represented in Figure 3.13. Tank A has an internal volume of $(205.14 \pm 0.48)\text{cm}^3$ and tank B has an internal volume of $(45.29 \pm 0.18)\text{cm}^3$. Both these volumes were determined using the procedure described before. The unit is composed by three pressure sensors from Lucas Schaevitz, with a precision of 0.1% FS, with ranges between 0 and 2 bara, 0 and 16 bara and 0 and 68.9 bara. The thermocouple used for measuring the temperature was of type K and a Polystat K6-1 thermostatic bath from Hubber was used for regulating the temperature.

The assembled unit is represented in Figure 3.17.

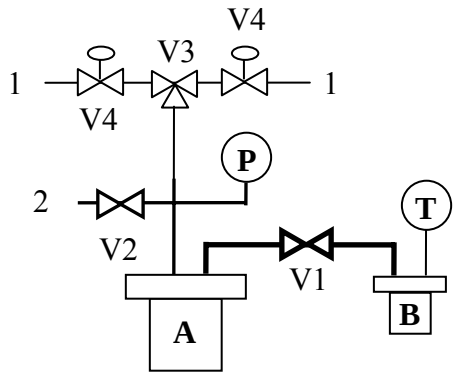

Legend: 1 – Gas inlet; 2 – Vacuum outlet
V1 and V2 – On-off valves ; V3 – 3-Ways valve; V4 – Needle valve
P – Pressure sensor 0-10 bara; T – Thermocouple.
3/4' tube, 1/4' tube, 1/8' tube

Figure 3.17. Sketch of the unit assembled for measuring adsorption equilibrium points by the volumetric method.

This unit is composed by two stainless steel tanks, A and B. Tank A has an internal volume of $(245.89 \pm 0.21)\text{cm}^3$ and tank B has an internal volume of $(52.68 \pm 0.07)\text{cm}^3$. Both volumes were determined using the procedure described before. The holes in tank A have an 1/4' NPT thread while the holes in tank B have a 1/4' NPT thread (in the tanks connection) and 1/8' NPT thread (for the thermocouple).

All the valves are in stainless steel and are from Swagelok, the 3/4' on-off valve has the reference SS-43S6-A, the 1/4' on-off valve has the reference SS-43S4-A,

the 1/8’ 3-ways valve has the reference SS-41XS2 and the 1/8’ needle valves have the reference SS-ORS2.

The pressure sensor used, model PMP 4010 from Druck, has a range from 0 to 10 bara with a precision of 0.08% FS. This sensor was powered with 15V, continuous current, and gives an output from 0 to 5 V, also in continuous current.

The thermocouple used for measuring the temperature was also of type K and a Polystat K6-1 thermostatic bath from Hubber was used for regulating the temperature.

A 3.1.6 References

Spiegel, M. R.; Abellanas, L., *Fórmulas e Tabelas de Matemática Aplicada*. Schaum-McGraw-Hill: Maia, 1989.

Wadsworth, H. M., *Probability Distributions and Statistical Inference*. McGraw-Hill: Atlanta, 1989.

Appendix 3.2 Gravimetric method

A 3.2.1 Experimental procedure

The unit used for determining the adsorption equilibrium points by the volumetric method is presented in the next figure.

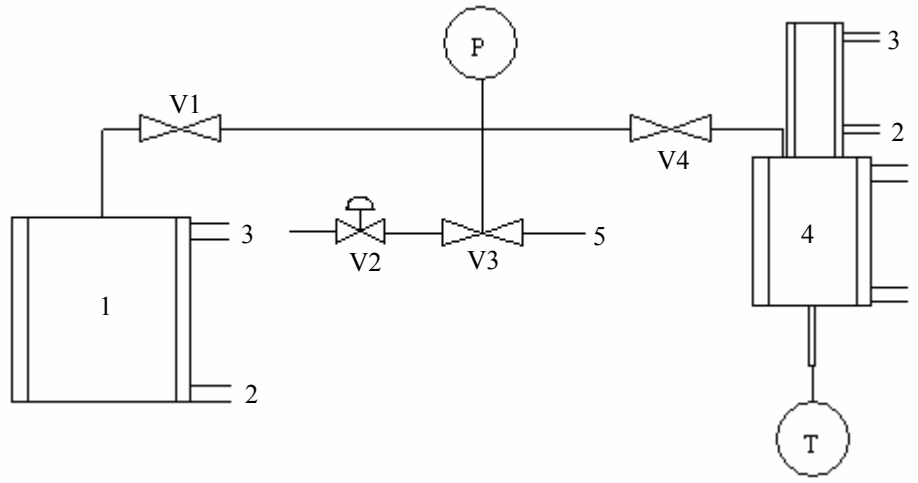

Legend: 1 – 5L Tank; 4 – Chamber where the sample is.
2 and 3 – Water inlet and outlet, respectively, for temperature control. 5 – Vacuum outlet.
V1 and V4 – On-off valve; V2 – Needle valve; V3 – 3-Ways valve.
P – Pressure sensor 0-7 bar.
T – Thermocouple.

Figure 3.18. Schematic representation of the experimental setup for measuring adsorption equilibrium data.

The 5L tank (1 in Figure 3.18) is used for keeping the pressure constant after the adsorption has begun. The valve V2 allows the control of the flow rate of the gas that is being fed to the system. The 3-ways valve V3 is used for selecting between feed and vacuum.

The temperature in the chamber where the sample is kept constant by the use of a thermostatic bath.

A 3.2.1.1 Measurement of the mass and volume of the sample basket and metallic shaft.

The temperature of the bath is set to 20ºC. Valve V1 is closed, valve V4 is opened and the system is evacuated through valve V3. Slowly, the chamber where the sample is filled with helium through valves V2 and V3 to the pressure of 6.5 bara. The mass is measured several times in positions 1 and 2 until agreeing values are obtained.

The pressure is decreased with the vacuum pump through valve V3. This procedure is repeated for several pressure values. Before each weight the balance is tared in position 0.

A 3.2.1.2 Measurement of the sample mass, volume and density

The procedure is similar to the one used for determining the mass and volume of the metallic shaft and sample basket.

Immediately after regenerating the adsorbent, the sample basket is filled with it. The temperature of the thermostatic bath is raised to 70ºC and the system is evacuated until the pressure and sample mass do not change in time. The temperature of the thermostatic bath is set to 20ºC and after it stabilizes the chamber where the sample is filled with helium until the pressure reaches 6.5 bara. The mass is registered in positions 1 and 2 until agreeing values are obtained. The pressure of the gas in the chamber is decreased and this procedure is repeated for several pressures.

Before each weight the balance is tared in position 0.

A 3.2.1.3 Measurement of the adsorption equilibrium points

The temperature of the thermostatic bath is set to the desired value. After the temperature stabilizes the system is evacuated. Valve V4 is closed and valve V1 opened. The tank is filled with the gas in study until the desired pressure is reached. Valve V4 is opened and after the mass stabilizes its value is registered, for about 10 minutes, in positions 1 and 2, at a rate of 3 points per second. Valve V4 is closed and the pressure in the tank is raised. Before each weight the balance is tared in position 0.

A 3.2.2 Relation between the impulsion and mass of the system

In the next figure are presented the objects that are weighted in positions 1 and 2 of the magnetic suspension balance.

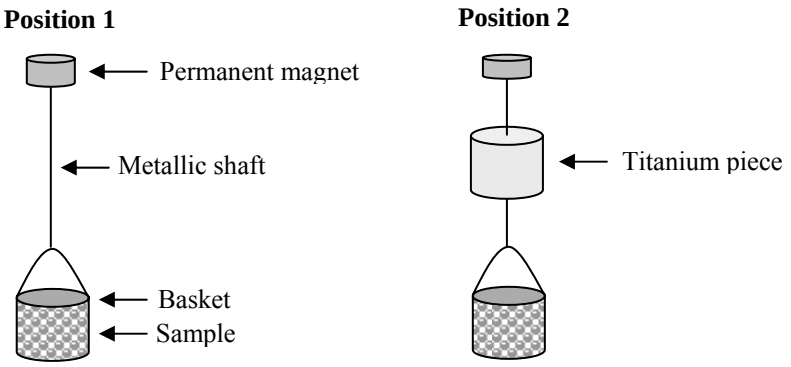

Figure 3.19. Objects weighted in each position of the magnetic suspension balance.

The mass measured in position 1, m_1, affected by the impulsion, is given by the following expression:

$$m_1 = m_{HBS} - V_{HBS} \cdot \rho_g , \tag{3.62}$$

where m_{HBS} and V_{HBS} are the real mass and volume, respectively, of the set composed by the metallic shaft (H), basket (B) and sample (S), ρ_g is the gas density.

The mass measured in position 2, m_2, affected by the impulsion, is given by:

$$m_2 = m_{HBS} + m_T - V_{HBS} \cdot \rho_g - V_T \cdot \rho_g , \tag{3.63}$$

where m_T and V_T are the real mass and volume of the titanium piece (T), respectively.

Equations (3.62) and (3.63) may be written as follows:

$$V_{HBS} \cdot \rho_g = m_{HBS} - m_1 \tag{3.64}$$

$$(V_{HBS} + V_T) \cdot \rho_g = m_{HBS} + m_T - m_2 \tag{3.65}$$

Dividing Equation (3.65) by Equation (3.64) and after some algebraic manipulations it is possible to obtain the following expression:

$$m_{HBS} = m_1 + \frac{V_{HBS}}{V_T} \cdot \left[m_T - (m_2 - m_1) \right] \tag{3.66}$$

This equation allows the removal of the effect of impulsion in the mass measured in position 1. For this, the mass must be measured in positions 1 and 2 and the

mass and volume of the titanium piece must be known, as well as the volumes of the system composed by the metallic shaft, basket, sample and titanium piece.

According to the error propagation theory (Spiegel and Abellanas, 1989), the error associated to the determination of m_{HBS}, $u(m_{HBS})$, is given by:

$$u(m_{HBS}) = \left\{ u(m_1)^2 + \left(\frac{1}{V_T} \left[m_T - (m_2 - m_1) \right] u(V_{HBS}) \right)^2 + \left(\frac{V_{HBS}}{V_T^{\,2}} \left[m_T - (m_2 - m_1) \right] u(V_T) \right)^2 + \right.$$
$$\left. + \left(\frac{V_{HBS}}{V_T} u(m_T) \right)^2 + \left(\frac{V_{HBS}}{V_T} u(m_1) \right)^2 + \left(\frac{V_{HBS}}{V_T} u(m_2) \right)^2 \right\}^{\frac{1}{2}} \tag{3.67}$$

A 3.2.3 Determination of the volume and mass of the set shaft/ basket

For the case where the basket is empty, Equation (3.66) can be written as:

$$m_{HB} = m_1 + \frac{V_{HB}}{V_T} \left[m_T - \left(m_2 - m_1 \right) \right] \tag{3.68}$$

This equation may be written in way that the mass measured in position 2 is related with the mass measured in position 1:

$$m_2 = C_1 \cdot m_1 + C_2 , \tag{3.69}$$

where C_1 and C_2 are constant and are given by:

$$C_1 = \frac{V_T}{V_{HB}} + 1 \tag{3.70}$$

$$C_2 = m_T - m_{HB} \frac{V_T}{V_{HB}} \tag{3.71}$$

By its turn, m_1 and m_2 are functions of the pressure. By weighting the system several times in a helium atmosphere in positions 1 and 2 and by fitting a line to the set of points (m_1 , m_2) it is possible to obtain the slope, C_1, of Equation (3.69).

Since the volume of the titanium piece, V_T, is given by the manufacturer of the balance, it is possible to determine the volume of the set shaft/ basket by rewriting Equation (3.70) as follows:

$$V_{HB} = \frac{V_T}{C_1 - 1} \tag{3.72}$$

The error associated to the determination of the volume of the set shaft/ basket is given by:

$$u(V_{HB}) = \sqrt{\left(\frac{1}{C_1 - 1} u(V_T)\right)^2 + \left(\frac{V_T}{(C_1 - 1)^2} u(C_1)\right)^2}, \tag{3.73}$$

where the error associated to the determination of the slope C_1, for a confidence interval of 95%, is given by (Ryan, 1989):

$$u(C_1) = t_{0.025} \cdot \mathrm{SE} = 2.042 \cdot \mathrm{SE}, \tag{3.74}$$

where SE is the standard error given by:

$$\mathrm{SE} = \frac{\sigma}{\sqrt{\sum_{i=1}^{N} (X_i - \bar{X})^2}}, \tag{3.75}$$

where N is the number of experimental points, X_i the value of the experimental point i and $\bar{X}$ the average value of the experimental points.

The mass in position 1 can be related with the pressure, P, by the following expression:

$$m_1 = m_{HB} - C_3 \cdot P, \tag{3.76}$$

where C_3 is a constant.

By fitting a line to all the points determined in position 1 as function of the pressure, it is possible to determine the mass of the set shaft/ basket, m_{HB}.

The error associated to the calculation of this mass is given by:

$$u(m_B) = \sqrt{u(m_1)^2 + (C_3 \cdot u(P))^2 + (P \cdot u(C_3))^2} \tag{3.77}$$

The error of the slope C_3, for a confidence interval of 95%, is given by:

$$u(C_3) = t_{0.025} \cdot \mathrm{SE} = 2.042 \cdot \mathrm{SE} \tag{3.78}$$

A 3.2.4 Determination of the volume and mass of the sample and mass of the titanium piece

The procedure followed for determining the volume and mass of the sample is similar to the one used for determining the volume and mass of the set shaft/ basket.

Equation (3.66) may be rewritten in such way that the mass measured in position 1 is related with the mass measured in position 2:

$$m_2 = C_4 \cdot m_1 + C_5, \tag{3.79}$$

where C_4 and C_5 are constant and are given by:

$$C_4 = \frac{V_\mathrm{T}}{V_\mathrm{HBS}} + 1 \tag{3.80}$$

$$C_5 = m_\mathrm{T} - m_\mathrm{HBS} \frac{V_\mathrm{T}}{V_\mathrm{HBS}} \tag{3.81}$$

By determining several times the masses m_1 and m_2, with helium at different pressures and by adjusting a line to the set of points (m_1, m_2), according to Equation (3.79), it is possible to compute the slope C_4.

With the following expression it is possible to determine the volume of the set shaft (H), basket (B) and sample (S):

$$V_\mathrm{HBS} = \frac{V_T}{C_4 - 1} \tag{3.82}$$

The error associated to the determination of this volume is given by:

$$u(V_{HBS}) = \sqrt{\left(\frac{1}{C_4 - 1} u(V_T)\right)^2 + \left(\frac{V_T}{(C_4 - 1)^2} u(C_4)\right)^2} \tag{3.83}$$

The error associated to the determination of the slope C_4, for a confidence interval of 95% is given by:

$$u(C_4) = t_{0.025} \cdot \mathrm{SE} = 2.042 \cdot \mathrm{SE} \tag{3.84}$$

Hence, the sample volume, V_S, may easily be determined by the following expression:

$$V_S = V_{HBS} - V_{HB} \tag{3.85}$$

The error associated to calculation of the sample volume is:

$$u(V_S) = \sqrt{u(V_{HBS})^2 + u(V_{HB})^2} \tag{3.86}$$

The measured in position 1 is related with the pressure as follows:

$$m_1 = m_{HBS} - C_6 \cdot P, \tag{3.87}$$

where C_6 is a constant.

By adjusting a line to the several points m_1 as function of the pressure, it is possible to determine the intercept, m_{HBS}.

The error in the determination of this mass, for a confidence interval of 95% is given by (Ryan, 1989):

$$u(m_{HBS}) = t_{0.025} \cdot \sigma \sqrt{\frac{1}{N} + \frac{\bar{X}^2}{\sum_{i=1}^{N} (X_i - \bar{X})^2}} \tag{3.88}$$

The mass of the sample may be determined by:

$$m_S = m_{HBS} - m_{HB} \tag{3.89}$$

The error associated to this determination is given by the following expression:

$$u(m_S) = \sqrt{u(m_{HBS})^2 + u(m_{HB})^2} \tag{3.90}$$

The density of the sample, ρ_S, may then be obtained by the following equation:

$$\rho_S = \frac{m_S}{V_S} \tag{3.91}$$

According to the error propagation theory (Spiegel and Abellanas, 1989), the error associated to the determination of the density of the sample is given by:

$$u(\rho_S) = \rho_S \cdot \sqrt{\left(\frac{u(m_S)}{m_S}\right)^2 + \left(\frac{u(V_S)}{V_S}\right)^2} \tag{3.92}$$

The mass determined in position 2 can be related with the pressure as follows:

$$m_2 = m_{HBST} - C_7 \cdot P \tag{3.93}$$

where C_7 is a constant and m_{HBST} is the mass of the set shaft, basket, sample and titanium piece.

Adjusting a line to the points m_2 obtained as function of the pressure it is possible to calculate the intercept, m_{HBST}.

The error associate to this determination, for a confidence interval of 95% is:

$$u(m_{HBST}) = t_{0.025} \cdot \sigma \sqrt{\frac{1}{N} + \frac{\bar{X}^2}{\sum_{i=1}^{N}(X_i - \bar{X})^2}} \tag{3.94}$$

The mass of the titanium piece may then be obtained by the following equation:

$$m_T = m_{HBST} - m_{HBS} \tag{3.95}$$

The error associated to the determination of the mass of the titanium piece is given by:

$$u(m_{\mathrm{T}}) = \sqrt{u(m_{\mathrm{HBST}})^2 + u(m_{\mathrm{HBS}})^2} \tag{3.96}$$

A 3.2.5 Determination of the concentration of the solute in the adsorbed phase

After evacuating the system, the masses m_1 and m_2 of the set shaft, basket, sample and titanium piece (only in position 2) are determined. The mass of the sample without impulsion may be obtained from the following expression that results from Equations (3.66) and (3.89):

$$m_{\mathrm{S}} = m_1 + \frac{V_{\mathrm{HBS}}}{V_{\mathrm{T}}}\left[m_{\mathrm{T}} - \left(m_2 - m_1\right)\right] - m_{\mathrm{HB}} \tag{3.97}$$

According to the error propagation theory, the error associated to the determination of the mass of the sample is given by:

$$u(m_{\mathrm{S}}) = \left\{ u(m_1)^2 + \left(\frac{1}{V_{\mathrm{T}}}[m_{\mathrm{T}} - (m_2 - m_1)] \cdot u(V_{\mathrm{HBS}})\right)^2 + \left(\frac{V_{\mathrm{HBS}}}{V_{\mathrm{T}}}[m_{\mathrm{T}} - (m_2 - m_1)] \cdot u(V_{\mathrm{T}})\right)^2 + \right.$$
$$\left. + \left(\frac{V_{\mathrm{HBS}}}{V_T} u(m_{\mathrm{T}})\right)^2 + \left(\frac{V_{\mathrm{HBS}}}{V_{\mathrm{T}}} u(m_1)\right)^2 + \left(\frac{V_{\mathrm{HBS}}}{V_{\mathrm{T}}} u(m_2)\right)^2 + u(m_{\mathrm{HB}})^2 \right\}^{\frac{1}{2}} \tag{3.98}$$

After doing a step in the pressure of the gas in study, and after the mass in position 1 does not change more than the precision of the balance (2×10^{-5} g), the mass in position 2 may be measured and the mass of the adsorbent may again be determined using Equation (3.97).

The variation of the mass of the sample, Δm_{S}, is given by:

$$\Delta m_{\mathrm{S}} = m_{\mathrm{S}}^{i} - m_{\mathrm{S}}^{i-1}, \tag{3.99}$$

where the superscripts i and $i-1$ stand for the current and previous measurements, respectively.

The error associated to this variation is given by:

$$u(\Delta m_S) = \sqrt{u(m_S^i)^2 + u(m_S^{i-1})^2} \tag{3.100}$$

Since the variation of the mass is due to the adsorption of the gas, the variation of the concentration of the solute in the adsorbed phase (Δq) is then given by:

$$\Delta q = \frac{\Delta m_S}{\mathrm{M} \cdot V_S} \tag{3.101}$$

The error associated to its determination is:

$$u(\Delta q) = \sqrt{\left(\frac{1}{MV_S} u(\Delta m_S)\right)^2 + \left(\frac{\Delta m_S}{MV_S^2} u(V_S)\right)^2} \tag{3.102}$$

The total concentration of the solute in the adsorbed phase at a given pressure is given by:

$$q^i = q^{i-1} + \Delta q^i, \tag{3.103}$$

where the superscripts i and $i-1$ refer to the current and previous pressures, respectively.

The error associated to this determination is given by:

$$u(q^i) = \sqrt{u(q^{i-1})^2 + u(\Delta q^i)^2} \tag{3.104}$$

A 3.2.6 Detailed description of the unit

The unit, represented in Figure 3.18, is composed by one pressure sensor from Druck, reference PMP 4010, of the range 0 to 7 bara, with an accuracy of 0.08% FS. The thermocouple used for the measurement of the temperature was of type K and a Polystat K6-1 thermostatic bath from Hubber was used for regulating the temperature.

The volume of the titanium piece, V_T, is $(4.37110 \pm 0.00219)\,\mathrm{cm}^3$, the mass of the set shaft and basket, m_{HB}, is $\left(3.94395 \pm 2 \times 10^{-5}\right)\mathrm{g}$ and the volume of the same set, V_{HB}, is $(0.46256 \pm 0.00726)\,\mathrm{cm}^3$. These values were determined using the procedure previously described.

A 3.2.7 References

Ryan, T. P., Linear Regression. In *Linear Regression*, Wadsworth, H. M., McGraw-Hill: New York, 1989.

Spiegel, M. R.; Abellanas, L., *Fórmulas e Tabelas de Matemática Aplicada*. Schaum-McGraw-Hill: Maia, 1989.

Appendix 3.3 Contamination of the adsorbents

A 3.3.1 Oxysiv 5 from UOP

The nitrogen adsorption capacity was measured, at 20ºC, for evaluating the influence of carbon dioxide in the adsorption capacity of Oxysiv 5, after some experiments where the zeolite was tried to be deactivated with carbon dioxide. These experiments are described in Table 3.15.

Table 3.15. Experiments related with the deactivation of Oxysiv 5 with carbon dioxide.

Sample	Experiment	Description
I	1	Measurement of the nitrogen adsorption capacity at 20ºC in a sample of "fresh" zeolite.
	2	Saturation at about 7 mbara of CO_2. Regeneration at 70ºC for 2h, using alternatively vacuum and helium at 8 bara.
	3	Regeneration in a muffle at 375ºC for 12h passing a current of dried air through the adsorbent.
	4	Saturation at about 7 mbara of CO_2. Regeneration at 70ºC for 2h, using alternatively vacuum and helium at 8 bara.
	5	Regeneration in a muffle at 375ºC for 24h without passing a current of dried air through the adsorbent.

The amount of carbon dioxide used is close to the amount the adsorbents are exposed to during the operation of a pressure swing adsorption unit.

The results of these experiments are presented in Figure 3.20.

Analysing the results it is possible to conclude that the only way to recover the full adsorption capacity of this adsorbent is by regenerating it at 375ºC in a muffle and passing a dried air current through the adsorbent.

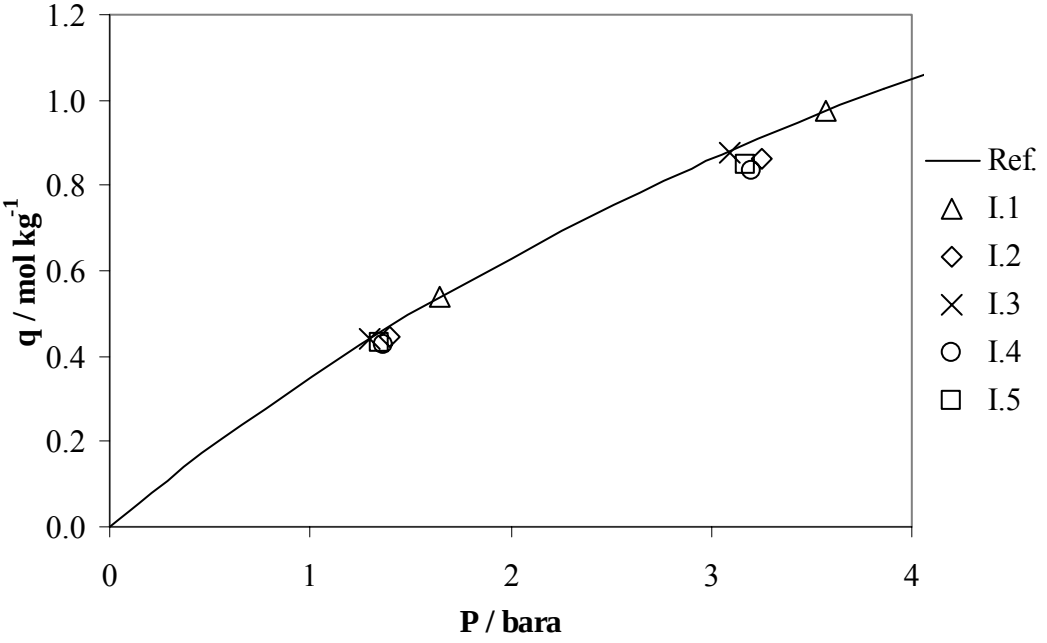

Figure 3.20. Nitrogen adsorption capacity at 20ºC. The reference adsorption isotherm (Ref.) is the nitrogen adsorption isotherm at 20ºC in a regenerated sample.

A study was conducted in a similar way, to evaluate the influence of water vapour in the adsorption capacity of Oxysiv 5. The experiments conducted are described in Table 3.16.

Table 3.16. Experiments related with the deactivation of Oxysiv 5 with water vapour.

Sample	Experiment	Description
II	1	Measurement of the nitrogen adsorption capacity at 20ºC of a sample of the zeolite regenerated in a muffle at 375ºC, for 12h and passing a dried air current through the adsorbent.
	2	Saturation with water vapour at 20ºC (about 23.4 mbara of water vapour). Regeneration at 70ºC for 2h using alternatively vacuum and helium at 8 bara.
	3	Regeneration in a muffle at 375ºC for 12h without passing a current of dried air through the adsorbent.

This experiment was repeated and the adsorbent was regenerated in a muffle at 375ºC with a current of dried air passing through the adsorbent and it was possible to recover the full adsorption capacity of the adsorbent.

The amount of water vapour used is close to the amount that the adsorbents are exposed to during the operation of a pressure swing adsorption unit.

The results of these experiments are presented in Figure 3.21.

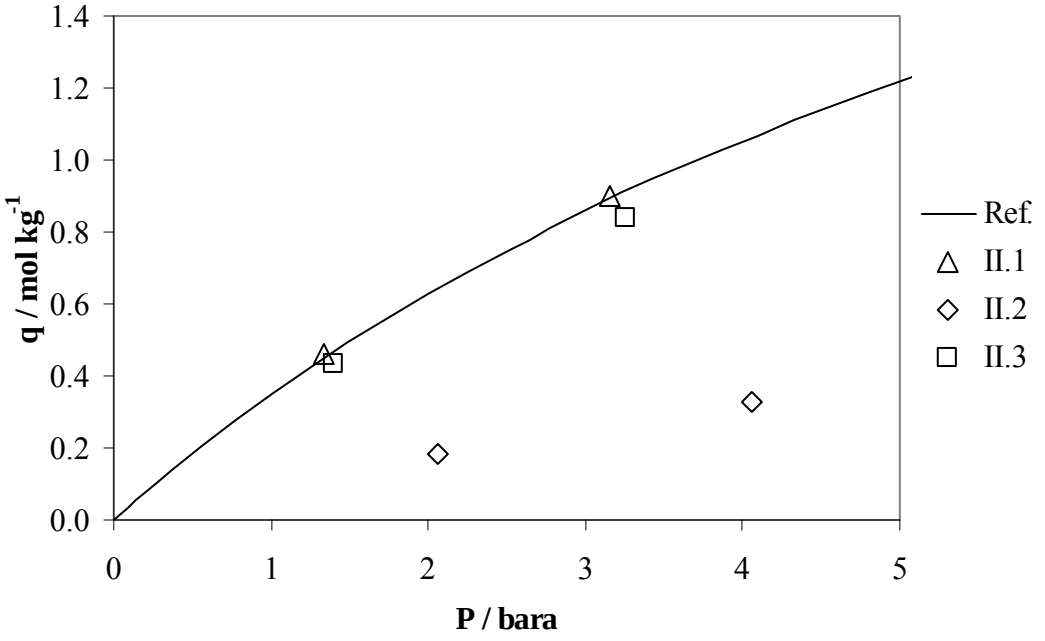

Figure 3.21. Nitrogen adsorption capacity at 20ºC. The reference adsorption isotherm (Ref.) is the isotherm of nitrogen at 20ºC in a sample regenerated.

Analysing the results it is possible to conclude that the only way to recover the full adsorption capacity of this adsorbent is by regenerating it in a muffle at 375ºC and passing a dried air current through the adsorbent.

A similar study was conducted for evaluating the influence of water vapour simultaneously with carbon dioxide in the adsorption capacity of Oxysiv 5. The experiments that were conducted are described in Table 3.17.

Table 3.17. Experiments related with the deactivation of Oxysiv 5 with water vapour simultaneously with carbon dioxide.

Sample	Experiment	Description
III	1	Measurement of the nitrogen adsorption capacity at 20ºC in a sample of zeolite regenerated in a muffle at 375ºC, for 12h and passing a dried air current through the adsorbent.
	2	Saturation with water vapour and carbon dioxide at 20ºC. Regeneration at 70ºC for 2h using alternatively vacuum and helium at 8 bara.
	3	Regeneration in a muffle at 375ºC for 12h without passing a dried air current through the adsorbent.

This experiment was repeated and the adsorbent was regenerated in a muffle at 375ºC with a current of dried air passing through the adsorbent and it was possible to recover the full adsorption capacity of the adsorbent.

The amounts of water vapour and carbon dioxide are close to the amount these adsorbents are exposed to during the operation of a pressure swing adsorption unit.

The results of these experiments are presented in Figure 3.22.

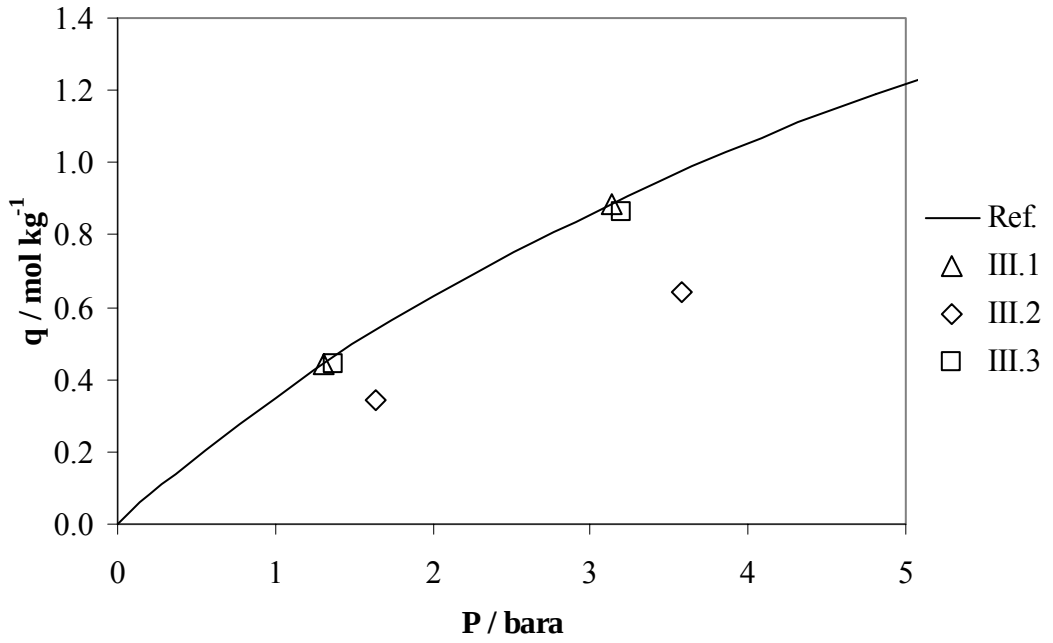

Figure 3.22. Nitrogen adsorption capacity at 20ºC. The reference adsorption isotherm (Ref.) is the nitrogen adsorption isotherm at 20ºC in a regenerated sample.

Analysing the results it is possible to conclude that the only way to recover the full adsorption capacity of this adsorbent is by regenerating it in a muffle at 375ºC and passing a dried air current through the adsorbent.

A 3.3.2 Oxysiv 7 from UOP

The nitrogen adsorption capacity was measured, at 20ºC, for evaluating the influence of carbon dioxide in the adsorption capacity of Oxysiv 7, after some experiments where the zeolite was tried to be deactivated with carbon dioxide. These experiments are described in Table 3.18.

Table 3.18. Experiments related with the deactivation of Oxysiv 7 with carbon dioxide.

Sample	Experiment	Description
I	1	Measurement of the nitrogen adsorption capacity at 20ºC of a sample of the zeolite regenerated in a muffle at 375ºC, for 12h and passing a dried air current through the adsorbent.
	2	Saturation at about 7 mbara of CO_2. Regeneration at 70ºC for 2h, using alternatively vacuum and helium at 8 bara.
	3	Regeneration in a muffle at 375ºC for 12h without passing a current of dried air through the adsorbent.

The amount of carbon dioxide used is close to the amount the adsorbents are exposed to during the operation of a pressure swing adsorption unit.

This experiment was repeated and the adsorbent was regenerated in a muffle at 375ºC with a current of dried air passing through the adsorbent and it was possible to recover the full adsorption capacity of the adsorbent.

The results of these experiments are presented in Figure 3.23.

Analysing the results it is possible to conclude that the only way to recover the full adsorption capacity of this adsorbent is by regenerating it at 375ºC in a muffle and passing a dried air current through the adsorbent.

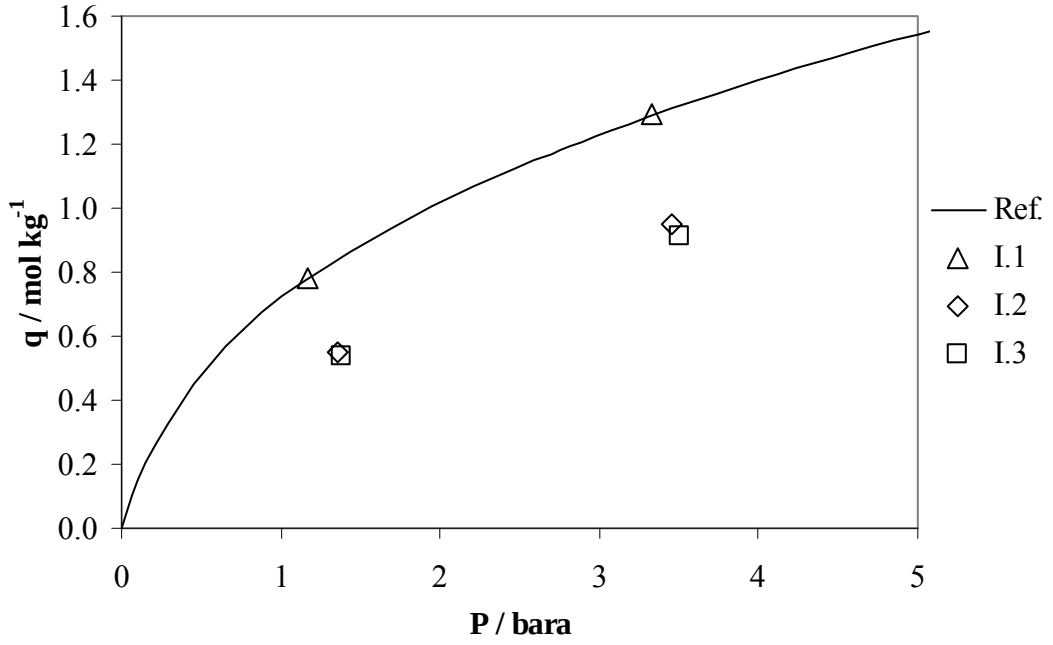

Figure 3.23. Nitrogen adsorption capacity at 20ºC. The reference adsorption isotherm (Ref.) is the nitrogen adsorption isotherm at 20ºC in a regenerated sample.

A study was conducted in a similar way, to evaluate the influence of water vapour in the adsorption capacity of Oxysiv 7. The experiments conducted are described in Table 3.19.

Table 3.19. Experiments related with the deactivation of Oxysiv 7 with water vapour.

Sample	Experiment	Description
II	1	Measurement of the nitrogen adsorption capacity at 20ºC of a sample of the zeolite regenerated in a muffle at 375ºC, for 12h and passing a dried air current through the adsorbent.
	2	Saturation with water vapour at 20ºC (about 23.4 mbara of water vapour). Regeneration at 70ºC for 2h using alternatively vacuum and helium at 8 bara.
	3	Regeneration in a muffle at 375ºC for 12h without passing a current of dried air through the adsorbent.

This experiment was repeated and the adsorbent was regenerated in a muffle at 375ºC with a current of dried air passing through the adsorbent and it was possible to recover the full adsorption capacity of the adsorbent.

The amount of water vapour used is close to the amount that the adsorbents are exposed to during the operation of a pressure swing adsorption unit.

The results of these experiments are presented in Figure 3.24.

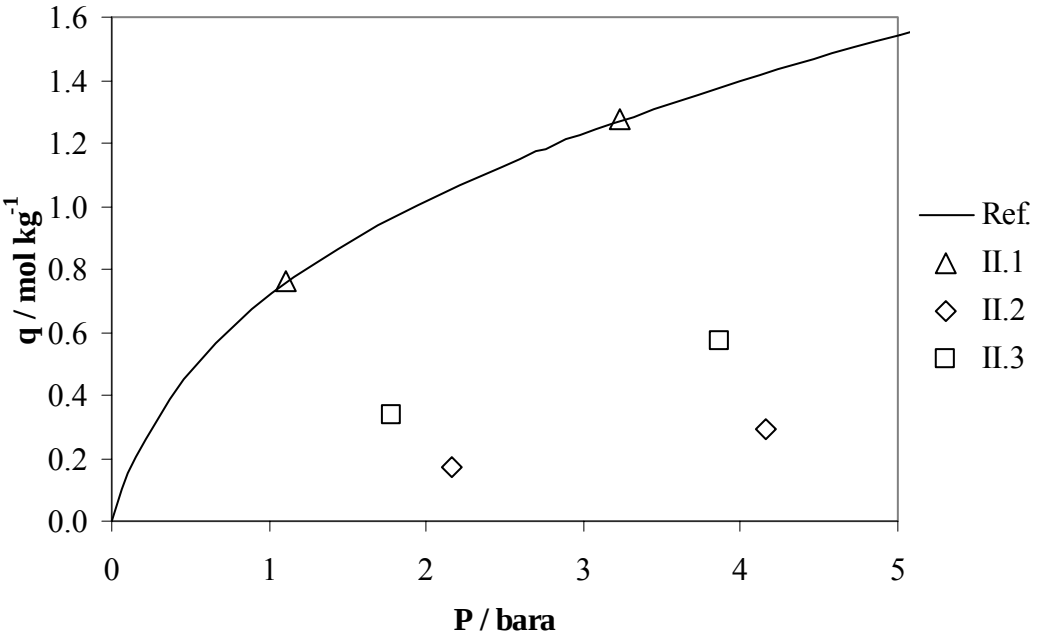

Figure 3.24. Nitrogen adsorption capacity at 20ºC. The reference adsorption isotherm (Ref.) is the isotherm of nitrogen at 20ºC in a sample regenerated.

Analysing the results it is possible to conclude that the only way to recover the full adsorption capacity of this adsorbent is by regenerating it in a muffle at 375ºC and passing a dried air current through the adsorbent.

A similar study was conducted for evaluating the influence of water vapour simultaneously with carbon dioxide in the adsorption capacity of Oxysiv 7. The experiments that were conducted are described in Table 3.20.

Table 3.20. Experiments related with the deactivation of Oxysiv 7 with water vapour simultaneously with carbon dioxide.

Sample	Experiment	Description
III	1	Measurement of the nitrogen adsorption capacity at 20ºC in a sample of zeolite regenerated in a muffle at 375ºC, for 12h and passing a dried air current through the adsorbent.
	2	Saturation with water vapour and carbon dioxide at 20ºC. Regeneration at 70ºC for 2h using alternatively vacuum and helium at 8 bara.
	3	Regeneration in a muffle at 375ºC for 12h without passing a dried air current through the adsorbent.

The amounts of water vapour and carbon dioxide are close to the amount these adsorbents are exposed to during the operation of a pressure swing adsorption unit.

This experiment was repeated and the adsorbent was regenerated in a muffle at 375ºC with a current of dried air passing through the adsorbent and it was possible to recover the full adsorption capacity of the adsorbent.

The results of these experiments are presented in Figure 3.25.

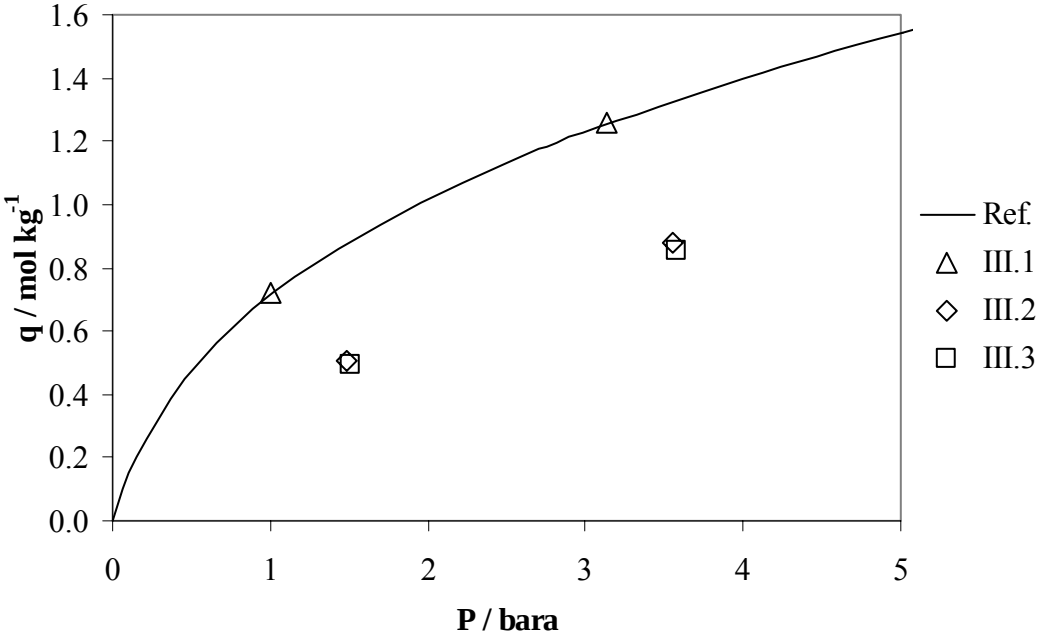

Figure 3.25. Nitrogen adsorption capacity at 20ºC. The reference adsorption isotherm (Ref.) is the nitrogen adsorption isotherm at 20ºC in a regenerated sample.

Analysing the results it is possible to conclude that the only way to recover the full adsorption capacity of this adsorbent is by regenerating it in a muffle at 375ºC and passing a dried air current through the adsorbent.

A 3.3.3 KEG415 from UOP/Bayer

The nitrogen adsorption capacity was measured, at 20ºC, for evaluating the influence of carbon dioxide in the adsorption capacity of KEG415, after some experiments where the zeolite was tried to be deactivated with carbon dioxide. These experiments are described in Table 3.21.

The amount of carbon dioxide used is close to the amount the adsorbents are exposed to during the operation of a pressure swing adsorption unit.

Table 3.21. Experiments related with the deactivation of KEG415 with carbon dioxide.

Sample	Experiment	Description
I	1	Measurement of the nitrogen adsorption capacity at 20ºC of a sample of the zeolite regenerated in a muffle at 375ºC, for 12h and passing a dried air current through the adsorbent.
	2	Saturation at about 7 mbara of CO_2. Regeneration at 70ºC for 2h, using alternatively vacuum and helium at 8 bara.
	3	Regeneration in a muffle at 375ºC for 12h without passing a current of dried air through the adsorbent.

This experiment was repeated and the adsorbent was regenerated in a muffle at 375ºC with a current of dried air passing through the adsorbent and it was possible to recover the full adsorption capacity of the adsorbent.

The results of these experiments are presented in Figure 3.26.

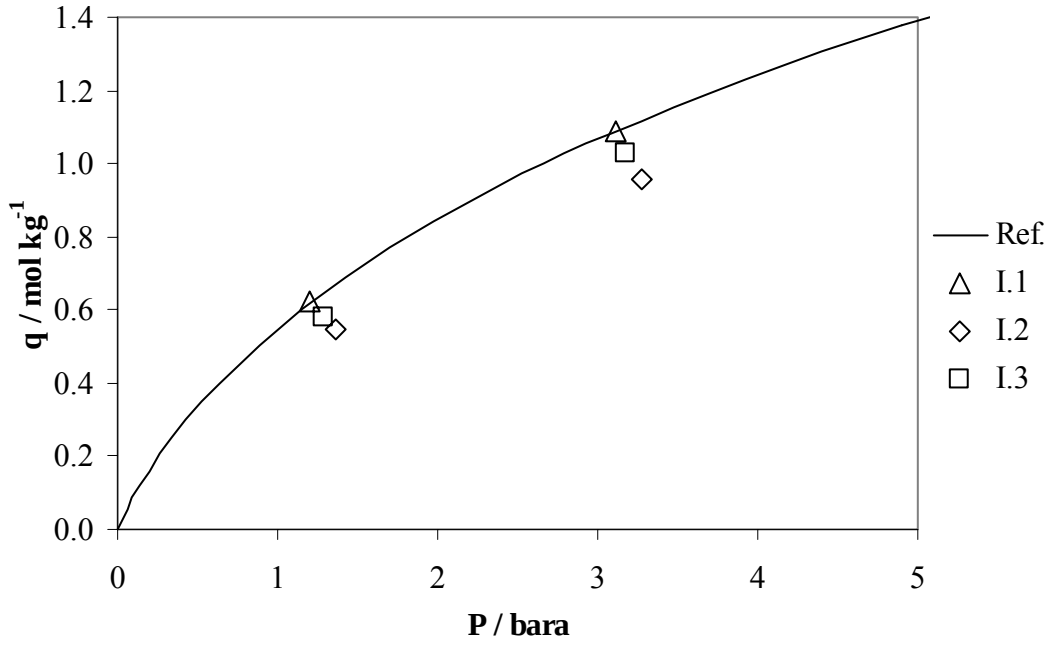

Figure 3.26. Nitrogen adsorption capacity at 20ºC. The reference adsorption isotherm (Ref.) is the nitrogen adsorption isotherm at 20ºC in a regenerated sample.

Analysing the results it is possible to conclude that the only way to recover the full adsorption capacity of this adsorbent is by regenerating it at 375ºC in a muffle and passing a dried air current through the adsorbent.

A study was conducted in a similar way, to evaluate the influence of water vapour in the adsorption capacity of KEG415. The experiments conducted are described in Table 3.22.

Table 3.22. Experiments related with the deactivation of KEG415 with water vapour.

Sample	Experiment	Description
II	1	Measurement of the nitrogen adsorption capacity at 20ºC of a sample of the zeolite regenerated in a muffle at 375ºC, for 12h and passing a dried air current through the adsorbent.
	2	Saturation with water vapour at 20ºC (about 23.4 mbara of water vapour). Regeneration at 70ºC for 2h using alternatively vacuum and helium at 8 bara.
	3	Regeneration in a muffle at 375ºC for 12h without passing a current of dried air through the adsorbent.

The amount of water vapour used is close to the amount that the adsorbents are exposed to during the operation of a pressure swing adsorption unit.

This experiment was repeated and the adsorbent was regenerated in a muffle at 375ºC with a current of dried air passing through the adsorbent and it was possible to recover the full adsorption capacity of the adsorbent.

The results of these experiments are presented in Figure 3.27.

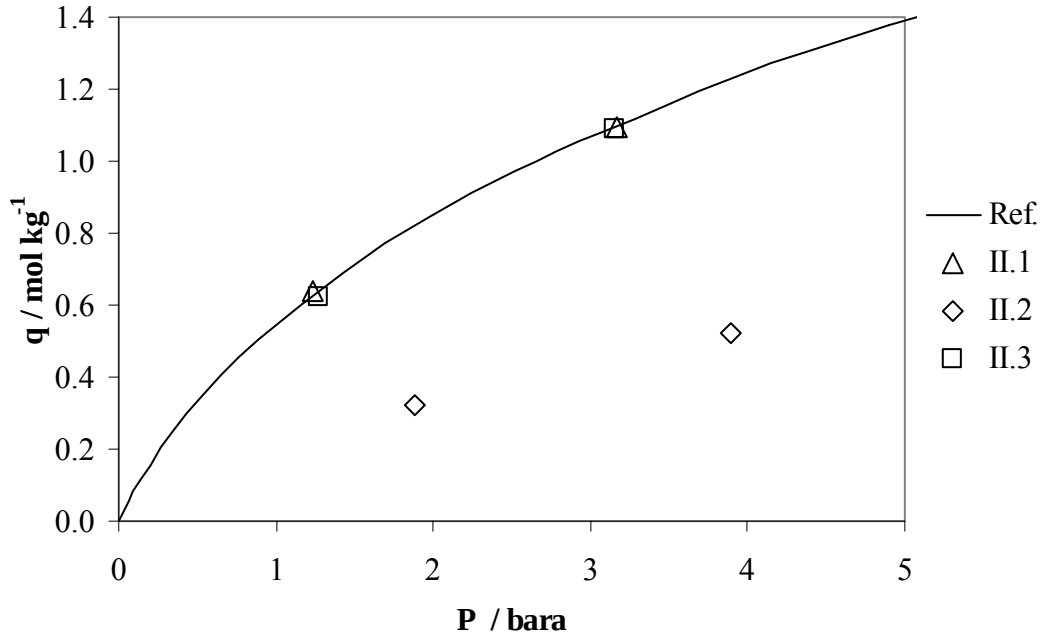

Figure 3.27. Nitrogen adsorption capacity at 20ºC. The reference adsorption isotherm (Ref.) is the isotherm of nitrogen at 20ºC in a sample regenerated.

Analysing the results it is possible to conclude that the only way to recover the full adsorption capacity of this adsorbent is by regenerating it in a muffle at 375ºC and passing a dried air current through the adsorbent.

A similar study was conducted for evaluating the influence of water vapour simultaneously with carbon dioxide in the adsorption capacity of KEG415. The experiments that were conducted are described in Table 3.23 .

Table 3.23. Experiments related with the deactivation of KEG415 with water vapour simultaneously with carbon dioxide.

Sample	Experiment	Description
III	1	Measurement of the nitrogen adsorption capacity at 20ºC in a sample of zeolite regenerated in a muffle at 375ºC, for 12h and passing a dried air current through the adsorbent.
	2	Saturation with water vapour and carbon dioxide at 20ºC. Regeneration at 70ºC for 2h using alternatively vacuum and helium at 8 bara.
	3	Regeneration in a muffle at 375ºC for 12h without passing a dried air current through the adsorbent.

This experiment was repeated and the adsorbent was regenerated in a muffle at 375ºC with a current of dried air passing through the adsorbent and it was possible to recover the full adsorption capacity of the adsorbent.

The amounts of water vapour and carbon dioxide are close to the amount these adsorbents are exposed to during the operation of a pressure swing adsorption unit.

The results of these experiments are presented in Figure 3.28.

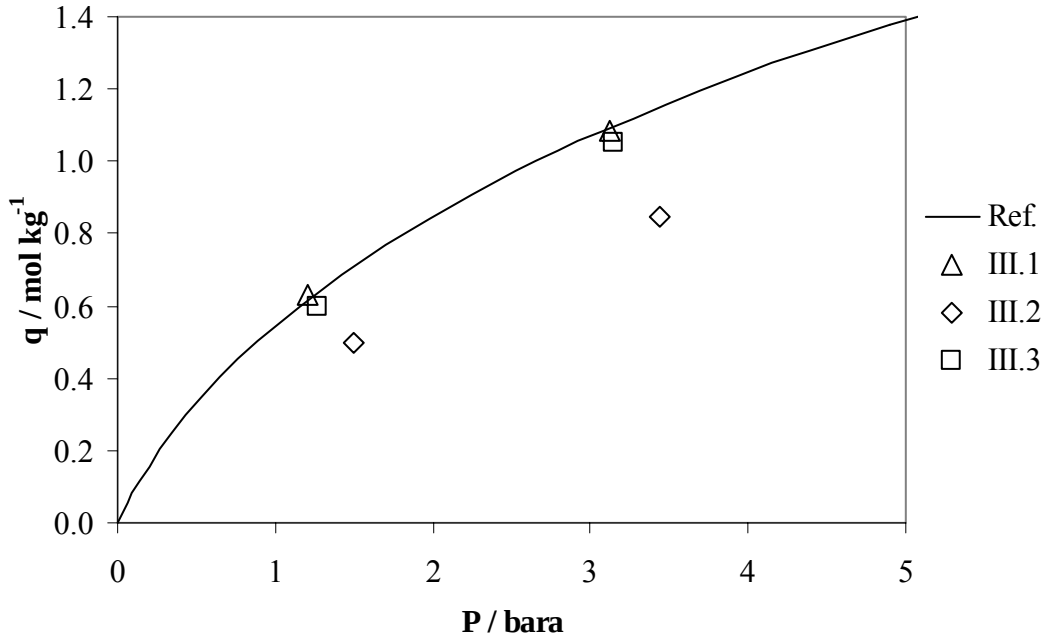

Figure 3.28. Nitrogen adsorption capacity at 20ºC. The reference adsorption isotherm (Ref.) is the nitrogen adsorption isotherm at 20ºC in a regenerated sample.

Analysing the results it is possible to conclude that the only way to recover the full adsorption capacity of this adsorbent is by regenerating it in a muffle at 375ºC and passing a dried air current through the adsorbent.

A 3.3.4 MS C 544 from Grace Davison

For evaluating the influence of carbon dioxide in the adsorption capacity of MS C 544, the nitrogen adsorption capacity was measured, at 20ºC, after some experiments where the zeolite was tried to be deactivated with carbon dioxide. These experiments are described in Table 3.24.

The amount of carbon dioxide used is close to the amount the adsorbents are exposed to during the operation of a pressure swing adsorption unit.

Table 3.24. Experiments related with the deactivation of MS C 544 with carbon dioxide.

Sample	Experiment	Description
I	1	Measurement of the nitrogen adsorption capacity at 20ºC of a sample of the zeolite regenerated in a muffle at 375ºC, for 12h and passing a dried air current through the adsorbent.
	2	Saturation at about 7 mbara of CO_2. Regeneration at 70ºC for 2h, using alternatively vacuum and helium at 8 bara.
	3	Regeneration in a muffle at 375ºC for 12h without passing a current of dried air through the adsorbent.

This experiment was repeated and the adsorbent was regenerated in a muffle at 375ºC with a current of dried air passing through the adsorbent and it was possible to recover the full adsorption capacity of the adsorbent.

The results of these experiments are presented in Figure 3.29.

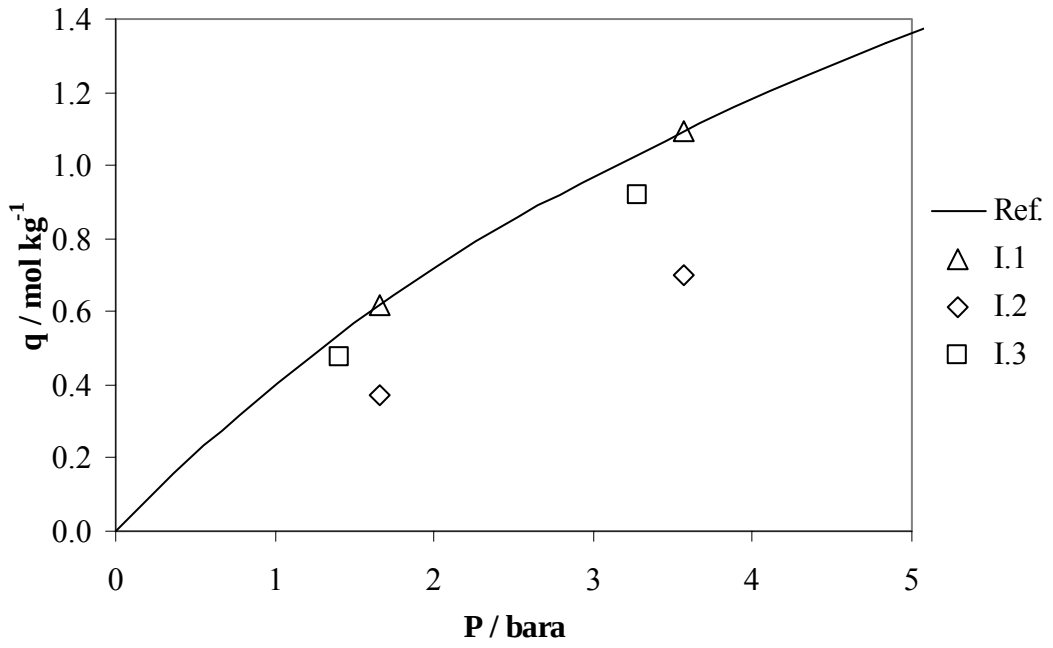

Figure 3.29. Nitrogen adsorption capacity at 20ºC. The reference adsorption isotherm (Ref.) is the nitrogen adsorption isotherm at 20ºC in a regenerated sample.

Analysing the results it is possible to conclude that the only way to recover the full adsorption capacity of this adsorbent is by regenerating it at 375ºC in a muffle and passing a dried air current through the adsorbent.

A study was conducted in a similar way, to evaluate the influence of water vapour in the adsorption capacity of MS C 544. The experiments conducted are described in Table 3.25.

Table 3.25. Experiments related with the deactivation of MS C 544 with water vapour.

Sample	Experiment	Description
II	1	Measurement of the nitrogen adsorption capacity at 20ºC of a sample of the zeolite regenerated in a muffle at 375ºC, for 12h and passing a dried air current through the adsorbent.
	2	Saturation with water vapour at 20ºC (about 23.4 mbara of water vapour). Regeneration at 70ºC for 2h using alternatively vacuum and helium at 8 bara.
	3	Regeneration in a muffle at 375ºC for 12h without passing a current of dried air through the adsorbent.

This experiment was repeated and the adsorbent was regenerated in a muffle at 375ºC with a current of dried air passing through the adsorbent and it was possible to recover the full adsorption capacity of the adsorbent.

The amount of water vapour used is close to the amount that the adsorbents are exposed to during the operation of a pressure swing adsorption unit.

The results of these experiments are presented in Figure 3.30.

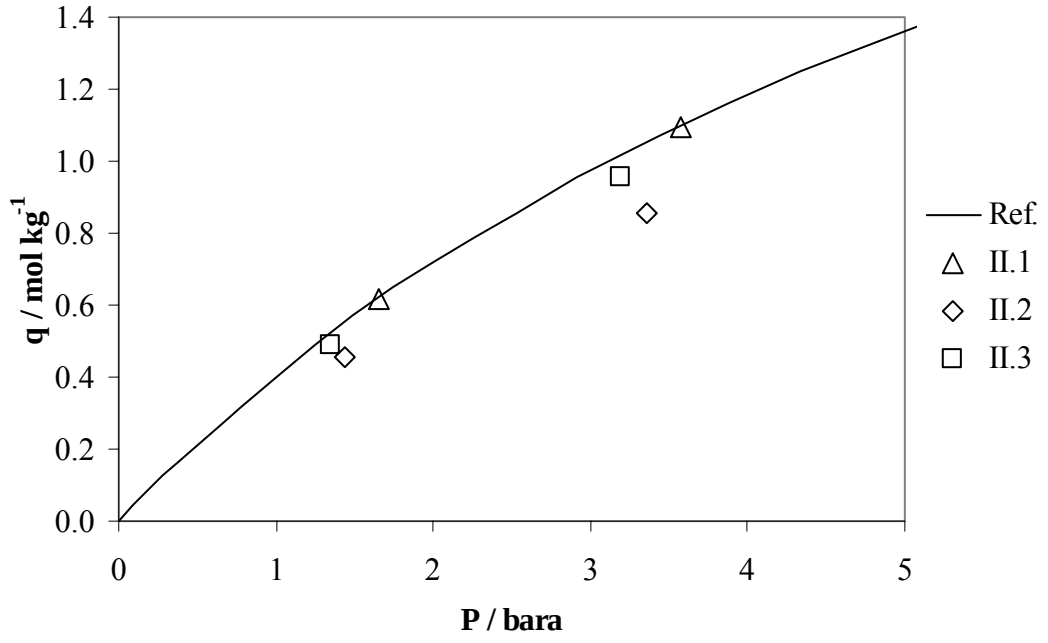

Figure 3.30. Nitrogen adsorption capacity at 20ºC. The reference adsorption isotherm (Ref.) is the isotherm of nitrogen at 20ºC in a sample regenerated.

Analysing the results it is possible to conclude that the only way to recover the full adsorption capacity of this adsorbent is by regenerating it in a muffle at 375ºC and passing a dried air current through the adsorbent.

A similar study was conducted for evaluating the influence of water vapour simultaneously with carbon dioxide in the adsorption capacity of MS C 544. The experiments that were conducted are described in Table 3.26.

Table 3.26. Experiments related with the deactivation of MS C 544 with water vapour simultaneously with carbon dioxide.

Sample	Experiment	Description
III	1	Measurement of the nitrogen adsorption capacity at 20ºC in a sample of zeolite regenerated in a muffle at 375ºC, for 12h and passing a dried air current through the adsorbent.
	2	Saturation with water vapour and carbon dioxide at 20ºC. Regeneration at 70ºC for 2h using alternatively vacuum and helium at 8 bara.
	3	Regeneration in a muffle at 375ºC for 12h without passing a dried air current through the adsorbent.

This experiment was repeated and the adsorbent was regenerated in a muffle at 375ºC with a current of dried air passing through the adsorbent and it was possible to recover the full adsorption capacity of the adsorbent.

The amounts of water vapour and carbon dioxide are close to the amount these adsorbents are exposed to during the operation of a pressure swing adsorption unit.

The results of these experiments are presented in Figure 3.31.

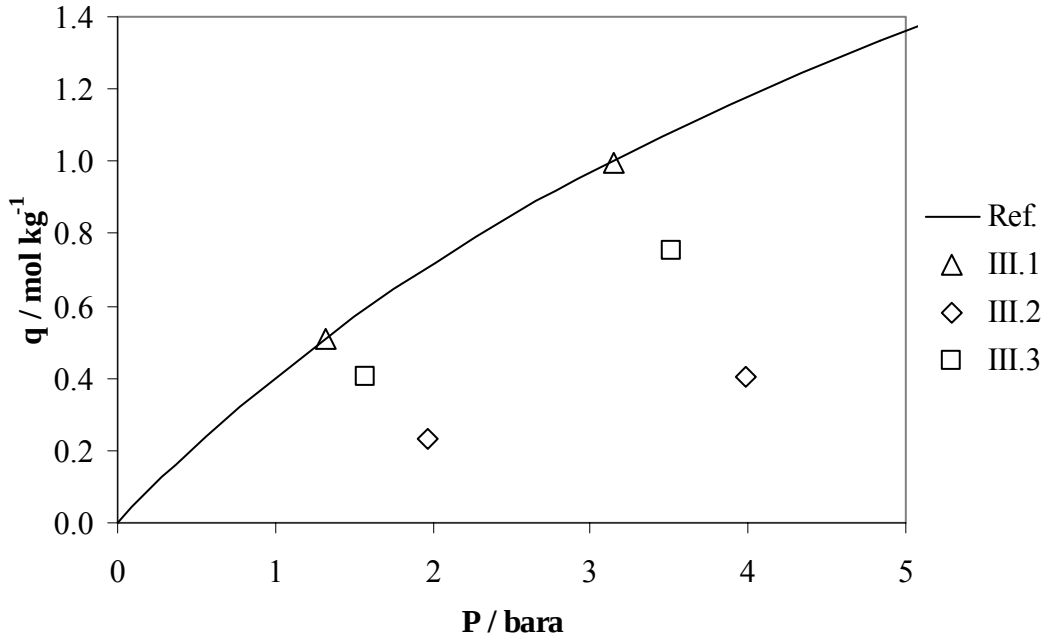

Figure 3.31. Nitrogen adsorption capacity at 20ºC. The reference adsorption isotherm (Ref.) is the nitrogen adsorption isotherm at 20ºC in a regenerated sample.

Analysing the results it is possible to conclude that the only way to recover the full adsorption capacity of this adsorbent is by regenerating it in a muffle at 375ºC and passing a dried air current through the adsorbent.

A 3.3.5 MS S 624 from Grace Davison

The nitrogen adsorption capacity was measured, at 20ºC, for evaluating the influence of carbon dioxide in the adsorption capacity of MS S 624, after some experiments where the zeolite was tried to be deactivated with carbon dioxide. These experiments are described in Table 3.27.

The amount of carbon dioxide used is close to the amount the adsorbents are exposed to during the operation of a pressure swing adsorption unit.

Table 3.27. Experiments related with the deactivation of MS S 624 with carbon dioxide.

Sample	Experiment	Description
I	1	Measurement of the nitrogen adsorption capacity at 20ºC of a sample of the zeolite regenerated in a muffle at 375ºC, for 12h and passing a dried air current through the adsorbent.
	2	Saturation at about 7 mbara of CO_2. Regeneration at 70ºC for 2h, using alternatively vacuum and helium at 8 bara.
	3	Regeneration in a muffle at 375ºC for 12h without passing a current of dried air through the adsorbent.

This experiment was repeated and the adsorbent was regenerated in a muffle at 375ºC with a current of dried air passing through the adsorbent and it was possible to recover the full adsorption capacity of the adsorbent.

The results of these experiments are presented in Figure 3.32.

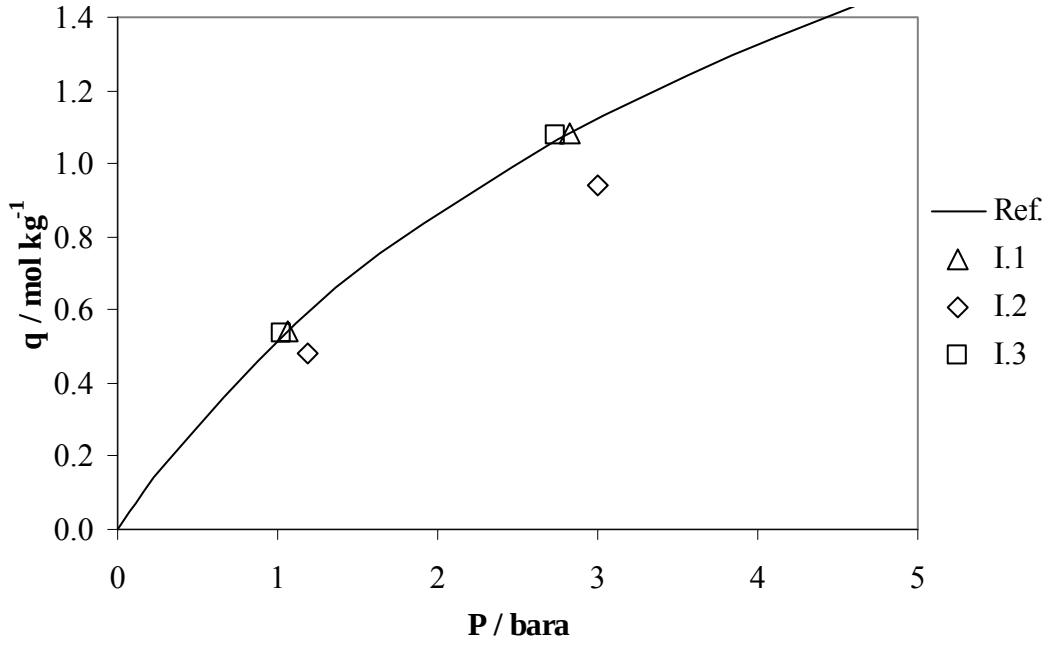

Figure 3.32. Nitrogen adsorption capacity at 20ºC. The reference adsorption isotherm (Ref.) is the nitrogen adsorption isotherm at 20ºC in a regenerated sample.

Analysing the results it is possible to conclude that the only way to recover the full adsorption capacity of this adsorbent is by regenerating it at 375ºC in a muffle and passing a dried air current through the adsorbent.

A study was conducted in a similar way, to evaluate the influence of water vapour in the adsorption capacity of MS S 624. The experiments conducted are described in Table 3.28.

Table 3.28. Experiments related with the deactivation of MS S 624 with water vapour.

Sample	Experiment	Description
II	1	Measurement of the nitrogen adsorption capacity at 20ºC of a sample of the zeolite regenerated in a muffle at 375ºC, for 12h and passing a dried air current through the adsorbent.
	2	Saturation with water vapour at 20ºC (about 23.4 mbara of water vapour). Regeneration at 70ºC for 2h using alternatively vacuum and helium at 8 bara.
	3	Regeneration in a muffle at 375ºC for 12h without passing a current of dried air through the adsorbent.

This experiment was repeated and the adsorbent was regenerated in a muffle at 375ºC with a current of dried air passing through the adsorbent and it was possible to recover the full adsorption capacity of the adsorbent.

The amount of water vapour used is close to the amount that the adsorbents are exposed to during the operation of a pressure swing adsorption unit.

The results of these experiments are presented in Figure 3.33.

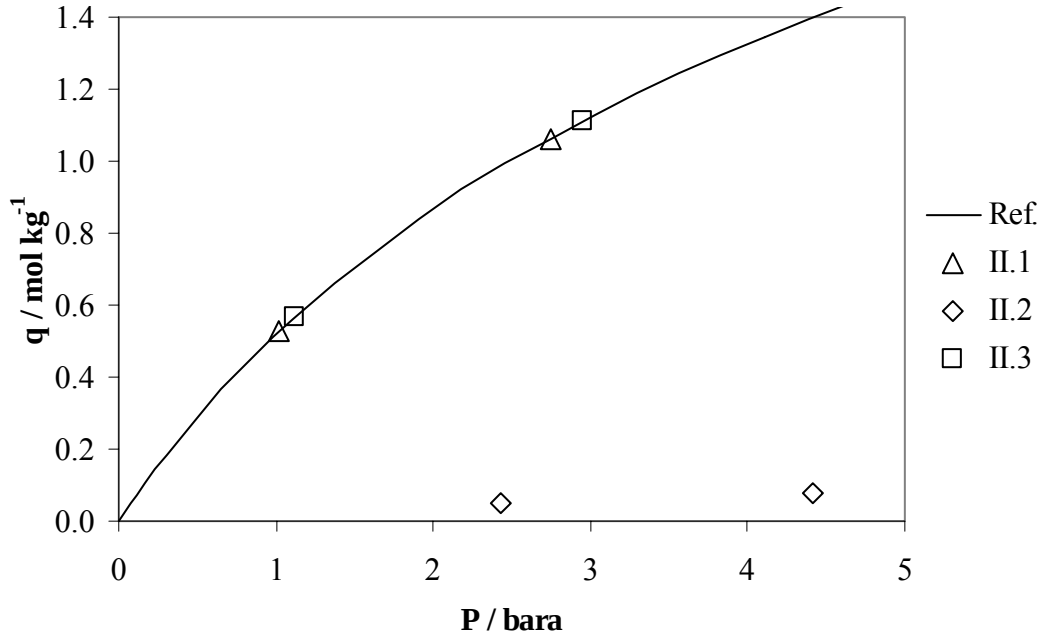

Figure 3.33. Nitrogen adsorption capacity at 20ºC. The reference adsorption isotherm (Ref.) is the isotherm of nitrogen at 20ºC in a sample regenerated.

A similar study was conducted for evaluating the influence of water vapour simultaneously with carbon dioxide in the adsorption capacity of MS S 624. The experiments that were conducted are described in Table 3.29.

Table 3.29. Experiments related with the deactivation of MS S 624 with water vapour simultaneously with carbon dioxide.

Sample	Experiment	Description
III	1	Measurement of the nitrogen adsorption capacity at 20ºC in a sample of zeolite regenerated in a muffle at 375ºC, for 12h and passing a dried air current through the adsorbent.
	2	Saturation with water vapour and carbon dioxide at 20ºC. Regeneration at 70ºC for 2h using alternatively vacuum and helium at 8 bara.
	3	Regeneration in a muffle at 375ºC for 12h without passing a dried air current through the adsorbent.

The amounts of water vapour and carbon dioxide are close to the amount these adsorbents are exposed to during the operation of a pressure swing adsorption unit.

The results of these experiments are presented in Figure 3.34.

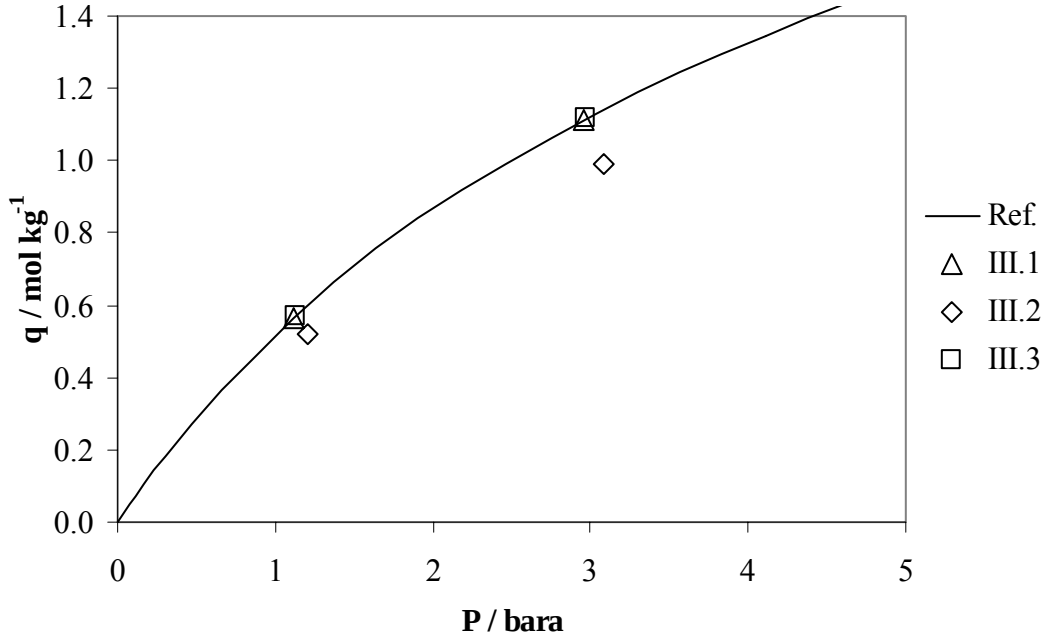

Figure 3.34. Nitrogen adsorption capacity at 20ºC. The reference adsorption isotherm (Ref.) is the nitrogen adsorption isotherm at 20ºC in a regenerated sample.

This experiment was repeated and the adsorbent was regenerated in a muffle at 375ºC with a current of dried air passing through the adsorbent and it was possible to recover the full adsorption capacity of the adsorbent.

Analysing the results it is possible to conclude that the only way to recover the full adsorption capacity of this adsorbent is by regenerating it in a muffle at 375ºC and passing a dried air current through the adsorbent.

A 3.3.6 Oxysiv MDX from UOP

The nitrogen adsorption capacity was measured, at 20ºC, for evaluating the influence of carbon dioxide in the adsorption capacity of Oxysiv MDX, after some experiments where the zeolite was tried to be deactivated with carbon dioxide. These experiments are described in Table 3.30.

Table 3.30. Experiments related with the deactivation of Oxysiv MDX with carbon dioxide.

Sample	Experiment	Description
I	1	Measurement of the nitrogen adsorption capacity at 20ºC of a sample of the zeolite regenerated in a muffle at 375ºC, for 12h and passing a dried air current through the adsorbent.
	2	Saturation at about 7 mbara of CO_2. Regeneration at 70ºC for 2h, using alternatively vacuum and helium at 8 bara.
	3	Regeneration in a muffle at 375ºC for 12h without passing a current of dried air through the adsorbent.

The amount of carbon dioxide used is close to the amount the adsorbents are exposed to during the operation of a pressure swing adsorption unit.

This experiment was repeated and the adsorbent was regenerated in a muffle at 375ºC with a current of dried air passing through the adsorbent and it was possible to recover the full adsorption capacity of the adsorbent.

The results of these experiments are presented in Figure 3.35.

Analysing the results it is possible to conclude that the only way to recover the full adsorption capacity of this adsorbent is by regenerating it at 375ºC in a muffle and passing a dried air current through the adsorbent.

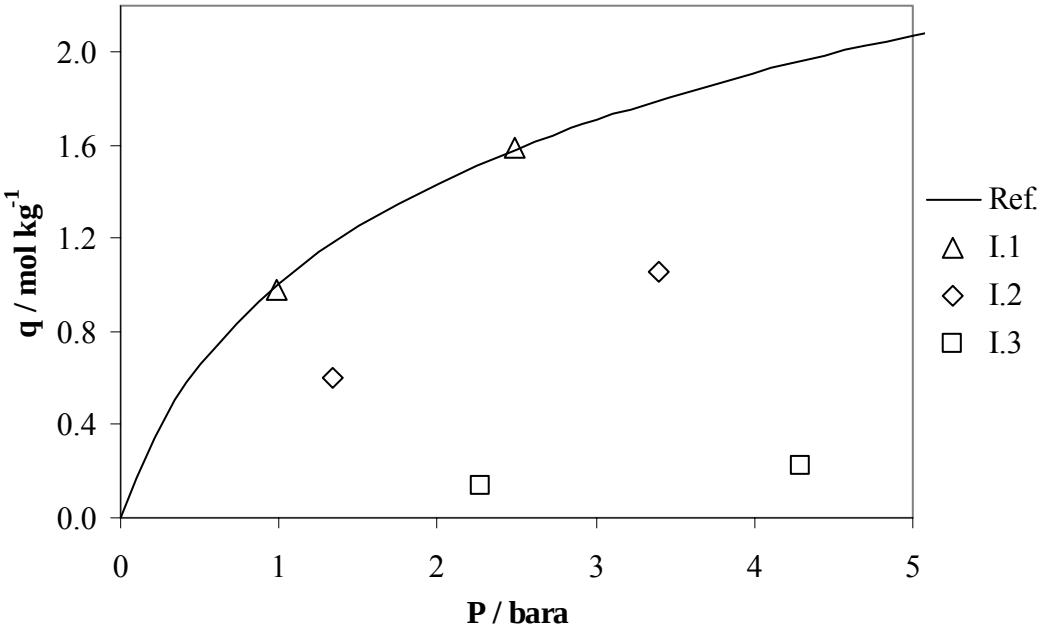

Figure 3.35. Nitrogen adsorption capacity at 20ºC. The reference adsorption isotherm (Ref.) is the nitrogen adsorption isotherm at 20ºC in a regenerated sample.

A study was conducted in a similar way, to evaluate the influence of water vapour in the adsorption capacity of Oxysiv MDX. The experiments conducted are described in Table 3.31.

Table 3.31. Experiments related with the deactivation of Oxysiv MDX with water vapour.

Sample	Experiment	Description
II	1	Measurement of the nitrogen adsorption capacity at 20ºC of a sample of the zeolite regenerated in a muffle at 375ºC, for 12h and passing a dried air current through the adsorbent.
	2	Saturation with water vapour at 20ºC (about 23.4 mbara of water vapour). Regeneration at 70ºC for 2h using alternatively vacuum and helium at 8 bara.
	3	Regeneration in a muffle at 375ºC for 12h without passing a current of dried air through the adsorbent.

This experiment was repeated and the adsorbent was regenerated in a muffle at 375ºC with a current of dried air passing through the adsorbent and it was possible to recover the full adsorption capacity of the adsorbent.

The amount of water vapour used is close to the amount that the adsorbents are exposed to during the operation of a pressure swing adsorption unit.

The results of these experiments are presented in Figure 3.36.

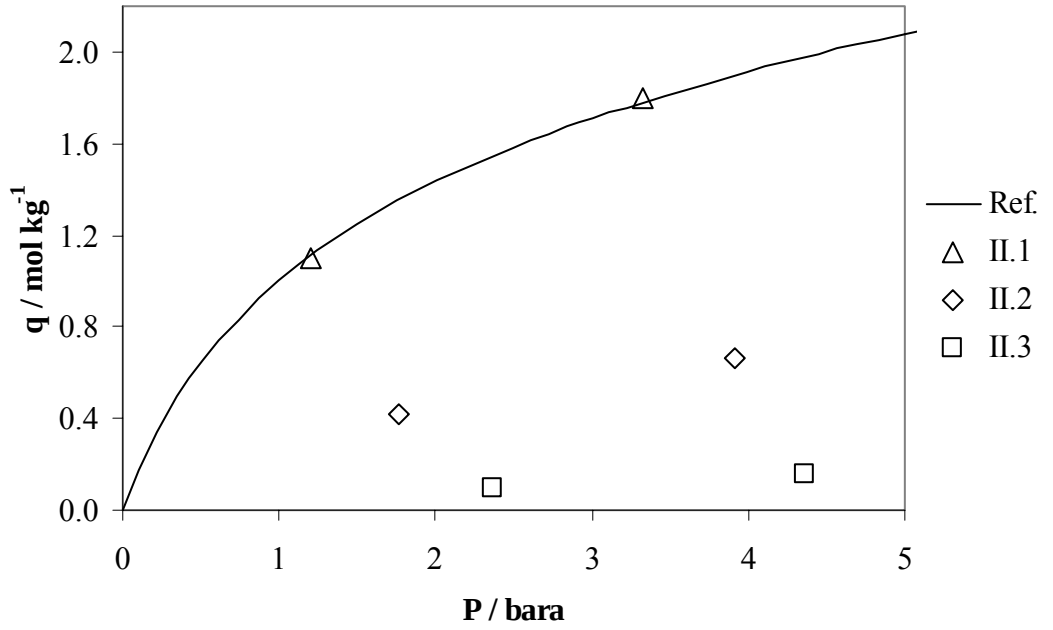

Figure 3.36. Nitrogen adsorption capacity at 20ºC. The reference adsorption isotherm (Ref.) is the isotherm of nitrogen at 20ºC in a sample regenerated.

Analysing the results it is possible to conclude that the only way to recover the full adsorption capacity of this adsorbent is by regenerating it in a muffle at 375ºC and passing a dried air current through the adsorbent.

A similar study was carried out for evaluating the influence of water vapour simultaneously with carbon dioxide in the adsorption capacity of Oxysiv MDX. The experiments conducted are described in Table 3.32.

The amounts of water vapour and carbon dioxide are close to the amount these adsorbents are exposed to during the operation of a pressure swing adsorption unit.

This experiment was repeated and the adsorbent was regenerated in a muffle at 375ºC with a current of dried air passing through the adsorbent and it was possible to recover the full adsorption capacity of the adsorbent.

Table 3.32. Experiments related with the deactivation of Oxysiv MDX with water vapour simultaneously with carbon dioxide.

Sample	Experiment	Description
III	1	Measurement of the nitrogen adsorption capacity at 20ºC in a sample of zeolite regenerated in a muffle at 375ºC, for 12h and passing a dried air current through the adsorbent.
	2	Saturation with water vapour and carbon dioxide at 20ºC. Regeneration at 70ºC for 2h using alternatively vacuum and helium at 8 bara.
	3	Regeneration in a muffle at 375ºC for 12h without passing a dried air current through the adsorbent.

The results of these experiments are presented in Figure 3.37.

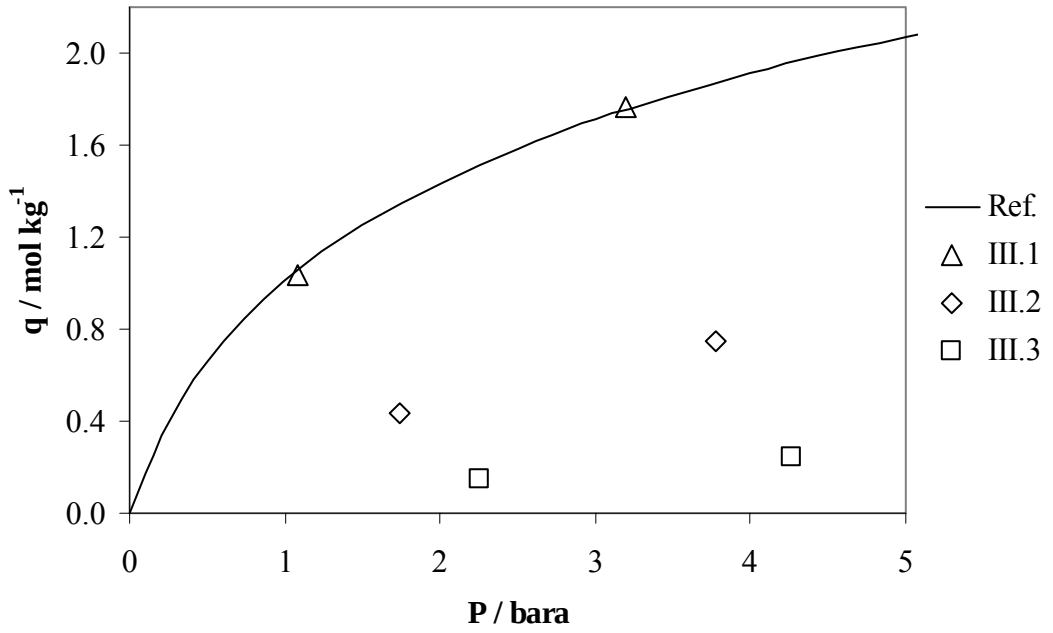

Figure 3.37. Nitrogen adsorption capacity at 20ºC. The reference adsorption isotherm (Ref.) is the nitrogen adsorption isotherm at 20ºC in a regenerated sample.

Analysing the results it is possible to conclude that the only way to recover the full adsorption capacity of this adsorbent is by regenerating it in a muffle at 375ºC and passing a dried air current through the adsorbent.

A 3.3.7 AgLiLSX from UOP

The nitrogen adsorption capacity was measured, at 20ºC, for evaluating the influence of carbon dioxide in the adsorption capacity of AgLiLSX, after some experiments where the zeolite was tried to be deactivated with carbon dioxide. These experiments are described in Table 3.33.

Table 3.33. Experiments related with the deactivation of AgLiLSX with carbon dioxide.

Sample	Experiment	Description
I	1	Measurement of the nitrogen adsorption capacity at 20ºC of a sample of the zeolite regenerated in a muffle at 375ºC, for 12h and passing a dried air current through the adsorbent.
	2	Saturation at about 7 mbara of CO_2. Regeneration at 70ºC for 2h, using alternatively vacuum and helium at 8 bara.
	3	Regeneration in a muffle at 375ºC for 12h without passing a current of dried air through the adsorbent.

The amount of carbon dioxide used is close to the amount the adsorbents are exposed to during the operation of a pressure swing adsorption unit.

This experiment was repeated and the adsorbent was regenerated in a muffle at 375ºC with a current of dried air passing through the adsorbent and it was possible to recover the full adsorption capacity of the adsorbent.

The results of these experiments are presented in Figure 3.38.

Analysing the results it is possible to conclude that the only way to recover the full adsorption capacity of this adsorbent is by regenerating it at 375ºC in a muffle and passing a dried air current through the adsorbent.

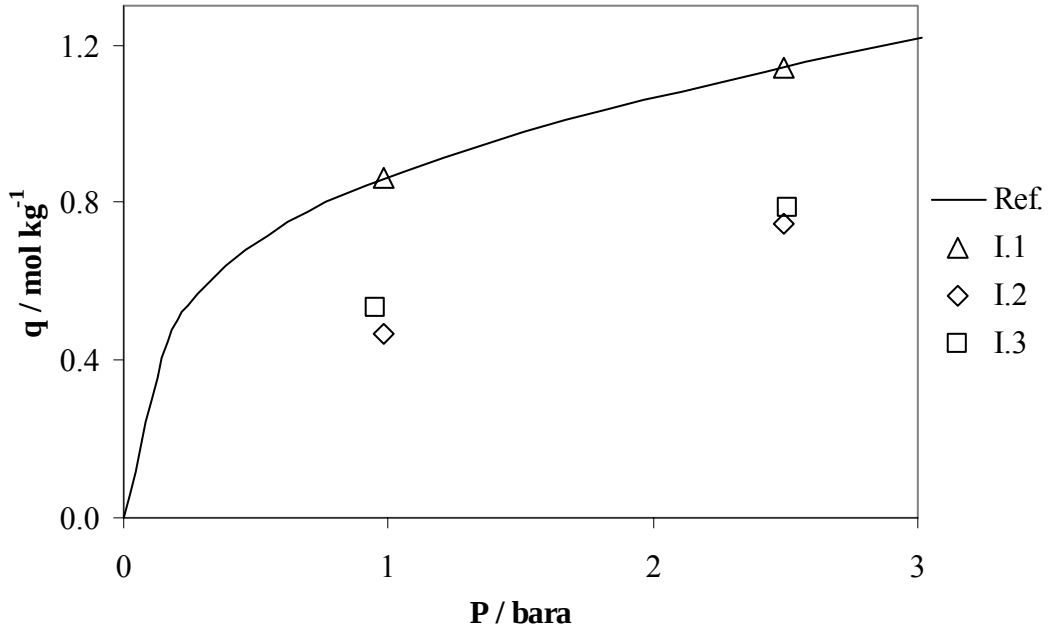

Figure 3.38. Nitrogen adsorption capacity at 20ºC. The reference adsorption isotherm (Ref.) is the nitrogen adsorption isotherm at 20ºC in a regenerated sample.

A study was conducted in a similar way, to evaluate the influence of water vapour in the adsorption capacity of AgLiLSX. The experiments conducted are described in Table 3.34.

Table 3.34. Experiments related with the deactivation of AgLiLSX with water vapour.

Sample	Experiment	Description
II	1	Measurement of the nitrogen adsorption capacity at 20ºC of a sample of the zeolite regenerated in a muffle at 375ºC, for 12h and passing a dried air current through the adsorbent.
	2	Saturation with water vapour at 20ºC (about 23.4 mbara of water vapour). Regeneration at 70ºC for 2h using alternatively vacuum and helium at 8 bara.
	3	Regeneration in a muffle at 375ºC for 12h without passing a current of dried air through the adsorbent.

This experiment was repeated and the adsorbent was regenerated in a muffle at 375ºC with a current of dried air passing through the adsorbent and it was possible to recover the full adsorption capacity of the adsorbent.

The amount of water vapour used is close to the amount that the adsorbents are exposed to during the operation of a pressure swing adsorption unit.

The results of these experiments are presented in Figure 3.39.

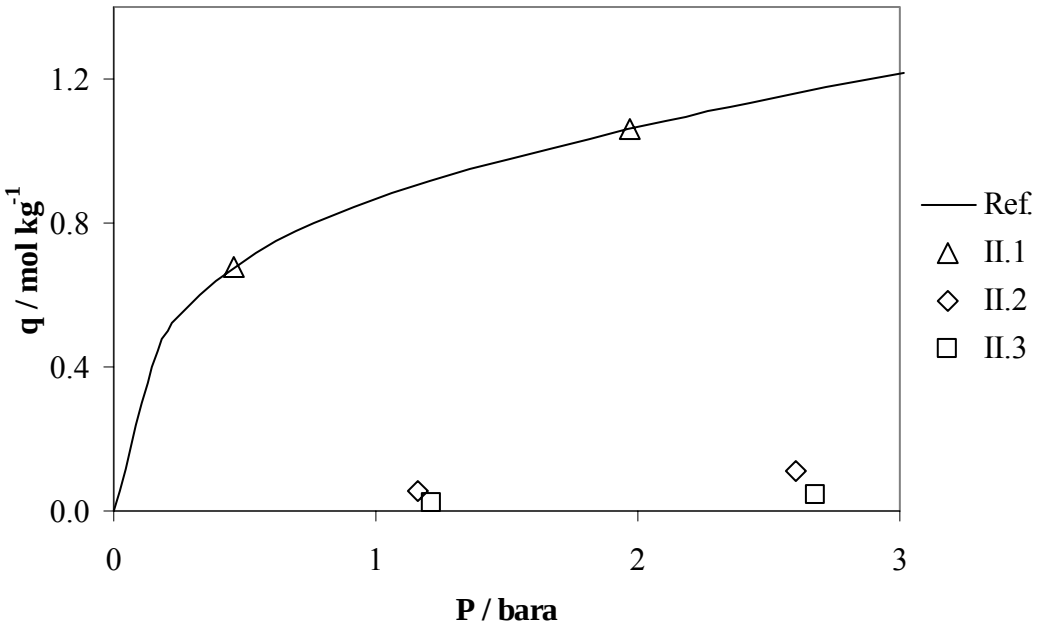

Figure 3.39. Nitrogen adsorption capacity at 20ºC. The reference adsorption isotherm (Ref.) is the isotherm of nitrogen at 20ºC in a sample regenerated.

Analysing the results it is possible to conclude that the only way to recover the full adsorption capacity of this adsorbent is by regenerating it in a muffle at 375ºC and passing a dried air current through the adsorbent.

A similar study was carried out for evaluating the influence of water vapour simultaneously with carbon dioxide in the adsorption capacity of AgLiLSX. The experiments conducted are described in Table 3.35.

The amounts of water vapour and carbon dioxide are close to the amount these adsorbents are exposed to during the operation of a pressure swing adsorption unit.

This experiment was repeated and the adsorbent was regenerated in a muffle at 375ºC with a current of dried air passing through the adsorbent and it was possible to recover the full adsorption capacity of the adsorbent.

Table 3.35. Experiments related with the deactivation of AgLiLSX with water vapour simultaneously with carbon dioxide.

Sample	Experiment	Description
III	1	Measurement of the nitrogen adsorption capacity at 20ºC in a sample of zeolite regenerated in a muffle at 375ºC, for 12h and passing a dried air current through the adsorbent.
	2	Saturation with water vapour and carbon dioxide at 20ºC. Regeneration at 70ºC for 2h using alternatively vacuum and helium at 8 bara.
	3	Regeneration in a muffle at 375ºC for 12h without passing a dried air current through the adsorbent.

The results of these experiments are presented in Figure 3.40.

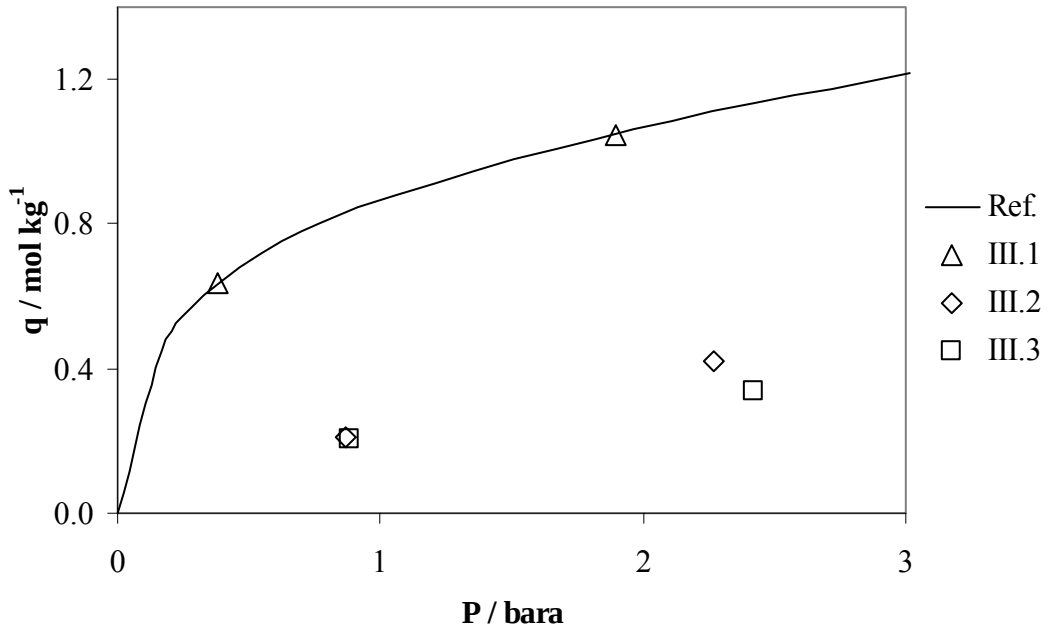

Figure 3.40. Nitrogen adsorption capacity at 20ºC. The reference adsorption isotherm (Ref.) is the nitrogen adsorption isotherm at 20ºC in a regenerated sample.

Analysing the results it is possible to conclude that the only way to recover the full adsorption capacity of this adsorbent is by regenerating it in a muffle at 375ºC and passing a dried air current through the adsorbent.

4. Mass Transport

4.1 Introduction

For the simulation, optimization and design of pressure swing adsorption (PSA) units, it is important to characterize the mass transport in the adsorbents used. Several approximations may be found for modelling the mass transport. An extensive review can be found in the work of Cruz (Cruz, 2003). This author divides the approximations in four groups: truncation of the analytical series, polynomial approximation of the particle concentration profile, use of efficient numerical methods for solving the particle mass balance and empirical and semi-empirical approximations.

The first approach was presented by Glueckauf in 1955 where the truncation of the variation of the concentration at the surface of the particle represented by an infinite series, leads to the linear driving force (LDF) model (Cruz, 2003). This model was also obtained by Liaw et al. in 1979 considering a parabolic concentration profile inside the particle (Cruz, 2003). Several other approximations are referred but for oxygen separation from air, which is governed by the adsorption equilibrium, the use of more complex models leads only to small differences on the results and to the increase of the computational time (Farooq et al., 1989).

Two methods may be used for determining the mass transport of the adsorbents: zero length column (Brandani and Ruthven, 2003, Brandani et al., 2003, Brandani, 1998, Brandani and Ruthven, 1996a, b, Brandani et al., 1996, Eic and Ruthven, 1988) and a gravimetric method (Ruthven et al., 1980).

In the zero length column (ZLC) method, some particles of the adsorbent are placed inside a small tube and a mixture of the carrier gas (helium, for example) and the gas in study is passed trough the adsorbent. By the analysis of one of the properties of the gas (thermal conductivity, for instance) along time and relating it with the concentration of the mixture, it is possible to determine the diffusivity.

For the gravimetric method, a magnetic suspension balance may be used for following the mass change along time of a sample of the adsorbent after a perturbation of the pressure of the gas inside the chamber of the balance. From this analysis the diffusivity of the gas may be determined.

In this Chapter, the critical characteristics of the adsorbents needed for the simulation of adsorption separation processes are presented as well as an estimate of the mass transfer coefficients.

4.2 Mass transport characterization

4.2.1 Gas flux in pores

4.2.1.1 Knudsen diffusion

This type of transport is due to the collisions of the molecules with the walls of the pores. The driving force is the partial concentration gradient and the parameter which characterizes it is the Knudsen diffusivity for species i, $D_{K,i}$. Knudsen diffusion depends of the molecular weight of the species that diffuses and the pore diameter. For the same concentration gradient, the molecules with a lower molecular weight travel faster than the ones with a higher molecular weight (Do, 1998).

The Knudsen diffusivity may be obtained by the following expression (Do, 1998):

$$D_K = \frac{2r_p}{3}\sqrt{\frac{8\Re T}{\pi M}}, \tag{4.1}$$

where r_p is the pore radius, $\Re$ is the universal gas constant, T is the absolute temperature and M the molecular weight. The effective Knudsen diffusivity, $D^e_{K,i}$, is given by (Do, 1998):

$$D^e_{K,i} = D_{K,i}/\tau, \tag{4.2}$$

where τ is the pore tortuosity. In zeolites, the typical value for tortuosity is 3 (Farooq et al., 1989).

4.2.1.2 Molecular diffusion

In this type of transport, the collisions between molecules are dominant relatively to the collisions with the walls. The parameter that characterizes this type of

transport is the binary diffusion coefficient, D_{ij}, of the species i and j. Due to the dependency of this parameter on the collisions between molecules, the binary diffusivity is a function of the total pressure and temperature (Do, 1998).

The binary diffusivity, expressed in cm^2/s, may be computed by the Chapman-Enskog equation (Do, 1998):

$$D_{12} = 0.0018583 \frac{\sqrt{T^3 \left(\frac{1}{M_1} + \frac{1}{M_2} \right)}}{P \sigma_{12}^2 \Omega_{D,12}}, \tag{4.3}$$

where P is the total pressure, expressed in atm, T is the absolute temperature, expressed in K, σ_{12} is the collision diameter, expressed in Å and $\Omega_{D,12}$ is a dimensionless function of the temperature and of the intermolecular potential field for a molecule of species 1 and a molecule of species 2. For non-polar molecules and for molecules that do not interact between themselves, the Lennard-Jones parameters may be used for species 1 and 2 (Do, 1998):

$$\sigma_{12} = \frac{\sigma_{11} + \sigma_{22}}{2}; \ \varepsilon_{12} = \sqrt{\varepsilon_{11} \varepsilon_{22}} \ . \tag{4.4}$$

Table 4.1 presents the Lennard-Jones parameters for oxygen, nitrogen and argon (Bird et al., 1960).

Table 4.1. Lennard-Jones parameters.

Gas	σ (Å)	ε/κ (K)
Nitrogen	3.681	91.5
Oxygen	3.433	113.0
Argon	3.418	124.0

The parameter $\Omega_{D,12}$ may be obtained from tables (Table B-2 from Bird *et al.*, 1960, for example) or computed from the following expression (Do, 1998):

$$\Omega_{D,12} = \frac{A}{\left(T^*\right)^B} + \frac{C}{\exp\left(DT^*\right)} + \frac{E}{\exp\left(FT^*\right)} + \frac{G}{\exp\left(HT^*\right)}; \ T^* = \frac{\kappa T}{\varepsilon_{12}}, \tag{4.5}$$

where T is the absolute temperature and the parameters A, B, C, D, E, F, G and H are:

A=1.06036 ; B=0.15610 ; C=0.19300 ; D=0.47635

E=1.03587 ; F=1.52996 ; G=1.76474 ; H=3.89411

4.2.1.3 Combination of the mechanisms Knudsen diffusion and molecular diffusion

According to the model based in the Fick law, the driving force is the concentration gradient. The parameter that characterizes the transport model is the coefficient of effective diffusivity in pores, $D^{e}_{p,i}$, computed by Bosanquet's formula (Cruz, 2003):

$$\frac{1}{D^{e}_{p,i}} = \frac{1}{D^{e}_{K,i}} + \frac{1}{D^{e}_{i,j}} \tag{4.6}$$

By its turn, the coefficient of effective mass diffusion, $D^{e}_{M,i}$, is given by the following expression (Cruz, 2003):

$$D^{e}_{M,i} = \frac{\varepsilon D^{e}_{p,i}}{\varepsilon + dq/dc}, \tag{4.7}$$

where ε is the adsorbent porosity, q is the concentration of the adsorbed phase and c is the concentration of the fluid phase. For a linear isotherm, $dq/dc = q_{ref}/c_{ref}$, where q_{ref} is the reference concentration of the adsorbed phase and c_{ref} is the reference concentration of the fluid phase.

4.3 Characterization of the adsorbents

4.3.1 Pore size distribution

Pores may be classified according to their sizes as macropores (diameter larger than 50nm), mesopores (diameter between 2 and 50nm), and micropores (diameter inferior than 2nm) (Figueiredo and Ramôa Ribeiro, 1989).

The macro- and mesopore size distribution may be obtained by mercury porosimetry.

Mercury contact angle, ϕ, is of 140º and therefore an excess of pressure, ΔP, must be applied for forcing the liquid to penetrate in the pores.

Considering a cylindrical pore with radius r_p, and making the force applied equal to the force due to the surface tension, it is possible to obtain the following expression (Washburn, 1921):

$$r_p = \frac{-2\sigma_S \cos\phi}{\Delta P}, \tag{4.8}$$

where σ_s is the surface tension which for mercury is of 0.480 N/m.

Mercury porosimetry consists in applying a given hydrostatic pressure and measuring the volume of mercury that penetrates in the solid. For each value of the pressure applied, ΔP_i, mercury penetrates in the pores with a radius higher than $r_{p,i}$, given by Equation (4.8). The pore size distribution consists in progressively increasing the pressure and measuring continuously the increase of volume of liquid that penetrates in pores (Gregg and Sing, 1982).

4.4 Models for mass transport

4.4.1 Linear driving force (LDF)

The linear driving force model (LDF), corresponds to a first order delay and may be deduced considering a parabolic profile inside the particle (Liaw et al., 1979). This hypothesis is only valid for long cycles (Sheng and Costa, 1997). The use of such a simple model is justified by the system type: for separations governed by the equilibrium, the use of more complex models leads only to small differences on the results and to the increase of the computational time (Farooq et al., 1989). The LDF model may be written as follows:

$$\frac{\partial \overline{q}_i}{\partial t} = k_i (q_{s,i} - \overline{q}_i), \tag{4.9}$$

where t is the time, q_i is the molar concentration of component *i* in the adsorbed phase, $q_{s,i}$ is the molar concentration of component *i* in the adsorbed phase, in the surface, $\overline{q}_i$ is the average molar concentration of component *i* in the adsorbed phase and k_i is the LDF kinetic coefficient of component *i*, given by:

$$k_i = 15\frac{D^{e}_{M,i}}{r^2}, \tag{4.10}$$

where r is the particle radius.

4.5 Experimental part

4.5.1 Particles and pores average diameters and porosity of the adsorbents

Table 4.2 presents the average pores diameter and porosity of the adsorbents Oxysiv 5, Oxysiv 7, KEG 415 and Oxysiv MDX from UOP; MS C 544 and MS S 624 from Grace Davison and AgLiLSX from Air Products and Chemicals, Inc. These values were obtained by mercury porosimetry. The average particle diameters are also presented and were determined by a particle size distribution analyser (Coulter Counter, model LS230 *small volume module plus*). This analyser allows the determination of the distribution of particles with diameters between 0.04 and 2000 μm.

Table 4.2. Average diameters and porosity of the adsorbents.

Adsorbent	Average pore diameter (μm)	Porosity	Average particle diameter (mm)
Oxysiv 5	0.5	0.336	0.61
Oxysiv 7	0.5	0.338	0.58
KEG415	0.7	0.365	1.70
Oxysiv MDX	0.4	0.315	0.61
MS S 624	0.8	0.253	2.10*
MS C 544	0.8	0.253	2.05*
AgLiLSX	0.5	0.471	1.01

* Data supplied by the manufacturer.

The porosimeter used was from Quantachrome, model POREMASTER 60 and allows the determination of the pore size distribution of pores with a diameter from 200 μm to 35 Å, analysing the intrusion and extrusion of mercury in the pores. The determination of the pore size distribution is composed by two operations: measurement at low pressures (from 0.5 to 50 psi) and measurement at high pressures (from 20 to 60000 psi).

4.5.2 LDF kinetic coefficients

Some experiments were conducted for determining the diffusivity of the adsorbents and so, obtaining the LDF kinetic coefficients. The zero length column (ZLC) method and the gravimetric method (using the magnetic suspension balance from Rubotherm) were used. Due to the very fast mass transport of oxygen, nitrogen and argon inside the particles of all the adsorbents studied neither of these two methods was able to give any result. Ruthven and Xu (1993) also tried to use the ZLC method for determining the mass transfer coefficients of a 5A type zeolite and also concluded that the diffusion of oxygen and nitrogen is to rapid to measure. They managed to measure it only at low temperatures (174 K and 193 K). For this reason, the correlations presented before were used to obtain an estimate of the LDF kinetic coefficients. These coefficients, at 1 bara and 20ºC, are presented in Table 4.3.

Table 4.3. LDF kinetic coefficient at 1 bara and 20ºC, for the adsorbents.

Adsorbent	k (s^{-1})	
	N_2	O_2
Oxysiv 5	15.5	40.8
Oxysiv 7	10.5	66.0
KEG415	0.9	2.7
Oxysiv MDX	4.2	34.3
MS S 624	0.7	1.9
MS C 544	1.6	4.3
AgLiLSX	2.0	20.2

As it can be seen, at 1 bara and 20ºC, Oxysiv 5 is the adsorbent with a fastest mass transfer for nitrogen and MS S 624 with the slowest.

4.6 Conclusions

The adsorbents physical properties (pore size distribution, porosity and particle diameter) were presented.

The LDF kinetic coefficients were tried to be obtained experimentally by the method zero length column (ZLC) and by a gravimetric method but due to the fast mass transport of oxygen, nitrogen and argon inside the adsorbent, none of the methods was able to give any result. For this reason, empirical correlations were used for evaluating this parameters for the three gases mentioned before. The adsorbent with a faster mass transfer for nitrogen was found to be Oxysiv 5 from UOP while MS S 624 from Grace Davison was found to have the slower mass transfer for nitrogen, also.

4.7 Notation

c	concentration in the fluid phase, $\text{mol}\cdot\text{g}^{-1}$
D_{ij}	binary diffusion coefficient of species *i* and *j*, cm^2s^{-1}
$D_{\text{K},i}$	Knudsen diffusivity for specie *i*, cm^2s^{-1}
$D^{\text{e}}_{\text{M},i}$	effective mass diffusion coefficient, cm^2s^{-1}
$D^{\text{e}}_{\text{p},i}$	coefficient of effective diffusivity in pores, cm^2s^{-1}
k_i	LDF kinetic coefficient of component i, s^{-1}
M	molecular weight, $\text{g}\cdot\text{mol}^{-1}$
P	total pressure, atm
q	concentration in the adsorbed phase, $\text{mol}\cdot\text{g}^{-1}$
$\Re$	universal gas constant
r	particle radius, cm
r_{p}	pore radius, m
T	absolute temperature, K

Greek variables

ΔP	pressure excess
ε	adsorbent porosity
ϕ	mercury contact angle
σ_{12}	collision diameter, Å

σ_s	surface tension, Nm^{-1}
τ	pore tortuosity

Subscripts

i	component *i*
ref	reference

Superscripts

e	effective

4.8 References

Bird, R. B.; Stewart, W. E.; Lightfoot, E. N., *Transport Phenomena*. Wiley International Edition: Singapore, 1960.

Brandani, F.; Ruthven, D., Measurement of adsorption equilibria by the zero length column (ZLC) technique part 2: Binary systems. *Industrial & Engineering Chemistry Research*, **2003,** 42, (7), 1462-1469.

Brandani, F.; Ruthven, D.; Coe, C. G., Measurement of adsorption equilibrium by the zero length column (ZLC) technique part 1: Single-component systems. *Industrial & Engineering Chemistry Research*, **2003,** 42, (7), 1451-1461.

Brandani, S., Effects of nonlinear equilibrium on zero length column experiments. *Chemical Engineering Science*, **1998,** 53, (15), 2791-2798.

Brandani, S.; Ruthven, D. M., Analysis of ZLC desorption curves for gaseous systems. *Adsorption-Journal of the International Adsorption Society*, **1996a,** 2, (2), 133-143.

Brandani, S.; Ruthven, D. M., Moments analysis of the zero length column method. *Industrial & Engineering Chemistry Research*, **1996b,** 35, (1), 315-319.

Brandani, S.; Xu, Z.; Ruthven, D., Transport diffusion and self-diffusion of benzene in NaX and CaX zeolite crystals studied by ZLC and tracer ZLC methods. *Microporous Materials*, **1996,** 7, (6), 323-331.

Cruz, P. Simulação e Optimização de Processos Cíclicos de Adsorção. PhD Thesis, Universidade do Porto, Porto, Portugal, 2003.

Do, D. D., *Adsorption Analysis: Equlibria and Kinetics*. Imperial College Press: London, UK, 1998.

Eic, M.; Ruthven, D. M., A New Experimental-Technique for Measurement of Intracrystalline Diffusivity. *Zeolites*, **1988,** 8, (1), 40-45.

Farooq, S.; Ruthven, D. M.; Boniface, H. A., Numerical-Simulation of a Pressure Swing Adsorption Oxygen Unit. *Chemical Engineering Science*, **1989,** 44, (12), 2809-2816.

Figueiredo, J. L.; Ramôa Ribeiro, F., *Catálise Heterogénea*. Fundação Calouste Gulbenkian: Porto, 1989.

Gregg, S. J.; Sing, K. S. W., *Adsorption, Surface Area and Porosity*. Second Edition. Academic Pres: London, 1982.

Liaw, C. H.; Wang, J. S. P.; Greenkorn, R. A.; Chao, K. C., Kinetics of Fixed-Bed Adsorption - New Solution. *Aiche Journal*, **1979,** 25, (2), 376-381.

Ruthven, D. M.; Lee, L. K.; Yucel, H., Kinetics of Non-Isothermal Sorption in Molecular-Sieve Crystals. *Aiche Journal*, **1980,** 26, (1), 16-23.

Ruthven, D. M.; Xu, Z., Diffusion of Oxygen and Nitrogen in 5A Zeolite Crystals and Commercial 5A Pellets. *Chemical Engineering Science*, **1993,** 48, (18), 3307-3312.

Sheng, P. Z.; Costa, C. A. V., Modified linear driving force approximations for cyclic adsorption-desorption processes. *Chemical Engineering Science*, **1997,** 52, (9), 1493-1499.

Washburn, E. W., Note on a method of determining the distribution of pore sizes in a porous material. *Proceedings of the National Academy of Sciences of the United States of America*, **1921,** 7, (4), 115-116.

5. Optimization of Pressure Swing Adsorption Processes

5.1 Introduction

The first pressure swing adsorption (PSA) unit was probably invented by Finlayson and Sharp in 1932 (GB Patent 365092). In their patent they describe a process with a single column with a pressurization step and a sequence of depressurizations (Espitalier-Noel, 1988). Around 1940 (DE Patent 871886), Kahle developed a system for air drying and carbon dioxide removal composed by two adsorption beds (Espitalier-Noel, 1988). In 1958 two different pressure swing adsorption units were patented for air separation: one by Skarstrom and another by Guérin de Montgareuil and Dominé. In Skarstrom's cycle, the saturated bed is purged at a low pressure by a fraction of the product (Yang, 1987). Guérin de Montgareuil and Dominé's unit was a very versatile PSA unit (Guérin de Montgareuil and Dominé, 1957) which could operate with several adsorbents (Espitalier-Noel, 1988) and the dessorption was performed with vacuum (Yang, 1987). However, due to the low separation factors between oxygen and nitrogen in the zeolites available back then, these cycles yielded only modest separations (Yang, 1987).

With the development of new adsorbents, the pressure swing adsorption and vacuum and pressure swing adsorption units became smaller and so, other applications became viable such as oxygen generators on-board military airplanes (Teague and Edgar, 1999) or for medical use (Jee et al., 2001). In hospitals, in 1975, PSA units were frequently used, producing 2 to 4 L/min of oxygen with a purity between 85 and 95% for treating patients with breathing illnesses. In 1976, Armond described an electrical compact device (Dee et al., 2003) which produced air for medical use using a zeolite (Espitalier-Noel, 1988). In 1984 (US Patent 4477264) Kratz and Sircar patented a medical oxygen generator for home use able of producing 90% of oxygen (Espitalier-Noel, 1988). Nowadays, about 500,000 of these units are sold worldwide and new cycles are still being invented: recently the company Sequal Technologies, Inc. developed a portable PSA unit with multiple columns for the production of oxygen for

medical use (Hill and Hill, 1998) which makes use of a rotary valve (Hill et al., 2001). These medical oxygen concentrators have a configuration that differs from the original Skarstrom's cycle in the simplicity of the assemblage and in the resulting complexity of the adsorption cycle. For economic reasons the solenoid on-off valves that are used in the Skarstrom's cycle to control the pressurization step are replaced by check valves and the needle valves often used in experimental PSA units for controlling the purge flow rate are replaced by calibrated orifices. As a result, the pressurization step cannot be controlled and it depends on the volume of the storage tank and on the production flow rate. The cycle has also only two stages, both with the same duration: a stage that begins with the column pressurization and ends after the production and a stage that begins with the column depressurization and ends after the purge.

In terms of optimisation, the conclusions obtained for a standard PSA or VPSA unit operating a Skarstrom's cycle are not applicable to these oxygen concentrators, which follow an adsorption cycle that is more complex to simulate and optimize. For example, the pressure history during a cycle in an oxygen concentrator changes completely when different product flow rates are selected, while in Skarstrom's cycle the pressure history stays approximately constant.

In 2003, Air Products and Chemicals, Inc. patented a vacuum and pressure swing adsorption unit for high purity oxygen (>99%) production directly from air (Dee et al., 2003). This unit uses an AgLiLSX type adsorbent also patented by this company (Chiang et al., 2002), which adsorbs more argon than oxygen.

In this Chapter, PSA and VPSA modes are compared for selected adsorbents as well as the performances obtained. Three equalization types are compared and a backfill step is studied. Some commercial units are analyzed and simulated and the results are compared with experimental data. An experimental PSA unit for high purity oxygen production is also presented and the experimental and simulation results are compared.

5.2 PSA units

5.2.1 Description of PSA units

The pressure swing adsorption (PSA) units are usually composed by two columns packed with an adsorbent, solenoid valves in the top and bottom of each column, a compressor and/or vacuum pump for VSA or VPSA, a storage tank for the product and valves or calibrated orifices for controlling the flow rates of the streams. A schematic representation of a PSA unit is presented in Figure 5.1.

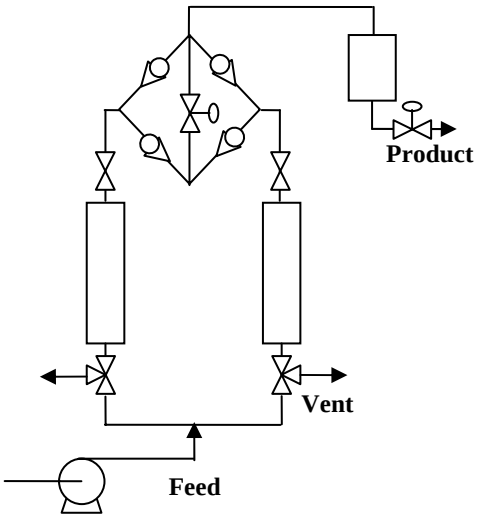

Figure 5.1. Sketch of a PSA unit.

Referring to Figure 5.1, when the unit is running, in one of the steps, the left column is being pressurized. This is achieved by opening the solenoid valve in the bottom of the left column, connecting, this way, the compressor with the column and closing the solenoid valve on the top of this column. The solenoid valve on the bottom of the column on the right is directed towards the vent and the valve on the top of this column is closed as well. After the left column is pressurized, production will start. For this, both solenoid valves on the top of each column are opened. Some of the product will go inside the right column for purging it. When this step ends, the left column will be depressurized; the solenoid valve on the top of the column is closed and the solenoid valve on the bottom is rotated towards the vent. Since the columns operate alternatingly, i.e., when one column is producing, the other is being purged and when one column is being pressurized the other is being depressurized, the solenoid valves of the column on

the right will switch to allow the pressurization. This cycle is known as the Skarstrom's cycle.

Instead of wasting all the energy stored in the form of pressure inside the column that will depressurize, some of the gas that is inside this column can be directed towards the other column that will be pressurized. This way, a fewer amount of air will be necessary to finish its pressurization. This step is called equalization.

Figure 5.2 presents a sketch of such units.

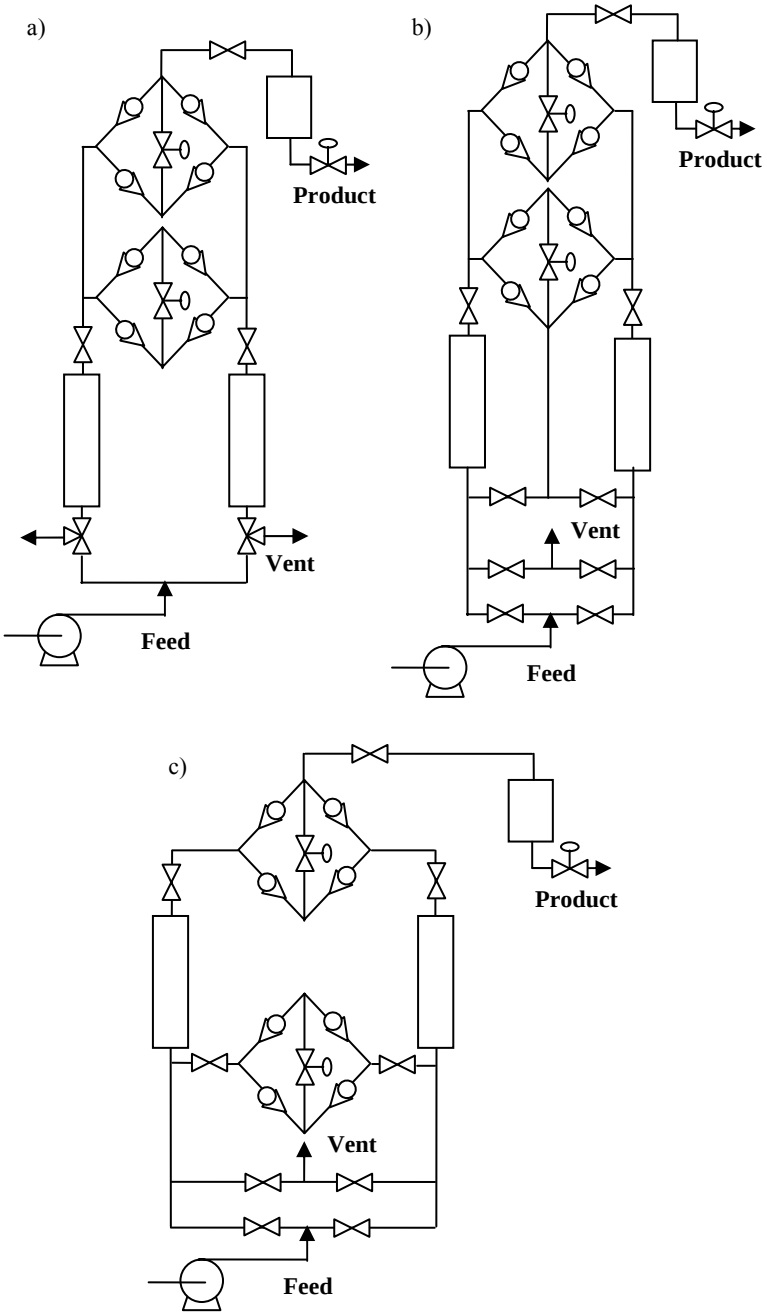

Figure 5.2. Sketch of a PSA unit with a) top-to-top, b) crossed and c) bottom-to-bottom equalization.

Other equalization steps may be employed such as bottom-to-bottom equalization, where the equalization stream passes from the bottom of a column to the bottom of the other or crossed equalization where the equalization stream passes from the top of a column to the bottom of the other.

Some applications require a fast re-start of the unit. For this a backfill step may be used (Liow and Kenney, 1990, Skarstrom, 1963). This cycle consists in pressurizing partially or totally the column at low pressure, using the product. This can be achieved by either using the product stored in the product tank or by using the purge stream but closing the valves on the bottom of the column.

Figure 5.3 a) and b) present a sketch of such units.

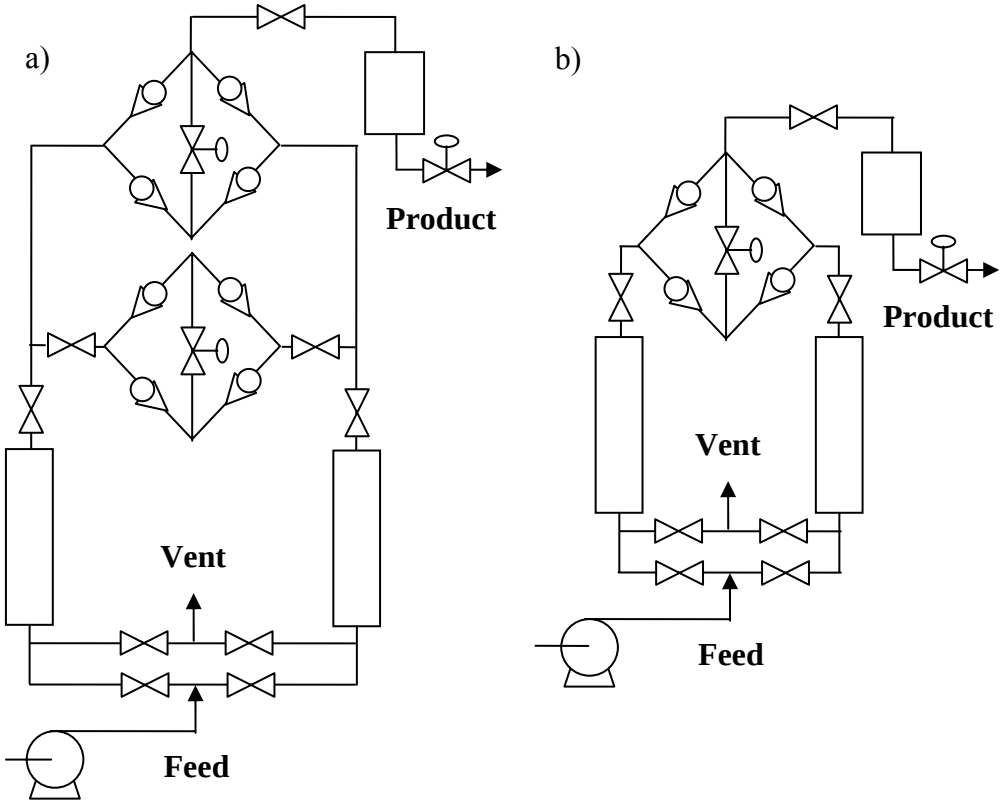

Figure 5.3. Sketch of a PSA unit with backfill using the product from a) the other column and b) the storage tank.

5.2.2 Cycles used in PSA units

5.2.2.1 Standard cycle without equalization (Skarstrom's cycle)

This is a very simple cycle. The pressure history of a unit running with this cycle looks like the one presented in Figure 5.4.

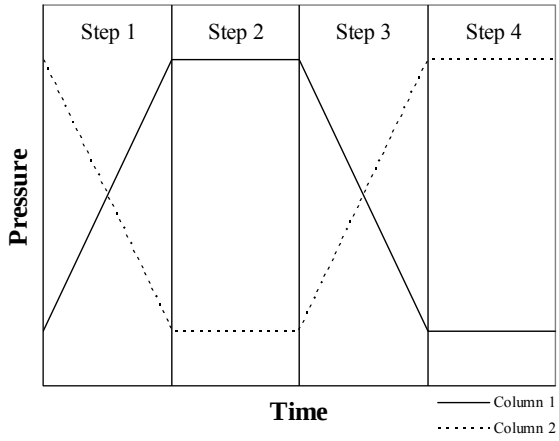

Figure 5.4. Pressure history of a unit running with the Skarstrom's cycle.

This cycle can be divided in four steps: step 1, where pressurization of column 1 and depressurization of column 2 occur; step 2, where production in column 1 and purge of column 2 occur; step 3, where column 2 is pressurized and column 1 depressurized and step 4 where column 2 produces and column 1 is purged.

5.2.2.2 Standard cycle with equalization

Figure 5.5 presents a typical pressure history of a unit running with this cycle.

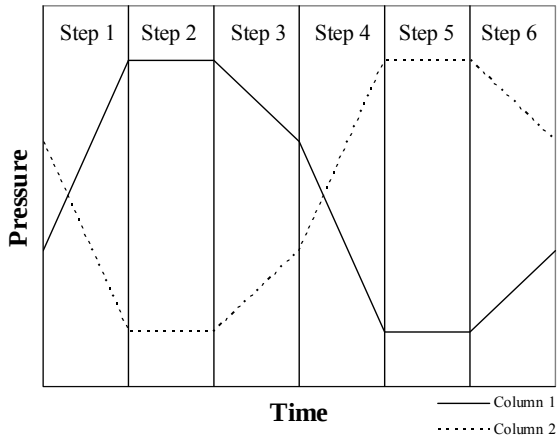

Figure 5.5. Pressure history of a unit running with a standard cycle with equalization.

This cycle can be divided in six steps: steps 1, 2, 4 and 5 are the same as steps 1, 2, 3 and 4 in the cycle without equalization; steps 3 and 6 are when the two columns are connected and gas flows from the column at higher pressure to the one at lower pressure - equalization.

5.2.2.3 Backfill

Figure 5.6 presents a typical pressure history of a unit running with a backfill cycle.

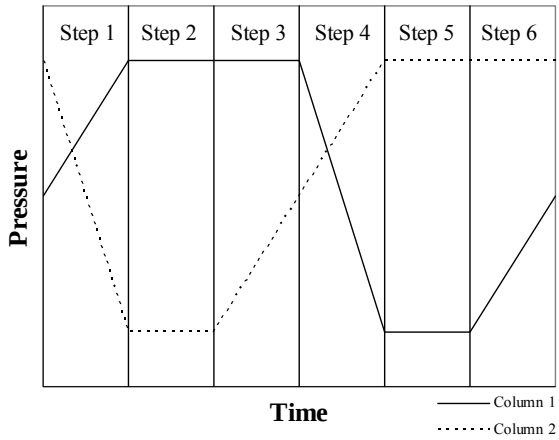

Figure 5.6. Pressure history of a unit running with a cycle with backfill.

This cycle can also be divided in six steps and steps 1, 2, 4 and 5 are the same as in the cycles previously presented. Steps 3 and 6 are when backfill occurs.

5.3 Commercial PSA units

5.3.1 PSA unit from Weinmann

OXYMAT®3 from Weinmann, GmbH, is composed by two adsorption columns packed with Oxysiv 5 from UOP, a storage tank, solenoid valves and a calibrated orifice for controlling the purge flow rate. It operates with four stages (six steps): pressurization/ production, equalization, depressurization/ purge and equalization again. Pressurization and production occur in stage 1. Simultaneously, stage 3 (depressurization and purge) takes place in the other column. Stages 2 and 4 (equalization) occur after stage 1 and 3, respectively. The duration of stages 1 and 3 is 7s and the duration of stages 2 and 4 is 1s. The unit operates between 1 and 3 bara.

The equalization occurs through the bottom of the columns (bottom-to-bottom equalization), however, this unit could operate with one of these three different equalization steps:

- Bottom-to-bottom equalization (BE) – the equalization stream exits from the bottom of one of the columns and enters at the bottom of the other;
- Crossed equalization (CE) – the equalization stream exits from the top of one of the columns and enters at the bottom of the other;
- Top-to-top equalization (TE) – the equalization stream exits from the top of one of the columns and enters at the top of the other.

These small pressure swing adsorption units with different equalization steps are represented in Figure 5.7. Other calibrated orifices were considered for modelling this unit and are also presented (for the feed, vent, equalization and before the storage tank).

The position of the valves are presented, for each stage, in Table 5.1.

Table 5.1. Position of the valves, in each stage, during the operation of the pressure swing adsorption unit.

Valve	Stage 1	Stage 2	Stage 3	Stage 4
VF	ON	OFF	ON	OFF
VE	OFF	ON	OFF	ON
V1	$1 \rightarrow 2$	$1 \rightarrow 2$	$1 \rightarrow 3$	$1 \rightarrow 2$
V2	$1 \rightarrow 3$	$1 \rightarrow 2$	$1 \rightarrow 2$	$1 \rightarrow 2$

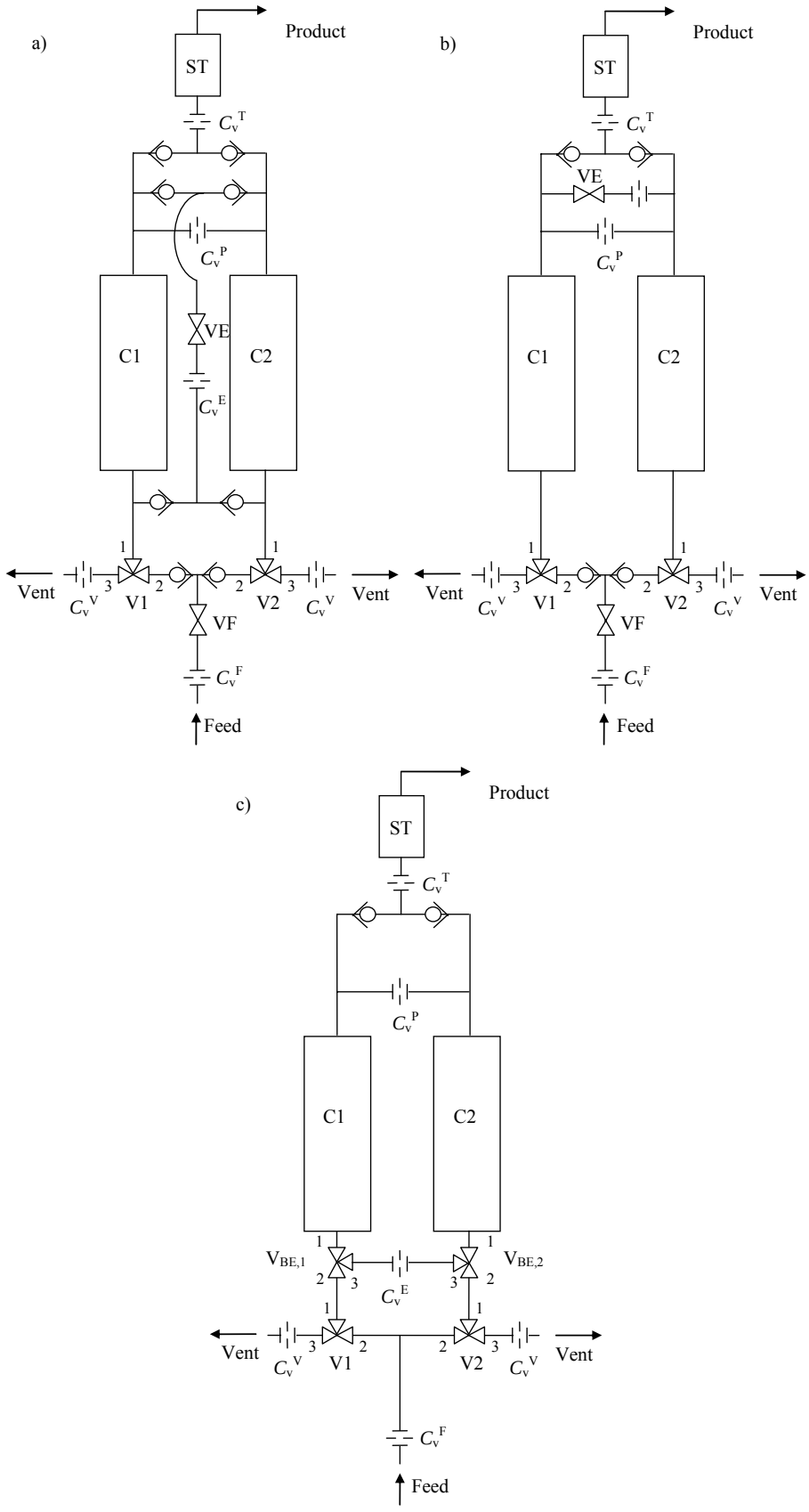

Figure 5.7. Sketch of a PSA unit with three different equalization steps: a) crossed, b) top-to-top and c) bottom-to-bottom.

Due to the units' configuration, in the equalization step there is always gas passing through the purge orifice from one column to the other. Therefore, in the units with a bottom-to-bottom equalization and with a crossed equalization, the tops of the columns are always connected and so, in addition to these equalizations, a sort of top-to-top equalization also occurs. The ratio between the purge orifice coefficient and the equalization orifice coefficient determines which of these equalizations has the most influence.

Another particularity is that due to the use of check valves before the storage tank (ST in Figure 5.7), whenever the pressure inside the storage tank is lower than the pressure inside one of the columns, there will be gas entering the tank, coming from one of the columns, regardless the stage the unit is at.

The pressure history inside the columns, during the unit's operation is presented in Figure 5.8.

Following in Figure 5.8 the pressure history inside column 1 (C1 in Figure 5.7), at the beginning of stage 1, this column is being pressurized while column 2 is depressurizing. When point B is reached, column 1 starts producing. This happens due to the presence of a check valve before the storage tank: while the pressure inside the columns is lower than inside the tank, the valves are "closed". Before point A is reached, the gas goes from column 2 to column 1, which can be seen as a complement to the equalization step. Afterwards, column 2 is purged with the gas coming from column 1.

In stage 2 the equalization step will take place. One may notice the different slopes of the equalization, pressurization and depressurization. This is due to different equalization, pressurization and vent orifices coefficients.

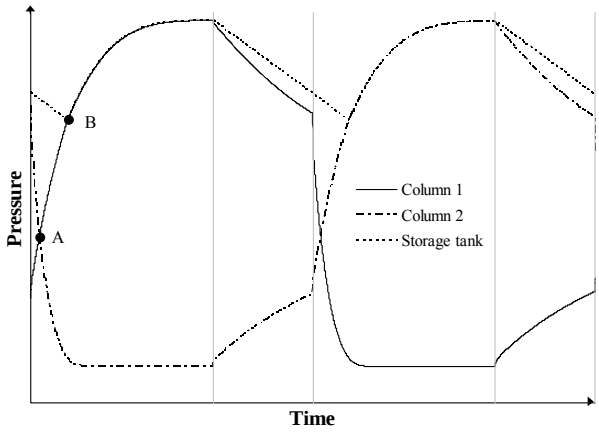

Figure 5.8. Pressure history inside the adsorption columns and the storage tank.

5.3.2 PSA unit from Sequal

INTEGRA™ from SeQual is composed by 12 adsorption columns and a rotary valve. This configuration has as main advantage the use of the compressor in a smoother way, i.e., the feed flow rate given by the compressor is nearly constant, while in conventional units, this flow rate fluctuates significantly. As a result the power consumption and noise are significantly decreased. This unit weights 24 kg and the maximum sound level produced is 47.6 dB (A).

5.3.3 VPSA unit from Air Products and Chemicals, Inc.

The VPSA unit from Air Products and Chemicals, Inc., produces 3 L_{STP}/min of oxygen at 93% and operates between 0.6 and 1.8 bara. It is composed by 4 adsorption columns, a rotary valve and a storage tank. This unit operates with 8 steps and is represented in Figure 5.9.

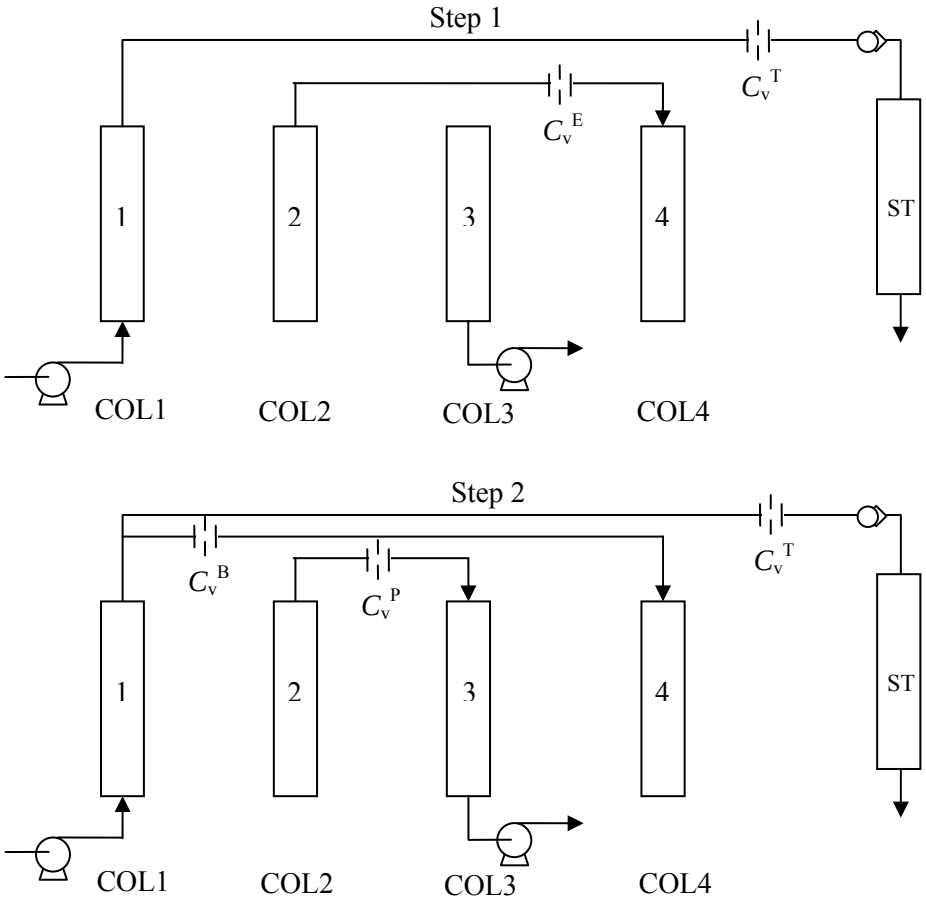

Figure 5.9. Sketch of the VPSA unit from Air Products and Chemicals, Inc.

Column 1 is producing in both steps (if the pressure inside the storage tank is lesser than inside the column) and in step 2 some of the product is backfilling column 4 (this is the same backfill step that was described before). In step 1, column 2 provides equalization to column 4 and in step 2, provides purge to column 3. Column 3 is evacuated in step 1 and purged in step 2. Column 4 is equalizing in step 1 and is backfilling in step 2.

With the rotation of the valves the columns go through all the steps as shown in Table 5.2.

Table 5.2. Position of the columns at each step.

Step	COL 1	COL 2	COL 3	COL 4
1	1	2	3	4
2	1	2	3	4
3	4	1	2	3
4	4	1	2	3
5	3	4	1	2
6	3	4	1	2
7	2	3	4	1
8	2	3	4	1

Figure 5.10 presents the pressure history inside the adsorption columns and the storage tank during the operation of the unit.

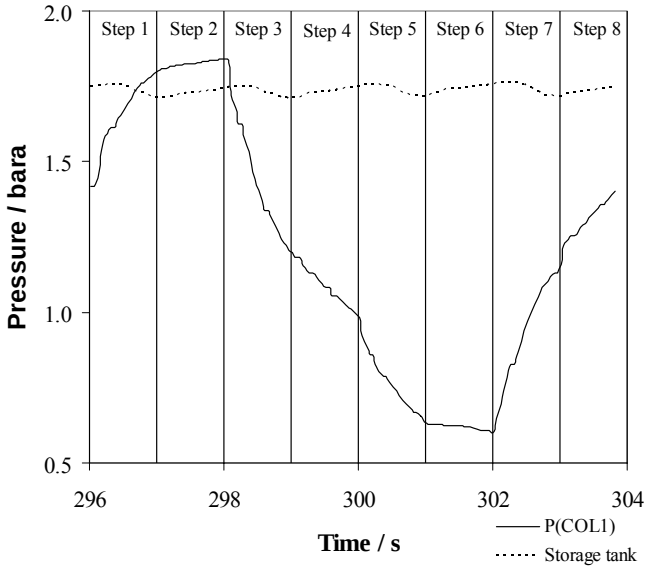

Figure 5.10. Pressure history inside the adsorption columns and the storage tank (experimental data supplied by Air Products and Chemicals, Inc.).

5.4 PSA units for high purity oxygen production

Due to the similar adsorption isotherms of oxygen and argon in traditional zeolites, the highest oxygen purity that can be achieved with a pressure swing adsorption (PSA) unit using these zeolites is around 95%.

In the past years some research has been carried out for the development of new adsorbents with selectivity for argon relative to oxygen, allowing the production of oxygen with purity above 95% by PSA. In 1999 Hutson et al. suggested the addition of silver to LiX zeolites in order to improve the air separation performance, by increasing the nitrogen adsorption capacity, and presented simulation results of a PSA unit producing oxygen with a purity of 96.42% and a recovery of 62.74% from a feed containing 22% of oxygen and 78% of nitrogen (Hutson et al., 1999). Although their adsorbent does not actually present selectivity of argon relative to oxygen, the argon adsorption capacity was increased. In 2001 Yang et al. presented similar results in a technical report (DE-FG26-98FT40115) submitted to the U.S. Department of Energy. In 2002 Air Products and Chemicals, Inc. patented an argon/oxygen selective X-zeolite (US 6432170 B1) described as AgLiLSX (low silica X) (Chiang et al., 2002). In 2003, a vacuum and pressure swing adsorption (VPSA) unit for the production of high-purity oxygen from air, using AgLiLSX is described in a patent by Air Products and Chemicals, Inc. (Dee et al., 2003). This unit may be composed by one layer of AgLiLSX or two layers of adsorbents: LiX and AgLiLSX. Simulation results are presented where the percentage of AgLiLSX in the bed is changed from 50 to 100% producing 99% oxygen with a recovery between 6 and 15 %, respectively. The unit is operated between 0.34 and 1.4 bara at 38ºC. According to the Air Products and Chemicals' patent, the recovery of a VPSA unit with unspecified volume and flow rates and producing 99% of oxygen is about 4% when fed with a current of 95% oxygen and 5% argon. This adsorbent allows also the production of high-purity oxygen directly from air which turns it very appealing since this can be achieved with a very simple unit.

Two other technologies may be used for producing high purity oxygen from air but are technologically more complex and make use of two steps. Both units have a pressure swing adsorption (PSA) unit packed with a zeolite for producing 95% of oxygen and 5% of argon. Next this current is fed to either a carbon molecular sieve (CMS) membrane module or another PSA unit packed with CMS adsorbent. In both

systems the product is obtained at low pressure and a compressor must be used to bring the product pressure to the operating requirements.

A PSA unit with an equalization step and using a traditional adsorbent (5A, NaX or LiX type zeolites) is expected to produce 95% of oxygen from air with a recovery around 60% (as it will be presented in this Chapter). The use of the new generation LiLSX type zeolite, such as Oxysiv MDX from UOP, will increase the recovery to around 80% (as it will also be presented in this Chapter).

The low separation factor of polymeric membranes, which hinders the production of high-purity oxygen, has led to the development of different configurations such as the continuous membrane column (CMC) (Ettouney and Majeed, 1997, Lababidi et al., 1996, Tsuru and Hwang, 1994) and the CMC in two strippers in series (TSS) mode (Ettouney and Majeed, 1997, Tsuru and Hwang, 1994) or membrane cascades (Agrawal, 1997, Agrawal and Xu, 1996, Xu and Agrawal, 1996). These multistage configurations make use of several membrane modules and the streams are recycled between the modules. Many arrangements of the modules are already patented (Behling et al., 2001, Dolle and Monereau, 2002, Gottzmann et al., 1994, Prasad, 1992, 1995, 1998, Thompson, 1994, Xu, 1993, 1994, Yee et al., 1995). The combination of polymeric membrane modules with PSA units for high purity oxygen production can also be found in the literature (Prasad et al., 1998, Tsuru and Hwang, 1994).

The ability of pore tailoring of the carbon molecular sieve membranes together with its high permeability and selectivity makes the use of this material very appealing since it allows the production of high purity oxygen with only one module. According to simulation results, a CMS membrane module with a selectivity of oxygen relative to argon of 14, using a feed pressure of 6 bara and a permeate pressure of 0.1 bara is able to produce 99.5% of oxygen with a recovery of 46%. This technology associated with a PSA packed with Oxysiv MDX is expected to yield a global recovery around 36%.

The third technology referred before for producing high purity oxygen, i.e., a PSA unit packed with zeolite followed by another PSA unit packed with carbon molecular sieve adsorbent can also be readily found in the literature (Armond et al., 1980, Bansal, 1990, Garrett, 1990, Haruna and Hayashi, 1987, Haruna et al., 1991, Hayashi et al., 1996, Jee et al., 2005, Miller and Theis, 1989a, b, Pinkerton, 1985, Rege and Yang, 2000, Richter et al., 1986). The second PSA produces 99.5% of oxygen when fed with a mixture of 95% of oxygen and 5% of argon with a recovery around 57% with the product obtained close to the atmospheric pressure or around 80%, with the product

obtained at low pressure (Jee et al., 2005). This system coupled with a PSA packed with a LiLSX type zeolite such as Oxysiv MDX may yield a maximum overall recovery around 64%. However, from the three technologies proposed, this one results in the largest unit.

The choice of the most suitable technology depends on the application characteristics. For small systems the PSA unit with AgLiLSX should be the most adequate. For systems where size isn't so important an economical balance should be made to find out which of these technologies is the best solution.

5.5 Mathematical model

The following assumptions were made in the formulation of the mathematical model: perfect gas behaviour, axially dispersed plug-flow, uniform cross-section void fraction, uniform adsorbent properties along the adsorption column, negligible radial gradients, instantaneous temperature equilibrium between gas, adsorbent and column wall, ideal distribution of the gas when it enters the adsorption column, negligible pressure drop (this assumption is usually valid for small units (Teague and Edgar, 1999) and isothermal operation, which, for oxygen separation and using small columns such as the ones employed in medical units is a reasonable approximation (Cruz et al., 2003)).

The model may be described by the following equations:

Inter-Particle Total Mass Balance

$$\varepsilon_b \frac{\partial c_T}{\partial t} = -\varepsilon_b \frac{\partial (u c_T)}{\partial z} - \sum_{i=1}^{nc} N_i \tag{5.1}$$

Inter-Particle Partial Mass Balance

$$\varepsilon_b \frac{\partial c_i}{\partial t} = \frac{\partial}{\partial z}\left(\varepsilon_b D_{ax} c_T \frac{\partial y_i}{\partial z} \right) - \varepsilon_b \frac{\partial (u c_i)}{\partial z} - N_i,\ i = 1, nc, \tag{5.2}$$

where c_T is the total molar concentration, ε_b is the bed void fraction, u is the interstitial molar velocity, z is the spatial coordinate, D_{ax} is the effective axial

dispersion coefficient, y_i is the molar fraction of component i in the gas phase, N_i is the molar flow rate of component i, c_i is the molar concentration of component i in the fluid phase, t is the time variable and nc the number of components in the mixture.

Intra-particle mass transfer

For the intra-particle mass transfer, the linear driving force (LDF) model, presented in Chapter 4, was used:

$$\frac{\partial \overline{q}_i}{\partial t} = k_i (q_{s,i} - \overline{q}_i), \tag{5.3}$$

where k_i is the LDF kinetic coefficient of component i, which is directly proportional to the effective diffusion coefficient in macro and mesopores, $q_{s,i}$ is the molar concentration of component i in the adsorbed phase, in the surface, and $\overline{q}_i$ is the average molar concentration of component i in the adsorbed phase.

The molar flux of component i in the adsorbent, N_i, is determined by:

$$N_i = (1-\varepsilon_b)\left[\rho_s \frac{\partial \overline{q}_i}{\partial t} + \varepsilon_p \frac{\partial \overline{c}_i}{\partial t}\right], \tag{5.4}$$

where ρ_s is the apparent density of the adsorbent and ε_p is the particle porosity. Instantaneous equilibrium between the inter- and intra-particle gas phases was considered (Cruz, 2003): $\partial \overline{c}_i / \partial t = \partial c_i / \partial t$.

Column mass balance

The column pressure history may be obtained by the following column mass balance (Teague and Edgar, 1999):

$$\varepsilon_b F_{in} \frac{P}{\Re T} = \varepsilon_b F_{out} \frac{P}{\Re T} + \varepsilon_b \frac{V}{\Re T} \frac{dP}{dt} + A \int_0^L \sum_{i=1}^{nc} N_i dz, \tag{5.5}$$

where F_{in} and F_{out} are the flow rates of the stream entering and leaving the column, respectively; L and V are the column length and volume, respectively; P is the total pressure; $\Re$ is the universal gas constant and T is the absolute temperature.

Storage tank total mass balance

$$F_{\text{in}}^{\text{T}} P^{\text{T}} = F_{\text{out}}^{\text{T}} P^{\text{T}} + V^{\text{T}} \frac{\text{d}P^{\text{T}}}{\text{d}t}, \tag{5.6}$$

where the superscript "T" stands for storage tank.

Storage tank partial mass balance

$$y_{i,\text{in}}^{\text{T}} F_{\text{in}}^{\text{T}} P^{\text{T}} = y_{i,\text{out}}^{\text{T}} F_{\text{out}}^{\text{T}} P^{\text{T}} + V^{\text{T}} \frac{\text{d}}{\text{d}t}\left(y_{i,\text{out}}^{\text{T}} P^{\text{T}} \right),\ i = 1, \text{nc} \tag{5.7}$$

Equations (5.1) to (5.7) may be written in the following dimensionless form:

Inter-particle total mass balance

$$\frac{\partial P^*}{\partial \theta} = -P^* \frac{\partial u^*}{\partial x} - T^* \sum_{i=1}^{\text{nc}} N_i^* \tag{5.8}$$

Inter-particle partial mass balance

$$\frac{\partial y_i}{\partial \theta} = -u^* \frac{\partial y_i}{\partial x} + \frac{1}{\text{Pe}} \frac{\partial^2 y_i}{\partial x^2} + \frac{T^*}{P^*} \left(y_i \sum_{j=1}^{\text{nc}} N_j^* - N_i^* \right),\ i = 1, \text{nc}, \tag{5.9}$$

where P^* is the dimensionless total pressure, $P^* = P/P_{\text{ref}}$; T^* is the dimensionless temperature, $T^* = T/T_{\text{ref}}$; θ is the dimensionless time variable, $\theta = t/\theta_{\text{ref}}$; θ_{ref} is the bed time constant defined as $\theta_{\text{ref}} = L/u_{\text{ref}}$; u^* is the dimensionless interstitial velocity, $u^* = u/u_{\text{ref}}$; x is the dimensionless spatial coordinate, $x = z/L$; N_i^* is the dimensionless molar flow rate of component i , $N_i^* = N_i \theta_{\text{ref}} / (c_{\text{ref}} \varepsilon_{\text{b}})$; c_{ref} is the reference fluid phase concentration, $c_{\text{ref}} = P_{\text{ref}} / \Re T_{\text{ref}}$ and Pe is the Peclet number for mass transfer, $\text{Pe} = u_{\text{ref}} L / D_{\text{ax}}$.

Intra-particle mass transfer

The linear driving force model in the dimensionless form is written as follows:

$$\frac{\partial \overline{q}_i^*}{\partial \theta} = R_{\mathrm{p}}^{\mathrm{b}} \alpha_i^{\mathrm{D}} (q_{s,i}^* - \overline{q}_i^*), \tag{5.10}$$

where $q_{s,i}^*$ is the dimensionless molar concentration of component i in the adsorbed phase, in the surface, $q_{s,i}^* = q_{s,i} / q_{\mathrm{ref}}$ and q_{ref} is the reference component dimensionless molar concentration in the adsorbed phase at reference conditions, $q_{\mathrm{ref}} = q(P_{\mathrm{ref}}, T_{\mathrm{ref}})$, α_i^{D} is the ratio between the LDF kinetic coefficients of component i and of the reference component, $\alpha_i^{\mathrm{D}} = k_i / k_{\mathrm{ref}}$; $R_{\mathrm{p}}^{\mathrm{b}}$ is the ratio between the bed time constant and the particle diffusion time constant, $R_{\mathrm{p}}^{\mathrm{b}} = k_{\mathrm{ref}} \theta_{\mathrm{ref}}$.

The dimensionless adsorbent molar flow rate of component i is given by:

$$N_i^* = \zeta_{\mathrm{a}} \frac{\partial \overline{q}_i^*}{\partial \theta} + \zeta_{\mathrm{p}} \frac{\partial \overline{c}_i^*}{\partial \theta}, \tag{5.11}$$

where ζ_{a} is the adsorbed phase capacity factor, $\zeta_{\mathrm{a}} = (1-\varepsilon_{\mathrm{b}}) / \varepsilon_{\mathrm{b}} \cdot \rho_{\mathrm{s}} \cdot q_{\mathrm{ref}} / c_{\mathrm{ref}}$ and ζ_{p} is the fluid phase capacity factor, $\zeta_{\mathrm{p}} = \varepsilon_{\mathrm{p}} \cdot (1-\varepsilon_{\mathrm{b}}) / \varepsilon_{\mathrm{b}}$.

Column mass balance

$$u_{\mathrm{in}}^* P^* = u_{\mathrm{out}}^* P^* + \frac{\mathrm{d}P^*}{\mathrm{d}\theta} + T^* \int_0^1 \sum_{i=1}^{\mathrm{nc}} N_i^* \mathrm{d}x \tag{5.12}$$

Storage tank total mass balance

Assuming that the adsorption column and tank have the same diameter, the storage tank total mass balance equation may be written in dimensionless form as follows:

$$u_{\mathrm{in}}^{\mathrm{T}*} P^{\mathrm{T}*} = u_{\mathrm{out}}^{\mathrm{T}*} P^{\mathrm{T}*} + \frac{L^{\mathrm{T}}}{L} \frac{\mathrm{d}P^{\mathrm{T}*}}{\mathrm{d}\theta}, \tag{5.13}$$

where u^{T*} is the dimensionless velocity of the gas entering or leaving the tank, L^{T} is the storage tank length and L is the length of the column.

Storage Tank Partial Mass Balance

$$\frac{dy_{i,out}^{T}}{d\theta} = \frac{L}{L^{T}}(y_{i,in}^{T}u_{in}^{T*} - y_{i,out}^{T}u_{out}^{T*}) - \frac{y_{i,out}^{T}}{P^{T*}}\frac{dP^{T*}}{d\theta},\ i = 1, nc \tag{5.14}$$

Pressure Drop Model in Orifices

The equation, written in dimensionless form, that describes the pressure drop in a valve or orifice is:

$$u^{*}P^{*} = C_{v} \cdot f(P_{u}^{*}, P_{d}^{*}, T^{*}, M), \tag{5.15}$$

where C_{v} is the dimensionless valve parameter,

$$C_{v} = 2.035\times10^{-2} \cdot \frac{T_{ref}}{\varepsilon_{b} \cdot A \cdot u_{ref} \cdot \sqrt{P_{ref}}} \cdot \frac{P^{0}}{T^{0}} \cdot K_{v} \tag{5.16}$$

K_{v} is the valve parameter, P_{u}^{*} and P_{d}^{*} are the dimensionless upstream and downstream pressures, respectively, M is the molecular weight of the gas passing through the orifice and it was considered to be given by $M = \sum_{i=1}^{nc} y_{i} \cdot M_{i}$; the superscript "0" stands for standard temperature and pressure conditions (STP) and (Chou and Huang, 1994)

$$f(P_{u}^{*}, P_{d}^{*}, T^{*}, M) = \begin{cases} 1.179\sqrt{\dfrac{P_{u}^{*2} - P_{d}^{*2}}{P_{d}^{*} \cdot M}} \cdot T^{*} & P_{d}^{*} > 0.53 \cdot P_{u}^{*} \\ P_{u}^{*}\sqrt{\dfrac{1}{P_{d}^{*} \cdot M}} \cdot T^{*} & P_{d}^{*} \le 0.53 \cdot P_{u}^{*} \end{cases} \tag{5.17}$$

Therefore, the dimensionless molar velocity, u^{*}, across the orifice in the feed, in the vent, before the storage tank and across the purge orifice was considered to be given by:

$$\text{Feed: } u_{in}^{*}P^{*} = C_{v}^{F} \cdot f(P^{H*}, P^{*}, T^{*}, M) \tag{5.18}$$

Storage tank: $u_{\text{in}}^{\text{T}*} P^{\text{T}*} = C_{\text{v}}^{\text{T}} \cdot f(P^*, P^{\text{T}*}, T^*, M)$ (5.19)

Purge: $u_{\text{purge}}^* P^* = u_{\text{purge,other column}}^* P_{\text{other column}}^* = C_{\text{v}}^{\text{P}} \cdot f(P^*, P_{\text{other column}}^*, T^*, M)$ (5.20)

Vent: $u_{\text{out,vent}}^* P^* = C_{\text{v}}^{\text{V}} \cdot f(P^*, P^{\text{L}*}, T^*, M)$ (5.21)

Equalization: $u_{\text{equalization}}^* P^* = C_{\text{v}}^{\text{E}} \cdot f(P^*, P_{\text{other column}}^*, T^*, M)$ (5.22)

Backfill: $u_{\text{backfill}}^* P^* = C_{\text{v}}^{\text{B}} \cdot f(P^*, P_{\text{other column}}^*, T^*, M)$ (5.23)

5.5.1 Boundary conditions

5.5.1.1 Standard cycle without equalization

When column 1 is pressurizing and column 2 is depressurizing (step 1), the boundary conditions are:

Column 1

$$x = 0: \ \frac{1}{\text{Pe}} \frac{\partial y_i}{\partial x} = u^* (y_i - y_{i,\text{in}})$$

$$u_{\text{in}}^* = \frac{C_{\text{v}}^{\text{F}}}{P_1^*} \cdot f(P^{\text{H}*}, P_1^*, T^*, M)$$

$$x = 1: \ \frac{\partial y_i}{\partial x} = 0$$

$$u^* = 0$$

Column 2

$$x = 0: \ \frac{\partial y_i}{\partial x} = 0$$

$$u^* = -\frac{C_{\text{v}}^{\text{V}}}{P_2^*} \cdot f(P_2^*, P^{\text{L}*}, T^*, M)$$

$$x = 1: \ \frac{\partial y_i}{\partial x} = 0$$

$$u^* = 0$$

When column 1 is producing and column 2 is purging (step 2), the boundary conditions are:

Column 1

$$x = 0: \ \frac{1}{\mathrm{Pe}} \frac{\partial y_i}{\partial x} = u^* (y_i - y_{i,\mathrm{in}})$$

$$u^*_{\mathrm{in}} = \frac{C^{\mathrm{F}}_{\mathrm{v}}}{P^*_1} \cdot f(P^{\mathrm{H}*}, P^*_1, T^*, M)$$

$$x = 1: \ \frac{\partial y_i}{\partial x} = 0$$

$$u^* = \frac{C^{\mathrm{P}}_{\mathrm{v}}}{P^*_1} \cdot f(P^*_1, P^*_2, T^*, M) + \frac{u^{\mathrm{T}*}_{\mathrm{in}} P^{\mathrm{T}*}}{\varepsilon_{\mathrm{b}} P^*_1}$$

Column 2

$$x = 0: \ \frac{\partial y_i}{\partial x} = 0$$

$$u^* = -\frac{C^{\mathrm{V}}_{\mathrm{v}}}{P^*_2} \cdot f(P^*_2, P^{\mathrm{L}*}, T^*, M)$$

$$x = 1: \ \frac{1}{\mathrm{Pe}} \frac{\partial y_i}{\partial x} = u^* (y_i - y_i\big|_{x=1,\mathrm{column1}})$$

$$u^* = -\frac{C^{\mathrm{P}}_{\mathrm{v}}}{P^*_2} \cdot f(P^*_1, P^*_2, T^*, M)$$

5.5.1.2 Standard cycle with equalization

When column 1 is pressurizing or producing and column 2 is depressurizing or purging the boundary conditions are the same as for the standard cycle without equalization. When the columns are equalizing (column 1 provides equalization to column 2 – step 3), the boundary conditions are:

Column 1

$$x = 0,\ x = 1:\ \frac{dy}{dx} = 0$$

Top-to-top equalization (TE) or crossed equalization (CE)

$$x = 0:\ u^* = 0$$

$$x = 1:\ u^* = \frac{C_v^E}{P_1^*} \cdot f(P_1^*, P_2^*, T^*, M)$$

Bottom-to-bottom equalization (BE)

$$x = 0:\ u^* = -\frac{C_v^E}{P_1^*} \cdot f(P_1^*, P_2^*, T^*, M)$$

$$x = 1:\ u^* = 0$$

Column 2

Top-to-top equalization (TE)

$$x = 0:\ \frac{dy}{dx} = 0$$

$$u^* = 0$$

$$x = 1:\ \frac{1}{\mathrm{Pe}} \frac{\partial y_i}{\partial x} = u^* (y_i - y_i|_{x=1,\mathrm{column1}})$$

$$u^* = -\frac{C_v^P}{P_2^*} \cdot f(P_1^*, P_2^*, T^*, M) - \frac{C_v^E}{P_2^*} \cdot f(P_1^*, P_2^*, T^*, M)$$

Crossed equalization (CE) or Bottom-to-bottom equalization (BE)

$$x=0:\ \frac{1}{\mathrm{Pe}}\frac{\partial y_i}{\partial x}=u^*(y_i-y_i\big|_{x=0,\mathrm{column1}})$$

$$u^*=\frac{C_\mathrm{v}^\mathrm{E}}{P_2^*}\cdot f(P_1^*,P_2^*,T^*,M)$$

$$x=1:\ \frac{\partial y_i}{\partial x}=0$$

$$u^*=0$$

5.5.1.3 Cycle with backfill

When column 1 is pressurizing or producing and column 2 is depressurizing or purging the boundary conditions are the same as for the standard cycle without equalization. When the unit is backfilling from the column producing (step 3) the boundary conditions are:

Column 1

$$x=0:\ \frac{1}{\mathrm{Pe}}\frac{\partial y_i}{\partial x}=u^*(y_i-y_{i,\mathrm{in}})$$

$$u_\mathrm{in}^*=\frac{C_\mathrm{v}^\mathrm{F}}{P_1^*}\cdot f(P^{\mathrm{H}*},P_1^*,T^*,M)$$

$$x=1:\ \frac{\partial y_i}{\partial x}=0$$

$$u^*=\frac{(C_\mathrm{v}^\mathrm{P}+C_\mathrm{v}^\mathrm{B})}{P_1^*}\cdot f(P_1^*,P_2^*,T^*,M)+\frac{u_\mathrm{in}^{\mathrm{T}*}P^{\mathrm{T}*}}{\varepsilon_\mathrm{b}P_1^*}$$

Column 2

$$x=0:\ \frac{\partial y_i}{\partial x}=0$$

$$u^*=0$$

$$x=1:\ \frac{1}{\mathrm{Pe}}\frac{\partial y_i}{\partial x}=u^*(y_i-y_i\big|_{x=1,\mathrm{column1}})$$

$$u^* = -\frac{(C_v^P + C_v^B)}{P_2^*} \cdot f(P_1^*, P_2^*, T^*, M)$$

The unit may also backfill only with the purge stream and so, $C_v^B = 0$.

5.5.1.4 Cycle of the unit from Weinmann without equalization

When column 1 is pressurizing/ producing and column 2 is depressurizing/ purging the boundary conditions are:

Column 1

$$x = 0: \ \frac{1}{\mathrm{Pe}} \frac{\partial y_i}{\partial x} = u^* (y_i - y_{i,\mathrm{in}})$$

$$u_{\mathrm{in}}^* = \frac{C_v^F}{P_1^*} \cdot f(P^{H*}, P_1^*, T^*, M)$$

$$x = 1: \begin{cases} \dfrac{\partial y_i}{\partial x} = 0 & , P_1^* \geq P_2^* \\ \dfrac{1}{\mathrm{Pe}} \dfrac{\partial y_i}{\partial x} = u^* (y_i - y_i\big|_{x=1,\mathrm{column2}}) & , P_1^* < P_2^* \end{cases}$$

$$\begin{cases} u^* = \dfrac{C_v^P}{P_1^*} \cdot f(P_1^*, P_2^*, T^*, M) + \dfrac{u_{\mathrm{in}}^{T*} P^{T*}}{\varepsilon_b P_1^*} & , P_1^* \geq P_2^* \\ u^* = -\dfrac{C_v^P}{P_1^*} f(P_2^*, P_1^*, T^*, M) & , P_1^* < P_2^* \end{cases}$$

Column 2

$$x = 0: \ \frac{\partial y_i}{\partial x} = 0$$

$$u^* = -\frac{C_v^V}{P_2^*} \cdot f(P_2^*, P^{L*}, T^*, M)$$

$$x = 1: \begin{cases} \dfrac{1}{\mathrm{Pe}} \dfrac{\partial y_i}{\partial x} = u^* (y_i - y_i\big|_{x=1,\mathrm{column1}}) & , P_1^* > P_2^* \\ \dfrac{\partial y_i}{\partial x} = 0 & , P_1^* \leq P_2^* \end{cases}$$

$$\begin{cases} u^* = -\dfrac{C_v^P}{P_2^*} \cdot f(P_1^*, P_2^*, T^*, M) & , P_1^* \geq P_2^* \\ u^* = \dfrac{C_v^P}{P_2^*} \cdot f(P_2^*, P_1^*, T^*, M) + \dfrac{u_{in}^{T*} P^{T*}}{\varepsilon_b P_2^*} & , P_1^* < P_2^* \end{cases}$$

Whenever the pressure inside the storage tank is higher than inside the columns, $u_{in}^{T*} = 0$. Otherwise: $u_{in}^{T*} \cdot P^{T*} = C_v^T \cdot f(P^*, P^{T*}, T^*, M)$.

5.5.1.5 Cycle of the unit from Weinmann

The boundary conditions, considering that column 1 is pressurizing/ producing and column 2 is depressurizing/ purging are the same as the ones presented for the unit from Weinmann without equalization. Afterwards, in the equalization step, there will be gas coming from column 1 to column 2. In this step, the boundary conditions for each equalization type are:

Column 1

$$x = 0,\ x = 1:\ \frac{dy}{dx} = 0$$

Top-to-top equalization (TE) or crossed equalization (CE)

$$x = 0:\ u^* = 0$$

$$x = 1:\ u^* = \frac{C_v^P}{P_1^*} \cdot f(P_1^*, P_2^*, T^*, M) + \frac{C_v^E}{P_1^*} \cdot f(P_1^*, P_2^*, T^*, M) + \frac{u_{in}^{T*} P^{T*}}{\varepsilon_b P_1^*}$$

Bottom-to-bottom equalization (BE)

$$x = 0:\ u^* = -\frac{C_v^E}{P_1^*} \cdot f(P_1^*, P_2^*, T^*, M)$$

$$x = 1:\ u^* = \frac{C_v^P}{P_1^*} \cdot f(P_1^*, P_2^*, T^*, M) + \frac{u_{in}^{T*} P^{T*}}{\varepsilon_b P_1^*}$$

Column 2

Top-to-top equalization (TE)

$$x = 0: \ \frac{dy}{dx} = 0$$

$$u^* = 0$$

$$x = 1: \ \frac{1}{\mathrm{Pe}} \frac{\partial y_i}{\partial x} = u^* (y_i - y_i|_{x=1,\mathrm{column1}})$$

$$u^* = -\frac{C_\mathrm{v}^\mathrm{P}}{P_2^*} \cdot f(P_1^*, P_2^*, T^*, M) - \frac{C_\mathrm{v}^\mathrm{E}}{P_2^*} \cdot f(P_1^*, P_2^*, T^*, M)$$

Crossed equalization (CE) or Bottom-to-bottom equalization (BE)

$$x = 0: \ \frac{1}{\mathrm{Pe}} \frac{\partial y_i}{\partial x} = u^* (y_i - y_i|_{x=0,\mathrm{column1}})$$

$$u^* = \frac{C_\mathrm{v}^\mathrm{E}}{P_2^*} \cdot f(P_1^*, P_2^*, T^*, M)$$

$$x = 1: \ \frac{1}{\mathrm{Pe}} \frac{\partial y_i}{\partial x} = u^* (y_i - y_i|_{x=1,\mathrm{column1}})$$

$$u^* = -\frac{C_\mathrm{v}^\mathrm{P}}{P_2^*} \cdot f(P_1^*, P_2^*, T^*, M)$$

5.5.1.6 Cycle of the unit from Weinmann with backfill

The boundary conditions, considering that column 1 is pressurizing/ producing and column 2 is depressurizing/ purging are the same as the ones presented for the unit from Weinmann without equalization. The boundary conditions for the backfill step are:

Column 1

$$x = 0: \ \frac{1}{\mathrm{Pe}} \frac{\partial y_i}{\partial x} = u^* (y_i - y_{i,\mathrm{in}})$$

$$u_\mathrm{in}^* = \frac{C_\mathrm{v}^\mathrm{F}}{P_1^*} \cdot f(P^{\mathrm{H}^*}, P_1^*, T^*, M)$$

$$x = 1: \ \frac{\partial y_i}{\partial x} = 0$$

$$u^* = \frac{C_{\mathrm{v}}^{\mathrm{P}}}{P_1^*} \cdot f(P_1^*, P_2^*, T^*, M) + \frac{u_{\mathrm{in}}^{\mathrm{T}*} P^{\mathrm{T}*}}{\varepsilon_{\mathrm{b}} P_1^*}$$

Column 2

$$x = 0: \ \frac{\partial y_i}{\partial x} = 0$$

$$u^* = 0$$

$$x = 1: \ \frac{1}{\mathrm{Pe}} \frac{\partial y_i}{\partial x} = u^* (y_i - y_i|_{x=1,\mathrm{column1}})$$

$$u^* = -\frac{C_{\mathrm{v}}^{\mathrm{P}}}{P_2^*} \cdot f(P_1^*, P_2^*, T^*, M)$$

5.5.1.7 Cycle of the unit from Air Products and Chemicals

The boundary conditions for step 1 are:

Column 1

$$x = 0: \ \frac{1}{\mathrm{Pe}} \frac{\partial y_i}{\partial x} = u^* (y_i - y_{i,\mathrm{in}})$$

$$u_{\mathrm{in}}^* \cdot P^* = \frac{Q_{\mathrm{STP}}^{\mathrm{F}} \cdot P_{\mathrm{STP}} \cdot T}{60 \cdot \varepsilon_{\mathrm{b}} \cdot A \cdot T_{\mathrm{STP}} \cdot u_{\mathrm{ref}} \cdot P_{\mathrm{ref}}}$$

$$x = 1: \ \frac{\partial y_i}{\partial x} = 0$$

$$u^* = \frac{C_{\mathrm{v}}^{\mathrm{P}}}{P_1^*} \cdot f(P_1^*, P_2^*, T^*, M) + \frac{u_{\mathrm{in}}^{\mathrm{T}*} P^{\mathrm{T}*}}{\varepsilon_{\mathrm{b}} P_1^*}$$

Column 2

$$x = 0: \ \frac{\partial y_i}{\partial x} = 0$$

$$u^* = 0$$

$$x = 1: \ \frac{\partial y_i}{\partial x} = 0$$

$$u^* = \frac{C_{\mathrm{v}}^{\mathrm{E}}}{P_2^*} \cdot f(P_2^*, P_4^*, T^*, M)$$

Column 3

$$x = 0: \ \frac{\partial y_i}{\partial x} = 0$$

$$u_{\mathrm{vent}}^* \cdot P^* = -\frac{Q_{\mathrm{STP}}^{\mathrm{V}} \cdot P_{\mathrm{STP}} \cdot T}{60 \cdot \varepsilon_{\mathrm{b}} \cdot A \cdot T_{\mathrm{STP}} \cdot u_{\mathrm{ref}} \cdot P_{\mathrm{ref}}}$$

$$x = 1: \ \frac{\partial y_i}{\partial x} = 0$$

$$u^* = 0$$

Column 4

$$x = 0: \ \frac{\partial y_i}{\partial x} = 0$$

$$u^* = 0$$

$$x = 1: \ \frac{1}{\mathrm{Pe}} \frac{\partial y_i}{\partial x} = u^* (y_i - y_i|_{x=1,\mathrm{column2}})$$

$$u^* = -\frac{C_{\mathrm{v}}^{\mathrm{E}}}{P_4^*} \cdot f(P_2^*, P_4^*, T^*, M)$$

The boundary conditions for step 2 are:

Column 1

$$x = 0: \ \frac{1}{\mathrm{Pe}} \frac{\partial y_i}{\partial x} = u^* (y_i - y_{i,\mathrm{in}})$$

$$u_{\mathrm{in}}^* \cdot P^* = \frac{Q_{\mathrm{STP}}^{\mathrm{F}} \cdot P_{\mathrm{STP}} \cdot T}{60 \cdot \varepsilon_{\mathrm{b}} \cdot A \cdot T_{\mathrm{STP}} \cdot u_{\mathrm{ref}} \cdot P_{\mathrm{ref}}}$$

$$x=1:\ \frac{\partial y_i}{\partial x}=0$$

$$u^*=\frac{C_{\mathrm{v}}^{\mathrm{P}}}{P_1^*}\cdot f(P_1^*,P_2^*,T^*,M)+\frac{C_{\mathrm{v}}^{\mathrm{B}}}{P_1^*}\cdot f(P_1^*,P_4^*,T^*,M)+\frac{u_{\mathrm{in}}^{\mathrm{T}*}P^{\mathrm{T}*}}{\varepsilon_{\mathrm{b}}P_1^*}$$

Column 2

$$x=0:\ \frac{\partial y_i}{\partial x}=0$$

$$u^*=0$$

$$x=1:\ \frac{\partial y_i}{\partial x}=0$$

$$u^*=\frac{C_{\mathrm{v}}^{\mathrm{P}}}{P_2^*}\cdot f(P_2^*,P_3^*,T^*,M)$$

Column 3

$$x=0:\ \frac{\partial y_i}{\partial x}=0$$

$$u_{\mathrm{vent}}^*\cdot P^*=-\frac{Q_{\mathrm{STP}}^{\mathrm{V}}\cdot P_{\mathrm{STP}}\cdot T}{60\cdot\varepsilon_{\mathrm{b}}\cdot A\cdot T_{\mathrm{STP}}\cdot u_{\mathrm{ref}}\cdot P_{\mathrm{ref}}}$$

$$x=1:\ \frac{1}{\mathrm{Pe}}\frac{\partial y_i}{\partial x}=u^*(y_i-y_i\big|_{x=1,\mathrm{column2}})$$

$$u^*=-\frac{C_{\mathrm{v}}^{\mathrm{P}}}{P_3^*}\cdot f(P_2^*,P_3^*,T^*,M)$$

Column 4

$$x=0:\ \frac{\partial y_i}{\partial x}=0$$

$$u^*=0$$

$$x=1:\ \frac{1}{\mathrm{Pe}}\frac{\partial y_i}{\partial x}=u^*(y_i-y_i\big|_{x=1,\mathrm{column1}})$$

$$u^* = -\frac{C_v^B}{P_4^*} \cdot f(P_1^*, P_4^*, T^*, M)$$

Whenever the pressure inside the storage tank is higher than inside the columns, $u_{in}^{T*} = 0$. Otherwise: $u_{in}^{T*} \cdot P^{T*} = C_v^T \cdot f(P^*, P^{T*}, T^*, M)$.

Q_{STP}^F and Q_{STP}^V are the feed and vent flow rates, respectively, in L_{STP}/min, which may be a function of the pressure inside the column, P^*.

5.5.1.8 Output molar velocity

For medical oxygen pressure swing adsorption units, it is important that the unit never stops producing and keeps a stable product flow rate Q_{prod}^0. For this reason, the dimensionless storage tank output molar velocity, $u_{out}^{T*} \cdot P^{T*}$, is assumed constant and equal to:

$$u_{out}^{T*} \cdot P^{T*} = \frac{Q_{prod}^0}{A \cdot u_{ref}} \frac{T}{T^0} \frac{P^0}{P_{ref}}, \tag{5.24}$$

where A is the column cross-sectional area and the superscript "0" stands for standard temperature and pressure conditions (STP).

5.5.2 Initial conditions

It was considered that, in the beginning, the columns and the storage tank are filled with air at atmospheric pressure, which corresponds to the low pressure, $P^* = P^{atm*}$ and $y_i = y_i^T = y_{i,in}, \forall x$.

5.6 Optimization strategy

5.6.1 Definition of the objective function

In the optimization of a pressure swing adsorption unit, the goal is to maximize the cumulative cash flow within the equipment life time, LT. The cumulative cash flow is a function of the operating costs, OC, of the investment, I, and of the product value, P_{val}.

Assuming 0% interest rate, the following objective function, F_{obj}, may be defined:

$$F_{\mathrm{obj}} = P_{\mathrm{val}} \cdot \mathrm{LT} - \mathrm{OC} \cdot \mathrm{LT} - I \tag{5.25}$$

The operating costs of an oxygen PSA unit are mainly due to the energy consumption to pressurize the feed. For a VPSA unit the energy consumption to depressurize the column must also be accounted. For a VPSA unit the operating costs can be defined as:

$$\mathrm{OC} = Q_{\mathrm{in}} \cdot W_{\mathrm{c}} \cdot \$\mathrm{EC} + Q_{\mathrm{v}} \cdot W_{\mathrm{v}} \cdot \$\mathrm{EC}\,, \tag{5.26}$$

where Q_{in} and Q_{v} are the average inlet and vent flow rates (expressed in $\mathrm{m}^3_{\mathrm{STP}}$/year), respectively, $\$\mathrm{EC}$ is the energy cost (expressed in \$/J) and W_{c} and W_{v} represent the theoretical amounts of work (expressed in J/ $\mathrm{m}^3_{\mathrm{STP}}$) done by the compressor and vacuum pump (naturally, for PSA units, $W_{\mathrm{v}} = 0$), respectively. For a single stage compressor, the theoretical amount of work is given by (Nilchan and Pantelides, 1998):

$$W_{\mathrm{c}} = \left(\frac{\gamma}{\gamma - 1}\right) P^0 \frac{T}{T^0} \left[\left(\frac{P^{\mathrm{H}}}{P_{\mathrm{atm}}}\right)^{\frac{\gamma-1}{\gamma}} - 1\right] \tag{5.27}$$

$$W_{\mathrm{v}} = \left(\frac{\gamma}{\gamma - 1}\right) P^0 \frac{T}{T^0} \left[1 - \left(\frac{P^{\mathrm{L}}}{P_{\mathrm{atm}}}\right)^{\frac{\gamma-1}{\gamma}}\right], \tag{5.28}$$

where γ is the ratio between the specific heat capacity at constant pressure and the specific heat capacity at constant volume (for air, $\gamma = 1.4$) and the superscript "0" stands for standard temperature and pressure conditions (STP).

The investment depends on the cost of the adsorbent, C_{ads}, the column, C_{col}, the storage tank, C_{ST}, the compressor, C_{comp}, the vacuum pump, C_{vpump} and other equipment such as valves, orifices, tubes and fittings, C_{other}. It may be given by the following expression:

$$I = C_{ads} + C_{col} + C_{ST} + C_{comp} + C_{vpump} + C_{other} \tag{5.29}$$

and

$$C_{ads} = V \cdot \$C_{ads} \tag{5.30}$$

$$C_{col} = (P^{H})^{\beta_1} \cdot V \cdot \$C_{col} \tag{5.31}$$

$$C_{ST} = (P^{H})^{\beta_2} \cdot V^{T} \cdot \$C_{ST} \tag{5.32}$$

$$C_{comp} = \kappa_1 (Q_{in})^{\gamma_1} + \kappa_2 (Q_{in} \cdot W_c)^{\gamma_2} \tag{5.33}$$

$$C_{vpump} = \kappa_3 (Q_v)^{\gamma_3} + \kappa_4 (Q_v \cdot W_v)^{\gamma_4} \tag{5.34}$$

$$C_{other} = \kappa_5 (Q_{in})^{\gamma_5}, \tag{5.35}$$

where $\$C_{ads}$ is the adsorbent price ($/m^3); $\$C_{col}$ is the column price that is a function of its volume, V; $\$C_{ST}$ is the storage tank price (when made of the same material, $\$C_{ST}$ is the same as $\$C_{col}$) and is a function of its volume, V^{T}; β_i, κ_i and γ_i are correlation parameters (Peters and Timmerhaus, 1980).

The product value may be defined as:

$$P_{val} = Q_{prod} \cdot \$P, \tag{5.36}$$

where Q_{prod} is the production flow rate (m^3_{STP}/year), and $\$P$ is the product price.

The objective function may be written as follows:

$$
\begin{aligned}
F_{\text{obj}}^{*} = \frac{F_{\text{obj}}}{Q_{\text{prod}}} = & \left[\$P - \left(\frac{Q_{\text{in}}}{Q_{\text{prod}}} W_{\text{c}} + \frac{Q_{\text{v}}}{Q_{\text{prod}}} W_{\text{v}} \right) \cdot \$\text{EC} \right] \cdot \text{LT} - \\
& - \frac{V}{Q_{\text{prod}}} \left[\$C_{\text{ads}} - (P^{\text{H}})^{\beta_1} \cdot \$C_{\text{col}} \right] - \frac{V^{\text{T}}}{Q_{\text{prod}}} (P^{\text{H}})^{\beta_2} \cdot \$C_{\text{ST}} - \\
& - \frac{\kappa_1}{Q_{\text{prod}}^{1-\gamma_1}} \left(\frac{Q_{\text{in}}}{Q_{\text{prod}}} \right)^{\gamma_1} - \frac{\kappa_2}{Q_{\text{prod}}^{1-\gamma_2}} \left(\frac{Q_{\text{in}}}{Q_{\text{prod}}} \cdot W_{\text{c}} \right)^{\gamma_2} - \frac{\kappa_3}{Q_{\text{prod}}^{1-\gamma_3}} \left(\frac{Q_{\text{v}}}{Q_{\text{prod}}} \right)^{\gamma_3} - \\
& - \frac{\kappa_4}{Q_{\text{prod}}^{1-\gamma_4}} \left(\frac{Q_{\text{v}}}{Q_{\text{prod}}} \cdot W_{\text{v}} \right)^{\gamma_4} - \frac{\kappa_5}{Q_{\text{prod}}^{1-\gamma_5}} \left(\frac{Q_{\text{in}}}{Q_{\text{prod}}} \right)^{\gamma_5}
\end{aligned}
\tag{5.37}
$$

For PSA units the parameters κ_3 and κ_4 are nil.

Assuming that the columns and storage tank have the same cross section area, we can write the objective function in terms of the product purity, Pur, product recovery, Rec, and the model parameter, R_{p}^{b}, as follows:

$$
\begin{aligned}
F_{\text{obj}}^{*} = & \left\{ \$P - \left[\frac{\text{Pur}}{y_{\text{O}_2,\text{in}} \cdot \text{Rec}} W_{\text{c}} + \left(\frac{\text{Pur}}{y_{\text{O}_2,\text{in}} \cdot \text{Rec}} - 1 \right) \cdot W_{\text{v}} \right] \cdot \$\text{EC} \right\} \cdot \text{LT} - \\
& - \frac{R_{\text{p}}^{\text{b}}}{k_{\text{ref}}} \left(\$C_{\text{ads}} - (P^{\text{H}})^{\beta_1} \cdot \$C_{\text{col}} \right) - \frac{L^{\text{T}}}{L} \frac{R_{\text{p}}^{\text{b}}}{k_{\text{ref}}} (P^{\text{H}})^{\beta_2} \cdot \$C_{\text{ST}} - \\
& - \frac{\kappa_1}{Q_{\text{prod}}^{1-\gamma_1}} \left(\frac{\text{Pur}}{y_{\text{O}_2,\text{in}} \cdot \text{Rec}} \right)^{\gamma_1} - \frac{\kappa_2}{Q_{\text{prod}}^{1-\gamma_2}} \left(\frac{\text{Pur}}{y_{\text{O}_2,\text{in}} \cdot \text{Rec}} \cdot W_{\text{c}} \right)^{\gamma_2} - \\
& - \frac{\kappa_3}{Q_{\text{prod}}^{1-\gamma_3}} \left(\frac{\text{Pur}}{y_{\text{O}_2,\text{in}} \cdot \text{Rec}} - 1 \right)^{\gamma_3} - \frac{\kappa_4}{Q_{\text{prod}}^{1-\gamma_4}} \left[\left(\frac{\text{Pur}}{y_{\text{O}_2,\text{in}} \cdot \text{Rec}} - 1 \right) \cdot W_{\text{v}} \right]^{\gamma_4} - \\
& - \frac{\kappa_5}{Q_{\text{prod}}^{1-\gamma_5}} \left(\frac{\text{Pur}}{y_{\text{O}_2,\text{in}} \cdot \text{Rec}} \right)^{\gamma_5}
\end{aligned}
\tag{5.38}
$$

For simplification, the operating costs can be ignored. Therefore, the optimization can be performed in order to maximize the recovery, Rec. This approach has the advantage of being independent of the adsorbent, column, storage tank and energy prices. Although the operating costs are not considered in the objective function, since they are inversely proportional to the recovery, for a given pressure envelope, by maximizing the recovery, the operating costs will be minimized.

The power consumption per product unit flow rate, Ψ, expressed as MJ/m^3_{STP}, of a VPSA unit may be calculated by dividing the operating costs (Equation (5.26)) by the product flow rate resulting in the following expressions:

$$\Psi = \int_0^{\theta_{1/2\,cycle}} \left\{ 10^{-1} \frac{\gamma}{\gamma - 1} P_{ref} \cdot \varepsilon_b \left\{ P_2^* \cdot u_v^* \left[1 - \left(\frac{P^{L*}}{P_{atm}^*} \right)^{\frac{\gamma-1}{\gamma}} \right] + P_1^* \cdot u_{in}^* \left[\left(\frac{P^{H*}}{P_{atm}^*} \right)^{\frac{\gamma-1}{\gamma}} - 1 \right] \right\} \right\} d\theta \quad (5.39)$$

For a PSA unit it is given by:

$$\Psi = \int_0^{\theta_{1/2\,cycle}} \left\{ 10^{-1} \frac{\gamma}{\gamma - 1} P^* \cdot P_{ref} \cdot \varepsilon_b \cdot u_{in}^* \left[\left(\frac{P^{H*}}{P_{atm}^*} \right)^{\frac{\gamma-1}{\gamma}} - 1 \right] \right\} d\theta, \quad (5.40)$$

where $\theta_{1/2\,cycle}$ is the dimensionless half cycle time ($\theta_{1/2\,cycle} = \theta_{press/prod} + \theta_{equalization}$).

The optimization was carried out using a successive quadratic-programming algorithm (SQP) described in Appendix 5.1.

5.6.2 Optimization variables

5.6.2.1 PSA unit from Weinmann

The unit's performance is influenced by the following variables:

- $\theta_{press/prod}$ - dimensionless pressurization/ production time;
- $\theta_{equalization}$ - dimensionless equalization time;
- L/L^T - ratio between the adsorption column and storage tank lengths;
- C_v^F - feed orifice parameter;
- C_v^T - storage tank orifice parameter;
- C_v^P - purge orifice parameter;
- C_v^E - equalization orifice parameter;
- C_v^V - vent orifice parameter.

The operating pressure envelope was not considered to be an optimization variable.

The dimensionless pressurization/production time, $\theta_{\text{press/prod}}$, represents the duration of stages 1 and 3, when pressurization and production take place for both columns. Along with the feed orifice parameter, C_v^F, the storage tank orifice parameter, C_v^T, the vent orifice parameter, C_v^V, the purge orifice parameter, C_v^P, and the ratio between the storage tank and column lengths, L/L^T, will highly influence the unit's performance as they will determine the amount of the bed's adsorption capacity effectively used. These last variables affect the pressure changing rate, influencing, this way, the product purity and recovery (Mendes et al., 2000).

Considering Figure 5.8, C_v^F will change the pressurization rate and C_v^V the depressurization rate. Point A will be reached sooner or later, as these parameters are respectively higher or lower. After this point is reached, column 2 will start being purged. Production will start after point B is reached. The values of C_v^F and L/L^T determine when and at which pressure this will happen (higher L/L^T values will result in a slower decrease of the pressure inside the storage tank). The storage tank and purge orifice parameters will influence the amount of gas that exits the adsorption bed.

The dimensionless equalization time, $\theta_{\text{equalization}}$, represents the duration of the equalization step (stages 2 and 4). Along with the equalization orifice parameter, C_v^E, this variable will influence the equalization step and, this way, the unit's performance. The higher the pressure level attained in the equalization step, the lower will be the amount of feed gas needed to achieve the intended operating pressure. Therefore, the higher will be the recovery. However, if the equalization time is too long, or the equalization orifice parameter is too high, the product purity will decrease, as well as the recovery.

5.6.2.2 Other PSA units

For the other PSA units presented before, the optimization variables are the same as the ones presented for the PSA unit from Weinmann. For the unit with a backfill step, the backfill orifice parameter, C_v^B, was also considered in the optimizations.

5.7 Experimental part

5.7.1 PSA unit from Weinmann

The performance of Oxymat 3 from Weinmann was evaluated for several product flow rates with the aim of validating the mathematical model which describes its operation.

5.7.1.1 Characteristics of the unit

OXYMAT®3 from Weinmann weights approximately 20 kg, its average power consumption is 360 W (1.6 A) and the maximum sound level produced is 40 dB (A).

Table 5.3 presents the characteristics of this unit.

Table 5.3. Characteristics of OXYMAT®3 from Weinmann.

Length (cm)	Column diameter (cm)	Storage tank length (cm)	K_v^P	K_v^T	K_v^V	K_v^E
29.5	8.0	12.5	0.0394	0.15	0.55	0.90

The purge valve parameter, K_v^P, was measured experimentally. The storage tank, the vent and the equalization valve parameters, K_v^T, K_v^V and K_v^E, respectively, could not be determined experimentally due to the configuration of the unit. These were therefore estimated, for one product flow rate, by fitting the simulated to the experimental pressure histories (columns and storage tank pressure histories). It was then verified that the simulated results obtained with these parameters yielded also very good agreement with the experimental data for the other flow rates.

With the intent of optimizing this unit, the feed flow rate given by the unit's compressor was experimentally determined, in order to incorporate this information in the optimization procedure. It was found to be given by the following correlation:

$$u_{in}^* \cdot P^* = \frac{10^{-3} \cdot P_{PTN} \cdot T}{60 \cdot \varepsilon_b \cdot A \cdot T_{PTN} \cdot u_{ref} \cdot P_{ref}} \left[0.0731 \left(P^* \cdot P_{ref} \right)^3 + \right.$$
$$\left. -0.288 \left(P^* \cdot P_{ref} \right)^2 - 6.517 \cdot P^* \cdot P_{ref} + 91.370 \right] \tag{5.41}$$

Unlike the equation previously proposed for computing the feed flow rate (Equation (5.18)), this equation implies the knowledge of the product flow rate and it must be kept in mind that the high pressure is not limited.

Since the bed length is 100 times larger than the adsorbent diameter and the bed diameter is 30 times larger than the adsorbent diameter, it is reasonable to consider negligible the wall effects (White and Barkley, 1989). Thus, assuming a packaging of small identical spherical particles, one can use the value of $\varepsilon_b = 0.36$ the bed void fraction.

The pressure drop along the bed was measured and verified to be negligible, validating the assumption made in the formulation of the model.

This methodology has the advantage of being independent of the product flow rates and this way, the velocity does not need to be previously known. This implies that the correlations to predict the Peclet number cannot be used, as they are a function of the velocity. However, for small scale units, the values for Peclet number vary from 500 to 1000. No noticeable changes on the process performance are verified for Peclet numbers higher than 600 (Farooq et al., 1989), therefore this value was used for all simulations.

Since the adsorption isotherms for oxygen and argon, for the adsorbents usually used in this kind of units, are almost identical, the feed was considered to be a pseudo binary mixture of 78% nitrogen and 22% oxygen.

5.7.1.2 Cycle without equalization – comparison between PSA and VPSA

Two types of units were studied: pressure swing adsorption (PSA) and vacuum and pressure swing adsorption (VPSA). The results of the optimization of these units operating with Oxysiv 5, Oxysiv 7 and MS S 624, as function of R_p^b ($R_p^b = k_{ref} \cdot L/u_{ref}$) are presented in the next figures. R_p^b is the ratio between the bed time constant and the particle time constant.

Figure 5.11 presents the maximum product recovery for a) the PSA unit and b) the VPSA unit (Santos et al., 2004). Both units were optimized for producing 99% of oxygen plus argon at 20ºC and operating between 3 bara and the atmospheric pressure (PSA unit) and between 1.2 bara and 0.4 bara (VPSA unit).

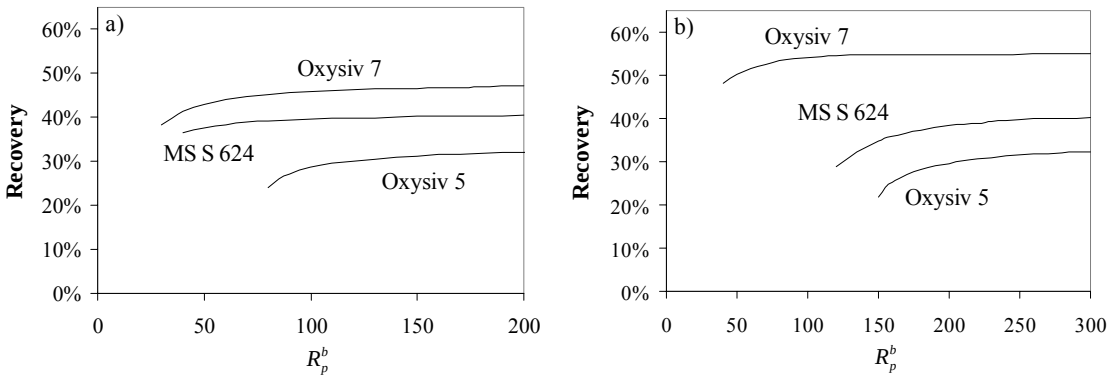

Figure 5.11. Maximum product recovery for a) the PSA unit and b) the VPSA unit.

Figure 5.12 presents the power consumption per unit product flow rate expressed as MJ/m^3_{STP} for a) the PSA unit and b) the VPSA unit.

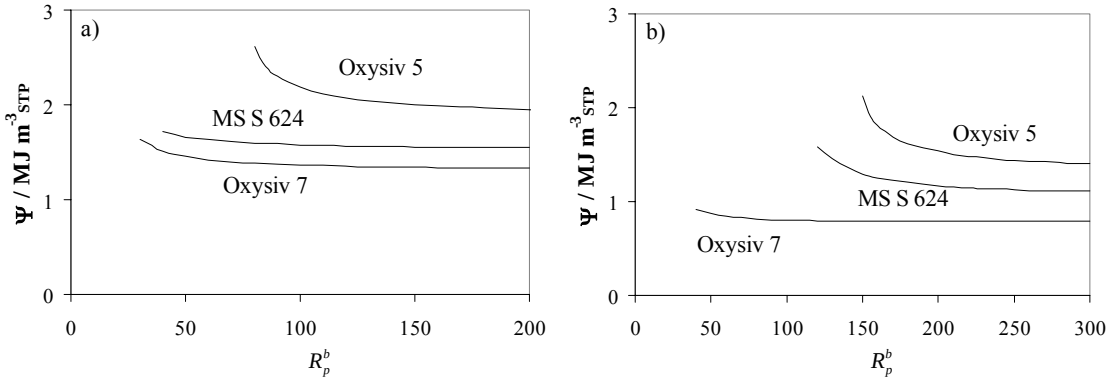

Figure 5.12. Power consumption per unit product flow rate, Ψ, for a) the PSA unit and b) the VPSA unit.

As it can be seen, both PSA and VPSA units have a high performance when using Oxysiv 7. This adsorbent allows the use of lower R_p^b values in VPSA mode, which means that the adsorption column can be smaller or the product flow rate can be higher comparatively to the other adsorbents. The smallest VPSA unit with Oxysiv 7 has about half the volume of the smallest unit with MS S 624 for the same production flow rate and purity. However, Oxysiv 7 is more expensive than the other adsorbents studied. Based on the results obtained, for the same recovery, the use of Oxysiv 7 is advantageous if it costs less than about twice the price of the other adsorbents.

The VPSA unit showed to have the lowest power consumption per unit product flow rate, however, except with Oxysiv 7, it should have about twice the volume or produce half the product flow rate of a PSA unit. In PSA, a unit with Oxysiv 7 or MS S

624 should produce twice the product flow rate or should have half the volume than with Oxysiv 5.

Relating the power consumption achieved with the three adsorbents we verified that PSA units with MS S 624 and Oxysiv 5 consume respectively, about 1.2 and 1.3 times more than the unit with Oxysiv 7. The power consumptions of a VPSA unit with MS S 624 and Oxysiv 5 are respectively 1.5 and 2 times greater than for a VPSA unit with Oxysiv 7.

The optimum ratios between the column and storage tank lengths for the PSA and VPSA units are presented in Figure 5.13 a) and b), respectively.

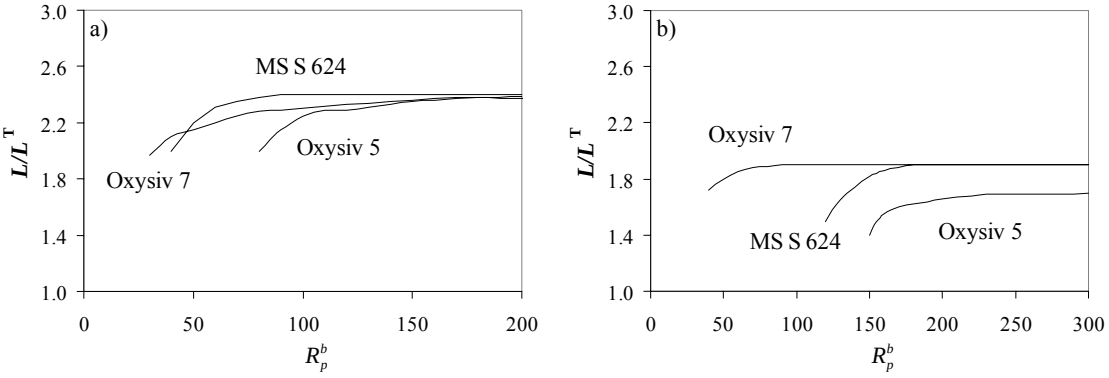

Figure 5.13. Optimum ratios between the column and storage tank lengths for the a) PSA unit and b) VPSA unit.

The optimum production time for the PSA and VPSA units are presented in Figure 5.14 a) e b), respectively.

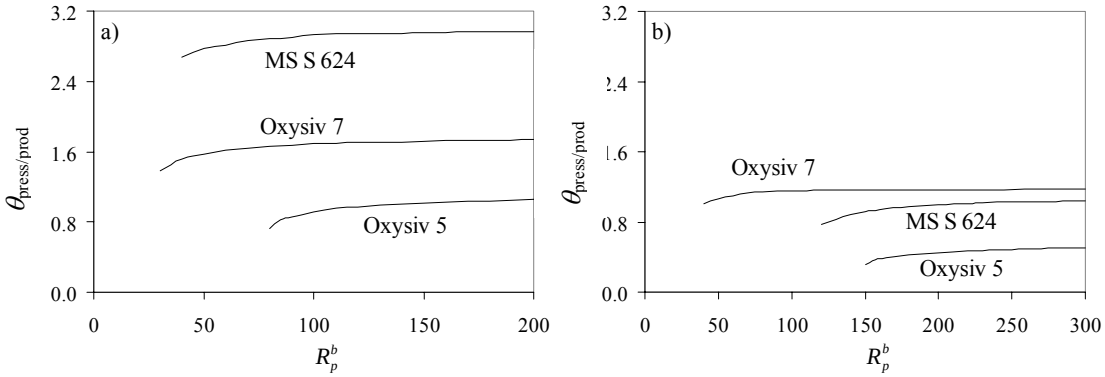

Figure 5.14. Optimum production time for the a) PSA unit and b) VPSA unit.

The optimum purge valve parameter for the PSA and VPSA units are presented in Figure 5.15 a) e b), respectively.

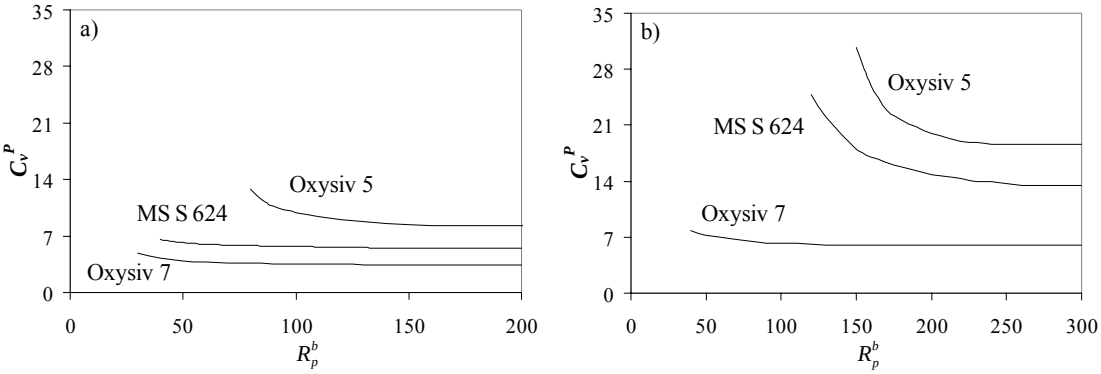

Figure 5.15. Optimum purge valve parameter for the a) PSA unit and b) VPSA unit.

It is observed that PSA allows, in comparison to VPSA, a higher ratio between the column and storage tank lengths, which means that smaller tanks can be used. For small R_p^b values, i.e., smaller units or higher product flow rates, the storage tank has to be larger. As a consequence, the unit will take more time to reach the cyclic steady state. Medical oxygen pressure swing adsorption units must start producing oxygen with purity above 82% in a very short time interval. Another disadvantage is that the optimum found for small R_p^b values is not robust, which means that little variations in the operating conditions result in significant variations in the unit performance. This "instability" can be observed in the abrupt variation of the optimization variables for small R_p^b values. Therefore this region should be avoided.

The PSA operating mode requires lower values of the purge valve parameters and longer cycles than VPSA. Oxysiv 7 and MS S 624 allow higher pressurization/ production times than Oxysiv 5 in both operating modes. This is expected since these two adsorbents show higher capacities for nitrogen than Oxysiv 5.

The optimal storage tank valve parameter, C_v^T, the feed valve parameter, C_v^F, and the vent valve parameter, C_v^V, are presented in Table 5.4, for the different adsorbents, and showed to be independent of the unit size and product flow rate.

Table 5.4. Optimum values of C_v^F, C_v^T and C_v^V for the different adsorbents (results for VPSA are between brackets).

Adsorbent	C_v^F	C_v^T	C_v^V
Oxysiv 5	155 (550)	73 (29)	228 (736)
Oxysiv 7	220 (513)	62 (63)	307 (691)
MS S 624	199 (650)	70 (75)	282 (736)

Analysing the results it is possible to conclude that an optimal unit should have pressure drops in the feed, vent and storage tank tubes as small as possible.

Experimental and simulation curves of purity and recovery as a function of the production flow rate are presented in Figure 5.16 and are in good agreement. The experimental data were obtained in Oxymat 3 from Weinmann without the equalization step. Each stage had a duration of 9s.

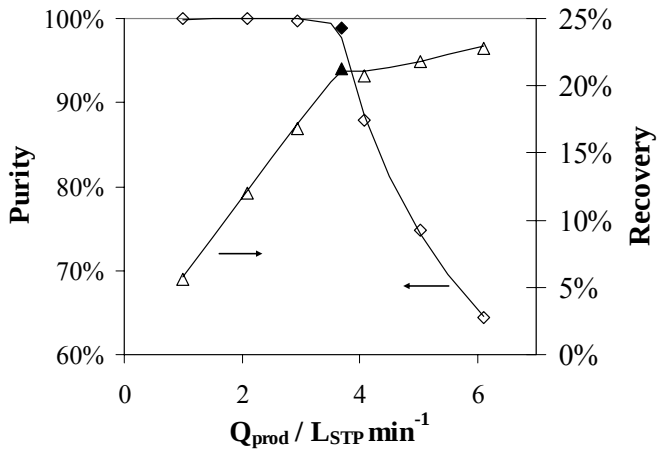

Figure 5.16. Comparison between simulated and experimental purity and recovery achieved on the unit studied (◇ Experimental purity, — Simulation purity, ◆ Simulated optimum purity, △ Experimental recovery, — Simulation recovery, ▲ Simulated optimum recovery).

The simulated pressure histories, inside the columns, for each operating condition tested were also in agreement with the experimental results, as can be seen in Figure 5.17.

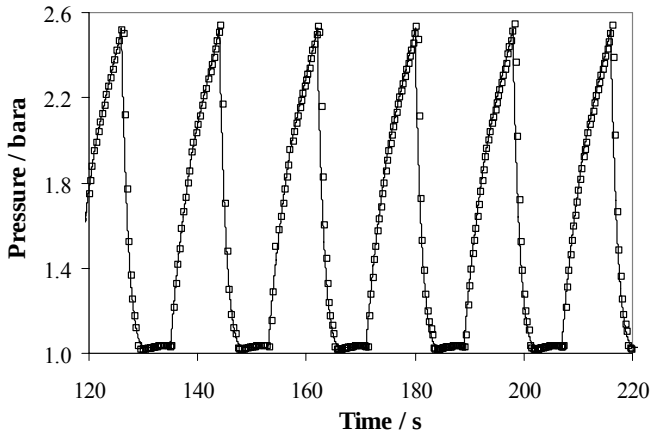

Figure 5.17. Comparison between simulated and experimental pressure history, inside the columns, achieved on the unit studied for a production flow rate of 5 L_{STP}/min (— Simulation, □ Experimental).

Analysing the previous figures it is possible to conclude that the simulator is able to represent very accurately the performance of a real unit.

The unit was optimized for a production flow rate of 3.7 L_{STP}/min ($R_p^b = 283.74$). This product flow rate is the highest that allows a product purity of 0.99 of the pseudo component (oxygen plus argon).

Analysing the physical characteristics of the existing unit, one notices that the storage tank and vent valve parameters already have high values, in agreement with the optimizations presented before. In addition, it must be noted that, for such high R_p^b, the value of L/L^T has only a minor influence on the process performance (simulations with L/L^T in the range from 1 to 3 showed no differences on purity and recovery). Thus, the only optimization parameters left are then $\theta_{press/prod}$ and C_v^P.

In this unit, further increasing $\theta_{press/prod}$ implies a higher pressure ratio (P^H/P^L)–as the compressor continues to pressurize the column, up to its maximum operation pressure –, which should correspond to higher purity and recovery (Mendes et al., 2000). However, this is not acceptable in practice, since $\theta_{press/prod}$ is already set to the highest value that allows a maximum column pressure just below the legislated limit (a special certificate would be required if the pressure exceeded 3 bara). For this reason, the pressurization/ production time is verified to be at its optimum value and the only optimization parameter left is C_v^P.

The simulated optimum was obtained for a normalised $C_v^P = 27.58$, which implies, for these operating conditions, $K_v^P = 0.0458$. The optimization result is presented in Figure 5.16. The purity constraint was respected and a recovery of 21.3% was achieved. As can be seen in Table 5.3, the value of K_v^P for the existing unit is already quite close to the estimated optimum.

5.7.1.3 Cycle with equalization

Units with three types of equalization steps were studied: top-to-top (TE), bottom-to-bottom (BE) and crossed (CE). The performance of these units was compared with the performance of a unit without equalization (NE), for the adsorbents Oxysiv 5,

Oxysiv 7 and MS S 624. The following results are presented as functions of the variable R_p^b ($R_p^b = k_{ref} \cdot L/u_{ref}$).

Figure 5.18, presents the maximum product recovery for each equalization type and adsorbent studied (Santos et al., 2006). The units were optimized for producing 99% of oxygen plus argon at 20ºC and operating between 3 bara and the atmospheric pressure.

Oxysiv 7 yields higher recoveries for the imposed product purity. This adsorbent also allows the use of lower R_p^b, i.e., smaller units or higher product flow rates. However, it is the most expensive, so economical judgment should be taken into account when selecting the unit's adsorbent.

Figure 5.18 shows that the unit recovery is always improved when an equalization step is added to the original cycle. In addition, it can be seen that top-to-top equalization presents better results for all the absorbents studied. Bottom-to-bottom and crossed equalizations display quite similar performances. In addition, it must be noted that top-to-top and bottom-to-bottom equalizations are more economical since they need fewer valves than crossed equalization (crossed equalization needs five more valves than the others).

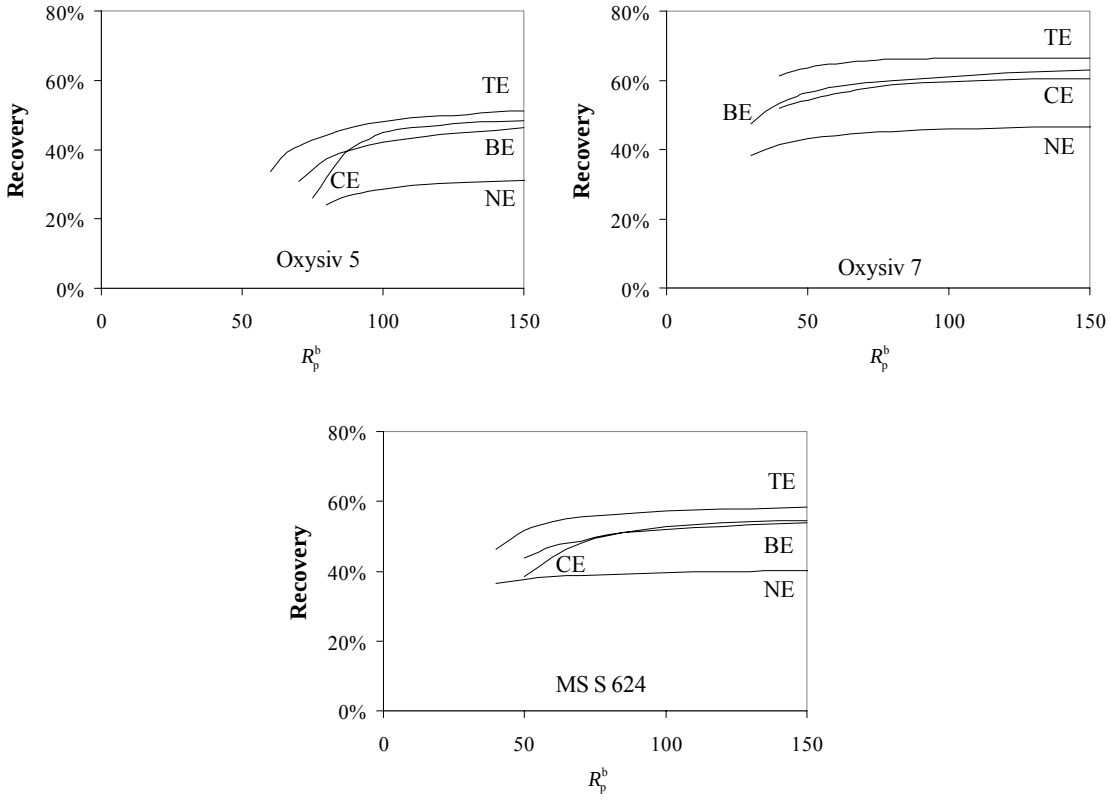

Figure 5.18. Maximum product recovery.

Besides the higher recovery and the lower unit cost, top-to-top equalization has also another advantage: in bottom-to-bottom equalization as well as in crossed equalizations steps, the gas enters the column that is being pressurized from the bottom. This flux can drag the contaminants eventually accumulated at the bottom of the adsorption column. This effect is certainly avoided by using top-to-top equalization. The use of this type of equalization will result in a delay of the adsorbent contamination and, consequently, in an extension of the equipment life-time. Therefore, top-to-top equalization appears to be the best choice for oxygen separation from air.

A decrease on the product recovery is noticeable, in Figure 5.18, for small R_p^b values. This strong variation is verified in almost all the variables optimized, which shows that this region is unstable and little variations in the operating conditions result in significant variations in the unit performance. For this reason, it is advisable to avoid this region.

The unit's power consumption for the different adsorbents and cycles studied are presented in Figure 5.19.

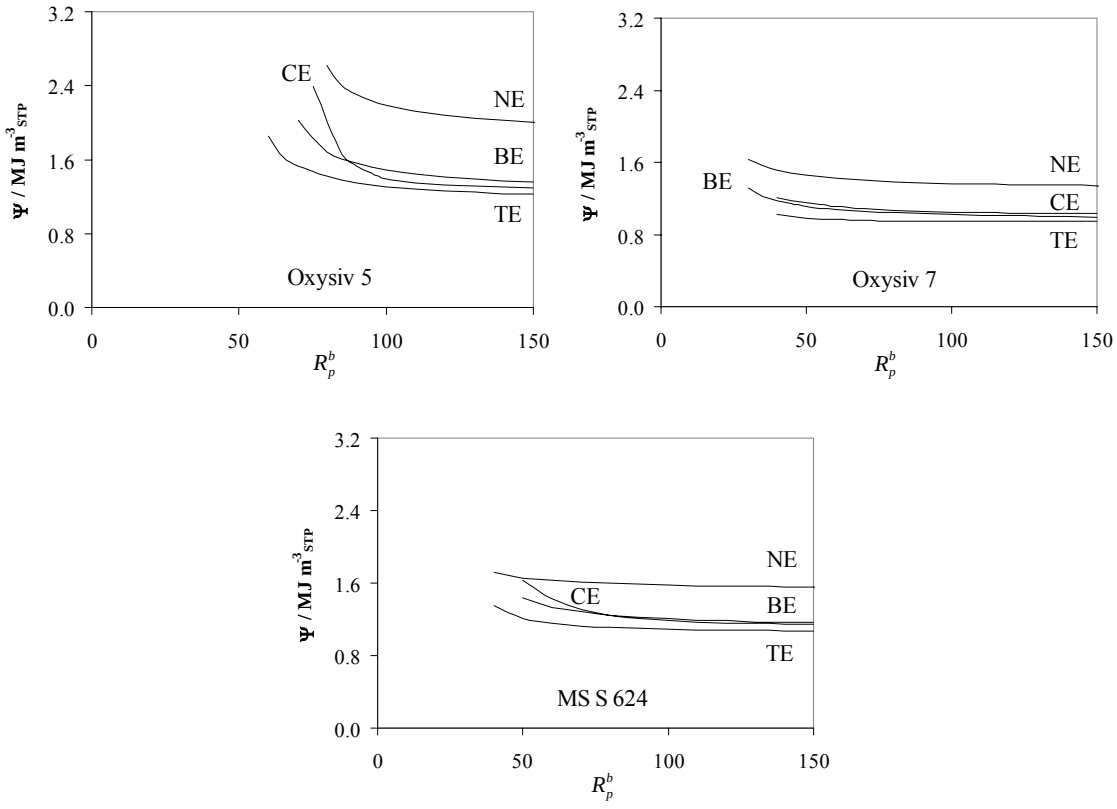

Figure 5.19. Power consumptions for each equalization type and adsorbent.

As it could be expected, the introduction of an equalization step reduces the unit's power consumption and, once again, top-to-top equalization gives the best results.

The optimum values for the unit's ratio between the column and storage tank lengths, the pressurization/ production time, the equalization time and the purge orifice parameter are presented in the next figures (Figure 5.20 to Figure 5.23).

Cycles without equalization require larger storage tanks (Figure 5.20). This feature causes the unit to take longer to reach the steady state, which is undesirable in oxygen concentrators. It is very important that the unit starts producing oxygen with purity above 82% in a short time. Even in cycles with equalization steps, for small R_p^b values, the ratio between the column and the storage tank lengths starts to decrease strongly, so this zone should be avoided.

As can be seen in Figure 5.21, when an equalization step is used, the pressurization/ production times do not differ significantly among adsorbents. However, units without equalization require longer pressurization/ production times.

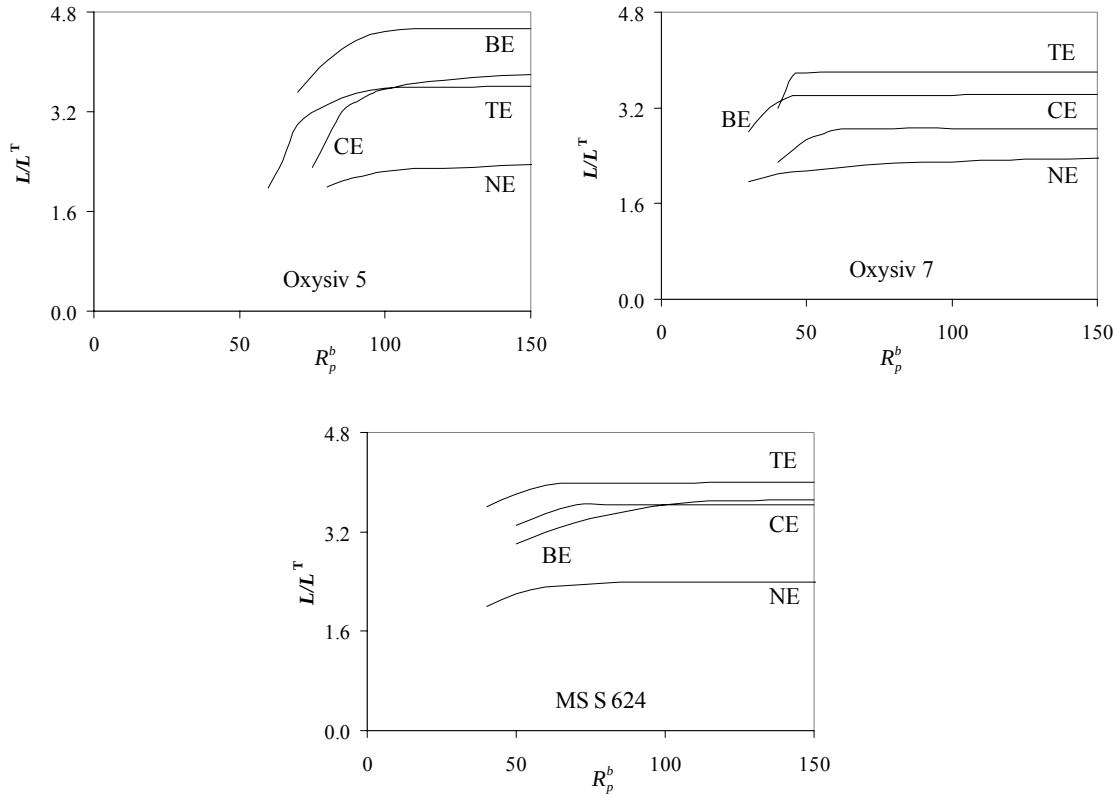

Figure 5.20. Optimum ratio between the column and storage tank lengths.

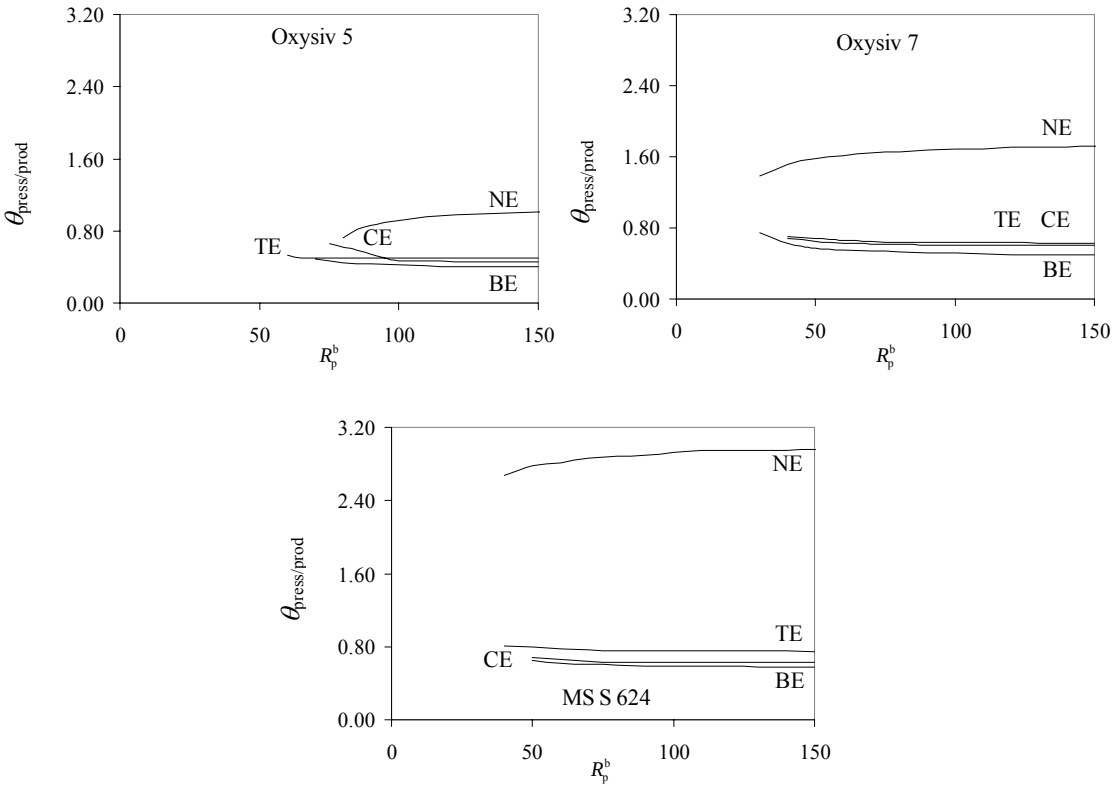

Figure 5.21. Optimum pressurization/ production time.

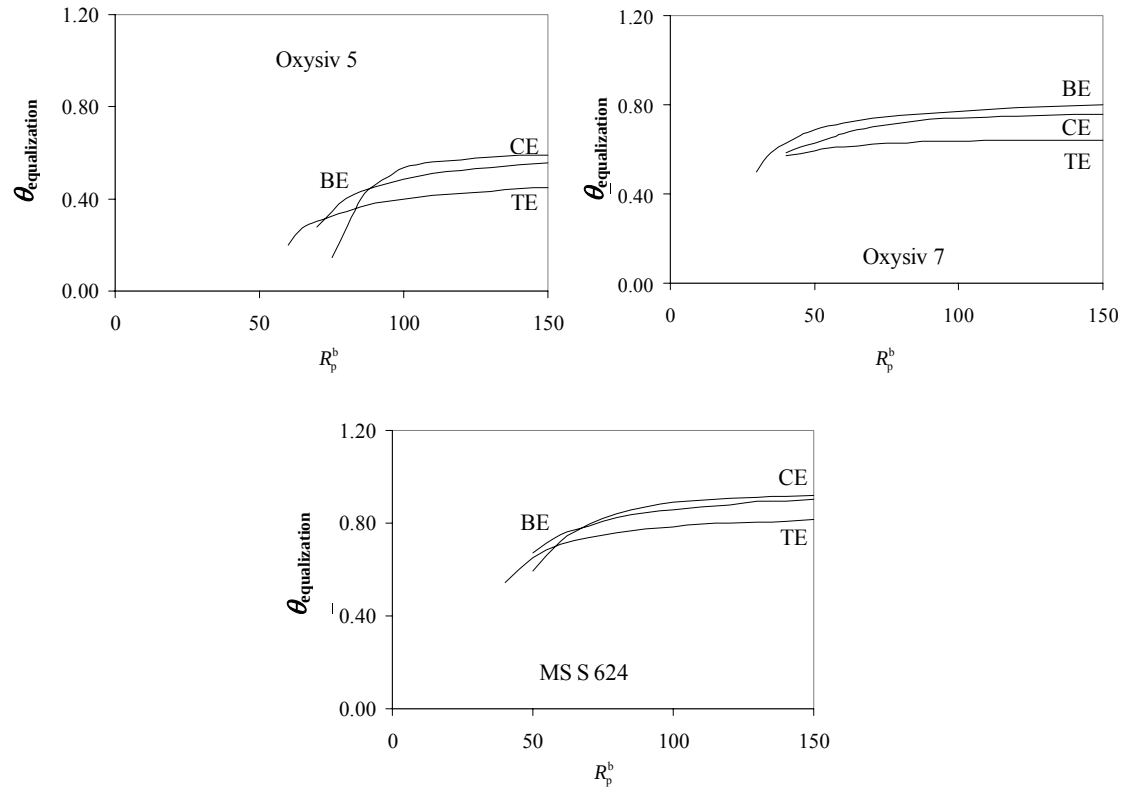

Figure 5.22. Optimum equalization time.

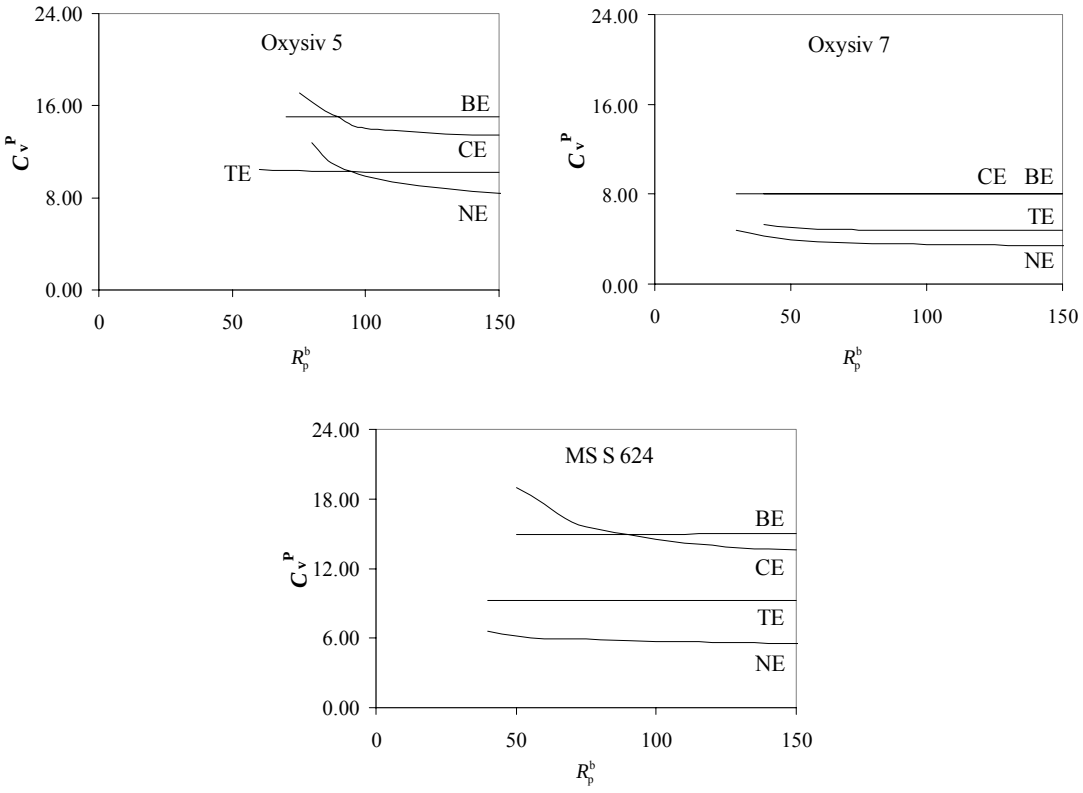

Figure 5.23. Optimum purge orifice parameter.

The dimensionless optimum feed, equalization, storage tank and vent orifices parameters showed to be independent of the unit size and product flow rate and their values are presented in Table 5.5.

Table 5.5. Dimensionless optimum Feed, Equalization, Storage Tank and Vent orifices parameters.

		C_v^F	C_v^E	C_v^T	C_v^V
Oxysiv 5	NE	199	-	73.4	228
	TE	205	28.46	47.9	424
	CE	238	0.63	58.0	423
	BE	238	1.26	55.0	423
Oxysiv 7	NE	220	-	62.0	307
	TE	360	15.57	4.76	440
	CE	232	3.68	5.28	316
	BE	232	3.83	4.05	316
MS S 624	NE	155	-	70.0	282
	TE	257	18.15	43.7	466
	CE	216	3.53	1.70	423
	BE	201	3.50	1.70	361

Top-to-top equalization needs a shorter equalization time, but it has a higher C_v^E (Table 5.5), which implies a higher gas flow rate during equalization or, in other terms, the energy stored inside the column in the form of pressure is more efficiently used. Top-to-top is also the equalization type that allows the lower C_v^P, which means that less product is wasted for the purge. In Table 5.5 it can be seen that, except for Oxysiv 5, the values of C_v^F and C_v^V in top-to-top equalization are high, which means that this type of equalization needs a low pressure drop in the feed and vent.

Experimental and simulation curves of purity and recovery as a function of the production flow rate are presented in Figure 5.24 and are in good agreement.

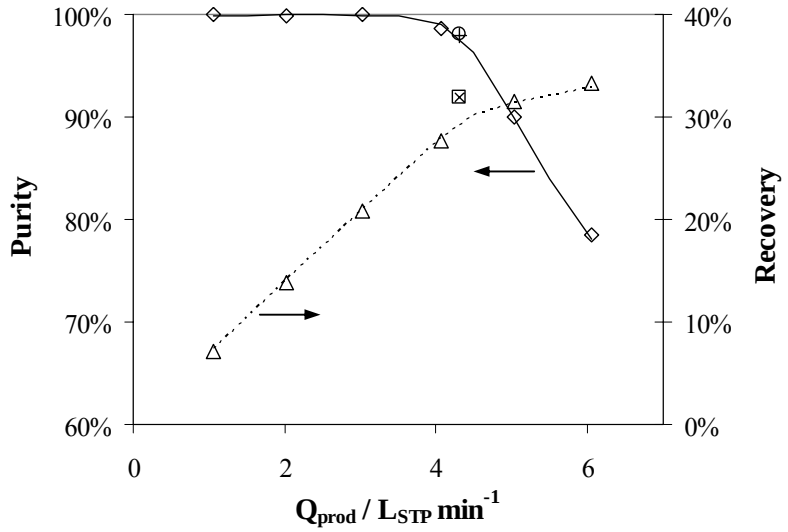

Figure 5.24. Comparison between simulated and experimental purity and recovery achieved on the unit studied using Oxysiv 5 (◇ Experimental purity, ── Simulation purity, + Simulated optimum purity, ○ Experimental optimum purity, △ Experimental recovery, - - - - Simulation recovery, × Simulated optimum recovery, □ Experimental optimum recovery).

The simulated pressure histories, inside the columns, for each operating condition tested were also in agreement with the experimental results, as can be seen in Figure 5.25.

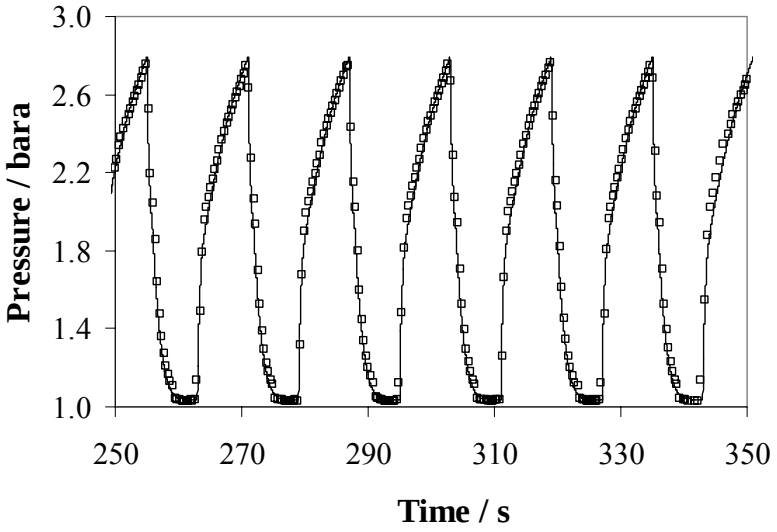

Figure 5.25. Comparison between simulated and experimental pressure history, inside the columns, achieved on the unit studied for a production flow rate of 2 L_{STP}/min (— Simulation, □ Experimental).

To better evaluate the performance of the simulator, Oxysiv 5 was replaced with MS S 624 and some experimental runs were carried out at different product flow rates and with the same operating conditions used with Oxysiv 5. The experimental and simulation results using MS S 624 are presented in Figure 5.26.

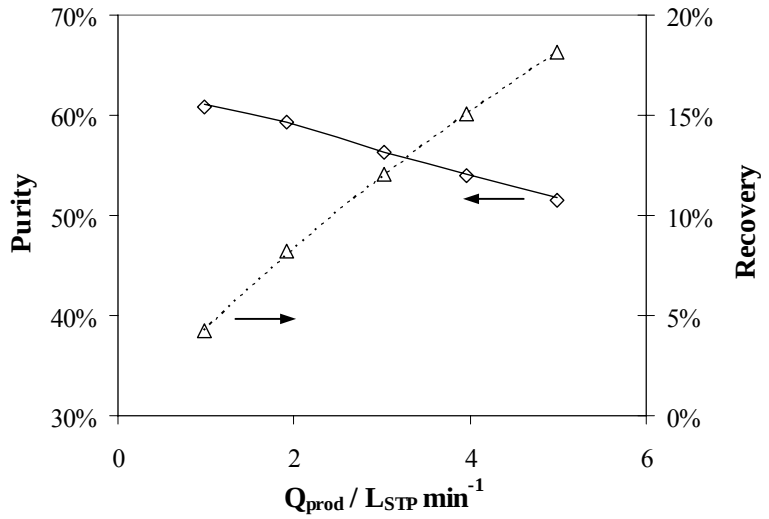

Figure 5.26. Comparison between simulated and experimental purity and recovery achieved on the unit studied using MS S 624 (◇ Experimental purity, — Simulation purity, △ Experimental recovery, - - - - Simulation recovery).

The pressure histories obtained from the simulations were also in agreement with the experimental results, for each operating condition tested with this adsorbent.

A batch of fresh adsorbent was used for all these experiments. Since untreated air was being fed to the columns, in order to check for possible water or carbon dioxide contamination effects, at the end of the experiments the first run (see Figure 5.24 and Figure 5.26) was repeated. Since both runs agreed, it was concluded that there was no contamination.

The previous figures (Figure 5.24 to Figure 5.26) confirm that the developed simulator is able to represent very accurately the performance of a real unit.

The optimization procedure described above was used for optimizing the commercial PSA unit, with Oxysiv 5, with a top-to-top equalization. A flow rate of 4.3 L_{STP}/min ($R_p^b = 244.15$) was chosen as it is the maximum flow rate that allows the production of the pseudo component (oxygen plus argon) with a purity of 0.99.

Comparing the unit's physical characteristics with the optimization results presented before, it is possible to conclude that the storage tank and vent orifices parameters are in agreement with these results as its values are already high, which means low pressure drop in the orifices. Simulations with L/L^{T} in the range from 1 to 5 with high R_p^b , revealed no significant difference in the unit's performance. For this reason this variable may be excluded from the optimization variables.

As mentioned before, these units have a legislated limit of 3 bara for the maximum operation pressure, above which a certificate is required. The $\theta_{press/prod}$ value influences directly the operating pressure as further increasing it will imply higher pressure ratio (P^{H}/P^{L})as the compressor continues to pressurize the column, up to its maximum operation pressure. Although this should correspond to higher purity and recovery (Mendes et al., 2000), for the reason pointed before, this is not desirable. The pressurization/ production time value was found to be at its optimum value and the only optimization parameters left are $\theta_{equalization}$, C_v^E and C_v^P.

For these operating conditions and for the purity constraint, the maximum recovery obtained was 34.1%, with $t_{equalization} = 1\ s$, $K_v^E = 0.6700$ and $K_v^P = 0.0162$. However, due to the existence of a small product outlet hole in the top of each column, the maximum equalization orifice parameter possible for this unit was found to be $K_v^E = 0.1100$, quite below the optimum value. Since the optimization results pointed out to a high equalization orifice parameter, a new optimization was performed with a

K_v^E set to 0.1100. The new maximum recovery, presented in Figure 5.24, was 31.9%, achieved with the optimum values of $t_{\text{equalization}} = 1\ s$ and $K_v^P = 0.0392$.

From the optimization results it is possible to conclude that the performance of the commercial unit can be improved with the use of a top-to-top equalization. Further improvements can be achieved if larger product outlet holes were used in the top of the columns.

This unit was optimized for producing 99% of oxygen plus argon with Oxysiv MDX from UOP with a top-to-top equalization at 20ºC and between 3 bara and the atmospheric pressure. The results are presented in Figure 5.27.

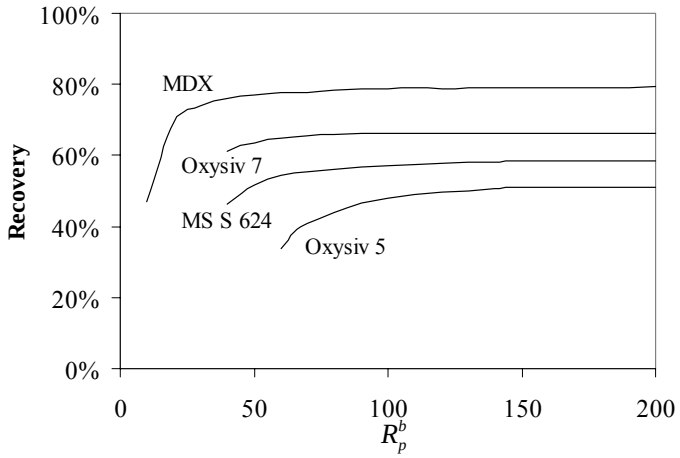

Figure 5.27. Maximum product recovery.

Figure 5.28 presents the optimum power consumption.

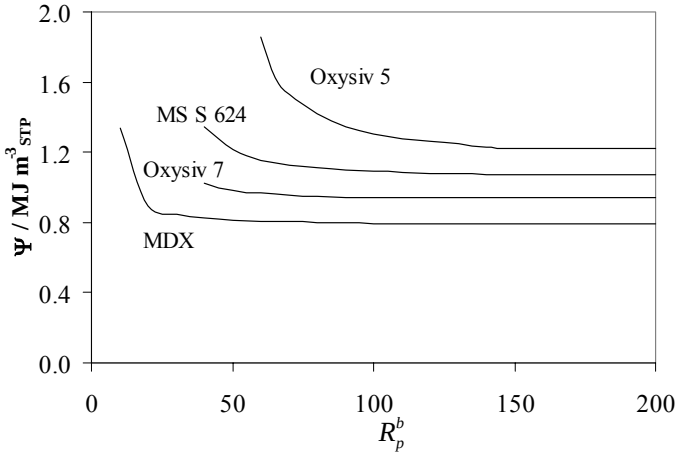

Figure 5.28. Optimum power consumption.

As it can be seen, Oxysiv MDX allows the highest recovery and the lowest power consumption.

The optimum values for the pressurization/ production time, the equalization time and the purge orifice parameter are presented in the next figures (Figure 5.29 to Figure 5.31).

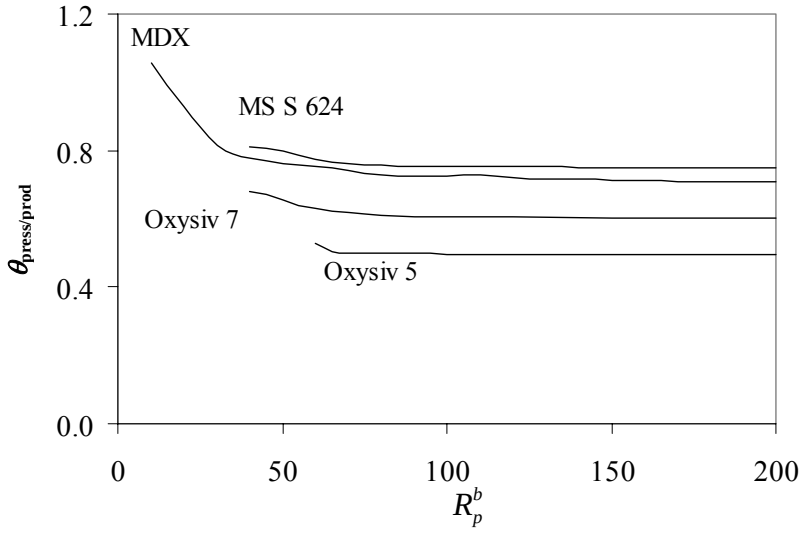

Figure 5.29. Optimum pressurization/ production time.

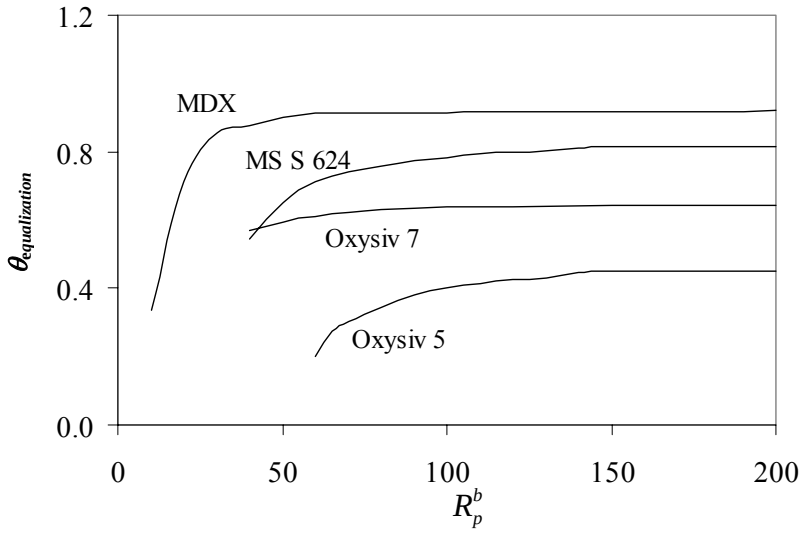

Figure 5.30. Optimum equalization time.

As it can bee seen, Oxysiv MDX requires the longest equalization time. The pressurization/production time required is between MS S 624 and Oxysiv 7.

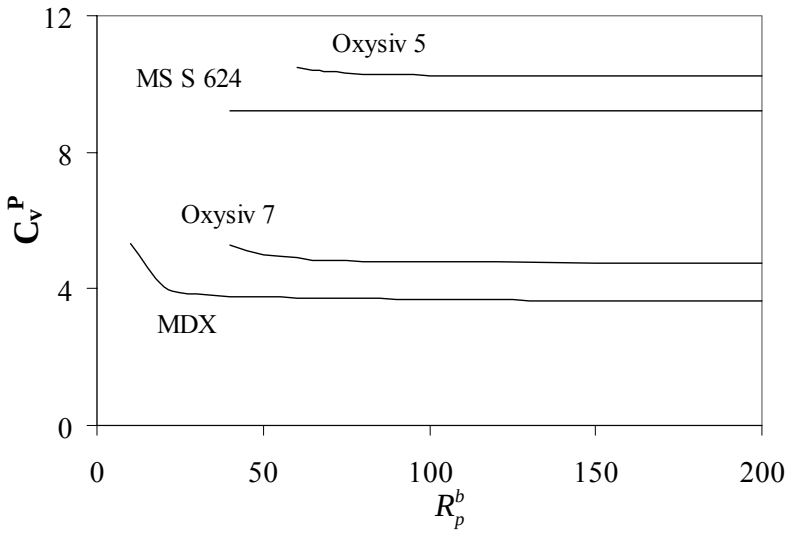

Figure 5.31. Optimum purge orifice parameter.

Analysing Figure 5.31, Oxysiv MDX uses the lowest purge, followed by Oxysiv 7 and MS S 624.

Table 5.6 presents the optimum feed, equalization, storage tank and vent orifices parameters.

Table 5.6. Optimum Feed, Equalization, Storage Tank and Vent Orifices Parameters.

	C_v^F	C_v^E	C_v^T	C_v^V
Oxysiv 5	205	28.46	47.9	424
Oxysiv 7	360	15.57	4.76	440
Oxysiv MDX	216	8.10	2.77	361
MS S 624	257	18.15	43.7	466

As it can be seen, Oxysiv MDX requires a small C_v^E.

5.7.1.4 Cycle with backfill

A PSA unit with product backfill supplied by the column that is producing was simulated and optimized. Figure 5.32 presents the maximum recoveries of the units with backfill (BF) with Oxysiv 5 and Oxysiv 7. The recoveries of the units with different equalizations are also presented for comparison. The units with backfill were also simulated at 20ºC and the pressure between 3 bara and the atmospheric pressure.

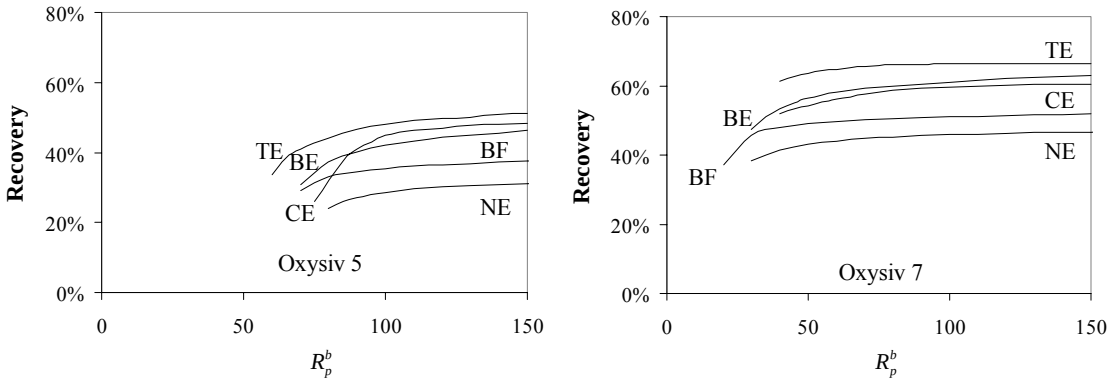

Figure 5.32. Maximum product recovery.

The use of a backfill step increases the product recovery. However, an equalization step allows an even higher recovery.

Figure 5.33 presents the power consumption of the units referred before with Oxysiv 5 and Oxysiv 7.

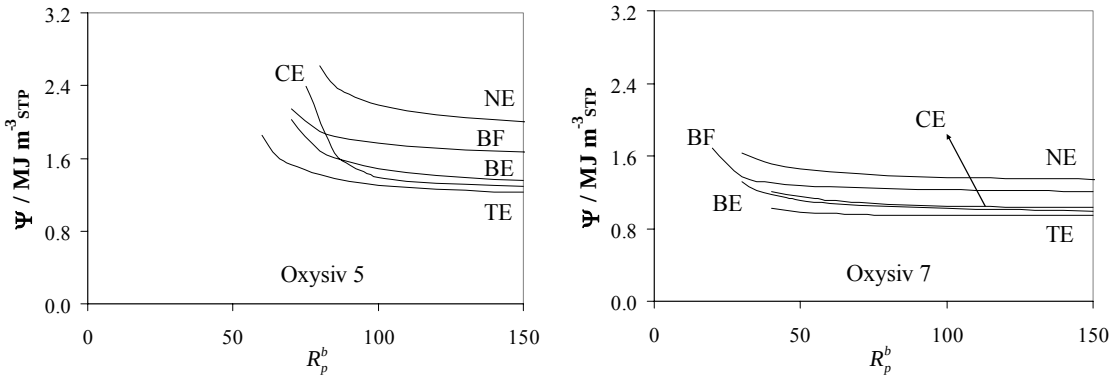

Figure 5.33. Optimum power consumption.

The backfill step also allows the decrease of the power consumption, when compared with a cycle without equalization. However, a unit with any of the equalizations studied before consumes less power.

The optimum ratio between the column and storage tank, the optimum pressurization/production time and the optimum equalization (for TE, BE and CE) and backfill (for BF) time are presented in the following figures (Figure 5.34 to Figure 5.36). Since during backfill the unit is producing, the pressurization/production time for the unit with this step (BF) includes the backfill time.

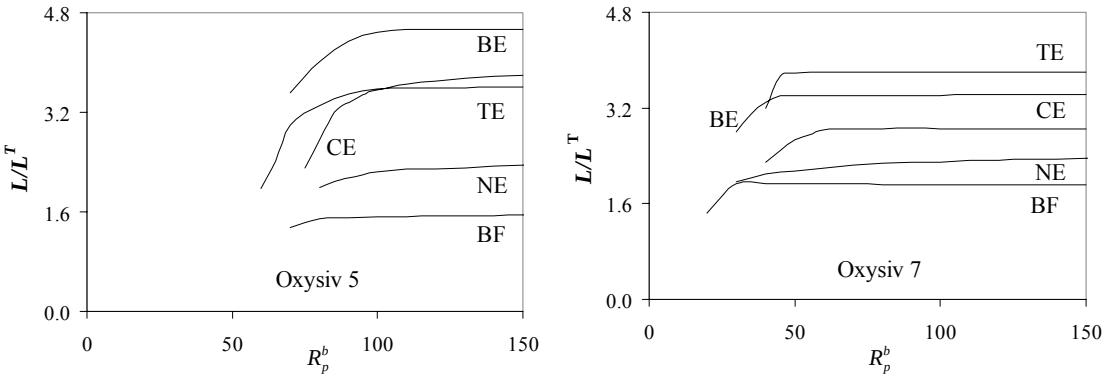

Figure 5.34. Optimum ratio between the column and storage tank lengths.

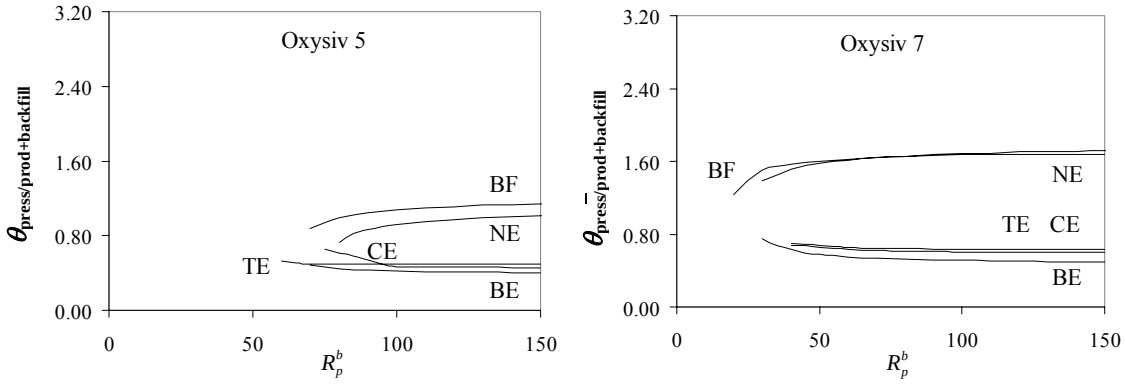

Figure 5.35. Optimum pressurization/ production and backfill (for BF) time.

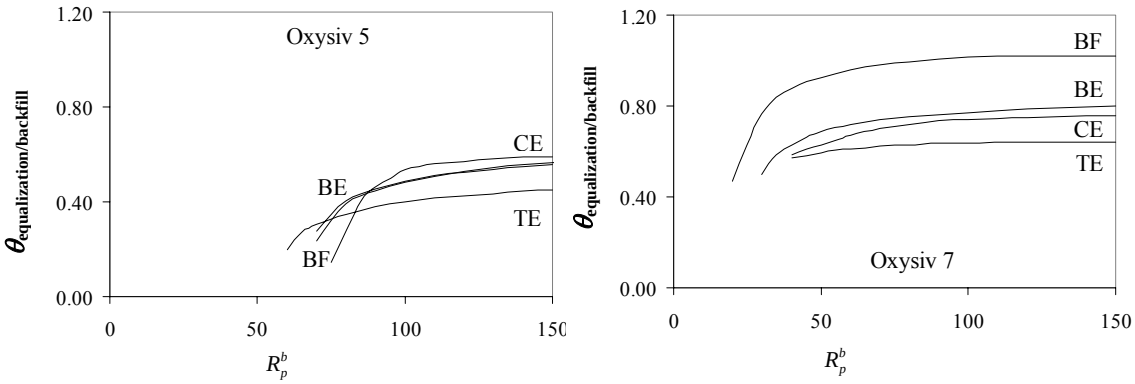

Figure 5.36. Optimum equalization (for TE, BE and CE) and backfill (for BF) time.

The backfill step allows the smallest storage tank as can be seen in Figure 5.34. With this step the unit will produce longer (Figure 5.35). For Oxysiv 5 and for the unit and conditions studied, the backfill time is very similar to the equalization time (Figure

5.36) of a unit with bottom-to-bottom equalization (BE). For Oxysiv 7 this time is much higher.

Table 5.7 presents the optimum feed, equalization, storage tank and vent orifice parameters for the units studied with Oxysiv 5 and Oxysiv 7.

The optimum operating conditions are very similar to the values of the optimization variables obtained for the unit without equalization except for the feed valve parameter for Oxysiv 5 and for the vent valve parameter for Oxysiv 7. The unit with backfill with Oxysiv 5 requires a smaller feed valve parameter which means a slower pressurization.

Table 5.7. Optimum feed, equalization, storage tank and vent orifices parameters for the units studied with Oxysiv 5 and Oxysiv 7.

		C_v^F	C_v^E	C_v^T	C_v^V
Oxysiv 5	NE	199	-	73.4	228
	TE	205	28.46	47.9	424
	CE	238	0.63	58.0	423
	BE	238	1.26	55.0	423
	BF	155	-	73.4	228
Oxysiv 7	NE	220	-	62.0	307
	TE	360	15.57	4.76	440
	CE	232	3.68	5.28	316
	BE	232	3.83	4.05	316
	BF	220	-	57.46	343

Figure 5.37 presents the product purity along the cycle for all the units referred before with Oxysiv 5, for $R_p^b = 100$.

As it can be seen, for Oxysiv 5 and for the conditions studied, the unit without equalization arrives faster to 82% of oxygen (85.64% of oxygen plus argon), which is the minimal legal limit for commercial medical oxygen concentrators, and to the optimized purity, 99% of oxygen plus argon.

For this adsorbent and at these conditions, no advantage was found for using this backfill step. Top-to-top equalization allowed a higher recovery and a faster increase of the product purity.

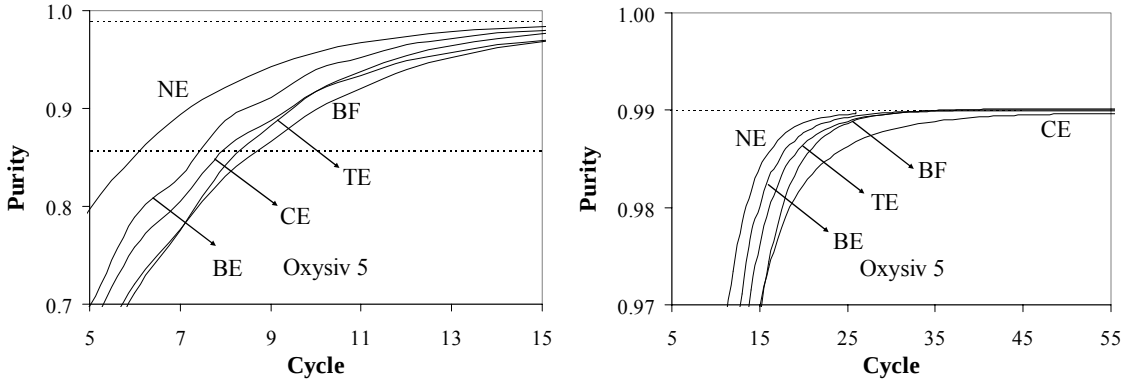

Figure 5.37. Product purity along the cycle for Oxysiv 5.

Figure 5.38 presents the product purity along the cycle for all the units referred before with Oxysiv 7, for $R_p^b = 100$.

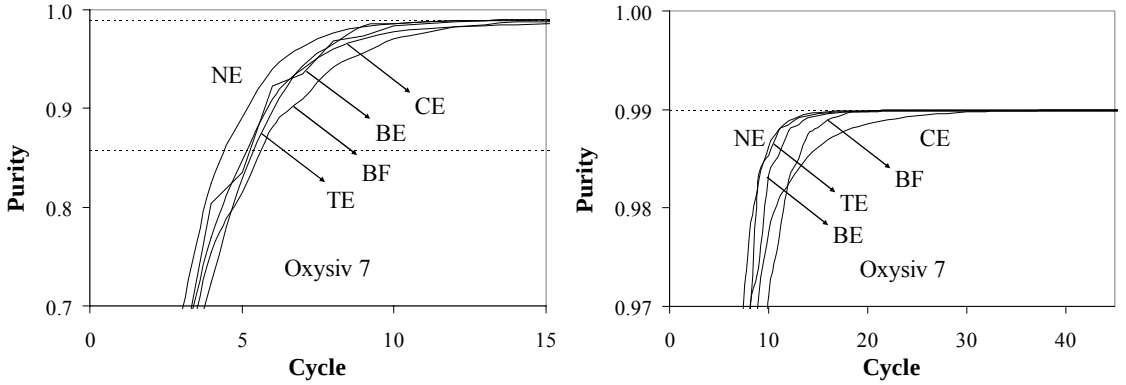

Figure 5.38. Product purity along the cycle for Oxysiv 7.

For Oxysiv 7 and for the conditions studied, the unit without equalization also arrives faster to 82% of oxygen and to 99% of oxygen plus argon (optimized purity).

As for Oxysiv 5, no advantage was found for using this backfill step with Oxysiv 7 and at these operating conditions. Top-to-top equalization allowed a higher recovery and a faster increase of the product purity.

5.7.2 PSA unit from Sequal

5.7.2.1 Experimental results

Table 5.8 presents the oxygen purity given by this unit at different flow rates.

Table 5.8. Oxygen purity at different flow rates.

Flow rate (L_{STP}/min)	T (ºC)	y_{O_2}
1.03	27.3	0.919
1.91	27.3	0.922
2.97	27.1	0.934
4.08	27.1	0.915
5.14	26.9	0.877

As it can be seen, comparing to the results presented in Figure 5.24, the performance of this unit, in terms of product purity is inferior to the unit from Weinmann.

5.7.3 VPSA unit from Air Products and Chemicals

5.7.3.1 Description of the unit

This experimental unit used is very similar to the commercial unit. The only difference is that instead of a rotary valve, solenoid valves are used. The columns have a length of 8.7 cm and an internal diameter of 5.25 cm and have two layers: one of activated alumina (2.6 cm of length) and another of Oxysiv MDX from UOP (6.1 cm of length).

5.7.3.2 Experimental results

The experimental results were supplied by Air Products and Chemicals, Inc. The feed was untreated air at 37.2 ºC and the step duration was 1 s. The product flow rate was 3 L_{STP}/min.

Figure 5.41a) presents the experimental feed flow rate given by the compressor as function of the feed pressure and Figure 5.41b) presents the experimental vent flow rate given by the vacuum pump as function of the vent pressure.

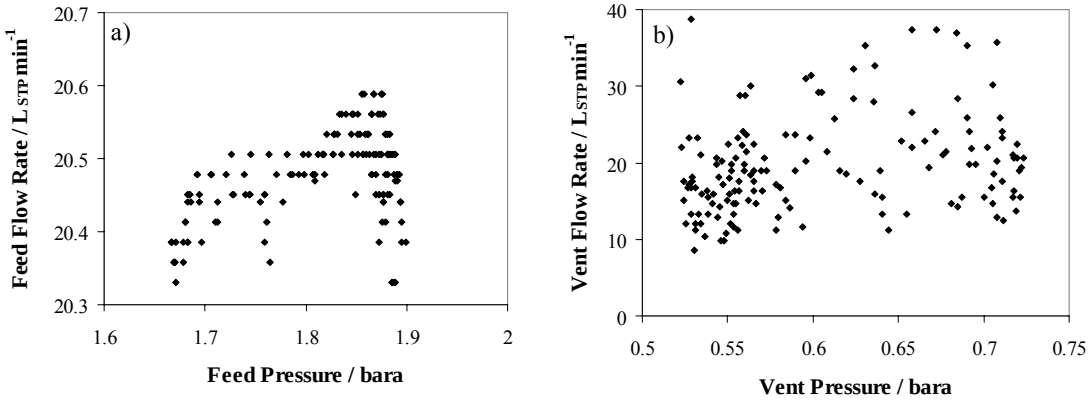

Figure 5.39. Experimental feed a) and vent b) flow rates versus corresponding pressure.

For the simulations, the feed flow rate was considered to be constant and equal to 20.48 L_{STP}/min. The vent flow rate was also considered to be constant and equal to 20.46 L_{STP}/min. The valve parameter C_v^P is 0.012, C_v^B is 0.014, C_v^E is 0.03 and C_v^T is 0.1.

Figure 5.40 presents the simulated and experimental pressure histories

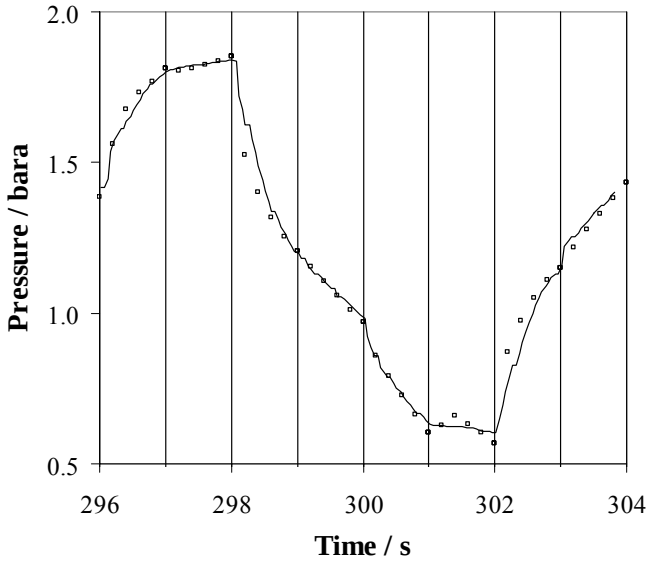

Figure 5.40. Simulated and experimental pressure histories (the line is the simulated pressure history and the doted line the experimental pressure history).

The simulated and experimental recovery and purity are presented in Table 5.9

Table 5.9. Experimental and simulated recovery and purity.

	Experimental	Simulated
Purity (%)	94.80	94.59
Recovery (%)	58.91	59.15

As it can be seen, the simulator was able to accurately represent the experimental unit.

5.7.4 Small experimental PSA unit with Oxysiv MDX

5.7.4.1 Description of the unit

The small experimental pressure swing adsorption unit was assembled in the framework of this Thesis. It was packed with Oxysiv MDX and was also used for high purity oxygen production. This unit is represented in Figure 5.41.

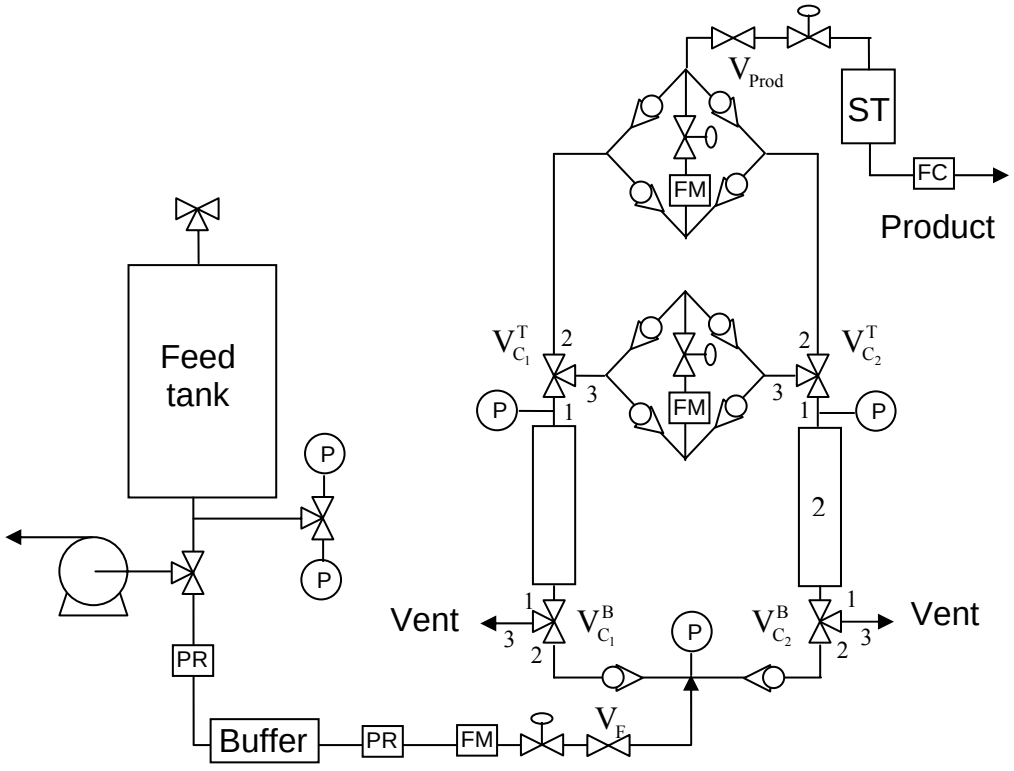

FM – Flow meter**; FC –** Flow controller**; PR –** Pressure reducer; **ST** – Storage Tank**.**

Figure 5.41. Sketch of the experimental PSA unit used with Oxysiv MDX and used for high purity oxygen production.

The unit has 3 stainless steel columns (one as storage tank for the product) with 27 cm of length and 1 cm of diameter. The buffer column is also in stainless steel and has 26 cm of length and 7.5 cm of diameter. The pressure inside the buffer tank is set to 0.5 bar above the high pressure of the unit for assuring a fast pressurization. The feed tank has 60 dm^3 and the unit is all built with Swagelok stainless steel fittings. The pipe and connectors in the bottom of the unit is all in 1/4" size for allowing fast pressurizations and depressurizations and in the top are all in 1/8" size. The metering valve in the feed is from Swagelok, reference SS-1RS4. The metering valves in the purge, equalization and before the storage tank are also from Swagelok, reference SS-2MG. The 3-way solenoid valves in the bottom and top of the columns are from ASCO and are certified for use with oxygen (they were cleaned and so do not have lubricant). The valves in the bottom are also in 1/4" size (reference SCE 370A056nV) and in the top are in 1/8" size (reference SC G325B031). The unit has two on-off valves from ASCO: in the feed, in 1/4" size (reference SCE370A056nV), for the equalization, and before the product storage tank in 1/8" size (reference SC G225B006NV).

The three pressure sensors in the unit are from Druck, model PMP 4010 and are from 0 to 7 bara. The two pressure sensors near the feed tank are for preparing the mixtures and are also from Druck, model PMP 4010; one is from 0 to 2 bara and the other is from 0 to 7 bara. The accuracy of these pressure sensors is 0.08% FS.

The pressure reducers are from Joucomatic (reference 34200314) and so are the pressure gauges attached to them (reference 34300015).

All the flow meters and controllers are from Bronkhorst. The flow meter in the feed is from 0 to 20 L_{STP}/min (reference F-112AC-HAD-22-V), the meter in the purge and in the equalization stream is from 0 to 10 L_{STP}/min (reference F-111C-HAD-22-V) and the flow controller in the product is from 0 to 100 mL_{STP}/min (reference F-201C-FAC-21-V). The accuracy of these flow meters and controllers is 0.2% FS

Two oxygen analysers were used: one from M&C, model PMA22, from 0 to 100% with an accuracy of 0.1% FS and another from Sable Systems, model PA-1B, also from 0 to 100% with an accuracy of 0.01% FS.

All the pressure sensors require 9 to 32 VDC and the output signals are from 0 to 5 VDC. The flow meters require 0 and +15 VDC and the flow controller requires 0, +15 VDC and -15 VDC. The output signals are from 0 to 5 VDC. The output signals were acquired in a personal computer with a National Instruments acquisition board, model PCI-6035E.

The solenoid valves require 0 and +24 VDC. The cycles were controlled with a programmable relay, model ZEN, reference 20C1DR-D-V1, powered with 24VDC.

Table 5.10 presents the position of the valves during the cycle.

Table 5.10. Position of the valves during the cycle.

Step	Valve					
	$V_{C_1}^B$	$V_{C_2}^B$	$V_{C_1}^T$	$V_{C_2}^T$	V_F	V_{Prod}
1	2→1	1→3	1→3	1→2	ON	OFF
2	2→1	1→3	1→2	1→2	ON	ON
3	1→2	1→2	1→3	1→3	OFF	OFF
4	1→3	2→1	1→2	1→3	ON	OFF
5	1→3	2→1	1→2	1→2	ON	ON
6	1→2	1→2	1→3	1→3	OFF	OFF

This unit operates with a standard cycle with a top-to-top equalization (TE), i.e., with steps well defined: pressurization, production and equalization.

The left column was packed with 90.5 g of MDX from UOP and the right column with 89.7 g.

5.7.4.2 Experimental results

For avoiding any contamination of the adsorbent, pure reconstituded air was used (21% of oxygen and 79% of nitrogen).

Table 5.11 presents the operating conditions of the experiments with Oxysiv MDX, from UOP, at 30ºC.

Table 5.11. Operating conditions of the experiments with Oxysiv MDX at 27ºC.

Run	t_{press} (s)	t_{prod} (s)	t_{eq} (s)	Product flow rate (mL_{STP}/min)
1	3.9	20.0	18.83	125
2	2.0	7.5	10.50	225

The experimental and simulation results (purity, Pur, and recovery, Rec) of these runs are presented in Table 5.12.

Table 5.12. Experimental and simulation results of the PSA unit with Oxysiv MDX.

Run	Experimental results (%)		Simulation results (%)	
	Pur	Rec	Pur	Rec
1	1.00	73.51	0.99	73.72
2	1.00	73.46	0.99	73.55

For calibrating the oxygen analyzers, a mixture of 90% of oxygen, 5% of nitrogen and 5% of argon was used as zero gas and pure oxygen was used as span.

Table 5.13 presents the valve coefficients determined experimentally for the runs presented before.

Table 5.13. Valve coefficients of the PSA unit with Oxysiv MDX.

Run	C_v^P	C_v^E
1	0.00045	0.00096
2	0.00080	0.00192

The feed, C_v^F, vent, C_v^V, and storage tank, C_v^T, valve parameters are respectively 0.025, 0.025 and 0.002.

Figure 5.42 presents the simulated and experimental pressure history for run 2.

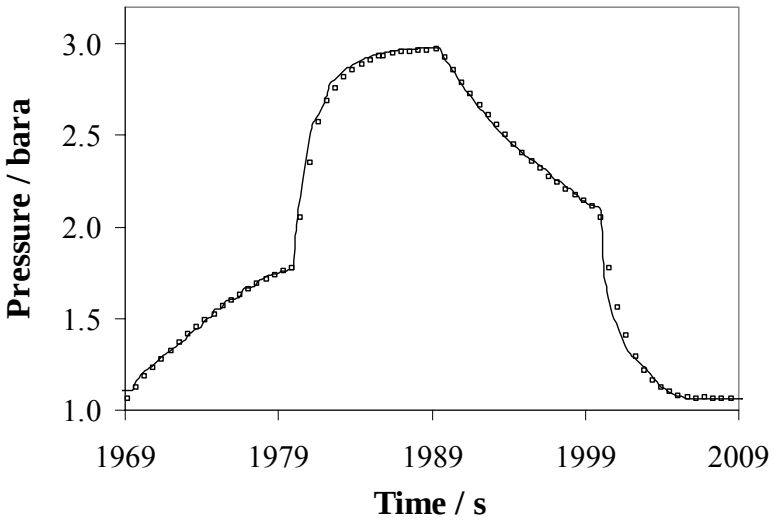

Figure 5.42. Simulated and experimental pressure history, inside the columns, achieved on the unit studied for run 2 (—Simulation, □ Experimental).

Analysing Table 5.12 and Figure 5.42 it is possible to conclude that the simulator was able to accurately represent the experimental results.

5.7.5 Small experimental PSA unit for high purity oxygen production

5.7.5.1 Description of the unit

The unit used for high purity oxygen production was the same as the one presented in the previous section.

The left column was packed with 101.86 g of AgLiLSX from Air Products and Chemicals and the right column with 101.37 g.

5.7.5.2 Experimental results

For avoiding any contamination of the adsorbent, mixtures of pure gases were prepared in the feed tank with the following concentrations: 78.12% of nitrogen, 20.95% of oxygen and 0.93% of argon (such as air) and 95% of oxygen and 5% of air (such as a product from a PSA unit).

Table 5.14 presents the operating conditions of the experiments with AgLiLSX at 30ºC.

Table 5.14. Operating conditions of the experiments with AgLiLSX at 30ºC.

Run	Feed composition (%)			t_{press} (s)	t_{prod} (s)	t_{eq} (s)	Product flow rate (mL_{STP}/min)
	O_2	Ar	N_2				
1	21	0	79	6.6	8.28	2.1	100
2	21	0	79	6.6	48.28	32.1	30
3	21	0	79	6.6	8.28	2.1	30
4	21	1	78	6.6	8.28	2.1	30
5	21	1	78	6.6	8.28	2.1	50
6	95	5	0	6.6	18.28	12.1	80
7	95	5	0	6.6	18.28	12.1	30
8	95	5	0	6.6	19.28	16.1	30
9	95	5	0	6.6	12.28	16.1	50

Runs 1 to 3 were conducted with pure reconstituted air.

The experimental and simulation results (purity, Pur, and recovery, Rec) of these runs are presented in Table 5.15.

For calibrating the oxygen analyzers, a mixture of 90% of oxygen, 5% of nitrogen and 5% of argon was used as zero gas and pure oxygen was used as span.

Table 5.15. Experimental and simulation results of the PSA unit with AgLiLSX.

Run	Experimental results (%)		Simulation results (%)	
	Pur	Rec	Pur	Rec
1	100	19.80	100	19.76
2	100	20.41	100	20.35
3	100	5.65	100	5.50
4	98.73	5.64	98.71	5.60
5	98.64	7.60	98.55	7.45
6	98.73	7.42	98.75	7.45
7	99.80	2.94	99.92	3.03
8	99.65	2.93	99.80	3.10
9	98.98	4.29	99.93	4.33

As it can be seen in Table 5.15, this adsorbent allows the production of high purity oxygen.

Table 5.16 presents the valve coefficients determined experimentally for the runs presented before.

Table 5.16. Valve coefficients of the PSA unit with AgLiLSX.

Run	C_v^P	C_v^E
1	0.0004	0.0020
2	0.0004	0.0020
3	0.0006	0.0050
4	0.0005	0.0030
5	0.0010	0.0020
6	0.0010	0.0048
7	0.0010	0.0048
8	0.0010	0.0015
9	0.0016	0.0017

Figure 5.43 presents the simulated and experimental pressure history for run 9.

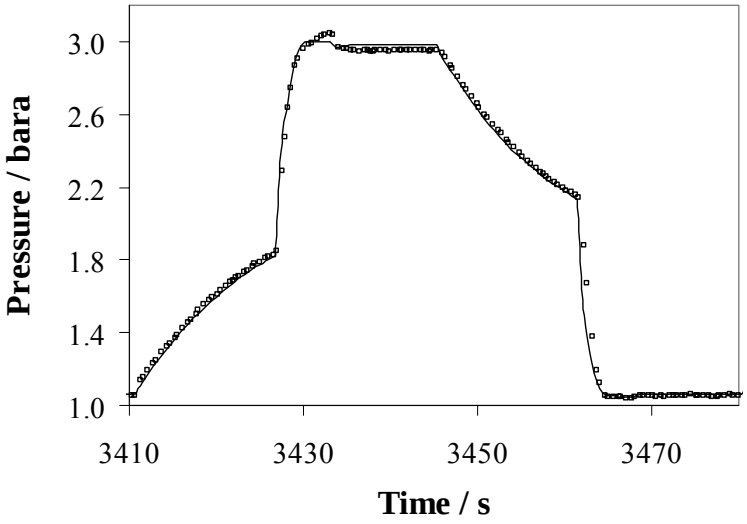

Figure 5.43. Simulated and experimental pressure history, inside the columns, achieved on the unit studied for run 9 (—Simulation, □ Experimental).

Analysing Table 5.15 and Figure 5.43 it is possible to conclude that the simulator was able to accurately represent the experimental results.

As referred before, Jee et al. presented a PSA unit with two adsorption columns with about 380mL packed with CMS adsorbent from Takeda (Jee et al., 2005). The feed is 95% of oxygen and 5% of argon and its flow rate is 4 L_{STP}/min. The high pressure is 5 bara. This unit produces around 1.6 L_{STP}/min of 99.87% oxygen with a recovery of 56.90%. According to the simulation results presented before, this unit coupled with a PSA unit packed with Oxysiv MDX would have a global recovery around 45%. It would be composed by two columns with about 1L (packed with Oxysiv MDX) and two columns with 380mL (packed with CMS adsorbent). The drawback of this technology is that the product is obtained at a pressure close to the atmospheric pressure and so, a third compressor might be needed to pressurize it.

A conventional oxygen concentrator for producing 95% of oxygen at this flow rate (1.6 L_{STP}/min), packed with Oxysiv 5, would need two columns with 800mL and would have a recovery around 35%.

Although the recovery given by this combination of units is high, technologically the unit is larger and more complex. In some applications where the size is important, it is advisable the use of AgLiLSX to directly produce high purity oxygen

or even a combination of a PSA with Oxysiv MDX, for example, with another PSA with AgLiLSX (although this combination is also complex, the product is obtained at high pressure).

5.8 Conclusions

Pressure swing adsorption cycles were compared with vacuum and pressure swing adsorption cycle mode. Cycles with three different types of equalization: top-to-top, bottom-to-bottom and crossed were compared as well. It was concluded that the top-to-top equalization is the best configuration since it allows higher recoveries, lower power consumption, requires fewer valves and avoids the dragging of the contaminants from the bottom of the column to the top. The bottom-to-bottom and crossed equalizations allow to obtain very similar performances. The use of any of these types of equalization allows a significant increase of the unit's performance.

As expected, a vacuum and pressure swing adsorption (VPSA) unit has a lower power consumption per product flow rate than a pressure swing adsorption (PSA) unit operating with the same pressure ratio although the VPSA unit is larger than the PSA unit.

The backfill step that was presented (the column producing backfills the other column) did not show to be advantageous in respect to the recovery and to the minimization of the time required to achieve the desired purity for a two bed unit. For the adsorbents and conditions studied a cycle without equalization arrives faster than with any other of the cycles studied. A cycle with top-to-top equalization allowed a high recovery and a fast increase of the product purity.

The adsorbent AgLiLSX from Air Products showed to allow the production of high-purity oxygen in a single step, although with a low recovery.

Oxysiv MDX from UOP allows the best performance in all the cycles studied, followed by AgLiLSX from Air Products and Chemicals, Oxysiv 7 from UOP, MS S 624 from Grace Davison and Oxysiv 5 from UOP. The use of Oxysiv MDX, AgLiLSX, Oxysiv 7 and MS S 624 in PSA units and MDX, AgLiLSX and Oxysiv 7 in VPSA units will have as a result, smaller units or higher product flow rates. However, Oxysiv MDX, AgLiLSX and Oxysiv 7 are more expensive than the other adsorbents studied.

The simulator was able to represent accurately a real unit when the contamination by carbon dioxide and water vapour is avoided. With the optimization strategy it was possible to achieve better operating conditions and design characteristics that improved the performance of the units.

The oxygen concentrator from Air Products and Chemicals, Inc. was studied and compared with the oxygen concentrators from Weinmann and Sequal and was found to have a higher performance while maintaining a small size and low noise levels and power consumptions – key issues for such units.

From a technological point of view, the use of rotary valves such as the ones used by Air Products and Chemicals and by Sequal has the advantage of avoiding the problems caused by the ware out of solenoid valves, especially in short cycles where the valves are constantly opening and closing, and problems caused by the dust resultant from the adsorbent which might cause leakages in the valves and consequently significantly reduce the performance of the unit. Another advantage comes from the fact that less piping is used, which will also reduce the chances of leakage.

5.9 Notation

A	area, m^2
c	molar concentration, mol/m^3
c_{ref}	reference molar concentration in fluid phase, $c_{ref} = P_{ref} / \Re T_{ref}$
C_v	dimensionless valve parameter
D_{ax}	effective axial dispersion coefficient, $m^2\ s^{-1}$
F	volumetric flow rate, $m^3_{STP}\ s^{-1}$
k	LDF kinetic coefficient, s^{-1}
K_v	valve parameter
L	adsorption column lenght, m
L^T	storage tank lenght, m
M	molecular weight, kg mol^{-1}
N	molar flow rate, mol $m^{-3}\ s^{-1}$
N^*	dimensionless molar flow rate, $N^* = N\theta_{ref} / (C_{ref}\varepsilon_b)$
nc	number of components in the mixture
P	total pressure, Pa
Pe	Peclet number for mass transfer, $\mathrm{Pe} = u_{ref} L / D_{ax}$
$\overline{q}$	average molar concentration in the adsorbed phase, mol kg^{-1}
q	molar concentration in the adsorbed phase, mol kg^{-1}
Q_{prod}	product flow rate, $m^3_{STP}\ s^{-1}$
$\Re$	universal gas constant, $(Pa \cdot m^3)/ (mol \cdot K)$

R_p^b ratio between the bed time constant and the particle diffusion time constant, $R_p^b = k_{ref}\theta_{ref}$

t time, s

T absolute temperature, K

u interstitial molar velocity, m s^{-1}

u^* dimensionless interstitial molar velocity, $u^* = u/u_{ref}$

u^{T*} dimensionless velocity of the gas entering or leaving the storage tank

V column volume, m^3

V^T storage tank volume, m^3

x dimensionless spatial coordinate, $x = z/L$

y molar fraction in the gas phase

z spatial coordinate, m

Greek variables

α_i^D ratio between the diffusivity coefficients, $\alpha_i^D = k_i/k_{ref}$

ε_b bed porosity

ε_p particle porosity

γ ratio between the specific heat capacity at constant pressure and the specific heat capacity at constant volume

ρ_s adsorbent apparent density, kg m^{-3}

θ dimensionless time, $\theta = t/\theta_{ref}$

θ_{ref} bed time constant, $\theta_{ref} = L/u_{ref}$

ζ_a	adsorbed phase capacity factor, $\zeta_a = (1-\varepsilon_b)/\varepsilon_p \cdot \rho_s \cdot q_{ref} / c_{ref}$
ζ_p	fluid phase capacity factor, $\zeta_p = \varepsilon_p \cdot (1-\varepsilon_b)/\varepsilon_b$
Ψ	power consumption per product unit flow rate, $\mathrm{MJ\,m_{STP}^{-3}}$

Subscripts

d	downstream
i	component i
ref	reference
T	total
u	upstream

Superscripts

*	dimensionless
0	standard temperature and pressure conditions (STP)
B	backfill
F	feed
H	high
E	equalization
L	low
P	purge
T	storage tank
V	vent

5.10 References

Agrawal, R., A simplified method for the synthesis of gas separation membrane cascades with limited numbers of compressors. *Chemical Engineering Science*, **1997,** 52, (6), 1029-1044.

Agrawal, R.; Xu, J. G., Gas separation membrane cascades .2. Two-compressor cascades. *Journal of Membrane Science*, **1996,** 112, (2), 129-146.

Armond, J. W.; Webber, D. A.; Smith, K. C. Gas Separation. U.S. Patent 4,190,424, 1980.

Bansal, R. K. Pressure Swing Adsorption Process and System for Gas Separation. U.S. Patent 4,973,339, 1990.

Behling, R.-D.; Peinemann, K.-V.; Ohlrogge, K.; Wind, J.; Silva, L. B. d. Multi-Stage Process for the Separation/ Recovery of Gases. U.S. Patent 6,221,131, 2001.

Chiang, R. L.; Whitley, R. D.; Ostroski, J. E.; Dee, D. P. Argon/ Oxygen Selective X-Zeolite. U.S. Patent 6,432,170, 2002.

Chou, C. T.; Huang, W. C., Incorporation of a Valve Equation into the Simulation of a Pressure Swing Adsorption Process. *Chemical Engineering Science*, **1994,** 49, (1), 75-84.

Cruz, P. Simulação e Optimização de Processos Cíclicos de Adsorção. PhD Thesis, Universidade do Porto, Porto, Portugal, 2003.

Cruz, P.; Santos, J. C.; Magalhães, F. D.; Mendes, A., Cyclic adsorption separation processes: Analysis strategy and optimization procedure. *Chemical Engineering Science*, **2003,** 58, (14), 3143-3158.

Dee, D. P.; Chiang, R. L.; Miller, E. J.; Whitley, R. D. High purity oxygen production by pressure swing adsorption. U.S. Patent 6,544,318 B2, 2003.

Dolle, P. O.; Monereau, C. Installation and Process for the Separation of Gas by Selective Permeation. U.S. Patent 6,458,190, 2002.

Espitalier-Noel, P. M. Waste recycle pressure swing adsorption to enrich oxygen from air. Ph.D., University of Surrey, Guildford, Surrey, UK, 1988.

Ettouney, H. M.; Majeed, U., Effect of cell configuration on separation characteristics of gas mixtures by polymeric membranes. *Separation and Purification Technology*, **1997,** 11, (2), 103-112.

Farooq, S.; Ruthven, D. M.; Boniface, H. A., Numerical-Simulation of a Pressure Swing Adsorption Oxygen Unit. *Chemical Engineering Science*, **1989,** 44, (12), 2809-2816.

Garrett, M. E. Separation of Gas Mixtures. U.S. Patent 4,989,083, 1990.

Gottzmann, C. F.; Prasad, R.; Fay, H. Multiple Purity Membrane Process. EP 0 596 268, 1994.

Guérin de Montgareuil, P.; Dominé, D. Procédé de séparation d'un mélange gazeux binaire par adsorption. FR 1,223,261, 1957.

Haruna, K.; Hayashi, S. Process for Producing High Concentration Oxygen by a Pressure-Swing-Adsorption Method. U.S. Patent 4,661,128, 1987.

Haruna, K.; Ueda, K.; Inoue, M.; Someda, H. Process for Producing High Purity Oxygen from Air. U.S. Patent 4,985,052, 1991.

Hayashi, S.; Kawai, M.; Kaneko, T., Dynamics of high purity oxygen PSA. *Gas Separation & Purification*, **1996,** 10, (1), 19-23.

Hill, C. C.; Hill, T. B. Fluid fractionator. U.S. Patent 5,730,778, 1998.

Hill, T. B.; Hill, C. C.; Hansen, A. C. Rotary valve assembly for pressure swing adsorption system. U.S. Patent 6,311,719, 2001.

Hutson, N. D.; Rege, S. U.; Yang, R. T., Mixed cation zeolites: LixAgy-X as a superior adsorbent for air separation. *Aiche Journal*, **1999,** 45, (4), 724-734.

Jee, J. G.; Kim, M. B.; Lee, C. H., Pressure swing adsorption processes to purify oxygen using a carbon molecular sieve. *Chemical Engineering Science*, **2005,** 60, (3), 869-882.

Jee, J.-G.; Lee, J.-S.; Lee, C.-H., Air separation by a small-scale two-bed medical O2 Pressure Swing Adsorption. *Industrial & Engineering Chemical Research*, **2001**, (40), 3647-3658.

Lababidi, H.; AlEnezi, G. A.; Ettouney, H. M., Optimization of module configuration in membrane gas separation. *Journal of Membrane Science*, **1996,** 112, (2), 185-197.

Liow, J. L.; Kenney, C. N., The Backfill Cycle of the Pressure Swing Adsorption Process. *Aiche Journal*, **1990,** 36, (1), 53-65.

Mendes, A. M. M.; Costa, C. A. V.; Rodrigues, A. E., Analysis of Nonisobaric Steps in Nonlinear Bicomponent Pressure Swing Adsorption Systems. Application to Air Separation. *Industrial & Engineering Chemical Research*, **2000,** 39, (1), 138-145.

Miller, G. W.; Theis, C. F. Molecular Sieve Oxygen Concentrator with Secondary Oxygen Purifier. U.S. Patent 4,880,443, 1989a.

Miller, G. W.; Theis, C. F. Secondary Oxygen Purifier for Molecular Sieve Oxygen Concentrator. U.S. Patent 4,813,979, 1989b.

Nilchan, S.; Pantelides, C. C., On the optimisation of periodic adsorption processes. *Adsorption-Journal of the International Adsorption Society*, **1998,** 4, (2), 113-147.

Peters, M. S.; Timmerhaus, K. D., *Plant Design and Economics for Chemical Engineering*. McGraw-Hill: New York, 1980.

Pinkerton, C. J. Portable Oxygen Enrichment and Concentration System. U.S. Patent 4,491,459, 1985.

Prasad, R. Three-Stage Membrane Gas Separation Process and System. U.S. Patent 5,102,432, 1992.

Prasad, R. High Purity Membrane Nitrogen. U.S. Patent 5,378,263, 1995.

Prasad, R. Advanced Membrane System for Separating Gaseous Mixtures. U.S. Patent 5,709,732, 1998.

Prasad, R.; Cook, P. J.; Gottzmann, F. Air Separation System and Method. U.S. Patent 5,827,351, 1998.

Rege, S. U.; Yang, R. T., Kinetic separation of oxygen and argon using molecular sieve carbon. *Adsorption-Journal of the International Adsorption Society*, **2000,** 6, (1), 15-22.

Richter, E.; Knoblauch, K.; Schlegel, R.; Körbächer, W. Process and Apparatus for Producing Oxygen with a Low Proportion of Argon from Air. U.S. Patent 4,566,881, January 28, 1986.

Santos, J. C.; Portugal, A. F.; Magalhães, F. D.; Mendes, A., Simulation and optimization of small oxygen pressure swing adsorption units. *Industrial & Engineering Chemistry Research*, **2004,** 43, (26), 8328-8338.

Santos, J. C.; Portugal, A. F.; Magalhães, F. D.; Mendes, A., Optimization of medical PSA units for oxygen production. *Industrial & Engineering Chemistry Research*, **2006**, (accepted).

Skarstrom, C. W. Timing Cycle for Improved Heatless Fractionation of Gaseous Materials. U.S. Patent 3,104,162, 1963.

Teague, K. G., Jr.; Edgar, T. F., Predictive dynamic model of a small pressure swing adsorption air separation unit. *Industrial & Engineering Chemical Research*, **1999,** 38, (10), 3761-3775.

Thompson, D. R. Multistage Membrane Control System and Process. U.S. Patent 5,281,253, 1994.

Tsuru, T.; Hwang, S. T., Production of High-Purity Oxygen by Continuous Membrane Column Combined with PSA Oxygen Generator. *Industrial & Engineering Chemistry Research*, **1994,** 33, (2), 311-316.

White, D. H.; Barkley, P. G., The Design of Pressure Swing Adsorption Systems. *Chemical Engineering Progress*, **1989,** 85, (1), 25-33.

Xu, J. Compressed Permeate Sweep Membrane Separation Process. U.S. Patent 5,252,219, 1993.

Xu, J. Low Pressure Feed Membrane Separation Process. U.S. Patent 5,36,427, 1994.

Xu, J. G.; Agrawal, R., Gas separation membrane cascades .1. One-compressor cascades with minimal exergy losses due to mixing. *Journal of Membrane Science*, **1996,** 112, (2), 115-128.

Yang, R. T., *Gas separation by adsorption processes*. Butterworths: Boston, 1987.

Yee, T. F.; Srinivasan, R. S.; Thorogood, R. M. Oxygen Production by Staged Mixed Conductor Membranes. U.S. Patent 5,447,555, 1995.

Appendix 5.1 Optimization algorithm

A 5.1.1 Successive quadratic programming algorithm

The successive quadratic programming algorithm (SQP) fits the function, locally, to a quadratic function and the restrictions to linear functions so that the quadratic programming may be used recursively. The optimum solution satisfies the Kuhn-Tucker necessary conditions. The algorithm may be described by the following steps (Cruz et al., 2005, Cruz et al., 2003, Edgar and Himmelblau, 1988):

1. Let $k = 0$.
   Pick r^0, $\mathbf{x}^0$, $\mathbf{B}^0$ **($\mathbf{B}^0$ = I)**,
   where **x** is the vector composed by the optimization variables, **B** is an estimate of the Hessian matrix and r is the weighting coefficient of the penalty function.

2. Compute the value of the restriction, $h(\mathbf{x}^k) = \text{Pur}_\text{R}\text{-Pur}$.
   Compute the objective function value, $f(\mathbf{x}^k)$.
   Compute the values of $\nabla\mathbf{f}(\mathbf{x}^k)$ and $\nabla\mathbf{h}(\mathbf{x}^k)$.

3. Estimate the Lagrange multiplier, $\mathbf{u}^k$
   $\mathbf{u}^k = \left(\nabla\mathbf{h}^k \cdot (\mathbf{B}^k)^{-1} \cdot (\nabla\mathbf{h}^k)^T\right)^{-1} \cdot (\nabla\mathbf{h}^k \cdot (\mathbf{B}^k)^{-1}\nabla\mathbf{f}^k - h^k)$,
   where f is the objective function $\text{f} = -\text{Rec}$.

4. Compute the new search direction, $\mathbf{s}^k$
   $\mathbf{s}^k = (\mathbf{B}^k)^{-1}((\nabla\mathbf{h}^k)^T \cdot u^k - \nabla\mathbf{f}^k)$.

5. Evaluate the weighting coefficient of the penalty function, **r**
   $\mathbf{r} = \max\left[|\mathbf{u}|, 0.5(|\mathbf{u}| + \mathbf{r})\right]$.

6. Compute the step size, λ^k, and the new **x**
   6.1. $\lambda^k = 1$ for $i = 0$;
   6.2. Compute $x^* = \min\left[\max(\mathbf{x}^k + \lambda^k \cdot \mathbf{s}^k, \mathbf{x}_\text{L}), \mathbf{x}_\text{H}\right]$,
   where $\mathbf{x}_\text{L}$ and $\mathbf{x}_\text{H}$ are the low and high bounds of the optimization variables, respectively;
   6.3. Compute $h(x^k) = \min(0, \text{Pur}_\text{R}\text{-Pur})$;
   6.4. Evaluate the objective function value, $f(x^k)$;
   6.5. If $\left\{ f(\mathbf{x}^*) - f(\mathbf{x}^k) + \sum r_j \left[|h_j(\mathbf{x}^*)| - |h_j(\mathbf{x}^k)| \right] \right\} > 0$ Then
   Let $\lambda^k = \lambda^k/2$; $i = i + 1$ and go to step 6.2;

Otherwise
Let $\mathbf{x}^{k+1} = \mathbf{x}^{*}$ and go to step 7.

7. Compute the values of $\nabla \mathbf{f}(\mathbf{x}^{k+1})$ and $\nabla \mathbf{h}(\mathbf{x}^{k+1})$.

8. Compute the new estimate for the Hessian matrix, **B**, using the method BFGS (Edgar and Himmelblau, 1988).
$$\mathbf{B}^{k+1} = \mathbf{B}^{k} + \frac{\Delta \mathbf{g}^{k} (\Delta \mathbf{g}^{k})^{T}}{(\Delta \mathbf{g}^{k})^{T} \Delta \mathbf{x}^{k}} - \frac{\mathbf{B}^{k} \Delta \mathbf{x}^{k} (\Delta \mathbf{x}^{k})^{T} \mathbf{B}^{k}}{(\Delta \mathbf{x}^{k})^{T} \mathbf{B}^{k} \Delta \mathbf{x}^{k}},$$
where $\Delta \mathbf{g}^{k} = \nabla_{x} L(\mathbf{x}^{k+1}, \mathbf{u}^{k+1}) - \nabla_{x} L(\mathbf{x}^{k}, \mathbf{u}^{k+1})$, $\Delta \mathbf{x} = \mathbf{x}^{k+1} - \mathbf{x}^{k}$ and L is the Lagrange function given by $L(\mathbf{x}, u) = f(\mathbf{x}) - \sum u_{j} h_{j}(\mathbf{x})$

9. Stop criteria used:
$\frac{\left\| x^{k} - x^{k-1} \right\|}{\left\| x^{k} \right\| + 1} \leq \varepsilon_{\mathrm{R}}$, $\left\| x^{k} - x^{k-1} \right\| \leq \varepsilon_{\mathrm{A}}$ and $\left| h(\mathbf{x}^{k}) \right| \leq \varepsilon_{\mathrm{A}}$, where ε_{R} is the relative error and ε_{A} the absolute error.
Stop if all criteria are obeyed. Otherwise, continue.

10. Let $k = k + 1$ and go to step 3.

A 5.1.2 References

Cruz, P.; Mendes, A.; Magalhães, F. D., On the Optimization of Cyclic Adsorption Separation Processes. *Aiche Journal*, **2005,** 51, (5), 1377-1395.

Cruz, P.; Santos, J. C.; Magalhães, F. D.; Mendes, A., Cyclic adsorption separation processes: Analysis strategy and optimization procedure. *Chemical Engineering Science*, **2003,** 58, (14), 3143-3158.

Edgar, T. F.; Himmelblau, D. M., *Optimization of chemical processes*. McGraw-Hill: Mexico, 1988.

6. General Conclusions and Future Work

This Thesis had as objectives the study of new adsorbents and cycles for pressure swing adsorption units used in medical applications. It was considered important to study the cycles used in commercial units for a better understanding of the technological solutions employed and how they influence the behaviour of the unit. This study aimed also to obtain directions for improving the performance of these units.

The simulation of adsorption processes involving zeolites with high capacities and selectivities requires accurate and fast numerical methods. The algorithm presented enforces both local and global flux conservation in space and time. The convection terms can be discretized using high-resolution schemes, ensuring boundedness. The algorithm was tested with a cyclic adsorption process and it was verified that the use of a finite volume method combined with the use of high resolution schemes such as SMART, allowed a good accuracy of the results and a fast convergence. For systems with more than two components, the χ-schemes with SMART formulation were used and the simulation results obtained were in good agreement with the experimental data.

The adsorption data was measured using two methods: gravimetric and volumetric. Both methods were shown to give agreeable results. Nevertheless, the errors of the values obtained by the volumetric method are much higher than the ones obtained by the gravimetric method.

The adsorption capacities of the adsorbents Oxysiv 5, Oxysiv 7, KEG415 (formerly from Bayer) and Oxysiv MDX from UOP, MS S 624 and MS C 544 from Grace Davison and AgLiLSX from Air Products and Chemicals, Inc., were determined. From the analysis of the monocomponent adsorption equilibrium data it was concluded that Oxysiv MDX, from UOP, is the best adsorbent for the separation of oxygen from air for concentrations under 95%. Good results may also be obtained in this range with AgLiLSX from Air Products and Chemicals Inc and Oxysiv 7 from UOP. AgLiLSX is the only adsorbent that allows the production of higher concentrations of oxygen since it shows selectivity for argon over oxygen.

The regeneration of the adsorbents was studied. It was concluded that the regeneration of Oxysiv 7 in a stagnant atmosphere causes an irreversible degradation of the adsorbent. It was also concluded that it is possible to fully regenerate a contaminated sample at about 375ºC and passing continuously helium or dried air.

Carbon dioxide and water vapour were found to contaminate most of the adsorbents studied and the extent of this contamination was measured. The contamination of a working pressure swing adsorption (PSA) unit with MS S 624 was studied. It was concluded that 30% of the column was contaminated, being the main contaminant water vapour. This contamination caused a loss of performance around 18%. It was also concluded that the density of the adsorbent gives a good indication about the activation state of the adsorbent.

The physical characteristics (pore size distribution, porosity and particle diameter) of the adsorbents were also measured and the LDF kinetic parameters were obtained with the use of empirical correlations for determining the diffusivities. The adsorbent with a faster mass transfer was found to be Oxysiv 5 from UOP while MS S 624 from Grace Davison was found to have the slower mass transfer.

Pressure swing adsorption cycles were compared with a vacuum and pressure swing adsorption cycle mode. Cycles with three different types of equalization: top-to-top, bottom-to-bottom and crossed and cycles with backfill and using multiple columns were compared as well. It was concluded that the top-to-top equalization is the best configuration since it allows higher recoveries, lower power consumption, requires fewer valves and avoids the dragging of the contaminants from the bottom of the column to the top.

As expected, a vacuum and pressure swing adsorption (VPSA) unit has a lower power consumption per product flow rate than a pressure swing adsorption (PSA) unit operating with the same pressure ratio although the VPSA unit is larger.

The backfill step that was presented (the column producing backfills the other column) did not show to be advantageous with respect to the recovery and to the minimization of the time required to achieve the desired purity. For the adsorbents and conditions studied a cycle without equalization arrives faster than with any other of the cycles studied. A cycle with top-to-top equalization allowed a high recovery and a fast increase of the product purity.

The adsorbent AgLiLSX from Air Products showed to allow the production of high-purity oxygen in a single step, although with a low recovery.

Oxysiv MDX from UOP allows the best performance in all the cycles studied, followed by AgLiLSX from Air Products and Chemicals, Oxysiv 7 from UOP, MS S 624 from Grace Davison and Oxysiv 5 from UOP. A PSA unit with a top-to-top equalization and packed with Oxysiv MDX was found to have the best performance

(allows a recovery around 70%) among the adsorbents and cycles studied. The use of Oxysiv MDX, AgLiLSX, Oxysiv 7 and MS S 624 in PSA units and Oxysiv MDX, AgLiLSX and Oxysiv 7 in VPSA units will have as a result, smaller units or higher product flow rates. However, Oxysiv MDX, AgLiLSX and Oxysiv 7 are more expensive than the other adsorbents studied.

Two commercial units (one from Air Products and Chemicals and the other from Weinmann) and a laboratorial unit with Oxysiv MDX and AgLiLSX were simulated. The simulator was able to represent accurately real units when the contamination of the adsorbent by carbon dioxide and water vapour is avoided. With the optimization strategy it was possible to achieve better operating conditions and design characteristics that improved the performance of the units.

As future work, the modelling of the water contamination in working PSA units and the optimization under these conditions considering the process variables such as cycle times, pressure envelope, purge and equalization flow rates as well as the ratio between the amount of adsorbent and the amount of adsorbent for treating the feed (silica gel or activated alumina, for example) would be of great importance.

The study of alternative processes for high purity oxygen production, such as a the combination of two PSA units, the second using the new carbon molecular sieve (CMS) adsorbents commercialized by CarboTech and Takeda or the combination of a PSA unit with a CMS membrane module and comparison with the one step production provided by the use of AgLiLSX would also be of great interest.